PROVENANCE AND PALEODRAINAGE OF LATE JURASSIC AND EARLY CRETACEOUS RESERVOIR SANDSTONES IN THE FLEMISH PASS AND ORPHAN BASINS

DAVID GEORGE LOWE

Provenance and Paleodrainage of Late Jurassic and Early Cretaceous Reservoir Sandstones in the Flemish Pass and Orphan Basins

By

© David George Lowe

A thesis submitted to the

School of Graduate Studies

in partial fulfillment of the

requirements for the degree of

Master of Science

Department of Earth Sciences

Memorial University of Newfoundland

November 2009

St. John's Newfoundland and Labrador

ABSTRACT

Late Jurassic to Early Cretaceous potential reservoir sandstones from three industry exploratory wells in the Flemish Pass and Orphan Basins were studied for provenance analysis. The sandstones from this study formed during intracratonic rifting that preceded the breakup between North America and its European conjugate margins and seafloor spreading in the North Atlantic. Most were deposited during the Tithonian and Neocomian North Atlantic Rifting stage, during which rifting intensified between Iberia and the Grand Banks and the deposition of important reservoir sandstones occurred regionally.

Heavy mineral fractions were isolated from cuttings samples from six syn-rift sandstone units. The studied sandstones range in age from Tithonian to Albian. Three heavy mineral approaches were used to determine provenance and make correlations: (1) U-Pb geochronology and petrography of detrital zircons, (2) detrital heavy mineral grain counts and ratios, and (3) geochemistry of detrital tourmalines.

Based mainly on detrital zircon ages and petrography and detrital tourmaline geochemistry, the predominant first-cycle sediment sources included the Neoproterozoic arc-phase igneous rocks of the Avalon Zone as well as the Ordovician to Devonian magmatic rocks and metasedimentary rocks present in the Central Mobile Belt. There is abundant petrographic and heavy mineral evidence to support significant recycling of material from cover sequences in these tectonic zones as well, likely including Early and Late Paleozoic sedimentary rocks which are ubiquitous in both zones.

Such a source signature requires uplifted source areas to be present in the west, including parts of the Bonavista Platform, Interior Newfoundland, Northeastern Newfoundland Shelf, and potentially parts of the Irish conjugate margin, including the Porcupine Bank. Thus, paleodrainage orientations and delivery of coarse clastic detritus into the Flemish Pass and Orphan Basins was predominantly from the west during the Late Jurassic to Early Cretaceous, as seafloor spreading began between the Grand Banks and Iberia. Based on this information, one would expect to find reservoir facies sandstone units of this age concentrated along the western margins of the Flemish Pass and Orphan Basins, with deteriorating reservoir grade towards the east.

A number of the studied sandstones in the Flemish Pass Basin show evidence for partial sourcing from the south, including proximal sources and distal sources as far south as the Avalon Uplift; verifying previous ideas that the Avalon Uplift existed as a significant positive regional tectonic element as incipient seafloor spreading began between Iberia and the Grand Banks. There is no evidence to support sourcing from the east, off of the Iberian margin or the Flemish Cap-Galicia Bank continental fragment, and material from these areas is instead interpreted to have been shed into the incipient Atlantic Ocean or Bay of Biscay.

Mesozoic aged detrital zircons were present in two samples, and proved useful for constraining the depositional age of these sandstones. The most likely known sources of these grains include the Budgell Harbour Stock, in Central Newfoundland, or an Early Cretaceous "granite basement" intercepted by the Bonavista C-99 well in the West Orphan Basin. Both of these potential sources are located to the west of the studied units.

Acknowledgements

I would like to thank my two thesis supervisors, Dr. Paul Sylvester and Dr. Michael Enachescu, for their technical, academic and professional guidance, and as well for giving me the opportunity to undertake this project and the freedom to gain some practical work experience as well. Also, I acknowledge and thank the people from the Creait Network at Memorial University, including Michael Tubrett, Michael Shaffer, Marc Beauchamp and Kate Souders. Without their technical expertise, this project would not have been possible. Also, thanks to Rick Hiscott and Greg Dunning, who, even though I did not ask for help often, gave me some pro-bono mentoring from time to time. Thanks to my employers and mentors at work, including some fine geologists at Petro-Canada (Michael Webb and John Gordon particularly) and the Newfoundland Geological Survey (Tim van Nostrand, and the rest), who contributed to my technical and professional growth as a geologist. Also, I would like to thank Gerald Sullivan from Petro-Canada and Jacqueline LeMoine at Husky for donations of sample materials, without which this project may have not gotten off of the ground. And thanks to all the people at the C-NLOPB for accommodating access to core and sample materials. Also, for that time that I had a flat tire and Dave and Jason from the C-NLOPB core repository helped me change my tire, extra thanks to those C-NLOPB employees.

Finally, I would like to thank all of the good friends I have made in St. John's for making this two-plus years experience some of the best times of my life. Most of you at some point were helpful with this project, whether you knew it or not, even though at most instances you would have seemed to have the opposite effect. And Mom and Dad, thanks for all your support during this period of my life.

Table of Contents

Table of Figures

Chapter 1: Introduction and Geological Setting

1.1 Introduction and Purpose

This thesis contains an in-depth study of East Coast Canada Mesozoic sandstone provenance using detrital heavy minerals. The sandstones were intercepted by industrial oil and gas exploration wells in the Flemish Pass and Orphan basins, which are located approximately 400 km northeast of St. John's, Newfoundland (Figure 1.1). These basins are fault-bounded Mesozoic aged basins that formed by attenuation of the continental crust during repeated Mesozoic rift periods that preceded the breakup and seafloor spreading between North America and its conjugate margins Iberia and NW Europe.

Covered by relatively thick passive margin sedimentary sequences, the basins are currently targets of oil and gas exploration because they are stratigraphically similar to the adjacent Jeanne d'Arc Basin, a prolific oil and gas province. The stratigraphic similarities include the presence of a mature Kimmerigian aged source rock as well as Late Jurassic to Early Cretaceous potential reservoir sandstone formations in the Flemish Pass Basin, considered analogous to the primary reservoir sandstone formations in the Jeanne d'Arc Basin (the Jeanne d'Arc, Hibernia, Avalon and Ben Nevis Formations) (Creaney and Allison, 1987; Foster and Robinson, 1993; Desilva, 2000). The distribution and geology of reservoir sandstones in the Jeanne d'Arc Basin are well constrained, based on the use of core analysis, well correlations and corroborating 2D 3D seismic interpretations (Tankard and Welsink, 1987; Enachescu, 1988; Sinclair, 1993; Enachescu

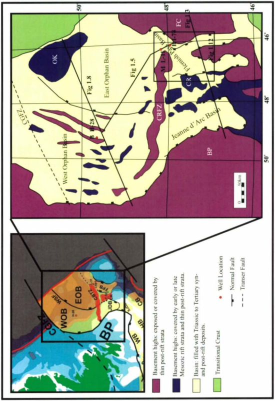

Figure 1.1: Regional location and geological map of the basins Offshore Newfoundland. Lines show locations of cross-sections in later figures in the chapter, and the inset box shows the location of figure 1.12. BP=Bonavista Platform; CGFZ=Charlie-Gibbs Fault Zone; CR=Central Ridge; CRFZ=Cumberland ridge fault zone; FC=Flemish Cap; OK=Orphan Knoll. Well locations P52=Panther P-52; I78=Baccalieu I-78; H28=Blue H-28; L11=MizzenL-11. (Modified from Enachescu 1987).

et al., 1994). However, unlike the shallow water Jeanne d'Arc Basin, the deep water Flemish Pass and Orphan basins have poor well control, due to the greater expense of drilling these areas; and thus, provenance, orientations, correlations, lateral reservoir quality variations and other depositional constraints of sandstones in these basins during this time are very poorly constrained. Also, our understanding of regional rifting, drainage and tectonics is limited, given only knowledge of provenance, paleodrainage orientations and uplift histories from studies in to the Jeanne d'Arc Basin.

The goals of this study are as follows:

1. To further constrain regional paleo-drainage, paleo-geography, uplift and basin configurations during rifting,
2. To determine constraints on the orientation, extent and quality predictions of Late Jurassic and Early Cretaceous reservoir facies in the Flemish Pass and Orphan Basins, based on regional paleodrainage models,
3. To make regional correlations between potential reservoir sandstones, and
4. To test the application of heavy mineral analysis and the analytical methods used (MLA and ICP-MS) to industry-related frontier exploration efforts.

Several syn-rift sandstones from the Flemish Pass Basin, ranging in age from Tithonian to Berriasian, and one Albian aged syn-rift sandstone from the West Orphan Basin were used in this study. This study utilizes several complimentary methods to interpret provenance, including thin section petrography (Chapter 3), provenance-sensitive heavy mineral ratios (Chapter 4), detrital tourmaline chemical discriminations (Chapter 5) and detrital zircon petrography and U-Pb geochronology (Chapter 6).

This chapter focuses on the regional geological setting of these syn-rift sandstones, with emphasis on basin and basement platform configurations and sedimentation during the Tithonian-Albian, as well as the geology and ages of various surrounding potential source areas. Also included are more detailed overviews of the geology and geologic evolution of the Flemish Pass and Orphan basins.

1.2 Mesozoic Offshore Newfoundland geological and tectonic setting

As shown in Figure 1.1, current day syn-rift Mesozoic rocks offshore Newfoundland are confined to a series of variably interconnected half-graben rift basins separated and bounded by pre-Mesozoic basement highs, and include the Jeanne d'Arc, West Orphan, East Orphan and Flemish Pass basins. These basins formed during the Mesozoic intra-continental rifting, spanning from the Permo-Triassic until the Mid Cretaceous, which was followed by North Atlantic seafloor spreading and passive margin sedimentation until recent times (Enachescu, 1987 and 1988; Tankard and Welsink, 1989; McAlpine, 1990; Enachescu et al., 2005).

The rift system and opening of the Atlantic was sequential and gradually moved from south to north during the Late Triassic to early Late Cretaceous, resulting in prolonged extension and basin formation on the Newfoundland continental shelf (Figure 1.2). The Jeanne d'Arc Basin preserves the deepest (~22km) and most complete syn-rift succession out of the Mesozoic basins offshore Newfoundland, due to its proximity to the main listric detachment, or basin bounding fault, and relatively continuous subsidence through the continental rift phases (Figure 1.3) (Keen et al., 1987; Enachescu, 1987;

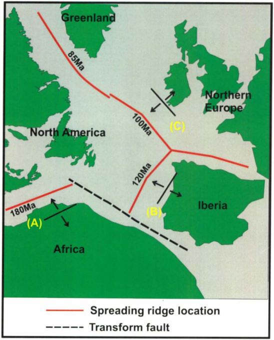

Figure 1.2: Reconstruction of the pre-rift North Atlantic area (compiled using Lefort (1983), Zeigler (1989), Verhoef and Srivastava (1989) and Scotese (2004)). Rifting in the North Atlantic was sequential, and the focus of rifting migrated from the south to north in the Mesozoic. The rifting orientations and approximate age of incipient seafloor spreading is shown for each regional rifting phase. First was the Tethys rift phase (A), focused between Africa and North America during the Triassic and Early-Mid Jurassic, and ending in seafloor spreading between these margins at 180 Ma. Second was the North Atlantic rift phase (B), focused between Iberia and the Grand Banks during the Latest Jurassic to Earliest Cretaceous (Kimmeridgian to Barremian), and ending in seafloor spreading between these margins at 120 Ma. Third was the Labrador Sea rift phase (C), focused between Northern Europe and North America during the Early Cretaceous (Aptian to Albian), and ending in seafloor spreading between these margins at 100 Ma.

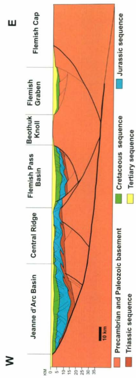

Figure 1.3: West to east cross section across the Jeanne d'Arc Basin, Central Ridge, Flemish Pass Basin, Beothuk Knoll, Flemish Graben and Flemish Cap. This figure depicts the deep crustal relationship between the Flemish Pass and Jeanne d'Arc basins. They form a "double failed rift" with synthetic and antithetic faults soling out along the main deep crustal listric detachment fault. The Central Ridge became a positive element in the Tithonian (Late Jurassic) and subsidence continued on either side. The Jeanne d'Arc Basin preserves the deepest syn-rift fill due to its location adjacent to the main listric detachment fault (Modified from Enachescu 1988).

Tankard and Welsink, 1987). It also hosts several offshore oil fields, has extensive well control, and has been studied extensively. Thus, the stratigraphy of the Jeanne d'Arc Basin is considered a good analogue for regional exploration and studies of syn-rift basin sedimentation elsewhere offshore Newfoundland (Figure 1.4). Three stages of rifting have been identified from studies of basin fill in the Jeanne d'Arc Basin, and these are shown to have affected many of the North Atlantic Basins regionally (Enachescu, 1987; Tankard and Welsink, 1987; Sinclair, 1995). The Three rift stages, according to Enachescu (1987), are: (1) the Tethys rifting stage, from Late Triassic to Early Jurassic, which resulted in the mid-Jurassic breakup between North America and Africa and subsequent seafloor spreading south of the Newfoundland Fracture Zone; (2) the North Atlantic rifting stage, from Late Jurassic to Early Cretaceous, which ended in incipient seafloor spreading and break-up between the southern Grand Banks and Iberia; and (3) the Labrador Sea rifting stage, occurring in the late Early Cretaceous (from the Barremian to Albian), that resulted in the final break-up between Iberia and the Grand Banks, propagation of incipient seafloor and eventual break-up between the Northeast Newfoundland shelf and Northern Europe, and rifting between Labrador and Greenland (Enachescu, 1987; Tankard and Welsink, 1989; McAlpine, 1990; Sinlcair, 1993). A fourth rifting stage that influenced the Orphan and Labrador area is related to Late Cretaceous to Tertiary rifting between Labrador and Greenland (Enachescu et al., 2005). Following the succeeding intra-continental rifting stages was the final post-rift stage, where thermal subsidence of the newly created continental margins dominated from Late Cretaceous (Early Tertiary in the north) onwards and passive margin sediments were deposited along the Atlantic shelf, slope and in deep water.

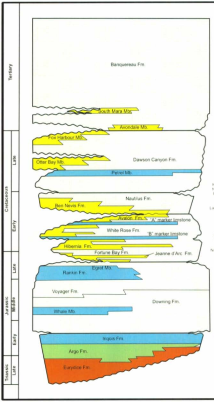

Figure 1.4: General Regional stratigraphy of the Jeanne d'Arc Basin. The primary oil and gas reservoir units are the Late Jurassic Jeanne d'Arc Formation and the Early Cretaceous Hibernia, Avalon and Ben Nevis Formations. The primary regional source rocks are the Egret Member of the Rankin Formation (Kimmerigian).

Syn-rift fill from the Tethys rift overlies pre-rift basement and is composed of Triassic early syn-rift continental red beds and evaporates. Mid- to Late Jurassic post-Tethys rifting strata are dominated by carbonates, but include the Kimmeridgian aged organic-rich carbonaceous shales of the Egret Member, which represents the proven regional oil and gas source rock. The Late Jurassic to Early Cretaceous sequences of the North Atlantic and Labrador Sea rift phases generally comprises a succession of terrestrial to marginal marine siliciclastics, which include the fluvial-deltaic and shoreface sandstones that make up the main oil and gas reservoirs (Jeanne d'Arc, Hibernia, Avalon and Ben Nevis Formations). The post-rift succession comprises strata from Late Cretaceous onwards, and is dominated by continental margin siliciclastics (Tankard and Welsink, 1989; McAlpine, 1990; Sinlcair, 1993). The same or similar package of Late Triassic to Mid-Late Cretaceous aged sequences are considered to exist in the Flemish Pass and East Orphan basins (Foster and Robinson, 1993; Enachescu et al., 2005). Wells in the Flemish Pass Basin have intercepted similar Late Jurassic to Early Cretaceous packages, and these packages have been traced from the Flemish Pass Basin into the East Orphan Basin (Figure 1.5) (Foster and Robinson, 1993; Enachescu et al., 2005). Additionally, the Great Barasway F-66 well, drilled in the East Orphan Basin in 2007, intercepted Jurassic and Cretaceous strata (C-NLOPB, 2009). In the West Orphan Basin, rifting began in the Albian, much later than in the East Orphan or Flemish Pass basins, so the age of syn-rift sedimentary infill only ranges from Early Cretaceous (Albian) to Paleocene (Enachescu et al., 2004; Enachescu et al., 2005; Hardy, 2008).

Out of the basins highlighted in Figure 1.1, the Flemish Pass, Jeanne d'Arc and East Orphan Basins were active depocentres of clastic material during the Tithonian to

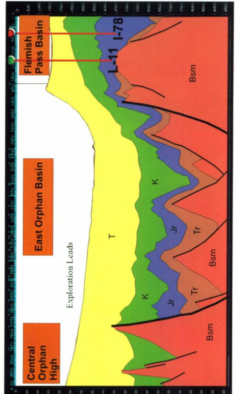

Figure 1.5: Composite seismic section of the East Orphan Basin and northern Flemish Pass Basin. This section shows continuity between the East Orphan and Flemish Pass Basins, suggesting that the northern Flemish Pass Basin is an elevated terrace of the East Orphan Basin. A major fault may be present at the southeastern boundary of the Orphan Basin. Modified from Enachescu et al. (2005).

Valanginian, during which time reservoir sandstones were deposited locally, at least in the Jeanne d'Arc and Flemish Pass basins, but presumably also in the East Orphan Basin (Tankard and Welsink, 1989; McAlpine, 1990; Sinlcair, 1993; Enachescu et al., 2005; Hardy, 2008). Syn-depositional communication between these basins is thought to have been likely (Enachescu et al., 2005) (Figure 1.6). The depositional constraints and insights into the provenance of such sandstones in the Jeanne d'Arc Basin have been described in detail, and are reviewed briefly in the next section, along with constraints on syn-rift sandstone deposition from other North Atlantic rift basins. The provenance and orientations of reservoir sandstones of the same age are not known in the Flemish Pass Basin, and this project addresses this lacking information. The provenance and implications for sand body orientations of Albian syn-rift sandstones in the West Orphan basin are also addressed, and similarly, contemporaneous regional rift evolution and sedimentation are described below.

1.3 Late Jurassic to Early Cretaceous Regional setting

During Mesozoic time, mainly from the Permo-Triassic until the Late Cretaceous, intra-continental rifting that preceded the breakup of Pangaea and opening of the Atlantic Ocean was extensive. The opening of the Atlantic was sequential and gradually moved from south to north during the Late Triassic to early Late Cretaceous, resulting in prolonged rifting in some areas (Figure 1.2). This prolonged rifting resulted in the formation of rift basins along the North Atlantic margins, including Iberian and Irish continental shelves (Figure 1.7). Figure 1.7 shows an approximate reconstruction of Late

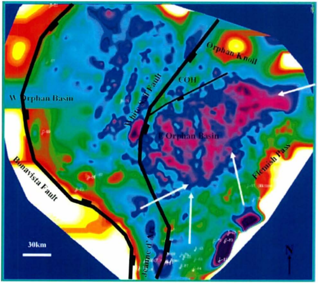

Figure 1.6: Workstation-generated map of seismic time-structure of the economic basement horizon over the Orphan Basin and the northern Flemish Pass and Jeanne d'Arc Basins. Also included are the approximate locations of the interpreted White Sail and Bonavista basin-bounding faults. Red and yellow areas are structural highs outside of the basinal areas. Green and light blue areas are structural highs within the basinal areas. Dark blue and purple areas are structural lows. COH= Central Orphan High. The white arrows indicate depressions where seaway communication between the East Orphan and adjacent basins was possible during the Triassic and Jurassic (From Enachescu et al. 2005).

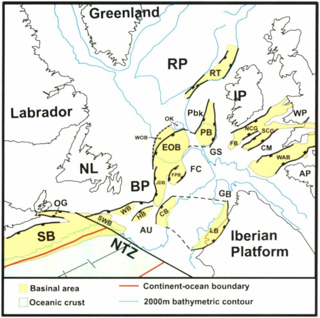

Figure 1.7: Late Jurassic to Early Cretaceous (Kimmerigian-Aptian) reconstruction of the North Atlantic showing the relative sizes and orientations of syn-rift basins and basement platforms at that time. The 2000 m bathymetric contour represents the approximate extent of continental basement. SB=Scotian Basin, NTZ= Newfoundland Transfer Zone, SWB= South Whale Bain, WB=Whale Basin, HB= Horseshoe Basin, CB=Carson (Salar) Basin, JDB= Jeanne d'Arc Basin, LB= Lusitanian Basin, GB=Galicia Bank, AU=Avalon Uplift, FC=Flemish Cap, FPB= Flemish Pass Basin, EOB=East Orphan Basin, WOB=West Orphan Basin, OK=Orphan Knoll, GS=Goban Spur, PB=Porcupine Basin, Pbk=Porcupine Bank, RT=Rockall Trough, RP=Rockall Platform, IP=Irish Platform, WP=Welsh Platform, FB=Fastnet Basin, NCG=North Celtic Graben, SCG=South Celtic Graben, CM=Cornubian Massif, WAB=Western Approaches Basin, AP=Amorican Platform. Reconstruction and platform and basin correlations are based on the work of Masson and Miles (1986), Keen et al. (1989), Verhoef and Srivastava (1989), Enachescu (1992), Srivastava et al. (2000), Enachescu et al. (2005) and Sibuet et al.. (2007).

Jurassic to Early Cretaceous (Tithonian-Albian) paleogeography, including intra-continental rift basins, various platform areas, and ocean spreading ridges at that time (see caption of Figure 1.6 for references). Basin connectivity was largely controlled by the orientations of basement platforms, which were exposed during much of this time. Thus, the orientations of these platforms presumably had important controls on paleodrainage and syn-depositional communication between basins, and additionally may have acted as thoroughfares for regional drainage systems into basins, or were uplifted periodically, providing detritus to basins. Figure 1.7 also includes potential basin and platform conjugate pairs. The pairing of conjugate platforms is important for reconstructing paleogeography, as well as for determining physical barriers to regional paleodrainage systems. Some of these conjugate pairings include the Porcupine Basin-Orphan Basin, Lusitanian Basin-Carson Basin, the Galicia Bank-Flemish Cap-Goban Spur, and Porcupine Bank-Orphan Knoll (Masson and Miles, 1984, 1986; Verhoef and Srivastava, 1989; Enachescu, 1992; Srivastava et al., 2000; Sibuet et al., 2007).

Similarly timed rifting events, occurring from the Permo-Triassic to the Paleocene, occurred in conjugate margin basins including the Porcupine, Lusitanian, and Celtic Sea basins, resulting in a broadly similar syn-rift stratigraphy in these basins as is present in the Jeanne d'Arc, Flemish Pass and Orphan basins on the North American margin (Masson and Miles, 1984, 1986; Sinclair, 1995; Hiscott, 1990; Johnston et al, 2001). In particular, these basins experienced markedly similar tectonic histories and contemporaneous source and reservoir rock deposition during the Late Jurassic to Early Cretaceous (Kimmeridgian to Aptian) (Sinclair, 1995)

This section briefly describes the general architectures and orientations of basins and platforms and deposition of reservoir facies into basins during the late Jurassic to Early Cretaceous. The best studied basins include the Scotian Basin, Orpheus Graben, Whale Basin, Jeanne d'Arc Basin, Flemish Pass Basin, Orphan Basin, Lusitanian Basin, Porcupine Basin, and Celtic Sea Basins; basement platforms include the Lahave Platform, Avalon Uplift/southern Grand Banks, Bonavista Platform, Flemish Cap, Galicia Bank, Goban Spur, Cornubian Platform, Porcupine Bank, as well the larger uplifted areas including the Newfoundland, Iberian, and Irish Platforms, and the Rockall Platform (Figure 1.7). The pre-Mesozoic geology of these areas is described in a later section of this chapter.

The Scotian Basin is a true rift basin that is comprised of a series of Triassic sub-basins dissected by shallow basement horsts and salt structures. Its western margin is a composite deep listric basin bounding fault and the LaHave Platform, and its eastern margin is the Atlantic Ocean and the continent-ocean boundary (Figure 1.7). It contains similar Tethys stage syn-rift deposits as are present in other basins (including red beds and evaporates), but strata younger than Bajocian (mid-Jurassic) are mostly platform carbonates and progradational post-rift clastics, deposited after the break-up between North America and Africa. Thus unlike many of the other north Atlantic rift basins, the Scotian Basin experienced only one rifting phase, followed by early and prolonged syn-rift sedimentation in an open shelf environment (Jansa and Wade, 1975; Welsink et. al, 1989; Wade and McLean, 1990). The Orpheus Graben had a similar depositional history and syn- and post-rift sedimentary fill as the Scotian Basin in the Mesozoic. However, it remains confined between basement platforms (the Scatarie Ridge and the Canso Ridge) and is bounded be reactivated transfer faults (Jansa and Wade, 1975; Welsink et. al, 1989) (Figure 1.7). These offshore Nova Scotia platforms and basins are not considered to have been regional sediment source areas to the Grand Banks basins or connected by regional drainage during the Late Jurassic to Early Cretaceous, because they were at the time located in a passive subsiding margin setting along the proto-Atlantic, and thus would have been an area of low and negative relief relative to the Grand Banks. Additionally, these basins are likely to have been separated from the Grand banks basins by the Avalon Uplift, an extensive uplifted area south of the Jeanne d'Arc and Flemish Pass basins where extensive uplift occurred from the Tithonian to the Aptian (Keen et. al, 1987; Tankard and Welsink, 1987; Enachescu, 1988; Sinclair, 1993). Pe-Piper and McKay (2006) show that during the Early Cretaceous, detritus entered the Scotian and Orpheus basins via a series of regional drainage systems extending to various parts of the Atlantic Canadian margin, including New Brunswick, Gaspe, Labrador-Quebec and western and southern Newfoundland.

Basins on the southern Grand Banks, including the Whale, Horseshoe and South Whale basins, are all half grabens bounded to the west by listric detachments along the Bonavista Platform, similar in overall structure to the Jeanne d'Arc and Flemish Pass basins (Enachescu, 1987; Keen et. al, 1987; Enachescu, 1988) (Figures 1.1 and 1.7). These basins experienced rift tectonism and syn-rift deposition during the Triassic to mid-Jurassic, and have early syn-rift deposits similar to the Jeanne d'Arc Basin, including red beds, evaporates, limestones and shales. However, a hiatus in deposition, coeval with uplift along with large parts of the southern Grand Banks, termed the Avalon Uplift, occurred between the Tithonian to Aptian, at a time when syn-rift deposition was prevalent in most other North Atlantic basins (Hubbard, 1988; Tankard and Welsink, 1987; Enachescu, 1988; Balkwill and Legall, 1989; Sinclair, 1993). Much of the material eroded from this area during the Tithonian-Aptian was deposited to the south, into the seaward edge of the South Whale Basin, which at this time was experiencing a post-rift stage, akin to that of the Scotian Basin, while other material was transported north, into the Jeanne d'Arc basin (Tankard and Welsink, 1987; Hubbard, 1988; Enachescu, 1988).

The Jeanne d'Arc basin is a deep half-graben failed rift basin, with 22km to pre-rift basement. It is bounded to the west by a deep crustal east-dipping listric fault (the Murre-Mercury fault) against the Bonavista Platform to the west, to the east by the Central Ridge high, to the south by the Egret fault and Avalon Uplift and to the north by the Cumberland Ridge (Tankard and Welsink, 1987; Enachescu, 1987; Keen et. al, 1987; Enachescu 1988) (Figures 1.1, 1.3 and 1.7). The Bonavista Platform is a peneplained basement uplift overlain with epeiric Mesozoic and thin Tertiary post-rift deposits, and forms the western shoulder of all of the rift basins Offshore Newfoundland (Enachescu, 1987; Tankard and Welsink, 1987; Grant and McAlpine 1990) (Figures 1.1 and 1.7). The Central Ridge comprises a group of northeast-southwest trending basement ridges overlain by a Late Triassic and Jurassic sequence with minor Cretaceous sediments filling in local grabens. Most of the uplift of the Central Ridge occurred from the Tithonian to the Berriasian due to activation of the supracrustal Egret and Voyager fault systems, at which time it would have formed a physiographic barrier between the Jeanne d'Arc Basin and Flemish Pass Basin (Enachescu, 1987, 1988; Tankard and Welsink, 1987; Foster and Robinson, 1993; DeSilva, 2000) (Figures 1.1 and 1.3). The Cumberland Ridge is a prominent east-west trending basement high and forms a physiographic barrier between the Orphan Basin and the Flemish Pass and Jeanne d'Arc basins and is covered by relatively thin Cretaceous and Tertiary sediments; although its role in Late Jurassic and Early Cretaceous drainage and deposition is unknown (Figures 1.1 and 1.5). The Avalon Uplift, as mentioned previously, was an area of rifting and subsidence until the Tithonian, at which time it was uplifted until the Berriasian, and again from the Valanginian until the Aptian. Uplift of this area is thought to have occurred due to transform movements along the Newfoundland transfer zone to the south and incipient break up between the southern Grand Banks and Iberia (Enachescu, 1987; Tankard and Welsink, 1987; Sinclair, 1993).

Deposition of course clastics (reservoir sandstones) into the Jeanne d'Arc basins peaked between the Tithonian to the Aptian; and coincides with the timing of rifting between the Grand Banks and Iberia until the break-up and seafloor spreading between these two continental fragments. The deposition of reservoir sandstones during this time was largely influenced by faulting and tectonic uplift and subsidence (Masson and Miles 1986; Tankard and Welsink, 1987; Sinclair, 1993). Syn-rift sandstone deposition began in the Tithonian, with the deposition of the fluvial-deltaic Jeanne d'Arc Formation. These sands entered the basin from the south and southeast mainly, and evidenced b the presence of channel-like incisions on the southern margin of the basin, and a concentration of the thickest and most aerially extensive fan delta sands in the southwest margin of the basin. Deposition was coeval with uplift of the Avalon Uplift to the south (Tankard and Welsink, 1987; McAlpine, 1990; Enachescu, 1994). In other parts of the basin, small marginal alluvial and marginal marine fans were deposited into the basin from local point sources, such as the margin of the Bonavista Platform (Tankard and Welsink, 1987). The second pulse of coarse clastic input is characterized by the deposition of the large sandy fan deltas of the Hibernia Formation, during the Berriasian. Uplift of and drainage off of areas to the west and south, including the Bonavista Platform and the Avalon Uplift, occurred during this time, resulting in a relatively restricted distribution of the Hibernia Formation into the southern and western margins of the basin (Tankard and Welsink, 1987; McAlpine, 1990). During the late Barremian, another pulse of coarse sedimentation occurred, resulting in the deposition of the stacked prograding shoreface, estuarine and coastal plain sand and mud packages of the Avalon Formation. This formation thickens into the southwestern margin of the basin, and presumably episodic margin uplift led to progradation of these sands from the Avalon Uplift to the southwest (Tankard and Welsink, 1987; McAlpine, 1990; Sinclair, 1993; Ainsworth et. al, 2005). The final major pulse of coarse clastic sedimentation occurred in the Aptian-Albian, with the transgressive shoreface and estuarine sands of the Ben Nevis Formation. Transport of clastic material into large estuaries during this time was though low gradient rivers draining off of areas to the southwest (Avalon Uplift and Bonavista Platform) (Tankard and Welsink, 1987; McAlpine, 1990; Sinclair, 1993).

The Flemish Pass basin is also a half graben basin bounded to the east by a deep listric fault, antithetic to the Murre-Mercury fault and informally known as the Voyager Fault (Foster and Robinson, 1993) (Figures 1.1, 1.3 and 1.7). It forms the outer part of a double-failed rift as described by Enachescu (1988). To the west, the Flemish Pass Basin is bounded by the Central Ridge high, to the East and south by the Flemish Cap-Beothuk Knoll and to the north by the Cumberland Ridge and East Orphan Basin (Enachescu, 1987; Keen et. al, 1987; Enachescu 1988; Enachescu et. al, 2005) (Figures 1.1, 1.3 and 1.7). It may have been in communication with the East Orphan Basin during periods of rifting and sedimentation (Enachescu at al., 2005) (Figures 1.5 and 1.6). Essentially, the Flemish Pass Basin contains syn- and post-rift deposits with a generally similar to that of the Jeanne d'Arc Basin, but with about half the depth to basement (Enachescu, 1988; Foster and Robinson, 1993). Deposition of course clastics into occurred at similar periods between the Tithonian and Aptian as they were deposited into the Jeanne d'Arc Basin; however, the extent, orientation and provenance of these sandstones are not known or poorly constrained (Foster and Robinson, 1993). The geology and geological evolution of the Flemish Pass Basin is described in detail later in this chapter.

The Flemish Cap is a physiographically isolated pre-rift basement fragment, forming the eastern margin of the Flemish Pass Basin (Figures 1.1 and 1.7). It consists of a central area of exposed basement, surrounded by on-lapping Tertiary and minor Cretaceous sedimentary rocks. Seismic interpretations across the Flemish Cap show no evidence for extensional basins or syn-rift strata, and for the most part the Flemish Cap is a coherent continental block covered by a veneer of post rift sediments (Grant, 1973; Enachescu, 1987, 1988; Grant & McAlpine 1990; Foster and Robinson, 1993; Hopper et al., 2006). Recent magnetic and gravity geophysical studies of incipient seafloor at the margin between the Newfoundland and Iberia show that the Flemish Cap and Galicia Bank behaved as a coherent continental block from the Late Jurassic until the Albian (Srivastava et al., 2000; Sibuet et al., 2007). Its role as a basement platform in Late Jurassic to Early Cretaceous paleodrainage and deposition of clastics is not known.

The Lusitanian Basin, located onshore and offshore western Iberia, is rift basin dissected by N-S and NW-SE normal faults and various salt diapirs, and has complicated structure and syn-rift sediments confined to multiple depocentres (Wilson et al., 1989;

Alves et al., 2003a, 2003b). It contains a broadly similar Mesozoic rift and post-rift stratigraphy as the Jeanne d'Arc Basin, and it is thought to have been connected to the Carson Basin before break up (Hiscott et al., 1990; Enachescu, 1992; Sinclair, 1995; Johnston et al., 2001) (Figure 1.7). From the Tithonian to the Berriasian, deposition of fluvial-deltaic sands into the Lusitanian Basin from hinterlands in the northeast (Iberian Massif), northwest and north (Galicia Bank?) was relatively constant. After a brief Berriasian hiatus, coinciding with a period of uplift and non-deposition, the same deposition of fluvial-deltaic sands from the north-northwest occurred from the Valanginian until the Aptian (Rey, 1972; Wilson et al., 1989; Alves et al., 2003a, 2003b).

The Galicia Bank is a structural basement high located east of mainland northern Spain (Figure 1.7). Morphologically, it is comprised of faulted basement, giving a horst-and graben structure, overlain by a relatively thin sedimentary cover ranging in age from Valanginian to recent (Ercilla et al., 2008). During most of the Late Jurassic-Early Cretaceous it formed a platform of undeformed pre-Mesozoic basement, and was connected to the Flemish Cap, forming a coherent continental block, until the Albian (Srivastava et al., 2000; Sibuet et al., 2007). Rifting and localized syn-rift sedimentation into grabens occurred from the Valanginian to Albian, and moved from the east to the west during this time. This diachronous rifting resulted in a basinal eastern interior and a prominent basement ridge at the western margin of the Galicia Bank, thus creating a localized barrier for sediments travelling westward from the Iberian Plateau (Ercilla et al., 2007).

The Orphan Basin is actually comprised of two half-graben rift basins with highly attenuated pre-rift basement. These are the West and East Orphan Basins, which are temporally distinct and are separated by an east-dipping listric detachment, called the White Sail Fault (Chian et al, 2001; Enachescu et. al, 2005) (Figures 1.1, 1.7 and 1.8). The basin bounding fault to the west, which separates the Orphan Basin from the undeformed Bonavista Platform/ Newfoundland Shelf, is considered a continuation of the deep listric fault along the western margin of the Jeanne d'Arc Basin, to the south (Enachescu et al., 2005; Hardy, 2008). The East Orphan Basin is the older part of the basin, containing syn- and post-rift successions from the Triassic to Cenozoic; whereas the West Orphan Basin contains syn- and post-rift fill that is no older than Albian (Enachescu et. al, 2005) (Figure 1.8). The geology and geological evolution of the Orphan Basin is described later in this chapter.

The Orphan Knoll is an under-extended continental fragment at the northeastern corner of the West Orphan Basin (Figures 1.7 and 1.8). It has subsided much more than the Flemish Cap and is overlain by Tertiary, Mesozoic and Lower Paleozoic sequences. The Mesozoic rocks include some Bajocian aged terrestrial sandstones and rare coals, implying that the Orphan Knoll was exposed up until the mid-Jurassic (Ruffman and van Hinte 1970; van Hinte et al. 1995). It is postulated to have been corrected to the Porcupine Bank preceding break-up (Verhoef and Srivastava, 1989).

The Porcupine Basin is a large and deep north-south oriented extensional rift graben, located offshore western Ireland, but once was located alongside the Orphan Basin, and It has been suggested that both of these basins comprised a coherent basin until the Aptian break-up between the North America and Northern Europe (Masson and

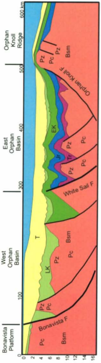

Figure 1.8: Geologic cross-section of the Orphan Basin. The White Sail fault separates the older East Orphan and younger West Orphan Basins. The Bonavista Fault is the major basin bounding fault, and defines the western limit of extension in the Orphan Basin. The basement structural architecture of the Orphan Basin is dominated by north-northeast/south-southwest and north-south trending elongate basement ridges and half-grabens, formed by large synthetic and antithetic faults to the basin-bounding fault. Some of the ridges and sub-basin troughs are comparable in size to the Central Ridge and Jeanne d'Arc Basin. Essentially, the East Orphan basin had a longer rifting history, active from the Triassic until the Late Cretaceous; whereas the West Orphan Basin is a younger rift system that was active only from the Early Cretaceous (Albian) until the Paleocene (From Enachescu 1987).

Miles, 1986; Keen et. al, 1989; Enachescu et. al, 2005) (Figure 1.7). It is bounded to the east, north and south by deep crustal normal faults, which lie adjacent to the Irish Platform, Slyne Ridge and Porcupine Bank, respectively. The Porcupine Bank, forming the western boundary, is an undeformed basement platform that was connected to the Orphan Knoll continental fragment before break-up (Verhoef and Srivastava, 1989). To the southeast it is bordered by the Goban Spur, and to the southwest by the continent-ocean boundary (Tate and Dobson, 1988; Croker and Klemperer, 1989). It contains Triassic to Early Cretaceous syn- and post- rift successions and Mid Cretaceous to recent post-rift fill stratigraphically similar to those present in the Jeanne d'Arc and other Offshore Newfoundland Basins (Croker and Shannon, 1987; Tate and Dobson, 1988; Sinclair 1995). During the Tithonian-Berriasian, sands were deposited mainly along the margins of the basin, as alluvial fans in the north and deep water turbitite fans in the south of the basin (Johnston et. al, 2001; Robinson and Canham, 2001). During the Valanginian-Aptian, the Porcupine Basin was largely fully marine, unlike the Jeanne d'Arc basin at this time, resulting in the deposition of shelfal mudstones, siltstones and minor thin sandstones in the North and progradation of deep marine turbidite fans and shelf clastics in the south (Johnston et al., 2001). Sands deposited into the Porcupine Basin during the Late Jurassic are thought to have been from the Irish Platform, to the east (Johnston et al., 2001; Smith and Higgs, 2001).

The Celtic Sea basins comprise a series of sub-parallel east-west oriented fault-bounded half-graben rift basins located to the south of the Iberian Plateau, and north of the Cornubian Platform (Figure 1.7). They include the Fastnet Basin, the North Celtic Basin and the South Celtic Basin. The Western boundary of these basins, especially the eastern edge of the Fastnet Basin, are characterized by thinning strata along the eastern edge of the Fastent high, to the west. The north and south Celtic Basins are dissected by basement highs; the Pembroke Ridge, an extension of the Welsh Platform, in the east, and the Labadie Bank in the west. They contain syn- and post-rift successions, with ages ranging from Permo-Triassic to mid-Cretaceous and a Late Cretaceous and Tertiary post-rift succession, broadly similar to those the Jeanne d'Arc Basin (Millson, 1987; Petrie et. al, 1989). Rifting and syn-rift sandstone deposition occurred mainly during the Berriasian to the Aptian, during which time stack alluvial fans built up, mainly on the northern margin of the Celtic basins. Most material is thought to have been derived from uplifted parts of southeast Ireland, to the northeast of the basins (Petrie et al., 1989).

The Goban Spur is a marginal plateau that has been highly faulted during the Mesozoic, and is located south of Ireland, east of the Porcupine Basin and southwest of the Fastnet basin (Figure 1.7). It is considered to be a continuation of the Cornubian Platform to the east, and during the late Jurassic-Early Cretaceous was probably connected to the Flemish Cap (Dingle and Scrutton, 1979; Masson and Miles, 1984, 1986; Keen et al., 1989; Verhoef and Srivastava, 1989). A shallow and relatively small Mesozoic basin formed on the Goban Spur, which has Early Jurassic to Early Cretaceous syn-rift sediments; however, during the Late Jurassic, the basin was uplifted along with the rest of the Goban Spur. Outside of the Basin, the Goban Spur is covered only by thin tertiary post-rift strata, and thus likely existed as an exposed basement platform during the Mesozoic rifting events (Dingle and Scrutton, 1979; Colin et al, 1992).

In addition to some of the basement platforms mentioned above, most of the Newfoundland, Irish, Welsh, Iberian, Amorican, Labradorean, Greenland and Rockall

Plateaus, including mainland and shelf areas, are thought to have been exposed during this time (Zeigler, 1989) (Figure 1.7). Some apatite thermobarometry data exists with regards to uplift of some of these areas during the Late Jurassic to Early Cretaceous. Hendriks et al. (1993) show that the long range inlier of Western Newfoundland was exposed by the Late Jurassic, and Holford et al. (2009) show that episodes of uplift in Ireland occurred in the mid-Jurassic and the Early Cretaceous. According to Turrin and Hemming (2000), basement on the Iberian margin, north of the Lusitanian Basin, experienced uplift during the Late Jurassic to Early Cretaceous.

1.4 Pre-Mesozoic Basement Geology

The pre-Mesozoic basement geology and general paleogeographic reconstructions for this part of the North Atlantic are outlined in Figures 1.9 and 1.10. The following section is a description of the previous studies of offshore and onshore pre-Mesozoic basement which could have been exposed as source areas for detritus during the Late Jurassic and Early Cretaceous times. Isotopic age constraints are also given for correlations to detrital zircon U-Pb geochronology from this study in later chapters.

1.4.1 North American Conjugate Margin

The most proximal pre-Mesozoic basement in the underlying the Grand Banks and Northeast Newfoundland shelf is part of the Neoproterozoic Avalon zone, which spans the area from the Charlie-Gibbs Fracture Zone south to the Collector Anomaly (Haworth and Lefort, 1978; King et al., 1985, 1986; Williams et al., 1999). The Avalon

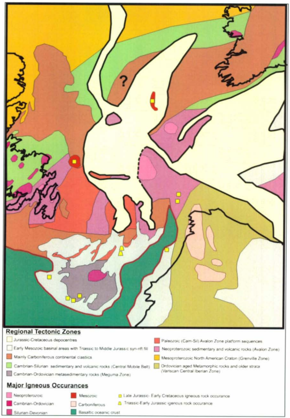

Figure 1.9: Approximate paleogeography and pre-Mesozoic basement regional geologic map during the North Atlantic rift phase (Tithonian to Valanginian). During this period, rifting was focused between Iberia and the Grand Banks, and incipient seafloor spreading began along this rift.

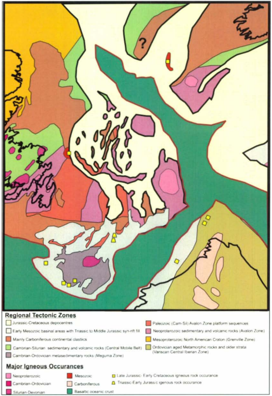

Figure 1.10: Approximate paleogeography and pre-Mesozoic basement regional geologic map during the Labrador Sea rift phase (Aptian-Albian). During this period, the primary axis of rifting propagated northwards between the Flemish Cap and Galicia bank, and seafloor spreading began between Iberia and the Grand Banks. Subsequently, rifting, leading to incipient seafloor spreading, began between North America and Northern Europe and in the Bay of Biscay.

zone onshore and offshore is comprised of Neoproterozoic arc-phase volcanic and magmatic units, late Neoproterozoic cover sequences and early Paleozoic cover sequences. Arc-phase igneous rocks have been traced in the offshore acoustic basement using magnetic anomalies; however, with a few exceptions (e.g. the Flemish Cap), Precambrian igneous basement has not been encountered as Pre-Mesozoic sub crop (Haworth and Lefort, 1978; King et al., 1985). The Late Neoproterozoic cover sequences present in the onshore presumably extend and sub-crop offshore along the eastern margin of the Bonavista Platform, the Central Uplift area, and beneath the shallow cover sequences of the Flemish Cap (King et al., 1985; Bell and Howie, 1990). Early Paleozoic (Cambrian to Silurian) clastic cover sequences occur in the northeastern and western Grand Banks (Avalon Uplift and Bonavista Platform areas), on the shelf and slope area beneath the West Orphan Basin as well as beneath the Northern Jeanne d'Arc and Flemish Pass Basin (King et al., 1986; Bell and Howie, 1990) (Figures 1.9 and 1.10). The Cumberland ridge has been interpreted as a volcanic mountain range formed as the result of either a Hercynian shear zone (Lefort and Haworth, 1978; Haworth and Lefort, 1979; Enachescu, 1987) or a mafic complex involved in the Acadian Orogeny (Jacobi and Kristofferson, 1981) or simply as a Mesozoic transfer zone that formed a complex chain of basement horsts during extension (Enachescu, 1987).

Arc phase magmatic and volcanic igneous formations of the exposed Avalon zone in Eastern Newfoundland, including the Rock Harbour, Marystown and Harbour Main Groups and Hollyrood Granite, have U-Pb zircon ages ranging from 586 to 632 Ma. One unrelated outlier, the Wandsworth Gabbro of the Burin Ophiolite Group on the Burin Peninsula, was dated at 763 ± 2.2 Ma (Krogh et al., 1987). Baddeleyite from mafic sills on Cape St. Mary's on the Avalon Peninsula were dated to 441± 2 Ma, indicating the occurrence of localized Silurian orogenic volcanic rocks in the Avalon Zone (Greenough et al., 1993). Precambrian granodiorite has been sampled on the Flemish Cap, which yielded discordant U-Pb zircon ages with upper intercepts of 751 and 833 Ma, representing an age of intrusion between 750 Ma and 830 Ma. It is interpreted to represent an offshore extension of the Avalon Zone; albeit one that potentially represents an older magmatic phase (King et al., 1985).

Neoproterozoic clastic sequences, including the Conception, Harbour Main, Marystown and St. John's Groups are extensively exposed onshore; however, their offshore basement sub crop extensions are poorly constrained and it appears that early Paleozoic cover sequences overly Precambrian basement offshore (King et al., 1986). There are only several locations offshore where Avalonian Precambrian cover sequences have been cored in the pre-Mesozoic sub crop: the Virgin Rocks – Eastern Shoals area (east of the Jeanne d'Arc Basin), and on the Flemish Cap (Lilly, 1966; King et al., 1985). Detrital zircons from the Precambrian main arc-phase sediments (Conception Group) are dominantly 570 – 620 Ma. Younger arc-platform transition sediments (Musgravetown and St. John's groups) contain dominantly 600 – 650 Ma detrital zircons with very minor Mesoproterozoic and Paleoproterozoic detrital zircons (Pollock et al., 2009).

The Cambrian-Ordovician sequences present offshore are considered analogous to those present on the Avalon Peninsula, particularly from the Bell Island Group in the Conception Bay area (King et al., 1986). The Cumberland B-55 well penetrated almost 400 m of Ordovician shales and siltstones, and the Linnet E-63 penetrated 320 m of Lower Paleozoic shales and siltstones. Kyle L-11, in the Flemish Pass Basin also drilled through almost 700 m of metasedimentary basement rocks (C-NLOPB, 2004). Detrital zircons from the equivalent Cambrian-Ordovician cover sequences on the Avalon Peninsula are dominantly Neoproterozoic to Early Cambrian (500-680 Ma) in age; however, Mesoproterozoic (1.0-1.6 Ga), Paleoproterozoic (1.9-2.3 Ga) and minor Late Archean (2.7-2.8 Ma) detrital zircons are also present (Pollock et al., 2009).

The Cambrian-Ordovician metasedimentary turbidites and associated Late Devonian granites of the Meguma Zone are present beneath the southern Grand Banks, and comprise the pre-Carboniferous basement of the Avalon Uplift. This is supported by tracing of subsurface magnetic anomalies; in particular, the Collector Anomaly, which is an extension of the Cobequid-Chedabucto fault zone in Nova Scotia, representing the boundary between the Meguma and Avalon zones (Haworth and Lefort, 1978) (Figures 1.9 and 1.10). A K-Ar whole-rock isotopic age of 376 ± 17 Ma of 'granite basement' at the base of Jaeger A-49 also supports the presence of the Meguma Zone in this area, as it is known to be uniquely abundantly intruded by such Late Devonian (Acadian) granites (Kreuger Enterprises, 1972; Clarke et al., 1997; Kontak et al., 2004). Detrital zircons taken from the Goldenville Formation metasediments of the Meguma Zone in southern Nova Scotia had predominantly Late Neoproterozoic (550-750 Ma), Middle Paleoproterozoic (2.0-2.2 Ga) and a significant amount of Archean (2.8-3.0 Ga) ages (Krogh and Keppie, 1990). Further studies of a younger sequence in the Meguma Zone yielded similar detrital zircon ages, except lacking Archean aged grains and having a small population of rare Mesoproterozoic aged grains (1.0-1.2 Ga) (White et al., 2008). Metaluminous to peraluminous granites are common in the Meguma Zone and are Middle to Late Devonian in age (380 Ma- 365 Ma), corresponding to emplacement during the

Acadian orogeny (Clarke et al., 1997, Kontak et al., 2004). Metamorphic and granitic tourmalines occur abundantly in the metasedimentary and granitic rocks of the Meguma Zone, respectively; with metasedimentary grains more commonly having schorl-like compositions, and granitic tourmalines more commonly having dravite-like compositions (Raeside et al., 1988; Clarke et al., 1989).

Rocks of the Central Mobile Belt, comprising sedimentary and volcanic remnants of the Iapetus Ocean, occur in central Newfoundland and extend as pre-Carboniferous basement offshore northwest of the Charlie-Gibbs Fracture Zone (Figures 1.9 and 1.10). They predominantly comprise Cambrian to Silurian sedimentary and metasedimentary rocks, volcanic rocks and gabbros, as well as Silurian to Devonian granites. Detrital zircons from a Cambrian aged low grade metasedimentary unit (the Jonathans Pond Formation) along the eastern portion of the Central Mobile Belt in the Gander Zone of Newfoundland have mainly Mesoproterozoic (1.0-1.3 Ga), Paleoproterozoic (2.0-2.2 Ga) and Archean (~2.7 Ga) ages, with the exception of a single Late Neoproterozoic- Early Cambrian (~540 Ma) grain (O'Neill 1991). Further east in the Central Mobile Belt (from within the Exploit Subzone) Late Ordovician to Silurian sedimentary successions contain detrital zircons dominated by Ordovician to Late Neoproterozoic (450-550 Ma), Mesoproterozoic (1.0-1.5 Ga), Late Paleoproterozoic (1.6-1.8 Ga), and minor Late Archean (2.7-2.5 Ga) ages (Pollock et al., 2007). Magmatic rocks in the Central Mobile Belt have ages ranging from Late Cambrian to Early Devonian, and generally, the ages of these intrusive rocks become older towards the west; however, granitic and volcanic rocks with U-Pb ages ranging through Late Ordovician and Early Devonian are common throughout central Newfoundland (Dallmeyer et al., 1981; Chorlton and Dallmeyer, 1986;

Dickson, 1990; O'Neill, 1991; Dube et al., 1996; Valverde-Vaquero et al., 2003; Valverde-Vaquero et al., 2006). Late Devonian granites are rare, but do also occur in the Gander Zone (Currie, 1995). Metamorphic tourmalines are ubiquitous in metasediments adjacent to granites and fault zones in the Gander Zone (O'Neill, 1991).

The Notre Dame and Belle Isle subbasins on the Northeast Newfoundland shelf contain Carboniferous continental clastics, and have been intercepted by several offshore wells (Figures 1.9 and 1.10). Hare Bay E-21, located on the shelf area of the West Orphan Basin, penetrated almost 1500 m of Pennsylvanian red-brown sandstones and siltstones. These may be equivalent to the upper Windsor Group and basal Canso Group exposed on mainland Nova Scotia and New Brunswick (BP Canada, 1979; Bell and Howie, 1990). Upper Paleozoic (Devonian-Pennsylvanian) cover sequences are also present within a large east-west trending syncline below the central Grand Banks (on the Avalon Uplift) and offshore south of the Avalon Peninsula. These are interpreted to include the Devonian-Mississippian shale and sandstone of the Horton Group, Mississippian evaporates and shale of the Windsor Group, Mississippian-Pennsylvanian red shale and sandstone of the Canso and Riversdale Groups, and Pennsylvanian red sandstone and shale of the Pictou Group (Barss et al., 1979; Bell and Howie, 1990). On mainland Nova Scotia, ages of detrital zircons from the Horton Group in the late Paleozoic St. Mary's Basin cluster in a bimodal manner into Neoproterozoic (550 – 700 Ma) and Paleoproterozoic (2.0 – 2.2 Ga) age groups, and are interpreted to be derived mainly from uplifted portions of the Meguma Zone. Minor Devonian (370 – 380 Ma) and Silurian (411 Ma) detrital zircons were also present (Murphy and Hamilton, 2000).

A Lower Paleozoic carbonate sequence has been interpreted on top of parts of the Orphan Knoll; based on angular Ordovician and Devonian limestone cobbles dredged from shallow deposits near the top of the Knoll that are considered to be in situ fragments (van Hinte et al., 1995). They may correlate with the Lower Paleozoic Carbonates offshore western and northern Newfoundland that formed on the passive Laurentian Margin and subsequent Paleozoic foreland basins. However, geophysical evidence suggests the Orphan Knoll is most likely a fragment of the Avalon Platform (Haworth and Lefort, 1978) covered in places by Mesozoic sediments (Enachescu et al., 2005).

A number of wells offshore have intercepted Mesozoic syn-rift igneous rocks, including a granitic rock in the West Orphan Basin, and various Mesozoic syn-rift volcanics in the southern and central Grand Banks. The Bonavista C-99 well intercepted 100 m of granite and/or pegmatitic granite which yielded a K-Ar whole-rock isotopic age of 146 ± 6 Ma (BP Canada, 1975). Triassic-Jurassic basalts were encountered in Spoonbill C-30 and Cormorant N-83 wells; however these basalts have not been dated (Amoco et al., 1973; Jansa and Pe-Piper, 1986). In the Southern Grand Banks, several wells intercepted Late Jurassic- Early Cretaceous volcanic rocks. In Brant P-87, 55 m of basalt and pyroclastics and 123 m of diabase sills or flows were dated at 135 ± 6 Ma. In Twillick G-49, a 15 m thick porphyritic diabase was dated at 177 ± 5 Ma. In Emerillon C-56, a 21 m thick diorite dyke was dated at 96.4 ± 3.8 Ma. All of these ages were determined by whole rock K/Ar isotopic ratios (Jansa and Pe-Piper, 1988). The Budgell Harbor Stock, a small alkaline ultramafic pluton located on land in Central Newfoundland, has a K-Ar biotite age of 139 ± 9 Ma (Helwig et al., 1974).

1.4.2 Irish Conjugate Margin

Because of the proximity of the Irish and Iberian conjugate margins during the time which the units from this study were deposited, they would have been potential source areas. Therefore, it is pertinent to summarize the geology of these areas, with emphasis on any crustal ages that could be used to discriminate sourcing from potential European hinterlands in these areas from those on the North American conjugate margin, using detrital zircon geochronology as the primary proxy for provenance analysis.

The pre-Mesozoic basement geology on the Irish conjugate margin is largely comprised of Early to Middle Paleozoic sequences from the closure of the Iapetus (analogous to the Central Mobile Belt in Newfoundland) that is largely overlain by Late Paleozoic (mainly Carboniferous) clastics and carbonates (Figures 1.9 and 1.10). Several large plutons and batholiths are present that have Late Silurian to Early Devonian ages. The largest of these exposed plutons is the Galway Granite, which has U-Pb zircon ages between 395 and 405 Ma (Early Devonian) (Feely et al. 2004). Other crystalline basement exposures on the Irish Mainland are older (Early Paleozoic and Mesoproterozoic) and sparsely exposed. Magmatic rocks from within the Slishwood Division of the Dalradian Supergroup in Northwestern Ireland have Early Ordovician U-Pb zircon ages ranging between 467 ± 6 Ma and 474 ± 5 Ma (Flowerdew et al., 2005). The Annagh Gneiss, which structurally underlies the Dalradian Supergroup in Northwestern Ireland, has late Mesoproterozoic U-Pb Zircon ages with a weighted mean age of 963 ± 8 Ma (Daly et al., 2005).

The offshore pre-Mesozoic basement geology is poorly constrained on the Irish conjugate margin. Presumably, the pre-Mesozoic basement underneath the Porcupine Basin, Porcupine Ridge and Galicia Bank areas forms a continuation along the Caledonian-Appalachian trend and Iapetus Suture Zone, including (from southeast to northwest) parts of Avalon Zone, Central Mobile Belt, Laurentian margin, and Grenville Zone (Figure 1.8). The Clare Lineament, a major east-southeast - west-northwest trending structure that dissects the Porcupine Basin, has been interpreted as a trans-Atlantic continuation of the Charlie-Gibbs Fracture Zone, and has been considered as the boundary between Avalon Zone basement, to the southeast, and Central Mobile Belt basement to the northwest (Johnson et al., 2001) (Figure 1.9 and 1.10). There is evidence to suggest the presence of Carboniferous cover sequences as pre-Mesozoic basement in the area as well. Although no Carboniferous basement has been drilled, reworked Carboniferous palynomorphs have been found in Early Mesozoic rift related clastics in the Porcupine Basin, indicating the presence of nearby Carboniferous-aged sources (Smith and Higgs, 2001). Additionally, a potential Mesozoic source of detrital zircons exits offshore Ireland. The Porcupine Median high, a 3-5 km thick seismically imaged feature in the centre of the Porcupine Basin, has been interpreted as an igneous feature of Berriasian to Valanginian age (Earliest Cretaceous) by Tate and Dobson (1988); however, this feature has not been sampled, and therefore its age, and composition, is unknown. Johnston et al. (2001) suggest a younger age, probably Aptian and coinciding with early seafloor spreading, for the Porcupine Median high.

1.4.3 Iberian Conjugate Margin

Paleozoic granitoids constitute much of the basement present in the Iberian Penninsula, particularly in the nearest areas on the northwestern Iberian Pennsinsula, where they make up most of the exposed rocks of the Variscan Central Iberian Zone (Figures 1.9 and 1.10). The U-Pb ages of these granitoids are predominantly Late Paleozoic, and were generated during three distinct time intervals: Mississippian (330-320 Ma), Pennsylvanian (310-300 Ma), and Early Permian (290-280 Ma) (Priem and Tex, 1984). Additionally, older but lesser exposed Early Ordovician gniesses are present as pre-Varsican basement in the area, with U-Pb ages ranging between 460 Ma and 490 Ma (Priem and Tex, 1984; Valverde-Vaquero and Dunning, 2000).

Much of the continental shelf areas offshore northern and central Iberia is interpreted to be underlain by pre-Mesozoic basement comprising extensions of the Central Iberian Zone, largely comprised of late Paleozoic (Carboniferous-Permian) granitoids (Priem and Tex, 1984; Capdevila and Mougenot, 1988). However, the continental slope, including the Galicia Bank, has been interpreted to be underlain by extensions of the Ossa Morena Zone based on lithologic comparisons to on land equivalents (Capdevila and Mougenot, 1988). On land, the Ossa Morena Zone predominantly contains Neoproterozoic metasedimentary rocks, as well as intrusive and volcanic igneous rocks that formed during three magmatic phases: 587 Ma to 535 Ma (Neoproterozoic), 530 Ma to 470 Ma (Cambrian to Early Ordovician) and 359 Ma to 330 Ma (Mississippian) (Romeo et al., 2006; Sola et al., 2008).

Mesozoic syn-rift volcanic rocks are also present on the Iberian Margin, most of which are present far to the south, within the southern Lusitanian Basin on land and offshore. The volcanics are predominantly mafic and occurred in four distinct cycles: Late Triassic to Early Jurassic (203-224 Ma), Early Middle Jurassic (160-190 Ma), Early Cretaceous (130-135 Ma), and Late Cretaceous (100-70 Ma) (Pinheiro et al., 1996). Additionally, metamorphosed Mesozoic syn-rift gabbro sills have been encountered on the continental slope on the western edge of the Galicia Bank, and have a U-Pb age of emplacement of 122 ± 0.3 Ma (Schaerer et al., 1995).

1.5 Geology and geologic evolution of the Flemish Pass Basin

1.5.1 Location and Regional Geology

The Flemish Pass Basin is located approximately 400 km east of Saint John's Newfoundland, under the Flemish Pass bathymetric low between the Flemish Cap and the Grand Banks (Figure 1.1). It covers an area of approximately 30,000 km^2 and occurs at ocean depths ranging from 400 to 1100 m (Foster and Robinson, 1993; DeSilva, 2000). Structurally, it is a half-graben that formed during Late Triassic to Early Cretaceous rifting. The depth to basement in the Flemish Pass Basin is about 10 to 15 km. It is bounded (a) to the southwest by the Central Ridge, (b) to the east by the Beothuk Knoll-Flemish Cap basement high, (c) to the north by the Cumberland Ridge, and (c) to the south by the Avalon Uplift (Enachescu et al., 1987; Foster and Robinson, 1991; DeSilva, 2000). It is the outer half-graben of the "double-failed rift", which also includes the Jeanne d'Arc Basin half-graben and the Central Ridge horst to the west (Enachescu,

1987) (Figure 1.3). The Cumberland Belt Fault Zone is not strictly a barrier between the Flemish Pass and East Orphan Basin. Seismic stratigraphic evidence suggests that the Flemish Pass Basin forms a terrace of the East Orphan Basin, and both basins are interpreted to have been connected through much of their rift phase development time (Enachescu et al., 2005) (Figure 1.5).

1.5.2 Tectonic and Geologic Evolution

The Mesozoic and Tertiary geology and geologic evolution of the Flemish Pass Basin is described in detail by Foster and Robinson (1993). The following section is a summary of their work. Their generalized stratigraphy of the Mesozoic rift and post-rift sequences is shown in figure 1.11.

The Mesozoic to recent sediments of the Flemish Pass Basin can be divided into four broad sequences. These include (1) Late Triassic to Late Jurassic syn- and post-rift deposits of the Tethys rift stage (MS1), (2) Berriasian to Aptian syn- and post-rift deposits of the North Atlantic rift stage (MS2), (3) Aptian to Albian syn-rift deposits of the Labrador Sea stage (MS3), and (4) Late Cretaceous to recent post-rift thermal subsidence deposits (PR). The first three sequences are localized in fault-bounded depocentres with differing orientations. During most of the Late Jurassic to Early Cretaceous, deposition of syn-rift clastics was confined to northern and southern subbasins, referred to as the Baccalieu subbasin and the Gabriel Subbasin, respectively (Foster and Robinson, 1993). This project focuses on the deposition of reservoir sandstones into the Baccalieu subbasin, which contains the Mizzen L-11, Baccalieu I-78

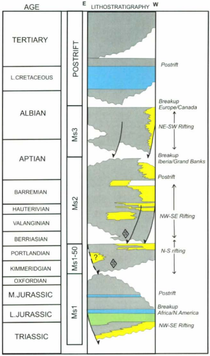

Figure 1.11: General regional stratigraphy of the Flemish Pass Basin, after Foster and Robinson (1993). Syn-rift sediments are shown adjacent to faults. The stratigraphy records four major sequences (Ms1, Ms2, Ms3 and Post rift) and one parasequence (Ms1-50). "S" marks the location of source rocks. (From Foster and Robinson, 1993).

and prospective Mizzen O-16 wells (Figure 1.12); although the orientation of deposition of coarse clastics into the Baccalieu subbasins should also have implications for the deposition of coarse clastics into the Gabriel subbasin.

The Tethys stage sequence (MS1; from Foster and Robinson 1993) is located between the top of the economic basement and a regional non-erosional unconformity that records an abrupt change from shallow marine to open deep marine deposition.

Very little has been established about the lower part of MS1 (Late Triassic to Early Jurassic sediments), due to a lack of well control and poor resolution in seismic sections. However, it is likely that they are similar to their counterparts in the Jeanne d'Arc Basin, and include equivalents to the Eurydice, Argo and Downing Formations (redbeds, evaporites, and marine mudstones, respectively). It is unclear whether massive salt and salt structures are present, although various authors studying seismic sections of the Flemish Pass Basin have alluded to their presence (Enchescu, 1987; Keen et al., 1987; Foster and Robinson 1993).

The Kimmeridgian to Berriasian sedimentary section of MS1 (MS1-50) is well constrained from wells and seismic sections. MS1-50 is generally interpreted to comprise post-rift deposits of the Tethys rifting stage overlain by syn-rift deposits of the North Atlantic rifting stage (Foster and Robinson, 1993; DeSilva, 2000). MS1-50 fills two east-west trending subbasins, including the Baccalieu subbasin, to the north (Figure 1.12). The orientation of the Baccalieu subbasin indicates north-south directed extension in the Flemish Pass Basin during this period, associated to movement between North America and Africa, and increased rifting between Iberia and the Grand Banks. The base of MS1-50 is defined by a Kimmeridgian Unconformity that records onlap of sedimentary rocks

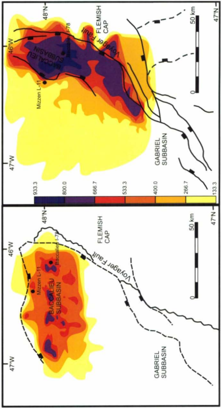

Figure 1.12: Structural and isopach maps of the MS1-50 parasequence (Kimmerigian to Berriasian) and the MS2 sequence (Berriasian to Aptian) in the Baccalieu Subbasin, modified from Foster and Robinson (1993). Depth scale is in ms.

towards the south and east in the northern subbasin, and towards the northeast in the southern subbasin. MS1-50 is characterized by the Baccalieu I-78 well, in which the section forms a shoaling upwards package, comprising, from bottom to top: marine shales, shallow marine sandstones interbedded with shales, overlain by thick non-marine sandstones. A similar change upward from open to marginal marine deposition has been interpreted for the MS1-50 sequence throughout the Flemish Pass Basin (Foster and Robinson, 1993). Source rocks occur in the lower part of MS1-50, and are present in the Baccalieu I-78 and Mizzen L-11 wells (Foster and Robinson, 1993; DeSilva, 2000; Enachescu et al., 2005).

The second rift parasequence, MS2, ranges in age from Valanginian to Aptian and is very well constrained by well and seismic data. Deposition of MS2 occurred during a brief post-rift subsidence phase from the Valanginian until the Hauterivian-Barremian, and then during the Labrador Sea rift phase until the Aptian. The clastic deposits of MS2 are relatively thick in the Baccalieu subbasin, which at the time of deposition had a NE-SW orientation (Figure 1.12). The orientation of this basin indicates northwest-southeast directed extension in the Flemish Pass Basin during this period, associated to rifting and incipient breakup between the Grand Banks and Iberia. It was also during this period when the supracrustal Flemish Pass and Voyager boundary faults were most active and most of the deepening of the Flemish Pass Basin occurred (Enachescu, 1987; Foster and Robinson, 1993) (Figure 1.12).

The base of MS2 is a regional unconformity representing regional subsidence and onlap of sediments. The top of the sequence is defined by an erosional unconformity, and has not been dated since it has been eroded in all of the wells. MS2 sediments are thickest in the Gabriel subbasin, where a lower sub-sequence of mudstones and turbidities is overlain by an upper sub-sequence of prograding coarse clastic wedges separated by high stand shale intervals. The lower sub-sequence records early syn-rift passive clastic deposition. The upper sub-sequence records multiple syn-rift shelf progradations, sourced from the north-west. The Baccalieu subbasin lacks a prograding shelf sub-sequence, and contemporaneous sediments are finer grained and poorly sorted, most likely representing syn-rift clastic deposition below wave base (Foster and Robinson, 1993).

As a result of a rotation to northeast-southwest directed regional extension in Aptian to Albian times during the Labrador Sea phase, northwest-southeast trending faults and depocentres in the Flemish Pass Basin formed. The sequence from this period, MS3, was deposited between and outside of the previous depocentres in the Baccalieu and Gabriel areas, mainly in an area that was previously a basement high. Therefore, the MS3 sequence is not represented in any wells in the area. Previous depocentres were uplifted during this period and the top of MS2 was eroded. The main MS3 depocentres contain flat parallel reflectors that onlap onto basin margins and have been interpreted as mainly deep marine mudstones and turbiditic sandstones. A channelized zone has been identified just to the southeast of the Baccalieu area that is interpreted as the main migration pathway for sediments. The top of MS3 is marked by the regional breakup (post rift) unconformity and has not been dated, but is probably Albian in analogy to the Jeanne d'Arc Basin (Foster and Robinson, 1993).

The drift stage sediments unconformably overly all of the previous sequences in the Flemish Pass Basins. They are more or less laterally extensive, and only fill shallow depressions over MS3 subbasins. The Albian to recent deposits record the progradation of a clastic shelf front from the east mainly, but also from the northwest (Flemish Cap area), interrupted by a regional Eocene tilting event (Foster and Robinson, 1993).

1.5.3 Oil and gas potential

In May 2004 the Canada-Newfoundland and Labrador Offshore Petroleum Board and the Geological Survey of Canada published a report that put the undiscovered recoverable petroleum reserves of the Flemish Pass Basin at 1.7 billion barrels, with expected field sizes ranging from 528 to 44 million barrels (Enachescu, 2006). The Flemish Pass Basin contains mature Late Jurassic source rocks and potential reservoir rocks of Late Jurassic and Early Cretaceous ages. Numerous large structural traps have been identified in the Flemish Pass Basin by industry 3-D seismic mapping, including some large faulted extensional anticlines and other such trapping systems that exceed Hibernia in size (DeSilva, 2000; Enachescu and Hogg, 2006).

Mature Late Jurassic source rocks and heavy oil have been discovered in both the Baccalieu I-78 and Mizzen L-11 wells of the northern Flemish Pass Basin. Baccalieu I-78 intercepted 164 m of upper Kimmeridgian source rocks with 2.2 to 3.6 percent TOC and a Hydrogen Index of 395 to 391, indicative of a Type II, or marine-type kerogen (DeSilva, 2000; McCracken, 2000). Mizzen L-11 intercepted 5 m of non-commercial oil pay in Early Cretaceous sandstone, and as well Jurassic sandstones with excellent reservoir characteristics (Enachescu, 2006). The Gabriel C-60 well never penetrated the Late Jurassic, but trace oils were found at about 4000 m in Cretaceous sandstones. These oils have a geochemical signature that indicate derivation from a Kimmeridgian source rock;

however, one that was deposited in a more oxidizing environment than the Egret Member in the Jeanne d'Arc Basin (Creaney and Allison, 1987). Creaney and Allison (1987) created a current day maturity map of the Kimmeridgian source rocks in the Flemish Pass Basin, in which the central areas of the basin contain thick source intervals that are currently in the oil window, overlain by potential Late Jurassic and Early Cretaceous reservoir intervals.

Recently, StatoilHydro has announced a significant discovery at the well Mizzen O-16, and subsequently has applied for a significant discovery license from the Canada Newfoundland and Labrador Offshore Petroleum Board; however, the details of this discovery, and of the well itself, remain classified at this time.

1.6 Geology and geological evolution of the Orphan Basin

1.6.1 Location and Geology

The Orphan Basin is the largest and deepest of the Newfoundland offshore basins, covering an area of 160,000 km^2 and ranging in depth from 1000 to 3000 m. It contains thick syn- and post- rift Mesozoic and Tertiary sedimentary infill overlying attenuated continental crust of the Avalon Zone. The highly attenuated basement has an average stretching factor of 2.5 (Enachescu et al., 2005). The Orphan Basin is located (1) south of the Charlie-Gibbs Fault Zone (CGFZ), (2) north of the Cumberland Belt Fault Zone (CBFZ), (3) west of the Continent-Ocean boundary (COB) and the Orphan Knoll-

Flemish Cap elevated trend, and (4) east of the Bonavista Platform and the basin-bounding Bonavista Fault (Figure 1.1).

Although the Cumberland Belt Fault Zone forms a chain of basement highs and is considered the southern limit of the Orphan Basin, seismic stratigraphic interpretations indicate that it has not been an uninterrupted barrier through the various phases of the basin evolution and sediment deposition. Localized basement depressions probably formed, allowing communication between bodies of water (seas or lakes) in the Northern Jeanne d'Arc, Flemish Pass and Orphan basins throughout the Jurassic and Cretaceous (Enachescu et al., 2005) (Figure 1.6).

The continent-ocean boundary is located approximately at the 4000 m bathymetric contour. There is approximately 110 km of transitional crust landward of the COB, comprising attenuated continental crust made up of highly tilted fault blocks of underlain by a shallow detachment surface and separated locally by linear ridges of exhumed mantle peridotite (Kearsey and Enachescu, 2005).

The Bonavista Fault is a northwest continuation of the Murre-Mercury basin-bounding fault system, and defines the western limit of extension in the Orphan Basin. The Bonavista Fault dips to the east, and the dip of this fault zone varies from steep to shallow along strike (Enachescu et al., 2005).

The basement structural architecture of the Orphan Basin is dominated by north-northeast/south-southwest and north-south trending elongate basement ridges and half-grabens, formed by large synthetic and antithetic faults to the basin-bounding fault. Some of the ridges and sub-basin troughs are comparable in size to the Central Ridge and Jeanne d'Arc Basin (Chian et al., 2001; Enachescu et al., 2005) (Figures 1.1, 1.5 and 1.8).

Based on tectonic and stratigraphic characteristics, the Orphan Basin can be subdivided into two large subbasins, the West and East Orphan basins. They are separated by the White Sail Fault, a deeply penetrating basement fault, roughly parallel to the Bonavista Fault, that trends northeast-southwest and dips to the east. It is a continuation of a crustal detachment lineament that continues southwards into the Jeanne d'Arc Basin (Chian et al., 2001; Enachescu et al., 2005) (Figures 1.1 and 1.8). The lithostratigraphy and Mesozoic geologic evolution of the East and West Orphan basins is best described by Enachescu et al. (2005). Several major unconformities have been defined from seismic interpretation, and represent the tops of the major seismic sequences. These include: (1) top of the pre-rift basement (the pre-rift unconformity), (2) the top of the Triassic rift sequence, (3) The top of the Jurassic, (4) the top of Early Cretaceous (a.k.a. the Avalon or "breakup" unconformity), and (5) the Top of the Cretaceous or Base Tertiary Unconformity.

Basement architecture differs in the West and East Orphan Basins. The basement ridges in the West Orphan Basin have been eroded by the Base Tertiary Unconformity as well as by the Avalon Unconformity. The highs are partially covered by pre-rift Paleozoic sedimentary cover, and are rarely also overlain by thin syn-rift Mesozoic sedimentary cover. The East Orphan Basin contains thick Mesozoic sedimentary cover, which overlies basement ridges. Jurassic and Cretaceous syn-rift sediments in the East Orphan Basin are structurally complex, with rollover anticlines and normal faulting that are attributed to movement of adjacent basement blocks (Figure 1.8).

1.6.2 Tectonic and Geologic Evolution

The Orphan Basin evolved over roughly 160 Million years, with four major rifting events occurring at roughly 210, 150, 120 and 60 Ma (Enachescu et al., 2005.). Rifting began in the east, and moved westward with each successive rifting stage. The first three rift stages correspond to the regional Tethys, North Atlantic and Labrador Sea stage rifts; the last rifting stage is the Late Cretaceous to Paleocene East Greenland stage. Each rifting episode was followed by a period of thermal subsidence, with the most rapid and significant subsidence occurring after the final rifting event in the Eocene. Very minor volcanic rocks have been identified throughout the entire Orphan Basin, indicating that the Orphan Basin was a non-volcanic failed rift (Chian et al., 2001; Enachescu et al., 2005).

The East Orphan Basin first underwent rifting during the regional Late Triassic to Early Jurassic Tethys rift stage, as indicated by the presence of Late Triassic and Jurassic syn-rift sedimentary rocks. The Triassic sequence is only present in the East Orphan Basin, where it may contain red beds and stratified evaporites (Enachescu et al., 2005). Massive salt structures, such as diapirs, have not been identified. An early to middle Jurassic post-rift sequence is also probably present. The DSDP site 111 well on the Orphan Knoll intercepted Mid Jurassic (Bajocian) continental to marginal marine fluvial sandstones (Ruffman and van Hinte, 1970). During the Tethys rifting, the East Orphan Basin was connected to the Porcupine Basin offshore Ireland, and the Flemish Cap was connected to the Galicia Bank. The White Sail Fault was the western limit of extension during this stage, and acted as the basin bounding fault. The West Orphan Basin was still an elevated peneplained part of the continent, and the western rift shoulder. Sediments were most likely derived from this western rift shoulder, from southern uplifted areas, and from rotated basement blocks within the East Orphan Basin. The earliest sediments were deposited in alluvial and lacustrine settings. This was followed by thermal subsidence, marine invasion, and deposition of mixed evaporites and continental clastics.

During the Late Jurassic to Early Cretaceous North Atlantic rifting stage, the East Orphan rift was reactivated. As the regional extensional vector rotated from a north-south to east-west orientation during the North Atlantic rift stage, trans-tension caused deformation of previous syn- and post-rift sedimentary rocks in the East Orphan Basin. The Orphan Knoll was emergent at this time and became a source of proximal sedimentation. Although the Grand Banks and Iberia continental margins separated during this stage, the Orphan Basin and Flemish Cap remained connected to the Irish conjugate margin. Late Jurassic to Early Cretaceous (Kimmeridgian to Albian) rift sediments from the North Atlantic rift stage are predominantly present in the East Orphan Basin, and extend into several deeper troughs, parts of the West Orphan Basin. The presence of these strata is supported by Jurassic and Early Cretaceous seismic markers that have been tied to wells in the North Flemish Pass Basin (Figure 1.5). The Jurassic to Early Cretaceous sequence thickens in half-grabens and is probably made up of continental siliciclastics and marine shales, analogous to those encountered in wells of the Flemish Pass and Jeanne d'Arc basins. The Early Cretaceous sequence may also contain sandstones and shales that are analogous to those in the Jeanne d'Arc Basin. Additionally, paleogeographic reconstructions indicate that the East Orphan Basin rift was connected to the Grand Banks and Irish conjugate margin via a regional epeiric sea, where organic-rich shallow marine shales (the regional oil and gas source rocks) were widely deposited during the Late Jurassic (Mason and Miles, 1986; Srivastava and Verhoef, 1992).

An Aptian to Albian sequence is present in both the West and East Orphan basins, related the regional Labrador Sea rift stage. Early in this rift stage, a triple junction with three incipient seafloor spreading centres formed just northeast of the Flemish Cap. The three spreading centre branches went (a) south, between Grand Banks and Iberia, (b) northwest between Northeast Newfoundland/Labrador and Northern Europe/Greenland, and (c) east, between Iberia and France, forming the Bay of Biscay. Evidence suggests that significant uplift and erosion in the West Orphan Basin occurred during the Labrador rifting stage during which, The Orphan Knoll and other intra-basin basement highs likely became sources for locally derived sediments (Enachescu et al., 2005). Towards the end of this stage, during the Albian, the western rifting margin of the Orphan Basin migrated westward past the White Sail Fault, forming the early eastern portion of the West Orphan Basin (Enachescu et al., 2005). This rifting was accommodated by eastward movement of the Flemish Cap micro plate, which at this time was still attached to the conjugate Galicia Bank, focusing rifting in the Orphan Basin rather than at the current Atlantic Ocean margin (Srivastava et al., 2000; Sibuet et al., 2007). Deposition of a syn-rift clastic sequence in the West Orphan basin during this period is supported by the presence of Albian syn-rift siliciclastics intercepted in the Blue H-28 well (Robertson Research, 1979). Based on further seismic studies, the upper boundary of this sequence is the regional break-up unconformity, the Avalon Unconformity, which separates it from the overlying Late Cretaceous to Tertiary post-rift deposits. The lithostratigraphy of the Lower Cretaceous sequence is interpreted to include siliciclastics such as marine shales and deltaic and/or shallow marine sandstones similar to Early Cretaceous deposits in the Jeanne d'Arc and Flemish Pass basins (Enachescu et al., 2005).

During the Late Cretaceous to Paleocene East Greenland stage, rifting movements were focused between Labrador and Greenland, north of the Charlie-Gibbs Fault Zone. South of the Charlie-Gibbs Fault Zone, rifting was mainly confined to the westernmost part of the West Orphan Basin. During this period, clockwise displacement of the Flemish Cap accommodated further opening of the West Orphan Basin. The Upper Cretaceous to Paleocene sedimentary sequence is located above the Avalon Unconformity and below the Base Tertiary Unconformity, and comprises mostly marginal to deep marine shales and mudstones. The sequence thins to the East, and is thickest over the West Orphan Basin. Repeated oblique-slip movements along the Charlie-Gibbs Fault Zone were transmitted through the entire Orphan Basin via smaller transform faults, causing basement block rotations as well as uplift, erosion and deformation of earlier Mesozoic syn-rift sedimentary rocks.

In the Early Tertiary, the entire Orphan Basin underwent rapid subsidence, followed by prolonged subsidence and passive margin sedimentation. The Tertiary sequence comprises thermal subsidence-stage deep marine shales deposited on the current passive margin. This sequence is thickest over the West Orphan Basin, where its average thickness in 4 km. Over the East Orphan Basin, the average thickness is only approximately 2 km (Chian et al., 2001; Enachescu et al., 2005).

1.6.3 Oil and Gas Potential

There is a strong probability that Late Jurassic source rocks are present in the East Orphan Basin, based on the continuation of the Jurassic sequence from the Flemish Pass Basin, and the presence of Jurassic sandstones on the Orphan Knoll (Enachescu et al., 2005; Ruffman and van Hinte, 1970). The Orphan Basin is predicted to have a similar geologic history, and therefore similar Mesozoic stratigraphy, to the Flemish Pass Basin, providing an expanded area covered by potential Late Jurassic mature source rocks and Jurassic and Cretaceous reservoirs (Enachescu et al., 2005; Enachescu, 2006). Numerous large structural traps, including rotated fault blocks and complex faulted anticlines, as well as stratigraphic traps including Late Cretaceous and Tertiary submarine fans, have been identified on industry 2D and 3D seismic data. At least six large structures in the East Orphan Basin have the potential to hold several billion barrels of oil-in-place. A new well in the East Orphan Basin, the Great Barasway F-66, has been drilled into the crest of a large rollover anticline, and is expected to have intercepted Early Cretaceous and Late Jurassic strata (Enachescu, 2006).

Since the West Orphan Basin is a younger rift, it is expected to generally lack any marine Late Jurassic sediments, including the regional Kimmeridgian source rocks. Good reservoir rocks of Early Cretaceous age were encountered in the Blue H-28 well and are expected to be present in Early Cretaceous strata throughout the basin. A number of different potential large hydrocarbon traps have been identified in Cretaceous sedimentary fill, including tilted fault blocks, draping anticlines over basement highs and stratigraphic pinchouts on the flanks of basement highs. Late Cretaceous and Tertiary aged large sand fans are present, and have potential as good hydrocarbon traps, although additional drilling and imaging is required to verify their potential. A thick Tertiary marine sequence (3 to 5 km thick) provides adequate burial for source maturation, as well as supplies a thick and extensive seal for any hydrocarbon reservoirs. The main issue in the West Orphan Basin is the relative scarcity of Jurassic source rocks. Albian-Aptian source rocks may be present, in analogy to the Hopedale Basin, offshore Labrador. More likely, the West Orphan Basin is gas prone (Enachescu, 2006).

Chapter 2: General Geology and Age of Sampled Intervals

2.1 Introduction

This chapter introduces the sandstone intervals which were used for heavy mineral provenance, as well as their age, lithology and petrography. Jurassic and Cretaceous intervals from Baccalieu I-78 and Mizzen L-11 in the Flemish Pass Basin, and a Cretaceous interval from Blue H-28 in the West Orphan Basin have been studied for provenance. (Figure 2.1) The studied sandstone intervals are from Mesozoic syn-rift (Late Jurassic and Early Cretaceous) coarse clastic sequences. Based on well correlation and seismic data these sandstones are thought to be chronostratigraphic equivalents to the prolific oil and gas reservoirs present in the Jeanne d'Arc Basin, which are oil producing in several fields. This chapter gives an overview of the geology of each interval, drawing from previous publications and industry reports, and from original core analysis.

2.2 Methods

Most of the geological information on the wells and analyzed intervals (including interval names, ages, cuttings lithologies and borehole logs) are from industry well reports and associated biostratigraphic and geological reports that were obtained from the office of the Canada- Newfoundland and Labrador Offshore Petroleum Board (C-NLOPB) in St. John's, Newfoundland. The ages of the intervals as described in this chapter are assigned biostratigraphically by previous researchers, by using age diagnostic

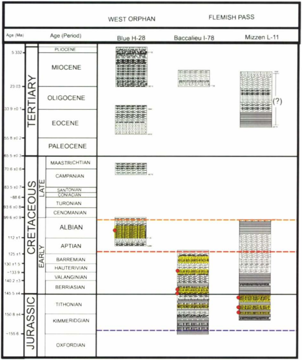

Figure 2.1: Chronostratigraphic chart of the three wells used in this study. The solid black lines are the period divisions. The dashed blue line represents the start of the North Atlantic rift stage, the dashed red line represents the start of the Labrador Sea rift stage, and the dashed orange line represents the start of the regional post-rift phase. Sample locations are shown as yellow dots. C1, C2, etc. show the location of cored intervals. Small numbers on the right side of the columns denote well depth (which is not uniform in scale). Age assignments for the sandstone intervals are from respective biostratigraphy reports available as C-NLOPB open file reports. Time scale is from the International Commission on Stratigraphy (ICS, 2009).

taxa of microfossils (diatoms, foraminifera, etc) and pollen. These are relative ages, corresponding recognized diagnostic taxa to age periods rather than absolute ages. The time scale used to correlate between relative and absolute ages in this thesis is the 2009 International Stratigraphic Chart (ICS, 2009).

General lithologic interpretations of the intervals are based on well site cuttings analysis and natural gamma ray log responses. Cuttings analyses are from the respective industrial well reports as reported by the well-site geologists. Gamma ray logs measure the natural gamma radiation by a rock formation as emitted by the K^{40}, Th^{232}, and U^{238}. Therefore, natural gamma ray measurements reflect the relative amounts of minerals bearing these elements in a rock formation. Such minerals include clays (e.g. illite and montmorillonite), muscovite, biotite, and potassium feldspars. Lithologies which contain these elements include clay-rich mudstones and shales, wackes and arkoses, and thus these lithologies will have relatively high or elevated natural gamma ray emissions relative to quartz arenite. The most radioactive lithology is shale, which is rich in clay minerals that either contain or have the ability to fix K, U and The ions from solution during deposition (Serra, 1984). Gamma radiation is measured by arbitrary units known American Petroleum Institute (API) units. These units were calibrated to an artificially radioactive concrete block with approximately twice the radioactivity of average natural shale, and were given an API value of 200 API units (Schlumberger, 2010).

In this study, core (sidewall and conventional) and thin sections were analyzed from the sampled intervals. Available conventional cores were viewed at the C-NLOPB core repository in St. John's, Newfoundland. The cored intervals were measured and logged for lithology and facies variations, trace and body fossil evidence and sedimentary structures. This information is supplemental, and detailed interpretations of depositional settings were not made, as the availability of core and well coverage makes it difficult, and such detailed interpretations are outside the scope of this study, and, because of an overall lack of core information of well correlations, would be conjectural. Only considerations of a formation's position relative to sea level during deposition and marine or non-marine influences, based mostly on previous studies, are used in provenance and sand deposition models in Chapter 6 of this thesis.

2.3 Lithostratigraphy and biostratigraphy of wells and sampled sandstones

2.3.1 Introduction

Mizzen L-11 well is an abandoned deepwater exploratory well located approximately 484 km east-northeast of St. John's Newfoundland (48.175486° N, -46.293208° W; Figures 1.1 and 2.2). It was drilled in 2003 by Petro-Canada, EnCana and Norsk Hydro, to a total depth (TD) of 3823 m and total vertical depth (TVD) of 3797.5 m. The well was drilled in 1153 m of water, on a large fault block on the southern flank of a large, complexly faulted, four-way dip closure in the Flemish Pass Basin. It intercepted approximately 800 m of Tertiary, 1000 m of Cretaceous and 350 m of Jurassic strata (Figure 2.2). This includes three Mesozoic reservoir targets: the Early Cretaceous "Baccalieu sandstone" (informal name) (3330-3430 m), and two Late Jurassic sandstones (3580 m-3630 m and 3730-3775 m). The Baccalieu Sandstone reservoir potential was poorly developed at this location; however, there was oil shows within it. The two

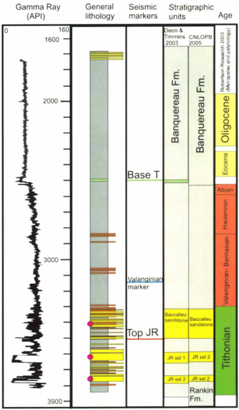

Figure 2.2: Combined gamma ray sonic, lithologic, stratigraphic, seismic stratigraphic and biostratigraphic log for the entire Mizzen L-11 well. On the lithology log, grey represents mainly shale/mudstone, orange is mainly siltstone, and yellow is mainly sandstone. Red dots mark the general sample locations.

Jurassic sandstones (informally referred to as Jurassic sandstone number 1 and Jurassic sandstone number 2) have excellent reservoir qualities, but are water saturated. The three intervals studied are therefore: (1) the Jurassic Sandstone # 2, (2) the Jurassic Sandstone # 1, and (3) the Baccalieu Sandstone (Deon and Timmins, 2003; Enachescu et al., 2005; C-NLOPB, 2007).

Baccalieu I-78 is an abandoned exploratory well located in the Northern Flemish Pass Basin (47.961525° N, -46.179656° W), approximately 426 km east of St. John's, Newfoundland. It was drilled in 1985 by a consortium led by Esso Parex at a water depth of 1092.8 m and had a total depth of 5134.5 m. It intercepted approximately 600 m of Tertiary, 1500 m of Early Cretaceous, and 1500m of Late Jurassic strata (Figure 2.3). Good quality reservoir was penetrated in the Cretaceous section, where 80 m of mature sandstone, referred to as Hibernia Formation equivalent, was encountered between 3195 m and 3275 m. A lesser reservoir was encountered, referred to as Avalon Formation equivalent, between 2030 m and 2220 m. Very little reservoir was encountered in the Jurassic section, and what was present was of poor quality. The Jeanne d'Arc Formation equivalent was encountered in the Jurassic section, between 3715 m and 3780m (MacAlpine, 1988; C-NLOPB, 2007). Four intervals have been sampled for provenance analysis in this well: (1) the Jeanne d'Arc equivalent sandstone, (2) Berriasian shales and sandstones underlying the Hibernia Formation equivalent, (3) the Hibernia Formation equivalent proper, and (4) the Avalon Formation equivalent. A limited amount of conventional drill core is available from this well.

Blue H-28 is located in the West Orphan Basin, approximately 375 km northwest of St. John's, Newfoundland (49.624025° N, -49.299494° W). It was drilled in 1979 by a

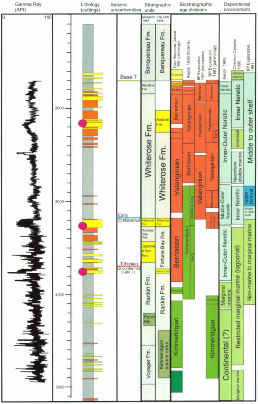

Figure 2.3: Combined gamma ray sonic, lithologic, stratigraphic, seismic stratigraphic and biostratigraphic log for the entire Baccalieu I-78 well. On the lithology log, grey represents mainly shale/mudstone, orange is mainly siltstone, and yellow is mainly sandstone. Red dots mark the general sample locations.

group led by Texaco into a basement high, at a water depth of 1487 m and to a total depth of 6103 m. The well encountered approximately 2000 m of Tertiary, 600 m of Cretaceous, and 800 m of Paleozoic strata (Figure 2.4). An early Cretaceous (probably Albian) 225 m-thick sandstone and shale interval was intercepted between 4950 m and 5175 m.

2.3.2 Mizzen L-11: Jurassic Sandstone #2

Heavy mineral grain counts, tourmaline geochemistry and U-Pb geochronology of detrital zircons were undertaken using cuttings from a sample between 3760 m and 3765 m (Figure 2.5). This interval is part of a sandstone unit occurring between 3741 m and 3769 m, informally referred to as Jurassic sandstone number 2, but also referred to as Tempest Sandstone Member. This was the second high quality reservoir sandstone that was encountered in Mizzen L-11, after Jurassic Sandstone # 1. This sandstone has excellent reservoir characteristics but is water-wet at this location (Deon and Timmons, 2003; Robertson Research, 2003; C-NLOPB 2007).

Biostratigraphy of the interval between 3735 m and 3823 m indicates a Tithonian age, and a depositional setting of a variably restricted shallow water shelf, with significant terrigenous influences. This unit has been interpreted to have accumulated by gravity flow processes off of an adjacent syn-depositional high (Robertson Research, 2003). The gamma ray sonic profile of this interval is generally blocky in the lower 15 m with a sharp lower contact and API values between 12 and 17, but in the upper 5 m API values gradually increase to 100. A prominent API high is present between 3754 m and

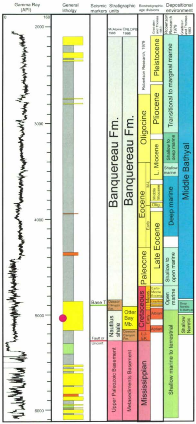

Figure 2.4: Combined gamma ray sonic, lithologic, stratigraphic, seismic stratigraphic and biostratigraphic log for the entire Blue H-28 well. On the lithology log, grey represents mainly shale/mudstone, orange is mainly siltstone, and yellow is mainly sandstone. Red dots mark the general sample locations.

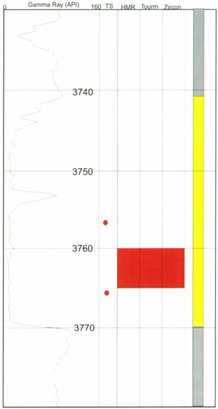

Figure 2.5: Lithologic and gamma ray sonic log of Jurassic Sandstone #2 in Mizzen L-11. Thin section locations are shown as red dots. Intervals which were used for heavy mineral analyses (HMR), detrital tourmaline geochemistry (tourm) and detrital zircon U-Pb geochronology (zircon) are highlighted in red.

3755 m (Figure 2.5). The cuttings descriptions indicate 60-90% medium to coarse grained moderately sorted quartz sandstone and 40-10% shale and minor siltstone, and that the proportion of sandstone decreases upwards (Deon and Timmons, 2003). Cuttings descriptions and the gamma ray profile indicate the presence of a fining-upwards and/or muddying-upwards quartz rich sandstone with a sharp basal contact.

2.3.3 Mizzen L-11: Jurassic Sandstone # 1

Interval 2 in Mizzen L-11 is located between 3615 m and 3625 m. Heavy mineral grain counts were compiled from cuttings between 3615 m and 3625 m, and detrital tourmaline geochemistry and U-Pb geochronology of detrital zircons were compiled from cuttings between 3620 m and 3625 m (Figure 2.6). This interval is part of a 45 m thick mature sandstone formation that occurs between 3595 m and 3640 m, and is referred to as Jurassic sandstone # 1 (Deon and Timmons., 2003).

Biostratigraphy of the interval between 3415 m and 3725 m indicates an early-late Tithonian age, as well as a depositional setting of a variably restricted shallow water shelf, with significant terrigenous influences. The presence of marine microplankton at 3615 m is thought to indicate a proximity to a maximum flooding surface. Ooliths present at 3625 m are thought to suggest input of components from a shallow water, high energy setting. This unit is thought to have been derived off of an adjacent syn-depositional high during lowstand or transgressive systems tracts, and may have been introduced by gravity flow processes (Robertson Research, 2003). The gamma ray profile of the sandstone is generally blocky with API values between 20 and 30. The upper and lower contacts of

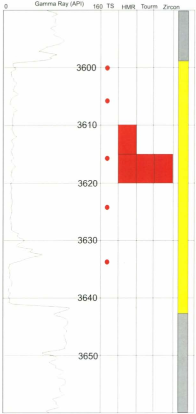

Figure 2.6: Lithologic and gamma ray sonic log of Jurassic Sandstone #1 in Mizzen L-11. Thin section locations are shown as red dots. Intervals which were used for heavy mineral analyses (HMR), detrital tourmaline geochemistry (tourm) and detrital zircon U-Pb geochronology (zircon) are highlighted in red.

this unit is defined by sharp increases in API indicating sudden changes in lithology at the top and base of the unit (Figure 2.6). Cuttings from the entire sample interval (3615 m to 3620 m) are described as 100% sandstone, comprised of mostly unconsolidated medium to coarse grained quartz grains. The grains are subangular to subrounded and moderately well to well sorted. There is minor white clay matrix, but no cement is present. The sandstone is interpreted to have good porosity (Deon and Timmons, 2003). The gamma ray profile and description of cuttings indicates quartz rich sandstone lacking large scale grading and with abrupt, possibly conformable or unconformable, contacts with mudstones or shales above and below.

2.3.4 Mizzen L-11: Baccalieu Sandstone

Interval 1 in Mizzen L-11 is located between 3410 m and 3420 m. Heavy mineral grain counts have been undertaken from cuttings over this entire interval, and additionally detrital tourmaline geochemical data and detrital zircon U-Pb geochronology has been compiled from cuttings between 3415 m and 3420 m (Figure 2.7).

The samples are taken from the middle of the Baccalieu sandstone formation, a unit of interbedded sandstone, siltstone and mudstone occurring approximately between 3335 m and 3500 m (Figs. 13 and 14). It has been considered a distal equivalent to the Early Cretaceous (Berriasian) Hibernia Formation equivalent from the Baccalieu I-78 well (Deon and Timmons, 2003). In contrast to this interpretation, biostratigraphy of the interval between 3415m and 3725m indicates an early-late Tithonian age. Biostratigraphy also indicates a depositional setting of a variably restricted shallow water shelf, with

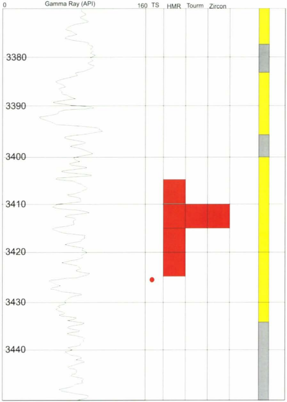

Figure 2.7: Lithologic and gamma ray sonic log of Baccalieu Sandstone in Mizzen L-11. Thin section locations are shown as red dots. Intervals which were used for heavy mineral analyses (HMR), detrital tourmaline geochemistry (tourm) and detrital zircon U-Pb geochronology (zircon) are highlighted in red.

significant terrigenous influences. A transgressive surface or maximum flooding surface is interpreted to be at or near 3415 m, based on the presence of marine microplankton. Similar to the older sands, sands from this unit are thought to have been derived off of an adjacent syn-depositional high, and may have been introduced by gravity flow processes; however the overall decrease in the volume of sands in this later interval has been interpreted to represent a reduction in fluvial input or submergence of proximal adjacent syn-depositional highs (Robertson Research, 2003).

Cuttings between 3410 m and 3415 m are approximately 60% sandstone and 40% shale. The sandstone is dominantly fine-grained and moderately sorted with generally sub-rounded grains. Framework grains include quartz and common feldspar that occur within a silty argillaceous matrix. The shale is medium grey and brown and is silty and calcareous. Between 3415 m and 3420 m the sandstone and shale lithologies are similar; however the proportion is 80% sandstone and 20% shale (Deon and Timmons, 2003). The gamma-ray API curve is jagged, and is interpreted to reflect the interbedded shales and sandstones present in this interval (Figure 2.7). Given the thickness of low API anomalies, the individual sandstone beds appear to be 4 to 8 m thick. Individual beds have average gamma ray sonic API values between 50 and 90 and blocky or increasing upwards profiles, possibly reflecting a mixture of relatively massive and fining- and/or muddying-upwards beds.

2.3.5 Baccalieu I-78: Early Cretaceous (Berriasian) Sandstones

Heavy mineral grain counts have been completed between 3295 m and 3305 m, and detrital tourmaline geochemisty completed from cuttings between 3295 m and 3300 m (Figure 2.8). Unfortunately, due to poor yields and small sample size, not enough detrital zircons were found at a size adequate for U-Pb geochronology.

This interval occurs below the Hibernia equivalent sandstone, to a depth of approximately 3310 m, and is composed of intercalated mudstone, sandstone and siltstone. It was cored between 3287 m and 3305.25 m. This interval also occurs within the MS1-50 parasequence of Foster and Robinson (1993), and as such is part of an overall shoaling-upwards succession that was interpreted to be derived largely from the north. Biostratigraphy indicates a latest Jurassic to earliest Cretaceous age, probably somewhere between Kimmeridgian and Berriasian, and a probable location of deposition in the outer to middle shelf or in a marginal marine realm (Esso Resources, 1986; Ascoli, 1990; Chevron Canada, 1990; BP Exploration, 1991). The cored interval is comprised of black shales and mudstones with finely intercalated lithic sandstone and siltstone layers from 3289 m to 3302.5 m, and interbedded coarse lithic wackes and matrix-supported muddy lithic conglomerates with minor shale and mudstone from 3287 m to 3289 m and from 3302.5 m to 3305 m (Figure 2.8).

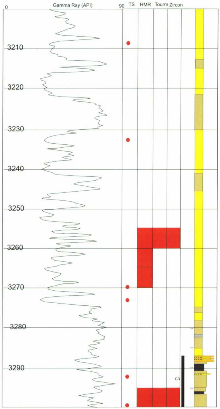

Figure 2.8: Lithologic and gamma ray sonic log of the Hibernia Equivalent sandstone (base at 3275 m), and underlying Berriasian shales and sandstones, in Baccalieu I-78. Thin section locations are shown as red dots. Intervals which were used for heavy mineral analyses (HMR), detrital tourmaline geochemistry (tourm) and detrital zircon U-Pb geochronology (zircon) are highlighted in red.

2.3.6 Baccalieu I-78: Early Cretaceous Hibernia Formation Equivalent

Heavy mineral grain counts, tourmaline geochemistry and U-Pb geochronology of detrital zircons have been completed from cuttings between 3255 m and 3260 m. Additional heavy mineral grain counts have been done for two samples between 3260 m and 3270 m (Figure 2.8).

This two sample interval occurs within an 80 m thick sandstone formation, which is considered an equivalent to the Hibernia Formation of the Jeanne d'Arc Basin (McAlpine, 1989; C-NLOPB, 2007). It is also informally referred to as the Baccalieu sandstone (Deon and Timmons, 2003). In the Jeanne d'Arc basin, the Hibernia Formation has been interpreted as a fluvial-deltaic succession that prograded from the south (Tankard and Welsink, 1987; McApline, 1990).

Foster and Robinson (1993) place the Hibernia equivalent interval at the top of the MS1-50 parasequence, which is an overall shoaling upwards parasequence overlain by a regional flooding surface. Deposition of MS1-50 was mainly controlled by north-south directed extension related to the Tethys rift stage; however, early northwest-southeast North Atlantic stage rifting may have influenced deposition of the upper part of MS1-50. Foster and Robinson (1993) postulated that the parasequence onlapped mainly from the north to the south, but that either the base or the top or both may represent a depositional unconformity, and potentially could accompany a change in the direction of sediment input. Biostratigraphy indicates an earliest Cretaceous age, probably Berriasian, and a probable location of deposition in a terrestrial realm (Esso Resources, 1986; Ascoli, 1990; Chevron Canada, 1990; BP Exploration, 1991).

The sandstone is characterized by gamma ray API values between 40 and 70 between depths of 3200 m to 3280 m. Sharp decreases in gamma-ray API occur at the top and base, indicating sharp lithologic boundaries (Figures 2.3 and 2.8). The lower contact may correspond to a depositional unconformity; however, the upper contact corresponds to a known Early Cretaceous seismic unconformity and flooding surface (Foster and Robinson 1993). There is no large scale grading apparent on gamma-ray logs, and as a whole, the Hibernia equivalent has a blocky profile (Figures 2.9 and 2.12). Cutting descriptions within this interval are summarized as predominantly sandstone with occasional shale and siltstone interbeds (Esso Resources Canada Ltd., 1985).

2.3.7 Baccalieu I-78: Early Cretaceous Avalon Fm Equivalent

A cuttings sample from 2165 m to 2170 m was used for heavy mineral ratios, detrital tourmaline geochemical analyses and detrital zircon U-Pb geochronology. Cuttings from 2175 m to 2180 m were used for heavy mineral ratios and detrital zircon U-Pb geochronology. Additionally, heavy mineral ratios were obtained from cuttings from 2170 m to 2175 m and 2180 m to 2185 m. Core is available between 2170 m and 2188 m, and was studied to interpret overall depositional setting of the interval (Figure 2.9).

This formation interval has been interpreted as analogous to the Avalon Formation of the Jeanne d'Arc Basin (McAlpine, 1989, C-NLOPB, 2007). In the Jeanne d'Arc Basin, the Avalon Formation is generally considered to be prograding stacked wave-dominated shoreface successions that were deposited during a forced marine regression related to Late Barremian/ Early Aptian uplift and erosion. Generally, sediments of the

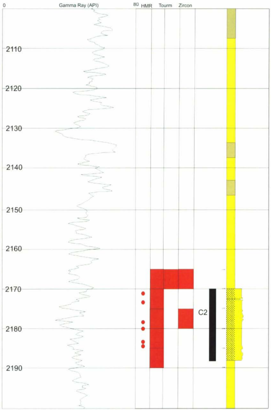

Figure 2.9: Lithologic and gamma ray sonic log of Avalon Formation equivalent in Baccalieu I-78. Thin section locations are shown as red dots. Intervals which were used for heavy mineral analyses (HMR), detrital tourmaline geochemistry (tourm) and detrital zircon U-Pb geochronology (zircon) are highlighted in red.

Avalon and Ben Nevis Formations in the Jeanne d'Arc Basin are considered to be supplied from uplifted areas in the south and west (including the Bonavista Platform and the Avalon Uplift) (Sinclair 1993).

Foster and Robinson (1993) place this interval into the MS2 sequence in the Flemish Pass Basin. The MS2 in the northern Flemish Pass basin is interpreted as a distal shoreline sequence that first prograded from the southeast during northwest-southeast rifting and activation of the Voyager fault system, and then retrograded before an abrupt change basin orientation and sediment supply occurred. The studied interval is from the coarsest section of MS2, where shoreline progradation was likely at its maximum.

Biostratigraphy indicates an earliest Cretaceous age for this interval, probably somewhere between Valanginian to Hauterivian (Ascoli, 1990; BP Exploration, 1991). The gamma-ray sonic log is gently sloping overall and no sharp changes in lithology are evident within the interval (Figures 2.3 and 2.9). The entire formation interval (approximately 2140 m to 2270 m) is characterized by an overall gradual upward coarsening or cleaning upwards. Micropaleotological and palynological analysis of this interval indicate a probable location of deposition in the middle to outer shelf (Chevron Canada, 1990; BP Exploration, 1991). A gradational upper contact is present somewhere approximately between 2120 m to 2130 m (Figure 2.9).

2.3.8 Blue H-28: Albian Sandstone

Interval 1 in Blue H-28 is located between 5005 m and 5030 m. Heavy mineral grain counts have been compiled from cuttings at 5005 m to 5010 m, 5010 m to 5015 m, 5015 m to 5020 m, 5020 m to 5025 m and 5025 m to 5030 m. Detrital tourmaline geochemistry and U-Pb geochronology of detrital zircons have been compiled from cuttings at 5025 m to 5030 m (Figure 2.10).

This interval is part of an Early Cretaceous sandstone unit, which is considered a possible lateral equivalent to the Otter Bay Member from the northern Jeanne d'Arc Basin (C-NLOPB, 2007). Biostratigraphic analyses indicates an Early Cretaceous, probably Albian, age of deposition, and a shallow marine to terrestrial (marginal marine) environment of deposition (Robertson Research, 1979; Gradstein and Thomas, 1983). The Gamma ray sonic profile of the surrounding interval (4990 m to 5050 m) is generally jagged to blocky with values between 40 and 60 API, indicative of sandstone with variable mud content. Several 3-6 m thick gamma ray highs (70-80 API) are present, and probably represent muddier and/or more fine-grained intervals. Large scale grading is not apparent, and the unit as a whole appears blocky; however, fining- and coarsening-upwards profiles are exhibited on the 1-10 m scale.

Cuttings from the interval between 4995 m and 5025 m are described as dominantly medium-grained moderately sorted quartz grains, and up to 10% feldspars with minor traces of mica and pyrite. Minor carbonate cements were noted, and the porosity is estimated to be as high as 10%. Below 5025 m, the cuttings are described as 70% medium-coarse grained, generally sub-angular, moderately well sorted quartz grains, 20% light grey to white siltstone with dolomitic cement, and trace feldspar and muscovite (Texaco Shell et al. 1979).

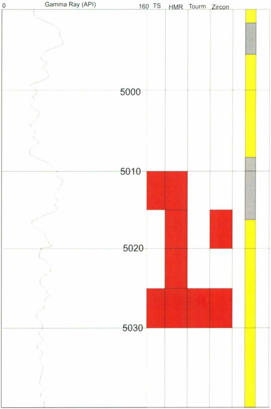

Figure 2.10: Lithologic and gamma ray sonic log of part of the Albian Sandstone in Blue H-28. Cuttings thin section locations are highlighted. Intervals which were used for heavy mineral analyses (HMR), detrital tourmaline geochemistry (tourm) and detrital zircon U-Pb geochronology (zircon) are highlighted in red.

2.4 Core descriptions

2.4.1 Baccalieu I-78: Early Cretaceous (Berriasian) Sandstones and shales

A conventional core between 3287 m and 3305 m was viewed and described (Figure 2.11). Medium- to coarse-grained lithic wacke and arenite and matrix-supported conglomerate beds dominate in the lower 2.5 m of the cored interval (3302.5 m to 3305 m), and these are interbedded with thin light grey mudstone. Matrix-supported conglomerate beds range in thickness from 2 to 35 cm and mudstone beds range from 0.5 to 6 cm thick. Clasts in the conglomerate are rounded to sub-angular and are mainly composed of black shale and white to beige medium-grained quartz sandstone. Sub-rounded rip-up clasts of laminated mudstone are present at the base of some of the sandstone/conglomerate beds. Interbedded mudstones are reddish brown or white, planar laminated, and lack trace fossils.

Most of the cored interval (3289 m to 3302.5 m) is dominated by black shales and mudstones with fine interbeds and intercalations of medium- to coarse-grained lithic sandstone (approximately 30% sandstone overall). Thicknesses of the sandstone intercalations range from 0.2 to 5 cm, and the average thickness is approximately 1 cm. Some of the intercalations have sharp and planar contacts, while others are low-angle cross-laminated, and resemble unidirectional current ripples. Some flaser-type bedding is also present. Body fossils are absent between 3295 m and 3302.5 m, and only minor *Chondrites* ichnofossils occur locally. Between 3289 m and 3295 m, trace and body fossils appear and increase in abundance upwards. Body fossils include bivalves and ammonites, and trace fossils are predominantly *Chondrites* with minor *Plantolites*

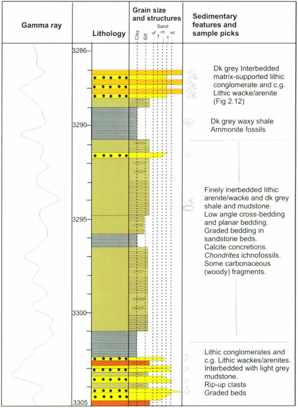

Figure 2.11: Core log for core 3 in Baccalieu I-78. Core 3 is within sample interval 3, from below the Hibernia Formation equivalent. Most of the cored interval (3288.5m-3302.5m) is dominated by shale with thin lithic sandstone intercalations. Above and below this are immature sandstones and conglomerates.

occurring nearer to the top of the section. Carbonaceous debris is also locally present between 3289 m and 3295 m.

The upper 2 m of the core (3287 m to 3289 m) is comprised mainly of matrix-supported lithic conglomerate interbedded with chaotic sandstone and mudstone layers. The lithic conglomerate beds are ungraded and range in thickness from 30 to 50 cm, and the sandstone layers are 10 to 13 cm thick. The conglomerate beds contain approximately 15-20% clasts and 80-15% matrix. The clasts are angular to sub-angular, and composed mainly of white to beige quartz sandstone and chert. Some carbonate fragments are also present, including bivalve and other shelly fragments. The matrix is composed of dark grey unsorted and ungraded silty to sandy mudstone. Sandstone layers are tightly but irregularly folded and boudined, indicating soft sediment deformation (Fig. 2.12).

2.4.2 Baccalieu I-78: Early Cretaceous Avalon Fm Equivalent

The cored interval between 2170 m and 2188 m is made up entirely of heavily bioturbated fine- to very fine-grained wacke, and lacks significant facies variation or sedimentary structures (Figure 2.13). Overall, it is poorly cemented, with the exception of several 15-20 cm thick reddish-brown siderite and/or hematite cemented horizons. Primary sedimentary structures are not evident due to bioturbation, which is intense and pervasively developed throughout the cored interval. The ichnofabric also shows a diverse assemblage of trace fossil types; trace fossils that have been identified include *Ophiomorpha*, *Teichichnus*, *Skilithos* and *Asterosoma*. The sizes of individual trace fossils ranges between 0.5-1.5 cm (Figure 2.14).

Figure 2.12: Photograph of to 3288.5 m to 3287 m of core 3 in Baccalieu I-78. The height of the cut sections is 75 cm. This section is comprised of poorly sorted matrix- supported lithic conglomerate interbedded with tightly folded and boudined lithic sandstone. The conglomerates are interpreted as debris flow deposits and the intervening sandstones are probably irregularly folded because of soft sediment deformation the occurred during debris flow deposition.

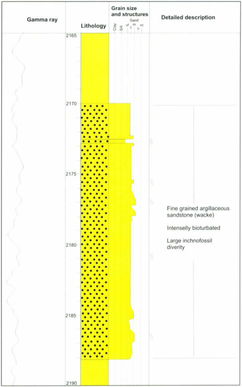

Figure 2.13: Core log for core 2 in Baccalieu I-78. Core 2 is from the Avalon Formation equivalent. Overall, it is a heavily bioturbated, fine grained argillaceous and poorly cemented sandstone.

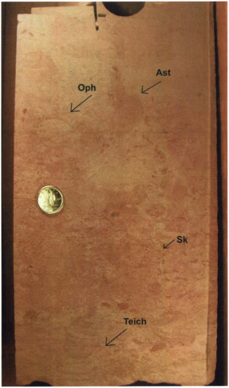

Figure 2.14: Photograph of a siderite-cemented portion of core 2, in Baccalieu I-78. This photograph demonstrates the intensity and diversity of trace fossils in this interval. The ichnofossil assemblage comprises ophiomopra (Oph), asterosoma (Ast), teichichnus (Teich), skilithos (Sk) and plantolites. The diversity and intensity of the trace fossils is indicative of a cruziana ichnofacies.

Chapter 3: Sedimentary Petrology

3.1 Introduction

Thin sections, where available, were analyzed from the sampled intervals, to give insight into the petrology and provenance characteristics of the sandstones. The purpose of doing thin section petrography was to assess provenance and sedimentary recycling using the compositions of constituent detrital grains, estimated compositions (mineralogical maturity), and textural maturity and of sandstones. It was also pertinent to identify any diagenetic overprints on the original sand composition (grain dissolution, quartz overgrowths) a well as the composition of detrital heavy mineral assemblages (e.g. authigenic phases or dissolution of detrital phases). Modal proportions of sandstone components are visually estimated, and high precision quantitative point count data was not obtained (see next section). Instead, the sandstone petrology is generally described and interpreted qualitatively, and is meant add information on aspects such as source area compositions, sedimentary recycling and transport distances, and to supplement interpretations made using high precision heavy mineral data later in this thesis.

3.1.1 Methodology

Thin sections were obtained at the C-NLOPB core repository and viewed using a petrographic microscope. The thin sections were previously stained using a combination of alizarin red-s and potassium ferricyanide blue in order to differentiate between different carbonate minerals (Dickson, 1966). Percentages of sand grains, matrix, porosity and cements were estimated visually using the visual percentage estimation charts of Folk (1951), Terry and Chilingar (1955) and Reid (1985). For the basis of classifications herein, the basic constituents of sandstone are framework grains, matrix, porosity, cement, authigenic minerals and accessory minerals. Framework grains are the primary detrital sand grains (0.06 mm -2 mm) present in the sandstone, and matrix are the primary detrital materials (clay, silt, or other fine material <0.06 mm) in the interstices representing its overall composition (Folk, 1968). The framework grains are classified as quartz, feldspar or lithic fragments. Other mineral grains, unless notably abundant, are defined as accessory minerals and not included proportionally when classifying the sandstone composition. Sandstones herein are classified using the classification scheme of Pettijohn (1975), which uses percentages quartz, feldspar and lithic framework grains (QFL), and independently the amount of matrix present to classify sandstones (Figure 3.1). All modal QFL proportions are normalized to percentages of sand sized grains, and do not include proportions of matrix, porosity or authigenic minerals. Also, they are presented as reconstructed modal proportions; that is, the percentages present at the time of deposition before diagenesis.

The textural maturity of sandstones is defined using the scheme of Folk (1951), wherein a hierarchical ordering of textural conditions must be met to define a sandstone at different levels of maturity, representing increasing levels of kinetic energy during transport and deposition. These textural conditions are (in order of maturity and required kinetic energy) the removal of clay matrix, sorting of sand grains and abrasion and rounding of sand grains. Under such a scheme, a sandstone is considered immature if it

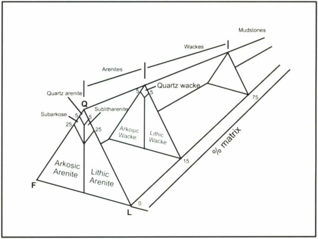

Figure 3.1: Classification scheme for sandstones, modified from Pettijohn (1975). Sandstones are classified based on modal abundances of quartz grains (Q), feldspar grains (F), and lithic grains (L), and also based on the percentage of detrital matrix present.

has >5% matrix, submature if it has <5% matrix but is not well sorted, mature if it is has <5% matrix and is well sorted, and supermature if it has <5% matrix, is well sorted, and the majority (>50%) of grains are rounded or well rounded. The classification scheme for grain sorting is after Folk (1951), which uses the standard deviation of the average grain size to define the degree of sorting. For the purposes of this thesis, sorting was visually approximated using the comparison charts of Compton (1962) and Pettijohn et al. (1987). The classification of the degree of roundness (very angular, angular, subangular, sub-rounded rounded and well rounded) is made herein visually using the comparison chart of Pettijohn et al. (1987).

Mineralogical maturity is defined by the percentage of quartz and chert grains, which are more resistant to physical and chemical breakdown during sedimentary processes than are feldspar grains or lithic grains (Pettijohn, 1975). Mineralogically mature sandstones are those with >90% quartz+chert grains, submature with 75-95% quartz+chert and submature with <75% quartz+chert.

Diagenesis can significantly alter the composition of sandstone at the time of deposition, and thus care must be taken to interpret diagenetic overprints on the original sand composition (Worden and Burley, 2003). The relative timing of porosity formation and cement growth and dissolution are considered in the context of their effect on the dissolution or growth of primary framework or accessory minerals that are diagnostic for interpretations of original depositional compositions and textures.

Porosity is the void space that occurs between framework grains, matrix and cement. Porosity is defined as either primary or secondary, and there are several types of primary and secondary porosity. Primary porosity is most commonly intergranular porosity; that is, the intergranular space left between grains and matrix after deposition, or more commonly the remaining intergranular space after compaction. Other types of primary porosity are intragranular; that is, they are a function of voids originally present in detrital grains, but this is not common. The most common types of secondary porosity are those that involve the dissolution of framework grains (e.g. feldspar or carbonate grains) or of authigenic carbonate and/or sulphate cements (Schmidt et al., 1977). Dissolution of detrital feldspars and lithic grains are common, and can alter the original sand composition and create artificially mineralogically mature sands (Burley, 1986; Wilkinson et al., 1997). Thus, the author is carful to note the occurrence and nature of secondary porosity.

Cements are authigenic void filling mineral growths that result in the lithification of sands into sandstones. Cement minerals commonly include silica (quartz), calcite, dolomite, and siderite, but can also include hematite, sulphates, phosphates and clays. They can form by precipitation from pore waters, nucleation off of framework grains, or replacement of or recystallization of framework grains or other cements (Burley and Worden, 2003).

3.1.2 Interpreting provenance characteristics

The composition of detrital sand grains in sandstones reflects the compositions of the source rocks from which the individual sand grains were derived, and thus framework mineralogy of sandstones has long been considered a good proxy for provenance; in particular, for determining the relationships between modal sand compositions (quartz, feldspar and lithic grains, or QFL) and tectonic affinities of source areas (Dickinson and Suczek, 1979). However, there are drawbacks to this approach, especially when discriminating quartz rich sands where it is easy to mismatch continental block and recycled orogen affinities because of variable inputs of sedimentary lithic grains (Dickinson et al., 1983; Cox and Lowe, 1995b). Additionally, and more critically, modal framework compositions are influenced by several other processes, including weathering, transport and diagenesis, and thus in many cases, are modified significantly from the compositions of their source rocks, and simple interpretations of source types based on modal mineralogy do not consider these factors adequately (Cox and Lowe, 1995a; Weltje and Eynatten, 2004). If one considers the processes, besides source composition, that effect modal sand composition, framework mineralogy becomes a useful tool for making inferences not only about source compositions, but also gives insight into sedimentary recycling, transport distances, and basin evolution (Cox and Lowe, 1995a).

The processes that have the most deal of influence on sediments from the source hinterland to the depositional basin are chemical weathering and transport. Chemical weathering has been shown to significantly change the modal compositions of sands from source to sink, particularly with regards to reducing or even eliminating libel lithic and feldspars, leading to increased mineralogical maturity that does not reflect the composition of the source area. In some cases, intense weathering can destroy the modal sand provenance completely (Johnsson et al., 1988). This effect is strongest when detritus is carried through long, low gradient and sinuous drainage systems in hot (tropical) humid climates, where storage of sand grains can occur for long periods of time in point bars before being carried to a larger depocentre (Cameron and Blatt, 1971; Suttner et al., 1981;

Grantham and Velbel, 1988; Johnsson, 1990). Unfortunately, it is hard to assess the degree to which weathering has modified the inherited compositions of sandstones. Abbink et al. (2001) provide some paleo-climate constraints from the Late Jurassic to the Early Cretaceous from cores in the nearby southern North Sea that may be useful. According to this study, the area experienced an arid and hot climate in the Late Kimmeridgian to the Tithonian, but switched to a more humid, tropical climate in the Earliest Cretaceous time. Therefore, Early Cretaceous sandstones may be expected to have experienced more extensive weathering than the Late Jurassic sandstones in this study.

The effects of transport on the modal compositions of sand from source to sink are similar, but less severe. During fluvial transport, the modal proportions and average sizes of lithic, feldspar and polycrystalline grains are reduced, and the amount of reduction increases with increased river length and decreased river gradient. Thus, the overall effect of transport is to increase the overall mineralogical and textural maturity of sandstone, but not to such a degree as weathering or recycling (Blatt and Christie, 1963; Suttner et al., 1981; Blassi and Manassero, 1990; Cox and Lowe, 1995a; Picard and McBride, 2007). The same is true during transport in the beach zone, where loss of feldspars and lithics may be even more severe due to constant abrasion (McBride et al., 1996). In general, the textural maturity of sandstones is thought to represent the amount of transport the parent material underwent and, to some extent, energy of the depositional settings. Some studies have shown that, generally, sand grains become more rounded after long shore transport, on coastal beach settings where depositional energy is high and reworking common, but that rounding is not as prevalent during fluvial transport (Picard and McBride, 2007).

Also, in some cases chemical weathering, particularly in warm and humid climates, has been shown to increase the roundness of quartz independent of transport (Crook, 1968). Long transport distance has been shown to decrease the overall grain size and increase the sorting of sand grains (Moss, 1972; Cox and Lowe, 1995a). However, in large fluvial drainage systems, this generalization that grain sorting increases downstream cannot always be maintained, as the textural maturity of sand downstream in the main tributary has actually been shown to decrease due to the addition of fresh material from local tributaries, such that material at the terminus of large rivers may actually be more poorly sorted than material in the middle reaches of the river (Ouma, 1967; Demir, 2003). Also, although rounding occurs in coastal settings, there is apparently no correlation between transport distance and grain roundness (McBride et al., 1996). In summary, single-cycle transport distance does not affect the textural or mineralogical maturity as much as other factors such as recycling and weathering. Thus it is difficult in many cases to interpret relative transport distances using the composition and texture of sandstone.

Understanding the effects of diagenesis is important for interpreting the original modal composition, at the time of deposition, of sandstones. Complete dissolution of feldspar grains, carbonate grains and carbonate cements can occur at depth, completely changing the modal mineralogy and creating secondary porosity (Burley, 1986; Wilkinson et al., 1997). Thus, in this investigation, the amount of formation of secondary porosity by grain dissolution is assessed in order to interpret the original modal composition and mineralogical maturity of the sandstone before diagenesis. Other effects of diagenesis can make it hard to determine the original framework composition and textural maturity of sandstones at the time of deposition. For example, feldspar and lithic grains can be altered and deformed, forming a pseudomatrix (Dickinson, 1970; Whettan and Hawkins, 1970). Quartz cements and overgrowths on detrital quartz sand grains can make interpretations with regards to textural maturity and sedimentary recycling difficult, because the boundary between detrital grains and overgrowths are generally invisible, unless the original detrital grain had an overgrowth or coating of clay or hematite. On the other hand, diagenesis could be beneficial for interpreting textural maturity, in the case of early pervasive carbonate cementation preventing quartz overgrowths and inhibiting feldspar and lithic grains.

The compositions of detrital sand grains in sandstone derived from a pre-existing sedimentary source reflect the ultimate source of those grains, rather than the proximal source, and thus correct recognition of the effects of sedimentary recycling is crucial for provenance analysis and paleodrainage reconstructions (Blatt, 1967). Increasing modal quartz content, sorting of grains into overall smaller size fractions, and rounding of grains should coincide with recycling of a pre-existing sediment into another, as much of the detrital material has gone through at least two if not successive episodes of weathering, transport, deposition and diagenesis (Suttner et al., 1981; Cox and Lowe, 1995b). Care must be taken in making such interpretations, because sands comprising mostly first cycle grains may also be mineralogically and texturally mature, if they were weathered extensively in humid climates, and experienced periods of high energy transport and deposition; although this is the exception (Cameron and Blatt, 1971; Suttner et al., 1981; Grantham and Velbel, 1988; Johnsson, 1990). The composition of recycled sandstones in some cases is shown to be generally quartz-lithic (sublitharenite compositions) with dominant quartz but significant amounts of clastic sedimentary and carbonate lithic grains; and, therefore such sandstones are mineralogically submature rather than mature (Dickinson and Suczek, 1979; Arribas and Tortosa, 2003; Critelli et al., 2003). In basins where much of the source material is recycled, inputs from fresh crystalline sources can be identified by the presence of detrital feldspars (Cox and Lowe, 1995a). Another key feature that would strongly indicate sedimentary recycling would be the presence of inherited diagenetic overgrowths on quartz (Sanderson, 1984). The evaluation of sedimentary recycling is done in the following chapters of this thesis using heavy minerals; however, it is worth noting that an abundance of ultrastable accessory minerals (zircon, tourmaline and rutile) is thought to represent their concentration through successive sedimentary cycles (Hubert, 1962)

3.2 Thin section Petrography

This section provides petrographic descriptions that focus on the various components present, including framework grains, matrix and authigenic phases, as well as textural characteristics. For each interval, a reconstructed or pre-diagenetic framework modal composition is given, as well as the name and mineralogical and textural maturities. Thin section analyses are summarized in Appendix 1.

3.2.1 Jurassic Sandstone #2

Three thin sections were analyzed from this formation, at 3765.5 m, 3765 m and 3756.5 m. The two sections at 3765.5 m and 3765 m are very similar; as both are pervasively cemented by ferroan dolomite, and have contain approximately 30-35%

ferroan dolomite cement, and both are quartz rich with subordinate lithic grains and a minor population of feldspar grains (Figure 3.2). Several factors indicate that the dolomite cement occurred early, before significant burial and compaction. First, the intergranular volume (volume between grains: cement+porosity+matrix) is estimated at around 40%, which is the typical porosity of sandstones before compaction (Beard and Weyl, 1973; Wordon and Burley, 2003). Second, there are no indicators of compaction, such as bent or deformed clay-rich lithic grains or sutured quartz grain contacts. Porosity is low in these samples (4-5%) and consists mainly of primary intergranular and secondary grain dissolution and intragranular dissolution porosity types. Grain dissolution seems to have primarily affected the feldspars, whereas intragranular dissolution has affected the lithic and feldspar grains (Figure 3.2 C).

Quartz overgrowths are visually apparent on some grains, but are presumed to be present on other grains based on the presence of euhedral faces on many grains (Figure 3.2). Later quartz overgrowths seem to be restricted to spaces between dolomite cements, creating meniscus like contacts, and some grains completely enveloped in cement show no evidence for overgrowths at all, indicating that dolomite cementation inhibited more extensive quartz overgrowths (Figure 3.2 A-B, D). The boundary between overgrowths and cores of some quartz can be seen due to the presence of clays between the core grain and overgrowth, revealing these grains to have had sub-rounded to rounded morphologies preceding silica overgrowths (Figure 3.2 A, D-F). Other quartz grains lacking overgrowths and lithic and feldspar grains or are sub-angular to rounded. Some of the quartz overgrowths that can be seen have angular abraded edges, and occur adjacent to silica-inhibiting dolomite cement (Figure 3.2 D). Rather than being formed authigenically

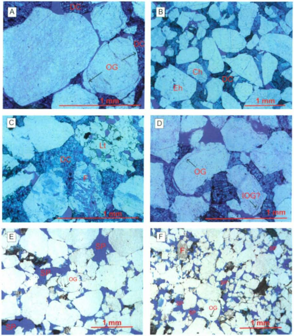

Figure 3.2: Photomicrographs of samples from Jurassic Sandstone #2, Mizzen L-11. **(A)** Quartz grains and ferroan dolomite cement (DC) at 3765.5 m. Silica overgrowths (OG), where visible, appear to be inhibited along contacts between quartz grains and dolomite cement, and reveal some grains (such as this one) to be rounded. **(B)** Detrital quartz and chert (Ch) grains surrounded by ferroan dolomite cement at 3765 m (DC). Silica cement is restricted to local grain contacts, and dolomite cement inhibits silica overgrowths. Grains are angular to sub-round. A euhedral, polycrystalline detrital quartz grain is also shown (Eh). **(C)** Sedimentary lithic grain (Lt) and partially dissolved feldspar (F) at 3765 m. **(D)** Visible silica overgrowths (OG) at 3765 m. An overgrowth on one grain shows that at the time of silica growth the grains was rounded, whereas now it is sub-angular, implying subsequent abrasion, and it is adjacent to dolomite cement, which inhibits overgrowths elsewhere in the sample. Thus, it is interpreted to be inherited (IOG). **(E)** Secondary porosity and compaction of quartz grains at 3756.5 m. The porosity is interpreted to have been created by the dissolution of grains, either feldspar or unstable lithic grains. A quartz overgrowth (OG) is also shown. **(F)** Another view from 3756.5 m showing secondary porosity (grain dissolution), a quartz overgrowth and a feldspar with abundant alteration.

in its current position, these overgrowths are interpreted to have been formed during a previous sedimentary cycle, abraded during transport, and re-deposited.

A small population (estimated ~0.5-1%) of euhedral grains is present (Figure 3.2 B). These euhedral grains are not interpreted to be the product of authigenic silica growth, for several reasons. First, they are texturally out of phase with all other grains in this sample, even those that have quartz overgrowths are not as perfectly euhedral. Second, some of these euhedral grains are enclosed in dolomite cement, which inhibited authigenic silica overgrowths elsewhere. Finally, some of these grains contain exotic mineral inclusions, including muscovite and garnet, and none contain inclusions of cement, which would be the case if they had grown authigenically.

Feldspars are present, estimated in small amounts (~1-2%), but the presence of partially dissolved and etched feldspar grains and grain dissolution porosity indicates that the sandstone might have contained 3-4% feldspar grains originally. Based on grain relationships, the paragenetic sequence probably began with minor quartz overgrowths (unless all inherited) possibly accompanied by some feldspar dissolution, followed by pervasive dolomite cementation, burial, and further quartz cementation and feldspar dissolution.

The sample at 3756.5 m is dissimilar in that there is almost no dolomite cement and more compaction appears to have occurred; but in most other ways it is similar (Figure 3.2 E-F). The intergranular volume is much lower than in the pervasively cemented sandstones below (~20%), and bent lithic grains, fractured lithic and mineral grains and suturing of grains are all abundant; indicating that compaction significantly affected this section (Figure 3.2 E-F). The dolomite cement rhombs present do not show signs of dissolution, indicating that this area was not pervasively cemented early on. Quartz overgrowths are more common in this sample, and most grains appear to have partial euhedral faces and grain contacts are interlocking (Figure 3.2 E-F). Authigenic quartz growth and cementation probably was more extensive here because of the absence of dolomite. A subpopulation of euhedral grains is also present here, as below. Lithic fragments have sub-angular to rounded morphologies. Grains where the overgrowth-core boundaries are visible can be seen to originally have had sub-angular to rounded morphologies (Figure 3.2 E-F). No evidence for the inheritance of silica overgrowths can be seen here.

The visually estimated reconstructed compositions of framework sand grains from these samples are Q(82-86), F(3-6) and L(8-13), and thus these samples are estimated to be a mineralogically submature sublitharenites. Grain sizes range from fine to very coarse, and the samples are visually estimated to be moderately sorted overall, with predominantly upper medium-lower coarse grain sizes. Grain morphologies are somewhat hard to determine where quartz overgrowths are present, but appear to range from angular to rounded. Lithic grains are predominantly sedimentary in origin, including siltstones mudstones, and chert. Feldspars are potassium feldspars, including Carlsbad twinned orthoclase and tartan twinned microcline. A significant proportion of quartz grains (estimated~5-10%) are polycrystalline with strain fabrics, and may be igneous or metamorphic in origin (Dickinson, 1970). Detrital zircons, tourmaline and rutiles are common at 3756.5 m. The rutile grains are not interpreted to be authigenic because they are angular to rounded. Several glauconite grains were also observed at 3756.5 m. Prevailing grain morphologies at the time of deposition are difficult to determine, since there appears to be a mixture of grains with inherited and secondary in-situ authigenic quartz overgrowths (of which it is difficult to estimate relative proportions) and other grains that show angular to rounded morphologies. In any case, the sandstones are defined as texturally submature since they are not well sorted. As mentioned previously, a small population of euhedral quartz grains are present (Figure 3.2 B). These grains are texturally out of phase with the rest of the framework material, and have sharply defined crystal faces, embayments, inclusions of muscovite and garnet and some are polycrystalline. An authigenic origin for these grains is not considered likely since authigenic quartz overgrowths on other grains appear to have been inhibited by dolomite cements, and because they contain exotic mineral inclusions. Thus, they are interpreted as euhedral detrital grains.

3.2.2 Jurassic Sandstone #1

Five thin sections were analyzed from this sample, at 3640 m, 3634.5 m, 3624 m, 3615.5 m and 3606 m. There are significant variations in sandstone compositions from the bottom to the top of this formation based on analysis of these samples. First of all, the percentage of cement, composed of ferroan and minor non-ferroan dolomite, decreases upwards from ~32% at 3640 m to <<1% at 3606 m (Figure 3.3). Limestone carbonate lithic grains are abundant (~5-10%) at 3640 m, 3634.5 m and 3624 m, but are absent at 3615.5 m and 3606 m.

The sample at 3640 m has relatively high intergranular volume (~35%) consisting mostly of pervasive ferroan dolomite cement. This sample is visually estimated to be

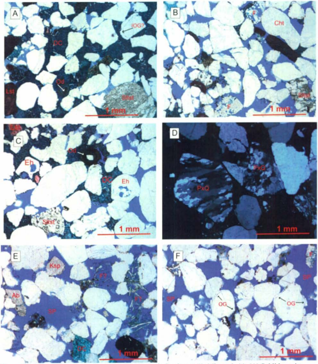

Figure 3.3: Photomicrographs of samples from Jurassic Sandstone #1, Mizzen L-11. (A) Sublitharenite cemented by ferroan dolomite at 3640 m. A quartz overgrowth (IOG) is interpreted as inherited since it has sub-angular (and thus abraded) edges. Limestone (Lst) and siltstone (Sltst) grains and ooids (Od) are also present. (B) Sample at 3634.5 m, including partially dissolved feldspar grains (F), chert (Cht) and Siltstone (Sltst) (C) Euhedral quartz grains (Eh) with pits and embayments at 3634.5 m, as well as siltstone (Sltst) and Limestone (Lst) grains and dolomite cement (DC). (D) Polycrystalline quartz grains (PxQ) at 3615.5 m, as seen in cross-polarized light. (E) Partially altered albite (Ab), K-feldspar (Ksp), secondary porosity and remnants of partially dissolved feldspars (F?) at 3606 m. (F) Quartz overgrowths (OG) are abundant, as seen at 3606 m. Where they can be seen, the original grains are rounded, implying that more of the quartz grains were originally rounded before silica overgrowths formed.

poorly sorted, and in light of this, an intergranular volume of 35% is quite close to what the original porosity value would have been before compaction (Beard and Weyl, 1973; Wordon and Burley, 2003). Based on this assumption and the absence of compaction related features (broken or bent grains, suturing), the pervasive ferroan dolomite cementation is interpreted to have occurred early (Figure 3.3 A). Quartz overgrowths are present in this sample, but mainly confined to spaces adjacent to remnant intergranular porosity (Figure 3.3 A). Most quartz grains that are enveloped by ferroan dolomite cement have sub-angular to rounded morphologies, but a few have euhedral faces suggesting the presence of quartz overgrowths. Some quartz grains where the grain-overgrowth boundary can be seen are partially abraded and totally enclosed within dolomite cement (Figure 3.3 A). They are interpreted as inherited. A few feldspar grains were observed, as well as mouldic grain dissolution porosity, indicating feldspar dissolution. Remnants of feldspar grains are also present in large patches of dolomite cement, implying the replacement of some feldspar grains by cement. Thus, detrital feldspars were more abundant in this sample preceding their dissolution and replacement.

In the rest of the samples, ferroan dolomite cement is patchy, filling large spaces between grains only locally, or not at all (Figure 3.3 B-F). Visually estimated porosity values are relatively high, ranging from approximately 20-30%. The porosity consists mainly of primary intergranular porosity, but also of a smaller yet significant proportion (2-5%) of secondary porosity. The secondary porosity is interpreted as predominately grain dissolution porosity based on the presence of grain shaped voids (grain moulds) lined with remnant clay minerals and feldspar overgrowths, and in the absence of any evidence for ferroan dolomite dissolution such as corroded grain boundaries (Figure 3.3

E-F). Most of the grain dissolution is interpreted to have been of detrital feldspars, based on the presence of some partially dissolved feldspar grains, remnant feldspar overgrowths and skeletal perthitic grains, and other feldspar grains present at various stages of alteration and dissolution (Figure 3.3 B, E-F).

Quartz overgrowths are relatively common in all samples except at 3640 m, where they were presumably inhibited by cement growth. It is difficult to determine the extent of authigenic quartz growth, because very few grains have visible overgrowth-core boundaries, but because of the abundance of euhedral faces and interlocking grain contacts suggest that silica overgrowths were abundant (Figure 3.3 B-F). Those grains where the core-overgrowth boundary is visible have sub-angular to rounded detrital core grains with significant silica overgrowths causing them to appear angular or subhedral (Figure 3.3 F). It is likely that many of the original detrital quartz grains in these samples were more rounded before authigenic cement growth, ranging in morphology from sub-angular to rounded. The lithic grains present are also sub-angular to rounded, further suggesting that these were the morphologies of quartz grains before silica overgrowths. There is no evidence to support the presence of inherited overgrowths on any grains.

The reconstructed framework compositions of these samples is visually estimated to be Q(71-82), F(3-9) and L(15-20), and thus they are estimated to range in composition from mineralogically submature to immature sublitharenites. Grain size ranges from fine to coarse, and in some samples from medium to coarse, and all of the samples with the exception of the section taken at 3640 m are well sorted. At 3640 m, the sample is poorly sorted and grains range in size from very fine to very coarse. With the exception of the sample taken at 3640 m, the sampled sandstones are defined as texturally mature, but not supermature because they are well sorted but are not dominated by rounded framework grains. The sample at 3640 m in defined as texturally submature because it is poorly sorted. It should be noted, however, that the grains in these samples are better rounded on average than in other sandstones in this study, and range from sub-angular to rounded. The feldspar grains present (in other words, those not dissolved) are sericitized and include relatively unaltered plagioclase and orthoclase (Figure 3.3 B, E).

Limestone (carbonate) lithic grains, mostly composed of non-ferroan calcite, are the predominant lithic grain type at 3640 m, 3634.5 m, and 3624 m, but are absent at 3615.5 m and 3606 m. The limestone grains include crystalline and fossiliferous types, as well as ooids cored by either calcite or quartz. Their absence at 3615.5 m and 3606 m implies that these grains may be absent throughout the upper part of the unit. They might have been present at one time but were subsequently dissolved. However, evidence of remnant feldspar overgrowths and partially dissolved feldspar grains indicates that most of the grain dissolution affected detrital feldspars (Figure 3.3 E), so it may be the case that limestone grains were never present in the upper part of this sandstone.

Most of the rest of the lithic grains are similar in composition to those present in Jurassic Sandstone #2, including siltstone, mudstone and chert. As in Jurassic Sandstone #2, significant mounts of quartz grains (~5-10%) are polycrystalline with strain fabrics (Figure 3.3 D). A very small percentage (<<1%) of euhedral quartz grains, similar to those noted from samples in the Jurassic Sandstone #2, were observed in these sample; however, due to the abundance of silica overgrowths in these samples it is more difficult to rule out an authigenic origin for these grains (Figure 3.3 C). Detrital zircons are abundant at 3624 m.

3.2.3 *Baccalieu Sandstone*

One thin section was analyzed at 3426 m. This sample is of sandstone comprised mainly of quartz and lithic grains and pervasively cemented by ferroan dolomite (Figure 3.4). Grain sizes ranges from fine to very coarse, but on average are fine, and the sample is visually estimated to be moderately or poorly sorted. There is essentially no porosity in this sample. Many of the lithic grains in this sample are composed of mudstone, and are flattened and bent around quartz grains and more coherent lithic grains. Also, the estimated intergranular volume in this sample is quite low (~15%). Therefore, it is likely that compaction probably occurred before the pervFasive ferroan dolomite cementation. Some silica overgrowths are present; however, the growth of silica cement is inhibited by mudstone fragments. Therefore, the few that are seen are interpreted as inherited (Figure 3.4 C). Feldspar grains are rare, and they do not show evidence for being significantly altered to clays or dissolved (Figure 3.4 D), and thus the amount of feldspar grains present is though to be the same as the original amount.

This sample has an estimated reconstructed modal framework composition of Q(64), F(1) and L(35), and thus in classified as a mineralogically immature lithic arenite. As previously mentioned, mudstone makes up many of the lithic grains, but a variety of other types are present including limestone, dolostone, siltstone and chert (Figure 3.4 A-C). Limestone and dolostone fragments are crystalline, micritic and fossiliferous, and some quartz and calcite cored ooids are also present. Detrital zircons and tourmalines are

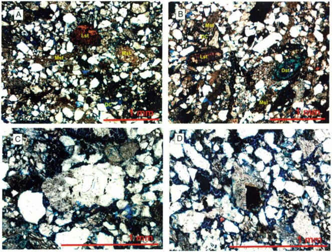

Figure 3.4: Photomicrographs of samples from 3426 m in the Baccalieu Sandstone, Mizzen L-11. **(A)** and **(B)** show the general composition of the sandstone at this location. Quartz and mudstone (Mst) lithic grains predominate, and the latter forms a pseudomatrix that makes the sample appear to be a wacke. Limestone and dolostone (Lst and Dst) grains are also common, and both crystalline and fossiliferous types are present. **(C)** In the centre of the photomicrograph is a silica-cemented siltstone, showing the potential for inheritance of quartz overgrowths. Larger quartz fragments in the sample also show inherited quartz overgrowths. **(D)** Feldspar grains, such as the one in the centre of this photomicrograph, are rare, but are relatively unaltered.

abundant in this sample. Glauconite is also present. Grain morphologies are angular to sub-rounded. The sample is classified as texturally submature, do to its poor sorting.

3.2.4 Baccalieu I-78: Early Cretaceous (Berriasian) Sandstones

Two thin sections were analyzed at 3292.2 m and 3304.5 m. This section at 3292.2 is of lithic sandstone cemented by ferroan dolomite. No porosity or matrix is present. Compaction appears to have occurred before cementation, as most soft lithic grains are flattened and deformed parallel to bedding, and the intergranular volume is approximately 5% (Figure 3.5 A). There are no feldspars or evidence for the past presence of feldspars, such as partially dissolved or altered grains, secondary porosity, or pseudomatrix. Visually, the sand grains are estimated to be moderately to well sorted, and overall are upper medium to coarse grained. Most of the grains are angular to sub-angular. Lithic grains, which form the bulk of this sample, are composed predominantly of mudstone and shale, with lesser amounts of siltstone and chert, and very minor calcareous limestone (Figure 3.5 A).

The section at 3304.4 m is different texturally. It is poorly sorted, with very angular to angular framework grains (Figure 3.5 B). Calcite cement is present but is minor due to low intergranular values. No porosity is present. The framework composition is similar to the sample at 3292.2 m, with predominant sedimentary lithic grains, very little quartz and no feldspar. Most lithic grains are siltstone fragments, but mudstone, sandstone and bioclastic limestone fragments are also abundant. Ooids are also very abundant (Figure 3.5 B).

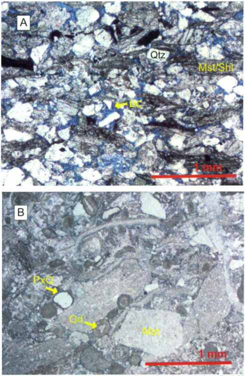

Figure 3.5: Photomicrographs of samples from the Berriasian aged sandstones in Baccalieu I-78. Both samples are lithic arenites. **(A)** Lithic grains composed of mudstone and shale (Mst/Shl) dominate at 3292.2 m, with lesser amounts of quartz (Qtz). The sandstone here is cemented by ferroan dolomite cement (DC). **(B)** The sample at 3304.5 m is poorly sorted and contains less quartz (most of which is polycrystalline, PxQ) and more lithic grains than at 3292.2 m. Ooids (Od) are also common here.

The estimated modal framework compositions of these samples are Q(5-15), F(0) and L(85-95), and thus the samples are estimated to be mineralogically immature lithic arenites. Texturally, the sample at 3292.2 m is mature, while the sample at 3304.5 m is submature.

3.2.5 Hibernia Formation Equivalent

Thin sections from this unit were analyzed from 3199.4 m, 3209 m, 3232.7 m and 3273.2 m. Despite the size of section between these sample locations, the composition and textures of all of the analyzed samples are very consistent. Grain sizes are consistent between all samples, ranging from fine to medium, but most grains are fine and the samples are visually estimated to be well sorted. Most samples contain very little or no cement (except at 3273.2 m), significant amounts of clay matrix and mostly primary intergranular porosity. The clay matrix may in large part be a "pseudomatrix", made up of what was originally mudstone or other clay rich libel lithic grains that were deformed around quartz grains and coherent lithic grains during compaction. This interpretation is evidenced by the compaction of discrete fragments of distinct looking clay material between quartz grains (Figure 3.6 C).

Cementation by ferroan dolomite is only abundant at 3273.2 m, where it has filled primary intergranular porosity. The cementation is not thought to have occurred after compaction because the intergranular volume is low (~10%) and soft lithic fragments are bent and deformed around quartz grains. In the rest of the samples, ferroan dolomite cement is rare or absent. Porosity values are also low in most samples, and porosity types

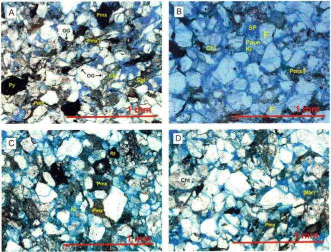

Figure 3.6: Photomicrographs of samples from the Hibernia Formation Equivalent in Baccalieu I-78. In all samples, libel lithic grains, mostly mudstone and clay-rich grains, are deformed between coherent quartz grains, forming a "pseudomatrix" (Pmx). **(A)** Quartz overgrowths (inherited?) (OG) can be seen at 3199 m, as well was detrital chlorite (Chl), shale fragments (Shl) authigenic pyrite (Py), and clay matrix and/or pseudomatrix (Pmx). **(B)** Several detrital feldspars (F), partially altered to clay minerals, are present at 3209 m, as well as kaolinte pseudomatrix (Pmx:Kl) and secondary porosity(Sp), which may have formed by the breakdown of feldspars. Other clay rich pseudomatrix (Pmx) is present here, as well as detrital chlorite (Chl). **(C)** At 3232 m, it is clear that interstitial clay matrix is probably pseudomatrix (Pmx) originating as clay-rich lithic grains that were subsequently altered and/or deformed between quartz and coherent lithic grains. Also shown is rutile, which is intergrown with a small silt sized quartz grain, and may be authigenic in origin **(D)** This view at 3232 m shows a relatively quartz-rich part of the section, with matrix and pseudomatrix (Mtx and Pmx) as well as detitial muscovite (Ms) and chert (Cht).

are mainly restricted to primary intergranular porosity. Compaction has occurred, evidenced by low intergranular volumes (15-25%), and in some cases intense deformation of lithic grains around more competent quartz grains (Figure 3.6 A, C). There is only rare evidence to suggest that dissolution of has occurred (Figure 3.6 B). Quartz overgrowths were rarely observed; and may be interpreted as inherited overgrowths, based on abrasion around their edges and an overall lack of silica cement observed in the samples. Authigenic siderite and pyrite are present locally. A euhedral rutile was observed at 3232.7 m, and appeared to be intergrown with other detrital material, suggesting either that it is authigenic TiO_2, or has an authigenic overgrowth (Figure 3.6 C).

Feldspars are rare, and there is no evidence to suggest that dissolution of these grains occurred; however, most grains of feldspar are partially sausseritized or altered to clay minerals (Figure 3.6 B). Rare secondary porosity and kaolinte "pseudomatrix" was also seen locally, suggesting the breakdown of feldspar grains (Figure 3.6 B). Such evidence suggests that some of the feldspars may have been completely altered and now appear as interstitial clay. Thus the matrix present in these samples may be, in large part, a pseudomatrix created by the deformation and alteration of lithic grains and alteration of detrital feldspar grains, similar to that noted by Dickinson (1970) and Whettan and Hawkins (1970); and the original proportion of detrital feldspars may have been higher than what is now observed.

It is difficult to precisely reconstruct modal abundances given the interpretation that a pseudomatrix had formed by the breakdown of less stable grains. The reconstructed modal framework compositions are made assuming that some matrix was detrital in nature; but, it is hard to determine how much. Much harder to reconstruct is the original percentage of feldspar grains that may have been present, if at all much different from what is presently observed. Estimated reconstructed modal abundances are Q(72-78), F(3-5) and L(17-24). Therefore, the samples are estimated to have the composition of mineralogically submature sublitharenites to immature lithic arenites. Compositions of lithic grains include mudstone, shale, limestone (fossiliferous and crystalline), dolostone, siltstone, and chert (Figure 3.6 A-D). Detrital zircons, tourmalines and rutiles are present and variably abundant. Detrital muscovite and chlorite are also present in small amounts (Figure 3.6 A-B, D).

3.2.6 Avalon Formation Equivalent

Samples from this unit were analyzed at 2183 m, 2180 m, 2177.8 m and 2177 m. Most of the samples are similar, comprising fine sand and abundant clay matrix, with the exception of 2177.8 m, which has almost no matrix (Figure 3.7). Texturally, the samples show a strong ichnofabric that is characterized by inhomogeneous mixing between clay matrix and fine sand particles. In some areas of the sections, porosity is enhanced and sand predominates, while in other areas clay matrix has completely occluded all porosity (Figure 3.7). Clearly the ichnofabric is strong, and the effect of burrowing on modifying original depositional textures and mixing clay and sand is probably significant. Very little authigenic minerals are present and include siderite and pyrite. Quartz overgrowths are not evident.

Detrital feldspars are present, but rare, in these samples, apparently including some small amounts of albite (Figure 3.7 B). Most of the feldspar grains are present in

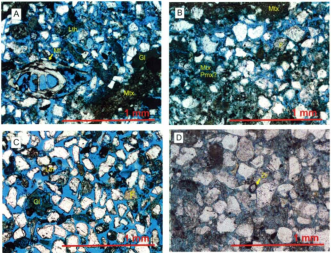

Figure 3.7: Photomicrographs of samples from the Avalon Formation Equivalent in Baccalieu I-78. Due to the bioturbation of this unit, mixtures of clay and sand, low porosity clay rich zones and high porosity sand rich zones are irregularly distributed. **(A)** Microfossils (Mf, a foram?) at 2171 m. There are present in all samples, as well as glauconite (Gl). Lithic grains (Lth) are predominantly clay rich mudstones or siltstones. **(B)** Feldspars (F), such as the ones shown at 2171 m, are present in all samples, but relatively uncommon; and where they do occur they are generally partially altered. Because of the large amounts of matrix, as well as the effects of textural inversions induced by bioturbation, it is hard to distinguish between matrix and pseudomatrix (if the latter is even present). **(C)** A high porosity sand rich zone at 2177 m, showing mostly quartz but also sedimentary lithics (Lth), feldspar (F) and glauconite (Gl). **(D)** Detrital zircons, such as the one shown at 2180 m, are common accessory minerals, as are detrital tourmalines.

various stages of alteration into sericite and other clay minerals, and there is no evidence to suggest dissolution of feldspar grains, such as secondary porosity or intragranular dissolution porosity in any of the grains. Assuming that much of the grains had been broken down into clays forming a pseudomatrix, it is still difficult to estimate a reconstructed proportion of the detrital feldspar originally present, because estimating pseudomatrix proportions is made difficult. This is because the samples appear to have originally contained abundant detrital clay matrix, and because it is difficult to quantify the effects of the bioturbation with regards to mixing between clays and sands in adjacent beds and texturally inverting material. The burrowing may have increased the depositional proportion of clays and sands, as well as redistributing or removing pseudomatrix. Given that the estimated proportions of detrital feldspar grains present is between 1% and 3%, reconstructed proportions may be anywhere between 5% and 10%, or may the same as the present values estimated.

As mentioned above, modal sand grain compositions are difficult to reconstruct in this case, due to the effects of bioturbation. The estimated framework proportions of the samples, without trying to reconstruct original compositions, are Q(79-90), F(4-6) and L(6-16). Based on the sand-sized population, the samples are defined as mineralogically submature. Estimated classifications include arkosic wacke, lithic wacke, and lithic arenite. Visually, the sand grains are interpreted as well sorted. Because of the high percentage of matrix in all samples except at 2177.8 m, most sections are classified as texturally immature. However, it is hard to determine the effect of bioturbation on the abundance of clay matrix and textural inversions observed, as it has been shown that intense ichnofabrics can significantly alter the original textures and distribution of clays and sands (Pemberton et al., 2001; Taylor et al., 2003). Lithic grains include chert and mudstone. Accessory heavy minerals are present and include zircon, tourmaline and rutile (Figure 3.7 D). Glauconite, muscovite grains and foraminiferous microfossils are also present (Figure 3.7 A, C).

3.3 Petrographic interpretations

3.3.1 *Jurassic Sandstone #2*

The textural sub-maturity of material in this unit alludes to a mixture of grain components with differing sources and/or weathering and transport histories. For example, grain sizes and morphologies of the detrital grains are highly variable, ranging from rounded to angular, and with even a small population of euhedral detrital grains (Figure 3.2 B). In this way, not only are the framework grains poorly sorted, but they display inherent differences in sizes and morphologies, interpreted to have been induced by varying provenance and transport histories.

Several factors suggest that at least a significant portion of grains are recycled from previous sediments. First of all, the bulk modal composition is mineralogically submature, with predominant monocrystalline quartz grains and subordinate lithic grains of sedimentary origin, which is similar to the modal sand composition of sand derived from pre-existing sedimentary rocks in several documented cases (Dickinson and Suczek, 1979; Critelli et al., 2003; Arribas and Tortosa, 2003). Also, there is some textural evidence to support the presence of inherited quartz overgrowths, and abundant ultrastable heavy minerals are present in one sample, both of which are diagnostic characteristics of sedimentary recycling (Hubert, 1962; Sanderson, 1984). Conversely, however, the poor to moderate sorting, average large size of grains and presence of large potassium feldspars, lithic grains, euhedral quartz and polycrystalline quartz indicates a lack of prolonged attrition of grains, thus suggesting that recycling may not have been a factor (Blatt and Christie, 1963; Suttner et al., 1981; Cox and Lowe, 1995a). It is likely, since the proportion of feldspar and polycrystalline quartz are relatively low, and that the lithic grains are themselves sedimentary in origin, that recycling of material was significant, but also were inputs from first-cycle sources. It is difficult to quantify the proportion of material which may have been recycled, but due to the abundance of monocrystalline quartz and especially of sedimentary lithic grains, it is interpreted to have had a relatively large recycled component, but also notable inputs of first-cycle material. Heavy mineral analyses in the following chapters will further go to access the degree of recycling.

Intuitively, the poor sorting is interpreted to have been caused by rapid deposition of bed load material, and therefore can be thought of as a good representation of the entire sand size population as influenced by provenance and sorting during transport. Overall, the samples comprise texturally and mineralogically immature sand. It is possible for tributaries to deliver fresh material to large drainage systems at any point, thus downstream decreases in textural and mineralogical maturity are possible (Ouma, 1967; Blassi and Manassero, 1990; Demir, 2003; Picard and McBride, 2007). Also, transport alone, especially in high gradient drainage systems, cannot remove feldspar and libel lithic grains completely, only reduce them (Blatt and Christie, 1963; Suttner et al., 1981; Blassi and Manassero, 1990; Cox and Lowe, 1995a; Picard and McBride, 2007). Thus, low textural maturity, including poor sorting and lack of abundant well rounded grains, and mineralogical sub maturity does not necessarily indicate that transport distances for the bulk of the material was short. Most likely, the sandstone comprises a mixture of material that is derived proximally and distally, and may have been linked by a large drainage system, or may not have been.

In summary, the deposit is interpreted to comprise a mixture of recycled and first-cycle material and of distally and proximally sourced material. Recycled source lithologies appear to include undeformed siliciclastic rocks (mudstone, siltstone, chert, and probably sandstone) as well as some low-grade metasedimentary rocks. First cycle source lithologies correspond to angular and euhedral quartz grains, polycrystalline quartz grains and potassium feldspar grains, including microcline and orthoclase. The most likely source lithologies would be of felsic igneous rocks, definitely from granites but possibly also from felsic volcanics.

3.3.2 Jurassic Sandstone #1

This unit differs from Jurassic Sandstone #2 in several important ways. First of all, it is texturally more mature, being well sorted and having a grain population that appears to be overall more rounded. Secondly, and conversely, it is mineralogically more immature, having a higher range in reconstructed modal feldspar (2-8% in this unit, in contrast to 3-4% in Jurassic Sandstone #2) and lithic grains (10-15% in this unit, in contrast to 5-10% in Jurassic Sandstone #2). It should be noted, however, that these changes are not drastic. One notable change is the difference in the compositions of lithic and feldspar grains. In this unit, calcareous limestone grains are abundant and even predominant over of lithic grains locally, and in this unit albite grains are present as well as orthoclase and microcline.

There is not abundant textural evidence to support either recycling of material or long transport of material, even though material in this sample is overall more texturally mature. Although sorting of material has been liked the attrition of grains through recycling and/or long transport, sorting by these means leads to an overall reduction of grain sizes through time (Blatt and Christie, 1963; Cox and Lowe, 1995a). Here, this is not the case, since grain sizes are medium to coarse; thus the more likely mechanism for sorting in this case is bed load sorting in a high energy depositional regime. This inference is supported by the presence of ooids, which also occur in high energy depositional settings where agitation of grains occurs (Davies et al., 1978). It is it is clear that the roundness of grains is on average higher in this unit than elsewhere; however, in many cases grain roundness cannot be attributed to transport distance (Ouma, 1967; Cox and Lowe, 1995a; McBride et al., 1996; Demir, 2003; Picard and McBride, 2007).

The compositions of lithic grains, which includes calcareous limestone, siltstone, mudstone, chert and low grade metasedimentary rocks, indicates that sourcing from older sedimentary rocks, and thus recycling of material, occurred, providing some detritus. However, the presence of feldspars, some relatively unaltered and including albite, as well as polycrystalline, probably metamorphic, quartz indicates that significant inputs of proximally derived and/or first cycle material was present, and was more significant in this unit than in Jurassic Sandstone #2.

It is difficult again, as it was for Jurassic Sandstone #2, to determine the relative inputs from recycled versus first-cycle material, but clearly inputs from both were present, with more first-cycle material being present in this unit. Transport distances are hard to determine, either texturally or mineralogically, as the increased textural maturity of this unit may be the result of high energy deposition and transport over relatively short distances in such conditions, and because fluvial transport distance may not significantly affect the mineralogical maturity (Suttner et al., 1981; Blassi and Manassero, 1990; Cox and Lowe, 1995a; Picard and McBride, 2007). It is clear that proportions of some components, such as libel lithic grains, would probably have been reduced prolonged transport (>100 km), so that either these components are relatively proximally derived (but others may not be), or the proportion of these lithologies in distal hinterlands were much higher, and became reduced during transport; a process that has been recorded by Blassi and Manassero (1990), and Picard and McBride (2007).

In summary, this unit contains a mixture of first-cycle and recycled material, with more first-cycle input than the older Jurassic Sandstone #2. It is difficult to determine the proportions of recycled and first-cycle material. Similar to Jurassic Sandstone #2, none of the textural or mineralogical evidence is diagnostic for interpreting transport distances. The compositions of lithic grains show that some sources, probably proximal sources, include limestone carbonates and siliciclastic sedimentary rocks, some with low metamorphic grade. The presence of polycrystalline quartz (some with strain fabrics), euhedral quartz albite and potassium feldspar grains indicates potential first-cycle inputs from granites, gneisses and felsic to intermediate volcanic rocks.

3.3.3 Baccalieu Sandstone

This sandstone is classified as a mineralogically immature lithic arenite, with a modal abundance of lithic grains at ~35%. Most of the lithic grains are mudstones, but significant amounts of siltstone, fine grained sandstone and limestone grains are also present. Quartz is relatively abundant, not to the point of mineralogical maturity or submaturity, but is still the largest framework component. Sourcing is interpreted to have been predominantly from pre-existing sedimentary rocks, due to the abundance sedimentary lithic grains and quartz grains, some of which show inherited silica overgrowths (Figure 3.4 C). Feldspar grains are so rare that it is difficult to envision much fist-cycle input of material, and no other indicators of first cycle material are present. The transport distances for this sand was likely to have been relatively short, because of the mineralogical immaturity and the abundance of libel lithic grains, which would be expected to be significantly reduced during long (>100km) transport (Blassi and Manassero, 1990; Cox and Lowe, 1995a; Picard and McBride, 2007). However, although the input of libel lithic grains is presumably relatively proximal, other components such as quartz may have been derived from farther away, with the addition of libel grains occurring downstream due to addition of material from proximal tributaries.

3.3.4 Baccalieu I-78: Early Cretaceous (Berriasian) Sandstones

The sections analyzed from this interval are estimated to be mineralogically immature lithic arenites, comprising lithic grains at a high modal abundance (estimated~85-90%). The large majority of these grains are composed of mudstone and shale, with lesser amounts of siltstone and chert, and very minor calcareous limestone, implying that the source area contained abundant clastic sedimentary material (shale and mudstone mainly) with subordinate amounts of carbonates. The transport distances for this sand was likely to have been relatively short, because of the mineralogical immaturity and the abundance of libel lithic grains, which would be expected to be significantly reduced during long (>100km) transport (Blassi and Manassero, 1990; Cox and Lowe, 1995a; Picard and McBride, 2007). A scenario involving uplift of an adjacent rift shoulder or shoulders, and erosion of sedimentary rocks from this uplifted area or areas is likely.

3.3.5 Hibernia Formation Equivalent

These samples appear to be of sandstones that are mineralogically mature, but texturally immature, because they contain >5% matrix and are relatively enriched in quartz grains. However, when one considers the effect of pseudomatrix, in other words, false detrital matrix formed in-situ by the breakdown and compaction of lithics and feldspars into clay minerals, the samples can instead be considered to be mineralogically submature and texturally mature or submature. These criteria are thus used to interpret the provenance of this unit.

The well sorted nature and average small grain size of the sand fraction can be interpreted to represent one of two scenarios: (1) grain abrasion and attrition causing small grain sizes and/or upstream sorting out of larger grain fractions during prolonged transport (e.g. Moss 1972), or (2) inheritance of a well sorted and fine grain population with little modification from transport. The latter scenario might imply grain sorting and attrition occurring in a previous sedimentary cycle, as successive recycling of sandy material is thought to cause a gradual decrease in average grain size and increase in sedimentary sorting (Cox and Lowe, 1995a). Thus, it is possible that either long transport distances, or sedimentary recycling, or a combination of both could be attributed as creating the textural properties of these framework grains. However, such interpretations should include intimate knowledge of the depositional setting of the sandstone, or else the proximal causes of grain size sorting may be overlooked. For example, in fluvial settings better sorted suspended load material could be deposited close to coarse bed load material, through the deposition of overbank deposits. Therefore, grain sorting into small size fractions can occur locally, and interpreting the influence of large scale factors such as sedimentary recycling and transport distance also requires a detailed knowledge of the depositional setting.

Mineralogically, the samples are classified as submature; however, this is based on the inference that much of the original feldspar was altered into a clay mineral "pseudomatrix". In any case, as was discussed during interpretations of the older sandstone intervals, the modal framework composition, and classficiation of the samples as sublitharenites with exclusively sedimentary lithic grains and very little feldspar grains implies a predominance of sedimentary rocks in the source area, and thus sedimentary recycling (Dickinson and Suczek, 1979; Critelli et al., 2003; Arribas and Tortosa, 2003). For certain, this sandstone has less feldspar grains than, and an indeterminate amount (possibly very small) of completely altered or dissolved grains. This may reflect either (a) increased recycling from other intervals, (b) increased weathering or (c) increased transport distance. It may also have been a combination of these factors.

In summary, there is abundant evidence to support that much of the material in this sandstone was recycled and may have experienced long transport before being deposited. There does not appear to be abundant evidence of input from first-cycle sources; although feldspars may be derived from granitic or volcanic rocks, and detrital chlorite and muscovite may be from low grade or retrograde metamorphic assemblages.

3.3.6 Avalon Formation Equivalent

Samples from this unit show irregular distributions of sand and clay matrix and textural inversion, and core analysis shows an interval that is intensely bioturbated. Therefore, it is not possible in the scope of this study to interpret the original textures present. Some things that can be taken from the intensity of bioturbation are that (a) during, or soon after deposition, the setting was sufficiently low energy as to allow colonization, and (b) the sedimentation rate may have been quite low (Pemberton et al., 2001; Taylor et al., 2003). In any case, the textural inversions observed in thin section are interpreted to have been influenced by bioturbation.

Ignoring the matrix, the sand sized fraction is well sorted and overall quite fine grained. These textural characteristics can be attributed to sedimentary recycling, long transport distance, or a combination of both (Moss 1972; Cox and Lowe, 1995a); however, it should be noted, as for the Hibernia Formation equivalent, that an intimate knowledge of the depositional setting (in other words, proximal effects on textural maturity) should be established before such large scale interpretations are made based on textural evidence.

In these samples, feldspar is present, as are lithic grains; however, it is hard to determine what the proportions of these components were before intense bioturbation and diagenetic alteration. Since they are both present in small but significant amounts (4-5% modal abundance for feldspars, 2-10% for lithics) it is perhaps reasonable to assume that their modal compositions are similar to that of the underlying sandstones, which are predominantly sublitharenites (making these samples, technically speaking, lithic arenites). Therefore, the predominance of quartz with sedimentary lithic grains suggests that derivation from pre-existing sedimentary rocks was significant, with lesser amounts of first-cycle material (Dickinson and Suczek, 1979; Critelli et al., 2003; Arribas and Tortosa, 2003).

3.3.7 Summary

It would appear that recycling of clastic material contributed detritus to all intervals, and predominant in some, based on estimated modal compositions comprising mainly quartz and sedimentary lithics. The overprinting effects of weathering are not easily determined, but it may be that the Early Cretaceous sandstones (Berriasian Sandstones, Hibernia Fm and Avalon Fm) may have been more affected due to prevailing humid tropical conditions during that time (Abbink et al., 2001). In any case, intense weathering did not occur, as is evidenced by the presence of lithic grains and feldspars in all intervals. Framework material implying significant inputs of fist-cycle material, including feldspar (albite and K-spar), euhedral quartz grains and strained polycrystalline quartz grains, are present in small amounts in most intervals, but most abundant in Jurassic Sandstone #1. Most of the first cycle material is interpreted to have been igneous in origin.

Except in cases of textural and/or compositional immaturity (eg., Berriasian Sandstones in Baccalieu I-78), transport distances of detrital material is not easily interpreted using textural or compositional constraints. This is because many other factors (including weathering, recycling) have a much greater effect on these constraints; and, because the proximal effects of textural modification must be recognized through an intimate understanding of the depositional setting of the sandstone, which is not present in this case, where only well bore data is available. Thus, the issue of transport distance will be addressed later in the thesis, using constraints from detrital zircon geochronology and morphological analysis.

Chapter 4: Detrital Heavy Mineral Data

4.1 Introduction

This chapter gives a summary of proportions and ratios of detrital heavy minerals compiled using grain counts made with a scanning electron microscope. It also gives a discussion of using these heavy mineral ratios for provenance fingerprinting and for use as a proxy for mineralogical maturity and sedimentary recycling. The detrital heavy mineral methodology and data from each study interval are described in this chapter. Data sheets with heavy mineral data for each sample interval are located in Appendix 2 of this thesis. Grain counts of detrital heavy minerals (zircon, tourmaline, rutile, apatite, monazite, titanite and chromite) are used to calculate provenance-sensitive heavy mineral indexes to aid in provenance discrimination, sedimentary correlations, and assessing mineralogical maturity and/or sedimentary recycling. Backscattered electron images of some of the detrital heavy minerals are shown in Figure 4.1.

4.2 Methodology

4.2.1 Sampling and processing

Fifty gram industrial well cuttings samples were obtained from the C-NLOPB core repository and some supplementary 300-500 g were obtained from the respective well operators. Mature to sub-mature sandstone intervals were the main target for

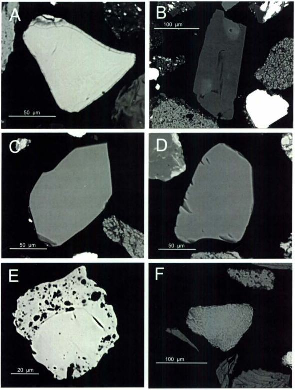

Figure 4.1: Backscattered electron images of various detrital minerals from this study. (A) Detrital chromite, from Mizzen L-11 3415m-3420m (Baccalieu Sandstone). (B) Detrital calcic amphibole from Mizzen L-11 3615m-3620m (Jurassic Sandstone #1). (C) Detrital apatite from Mizzen L-11 3615m-3620m (Jurassic Sandstone #1). (D) Detrital tourmaline from Baccalieu I-78 2165m-2170m (Avalon Fm Eq). (E) Detrital monazite from Baccalieu I-78 2165m-2170m (Avalon Fm Eq). (F) Detrital rutile from Baccalieu I-78 3300m-3305m (Berriasian Sandstones).

sampling, since these more sorted sediments are more likely to contain a higher proportion of detrital heavy minerals, including zircons (Cox, 2003).

The cuttings samples were first gently crushed to disaggregate mineral grains. Next the disaggregated samples were washed with warm water and dish soap and sieved through a 41 micron mesh in order to remove drilling mud and any particles too small for analysis. The cleaned cuttings were then separated into 41-500 micron and >500 micron size fractions. The 41-500 micron grains were used to obtain heavy mineral grains by gravity separation in the heavy liquid bromoform, with a specific gravity of 2.8 g/cm^3.

Heavy mineral grains from the 41-500 micron heavy fractions were split into 41-63 micron, 63-177 micron and 177-500 micron size fractions using a microsieve. The 63-177 micron heavy fractions were split using a sampler riffler and then mounted in 30 mm rings using a 2 part epoxy/resin procedure and polished to expose the grains. The reason for using this size fraction will be reviewed in the next section.

4.2.2 Analytical methods

Mineral identification and quantitative estimates of the proportions, and sizes and shapes of grains in the mounts have been made in automated fashion using a scanning electron microscope (SEM) equipped with and energy dispersive x-ray (EDX) spectrometer mineral liberation analysis (MLA) software. The samples were run in X-ray modal analysis mode (XMOD) as described in Gu (2003). The apparatus used includes an FEI Quanta 400 environmental SEM installed with a Bruker AXS XFlash® 3001 SDD x-ray detector. Mineral grain identification was achieved using MLA software from JKTech at the University of Queensland Australia. The MLA XMOD technique first relies on backscattered electron imaging (BEI) as a measure of average atomic number for discriminating grain and compositional boundaries, and then relies on rapid EDX spectrometry for obtaining mineral spectra of all outlined grains and areas within grains with varying backscattered electron intensities (Gu, 2003).

During the MLA run, voltage was set to 25 KeV, incident beam current was 12nA with a spot size of 7.3-7.5 microns, the working distance was 12mm, and x-ray acquisition time was 20ms. Between 10,000 and 40,000 particles were discriminated and analyzed by EDX in each sample (Appendix 2).

Mineral EDX spectra standards were compiled manually from within the samples by the identification of individual mineral spectra. These standards were then matched to all unknown spectra from each sample using the MLA Image Processing Tool software in order to identify all mineral phases. Grain counts of minerals of interest (including zircon, tourmaline, monazite, apatite, ilmenite, rutile and chromite) were then done manually using a search function on the MLA Viewer software.

It should be noted that it was the intention to also study detrital garnets; however, the MLA method did not effectively discriminate detrital garnets from the relatively abundant grains comprised of finely disseminated ankerite, pyrite, carbonates, micas and clays, due to similarities in EDX elemental peaks obtained from spot analyses.

The mineral barite ($BaSO_4$) was an abundant contaminant in all heavy mineral fractions, due to its presence as a drilling mud additive. The presence of barite is not expected to have altered the naturally occurring abundances of other important heavy minerals, as most industrial barite is derived from evaporate deposites, in close association to other sulphate minerals such as gypsum and anhydrite, and is not associated with the mineral phases from this study, which are associated with crystalline igneous and metamorphic rocks.

4.2.3 Heavy mineral analysis methods

Heavy mineral analysis (HMA) has commonly been applied to provenance studies of sandstones in the past (Hallsworth et al., 2000; Morton et al., 2002; Morton et al., 2005). This study follows the detrital heavy mineral methods as initially utilized by Morton and Hallsworth (1994) and refined by Morton and Hallsworth (1999). Their approach utilizes ratios of detrital heavy mineral pairs for "fingerprinting" sandstone provenance in order to detect changes in provenance through time and correlate units with similar provenance fingerprints on a basin-wide scale. The ratios use mineral pairs that are not significantly differentiated by hydraulic differentiation during transport and deposition or by dissolution during diagenesis. This is done by choosing pairs of minerals with similar densities ($dA/dB{\sim}1$) and that are stable during burial diagenesis. The conventional ratios include the apatite-tourmaline index (ATi: 100 x apatite count/(total apatite + tourmaline)), monazite-zircon index (MZi: 100 x monazite count/(total monazite + zircon)), rutile-zircon index (RZi: 100 x rutile count/(total rutile + zircon)) and the chromite-zircon index (CZi: 100 x chromite count/(total chromite + zircon)).

Because of inherent differences in the grain sizes of heavy minerals (for example, zircons are typically 40-200 μm, whereas garnets and tourmalines have a much greater size range) these ratios were measured for heavy minerals within a limited fine sand size bracket (63-177 μm) in which all of the heavy minerals are considered to exist inherently (following the method outlined by Morton and Hallsworth, 1994). Average sizes for each mineral phase in each sample have been calculated using MLA data and are given in **Appendix 2.** The ratios of the average sizes of mineral phases that constitute the provenance-sensitive mineral ratio pairs (e.g. average size monazite/ average size zircon, or M/Z_{size}) are also given for each sample in **Appendix 2**, and are shown to have values near 1 in most cases, implying that overprints of size sorting is negligible, and that the 63-177 μm size fraction is appropriate. For example, the average M/Z_{size} from all samples is 0.96 ± 0.5, the average A/T_{size} is 1.35 ± 0.5, the average R/Z_{size} is 1.15 ± 0.2 and the average C/Z_{size} is 1.1 ± 0.6. Therefore, overprints from the effects of hydraulic processes of grains from mineral pairs in this study should be negligible, given that both the densities and the grain sizes are very close.

All of the detrital phases used in the heavy mineral ratios (apatite, tourmaline, zircon, monazite, rutile and chromite) have been shown, in multiple cases of burial diagenesis up to 4 km, not to be subject to significant etching or dissolution (Morton, 1979; Smale and Morton, 1987; Milliken, 1988; Morton and Hallsworth, 1999). Interestingly, even though apatite is typically susceptible to acidic dissolution during weathering, it does not appear to be affected during burial diagenesis, even when dissolution of other unstable phases have occurred, presumably by the circulation of fluids rich in organic and carbonic acids. The reason for this is poorly understood (Morton and Hallsworth, 1999). Although garnet was not easily measured in the heavy mineral samples, it is a mineral that is susceptible to dissolution during burial diagenesis, especially past burial depths of 3 km (Morton, 1984), and thus it was considered justified that no great effort was made to measure the garnets.

The Zircon-Tourmaline-Rutile (ZTR) index is a measure of the percentage of combined zircon, tourmaline and rutile grains among all combined non-opaque and non-micaceous heavy minerals (zircon, rutile, tourmaline, apatite, monazite, chromite and titanite; ZTR= (Z+T+R)/(Z+T+R+A+Mz+Cr+Ti)*100). Because minerals such as apatite and monazite are susceptible to dissolution during weathering and transport (Morton and Hallsworth, 1999), the ZTR index is considered a good indicator for mineralogical maturity and sedimentary recycling; where detritus that is extensively or repeatedly subject to weathering and transport becomes enriched in the more chemically and mechanically stable heavy minerals (zircon, tourmaline and rutile) relative to more unstable heavy mineral species (Hubert, 1962). The same idea has been applied using bulk rock trace element geochemistry, where ratios of Zr/Sc increase relative to ratios of Th/Sc during sedimentary recycling as the result of enrichment of detrital zircons relative to detrital monazites (McLennan, 2001). Hubert (1962) showed how ancient feldspathic wackes have much lower ZTR indexes than quartz arenites. Potter (1978) showed a positive correlation between increasing mineralogical maturity of sand (including increased quartz content relative to feldspar and lithics and increased SiO_2/Al_2O_3) and the ZTR index; both of which were in relation to modern river sand deposition on passive margins where detritus was largely recycled form older sedimentary rocks and included abundant sedimentary lithic fragments. Dill (1995) also attributed high ZTR index values in Late Cretaceous sandstones to a mixture of sedimentary recycling and weathering of detritus. It has been suggested that ZTR indexes likely increase after time and burial due to intrastratial solution and dissolution of unstable species, as evidenced by higher ZTR indexes in older deeper buried sandstones (30-60%) with bulk mineralogical maturity similar to recent sediments with much lower ZTR values (<5%) (Hubert, 1962; Potter, 1978). However, such differences are arbitrary and likely arise by the use of mineral phases in the denominator of the ZTR index that are very susceptible to intrastratial solution (epidote, olivine, pyroxene, Al-silicates, etc.) which may exist in modern sands, but do not exist in older, more deeply buried sandstones. Thus, an absolute ZTR scale for comparing modern sands to ancient sandstones does not exist. In this study sandstones existing at similar depths and of similar ages are compared relatively using the ZTR index to understand relative differences in maturity and degree of sedimentary recycling/ first-cycle input, and only diagenetically stable minerals (apatite, tourmaline, zircon, monazite, titanite, rutile and chromite) are used, since the variations in the effects of intrastratial solution and dissolution of unstable phases between sampled units are not well understood. Other unstable mineral phases, if observed in any heavy mineral separates, are noted but not quantified. Modifications to the ZTR index by the overprints of size sorting during transport and deposition are considered negligible because the ratio of the average sizes of Z+T+R over the average sizes of Z+T+R+Mz+A+Cr+Ti has a value of 1.03 ± 0.16 (Appendix 2). Tourmaline and apatite have similarly lower densities (2.9-3.2), zircon, rutile, monazite and chromite have similarly higher densities (4.5-4.8), and titanite has an intermediate density (3.5-3.6), thus hydraulic fractionation based on differences in density is likely to occur. However, since low and high density minerals are present in the numerator and denominator, the ZTR value should remain relatively similar and representative under different hydraulic regimes of transport and deposition; for example, in lower flow regimes the value will approach T/T+A, but in higher flow regimes it will approach Z+R/Z+R+MZ+Cr.

There are some potential problems when using these approaches that must be addressed. One issue, which also relates to the analytical methods, involves the differentiation between detrital rutile and authigenic TiO_2 minerals. Authigenic rutile is common, and has been suggested to form from interstitial solutions rich in Ti ions, and generally take the form of interstitial euhedral crystals, or as overgrowths. The source of the Ti ions has been postulated to be derived from detrital rutile, other detrital TiO_2 minerals, ilmenite, sphene or biotite (Morad, 1986). One solution to the problem, proposed by Morton and Hallsworth (1994), is to count only rutile grains, which do not typically form authigenically, and exclude other TiO_2 phases (anatase and brookite) which more commonly form authigenically. However, since the MLA method used for this study relies on chemistry to identity different mineral phases, it is not possible to differentiate between the different TiO_2 minerals. Therefore, when considering the applicability and validity of the RZi and ZTR index, links back to petrographic constraints (in Chapter 3) will be made.

Another potential fallback of this method involves the use of detrital apatite and ATI values for provenance. Although it has been shown that apatite is not significantly affected by burial diagenesis, it has been shown that weathering during erosion, transport and alluvial storage significantly reduces the inherited proportion of detrital apatite and decreases apatite/tourmaline by dissolution of apatite grains by acidic groundwater (Morton and Johnsson, 1993; Morton and Hallsworth, 1994). Therefore, ATi values may decrease and ZTR values may increase as a result of chemical weathering rather than changes in provenance. Factors attributing to increased weathering of apatite include climate, relief and depositional setting. Low relief drainage in hot and humid climates will tend to lead to more intense weathering, and removal of apatite (Morton and Hallsworth, 1999). In marine sediments as well as in fluvial or aolean sands deposited in arid and semi-arid climates, weathering of apatite is not considered to be extensive, so ATi and ZTR values probably remain representative of provenance; however, in fluvial-deltaic sands deposited in humid tropical settings, ATi values will decrease and ZTR values will increase independent of provenance (Morton, 1986; Morton and Hallsworth, 1999). Unfortunately, as was the case with interpreting maturity from modal sand grain populations, the overprinting effects of weathering are not easily evaluated; but an assumption can be made that Early Cretaceous sandstones would have been more affected by weathering due to a more humid tropical regional climate at this time (Abbink et al., 2001). Apatite can also form authigenically, as nodular porous phosphate cements and overgrowths, an have been noted and studied in Early Cretaceous clastics in the nearby Scotian Basin (Pe-Piper and Weir-Murphy, 2008).

4.3 Heavy mineral data

4.3.1 Mizzen L-11 Interval 3: Jurassic Sandstone # 2

Heavy mineral counts were obtained from one 5 m sample interval, 3760 m to 3765 m. The heavy mineral assemblage comprises abundant tourmaline (49%) and zircon (39%). The remainder of the heavy mineral assemblage is comprised of 5% rutile, 2% apatite, 2% monazite, 2% chromite and 1% titanite (Figure 4.2). No ilmenite grains are

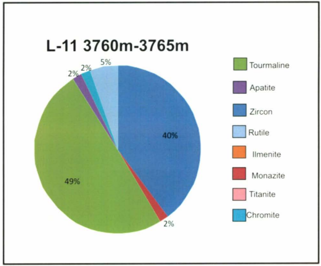

Figure 4.2: Pie chart giving proportions of detrital heavy minerals of interest from a sample interval (3760m-37656m) in the Jurassic Sandstone #2 in Mizzen L-11.

present. The sample has an ATi value of 3.5, a MZi value of 4.4, and an RZi value of 12. These values are comparatively low, and the ZTR index is high (95.5) owing to the abundance of detrital zircon and tourmaline grains (Figures 4.9, 4.10, 4.11).

4.3.2 Mizzen L-11 Interval 2: Jurassic Sandstone # 1

Heavy mineral counts were obtained from three 5m intervals between 3615 m and 3630 m. The mineral proportions comprise abundant apatite (22-35%). The samples also comprise 24-26% tourmaline grains, 13-21% zircon grains, 13-22% rutile grains, 2-7% ilmenite grains, 1-5% chromium spinel grains, 2-3% monazite grains and 2-4% titanite grains (Figure 4.3). Clearly, whatever the main source area of this interval is, there must be some rock type present which is rich in apatite. In addition, euhedral to subhedral detrital calcic amphibole and fluorite grains were observed in the heavy mineral fractions of this interval (Figure 4.1 B); however these grains have not been quantified since they are absent or rare in all of the other studied intervals.

The samples from this interval are well differentiated by their ATi values (Figures 4.9, 4.10). The RZi and MZi values are relatively well constrained, but values overlap with other intervals. MZi values range between 10 and 14, with an average value of 12.4. RZi values between 42.8 and 57.2, with an average of 50.3. ATi values range between 46 and 57.5, with an average of 53.2. ZTR values range between 58.9 and 71.6, with an average value of 63.4 (Figure 4.11).

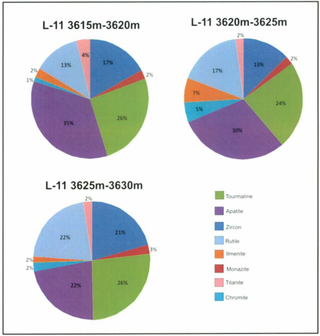

Figure 4.3: Pie chart giving proportions of detrital heavy minerals of interest from three 5-m sample intervals (3615m-3630m) in the Jurassic Sandstone #1 in Mizzen L-11.

4.3.3 Mizzen L-11 Interval 1: Early Cretaceous Baccalieu Sandstone

Heavy mineral counts in this interval were obtained from four 5 m sample intervals between 3405m and 3425m. All samples are characterized by heavy mineral suites with high rutile (31-37%), tourmaline (28-35%), as well as 16-27% zircon, and 4-10% monazite. Ilmenite grains are absent or rare. Apatite grains comprise 1-7% of the heavy mineral assemblages. Titanite grains comprise 0-4%. Chromite grains comprise 0-1% (Figure 4.4).

Values of the MZi index range from 13 to 28 with an average of 25. RZi values range from 57 to 70 with an average of 63. ATi values range from 1 to 18, with an average value of 11 (Figures 4.9, 4.10). The ZTR index of this interval ranges from 83 to 93, with an average of 88 (Figure 4.11).

4.3.4 Baccalieu I-78: Barremian Sandstones

Heavy mineral counts were obtained from two 5m sample intervals: 3295m-3300m and 3300m-3305m. The two samples have very similar mineral proportions, with high rutile (32-41%) and tourmaline (30-32%), as well as 14-25% zircon and 11% monazite. Combined ilmenite and apatite make up only 2% of both samples. No chromium-spinel grains are present in these samples (Figure 4.5). Heavy mineral proportions from this sample interval are comparable to heavy mineral proportions from the Baccalieu Sandstone sample interval in Mizzen L-11 (Figures 4.4, 4.5).

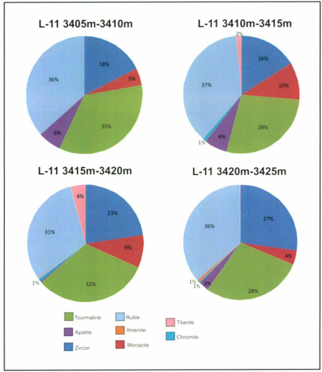

Figure 4.4: Pie chart giving proportions of detrital heavy minerals of interest from four 5-m sample intervals (3405m-3425m) in the Baccalieu Sandstone in Mizzen L-11.

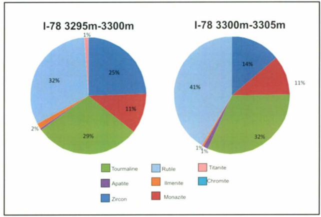

Figure 4.5: Pie chart giving proportions of detrital heavy minerals of interest from two 5-m sample intervals (3295m-3305m) from Barremian shales and sandstones below the Hibernia Equivalent in Baccalieu I-78.

The MZI and RZI mineral indexes work the best for discriminating this interval from others (Figures 4.9, 4.10). MZI values are between 31.2 and 43.6 and RZI values are between 56.4 and 74.7. These values overlap those from the Baccalieu Sandstone sample interval in Mizzen L-11, and are similar to those from Baccalieu I-78 interval 4 (Late Jurassic Jeanne d'Arc Formation Equivalent). RMI values are fairly well constrained (75 to 74) and fall in a range of RMI values that also occurs in samples from the Baccalieu Sandstone and Jurassic Sandstone # 2 in Mizzen L-11, and Baccalieu I-78 interval 4. Both ATI values are quite low, ranging from 1.3 to 4.1. ZTR values are tightly constrained and range between 88.1 and 87.7, with an average value of 88.0 (Figure 4.11).

4.3.5 Baccalieu I-78: Hibernia Formation Equivalent

Heavy mineral counts were obtained from three 5 m sample intervals between 3255 m and 3270 m. Detrital heavy mineral assemblages are consistent between 3260 m and 3270 m, but are different from the sample between 3255 m and 3260 m (Figure 4.6). The primary differences occur between the relative concentrations of rutile, tourmaline and titanite grains. Between 3255 m and 3260 m, there are 3% rutile grains, 9% titanite grains and 37% tourmaline grains. Between 3260 m and 3270 m, there are 30-35% rutile grains, 24-26% tourmaline grains and 0-1% titanite grains. Proportions of zircon grains are somewhat well constrained over the entire interval, with values ranging from 29-39%. Other mineral proportions are also more or less consistent over the entire interval, and

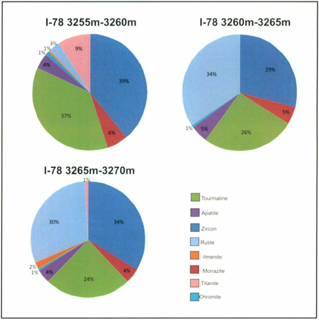

Figure 4.6: Pie chart giving proportions of detrital heavy minerals of interest from three 5-m sample intervals (3255m-3270m) from the Hibernia Formation equivalent in Baccalieu I-78.

comprise 4-6% monazite grains, 4-5% apatite grains, 0-2% chromite grains, and 0-1% ilmenite grains.

As a result of the variable rutile and tourmaline relative to other more consistent heavy mineral proportions, the RZi and ATi are not useful at discriminating this interval (Figures 4.9, 4.10). However, MZi discriminates the interval fairly well. MZi values range between 11.1 and 13.5, with an average value of 12.9. ZTR values are relatively inconsistent throughout the entire interval, ranging between 79.3 and 92.5, with an average value of 86.3 (Figure 4.11).

4.3.6 Baccalieu I-78: Avalon Formation Equivalent

Heavy mineral counts were obtained from four 5m sample intervals between 2165 m and 2185 m. In general, the four samples are characterized by a high proportion of ilmenite (21%-31%) and rutile (37%-52%). Zircon makes up 4-9% of the heavy mineral assemblages, Apatite makes up 1-8%, titanite makes up 2-4%, monazite make up 1-3%, and chromite makes up 0-1%. Tourmaline proportions are quite variable, ranging from 2% to 23% (Figure 4.7).

The mineral ratios best suited for discriminating this interval are the MZi and RZi indexes (Figures 4.9 and 4.10). RZi values are uniquely quite high, occurring between 80.5 and 92.5 with an average value of 85.7. MZi values are between 20.9 and 27.1, with an average value of 24.9. Due to the variable tourmaline concentrations, this interval is not well constrained using the ATi (values ranging between 5 and 46 with an average of

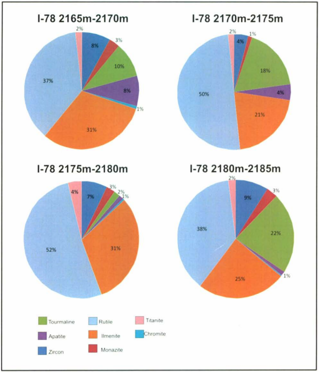

Figure 4.7: Pie chart giving proportions of detrital heavy minerals of interest from four 5-m sample intervals (2160m-2185m) from the Avalon Formation equivalent in Baccalieu I-78.

28.5). ZTR values range between 82.8 and 94.1, with an average value of 88.0 (Figure 4.11).

4.3.7 Blue H-28: Albian Sandstone

Heavy mineral grain counts were completed for five 5 m sample intervals between 5005 m and 5030 m. There is some variability in the mineral grain proportions between each sample interval, but there are some overall trends that make the heavy mineral assemblages from this interval unique. Tourmaline grains are the most abundant in all of the samples, comprising 34-65% of the assemblages. Zircon grain proportions are also variable, comprising 6-37% of the grains; however between 5010m and 5025m, the proportion of zircon grains is only 15-21%. Between 5005m and 5025m, rutile grains comprise 6-9% of grains, but between 5025m and 5030m, the make up 25% of the heavy mineral assemblage. The remainder of the mineral assemblages are made up of 6-13% apatite, 4-12% titanite, 0-1% monazite (with no monazite grains found between 5020m and 5030m), 0-4% ilmenite, and 0-5% chromite (Figure 4.8).

This interval is generally well discriminated using any combinations of ATi, MZi, and RZi (Figures 4.9, 4.10). MZi values are low owing to low detrital monazite abundances, and range between 0 and 6.7, with an average value of 2.8. Between 5005 m and 5025 m RZi values range between 15.4 and 36.4 with an average value of 27.9; however, the RZi value between 5025 m and 5030 m is 80.5, due to the abundance of rutile in this interval, giving an overall RZi average of 38.5. Values of the ATi range between 12.1 and 27.5 with an average of 17.5 for the entire 25 m sample interval. ZTR values range between 82.1 and 92.7, with an average value of 88.1 (Figure 4.12).

4.4 Discussion of Heavy Mineral data

4.4.1 Introduction

Figure 4.9 shows cross plots of all combinations of RZi, MZi, and ATi values using the heavy mineral assemblages from all of the samples used. Figure 4.10 shows cross plots of the average values of RZi, MZi, and ATi with standard errors from stratigraphic intervals with more than one representative sample. These plots are used for the purpose of provenance discrimination and correlation. Although some variation in the heavy mineral ratios may be inherent from within these individual formations, given the fact that individual data points represent 5 m of vertical section within each studied formation, the desired effect is to look at statistically meaningful, large scale variations between the heavy mineral "fingerprints" of each formation. For this method to be effective it would be ideal to have many data points for each formation, at higher resolution than every 5 m of section; however, the sample material for this project severely limits this ideal circumstance. Thus, the following section gives a summary of the distribution of data points from within each formation. Given such a small data set, only the Jurassic Sandstone # 1 from Mizzen L-11, the Avalon Formation equivalent from Baccalieu I-78 and the Albian Sandstone from Blue H-28 showed consistent variations that may be used as diagnostic heavy mineral provenance "fingerprints". However, this is

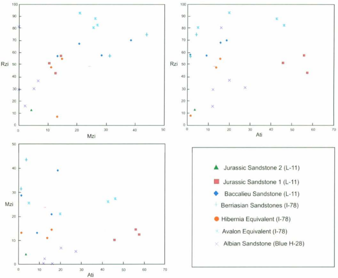

Figure 4.9: Cross-plots of heavy mineral index values from all samples. See section 4.2 for explanation of mineral indexes, and Section 4.3 and 4.4 for descriptions and interpretations.

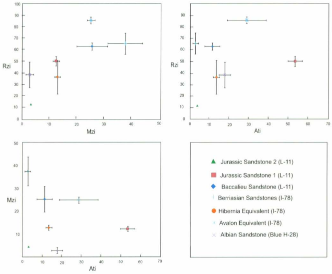

Figure 4.10: Cross-plots of averaged heavy mineral indexes from each sampled interval, with standard error bars. See section 4.2 for explanation of mineral indexes, and Section 4.3 and 4.4 for descriptions and interpretations.

provided that there is no evidence of other modifying factors such as weathering of apatite, or diagenetic growth of apatite or rutile.

4.4.2 Provenance Signatures of Sandstones

The Avalon equivalent in Baccalieu I-78 is discriminated from other studied intervals using these plots. In all possible combinations of cross-plotting RZi, MZi, and ATi, the standard error of averaged Avalon equivalent values do not overlap with the standard errors of any other averaged values (Figure 4.11). This supports a unique provenance signature for this interval, particularly with regards to uniquely high RZi values (80-90). However, other factors, such as the growth of rutile during diagenesis, should first be considered. No petrographic evidence was noted for the diagenetic growth of rutile; however, detailed diagenesis was not studied as part of this project. The heavy mineral separates contained abundant ilmenite grains and even biotite grains, which have been postulated to provide dissolved Ti ions for the authigenic growth of TiO_2 (Morad, 1985). Therefore, it is possible that the high rutile values are related to the authigenic growth of rutile, but there is no direct evidence for this.

The Jurassic Sandstone # 1 in Mizzen L-11 is well discriminated using ATi due to the uniquely high abundance of apatite with respect to tourmaline. Cross-plots using any of RZi and MZi versus ATi can be used to discriminate this interval. This is owing to the anomalously high proportions of apatite in samples from this unit. It is pertinent to consider an authigenic origin for these grains. Although authigenic phosphates are rare, they have been noted, even in Early Cretaceous clastics in the nearby Scotian Basin

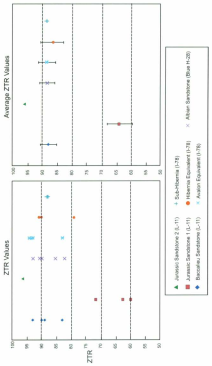

Figure 4.11: ZTR index values for every sample, arranged horizontally by interval. Also, averaged ZTR index values (with standard error bars) for each interval. See section 3.2 for explanation of the ZTR index.

(Pe-Piper and Weir-Murphy, 2008). No evidence of this was found of this in thin sections, however many apatite grains observed in the heavy mineral mounts have the nodular forms, crude concentric zoning, inclusions of pyrite and secondary porosity characteristic of the authigenic apatite noted by Pe-Piper and Weir-Murphy (2008) (Figure 4.12). This would imply that the anomalously high apatite in the heavy mineral fraction and characteristic ATi values are actually the result of authigenic growth, rather than provenance. However, it should be noted that apatite grains were not systematically imaged, so the ratio of uniform or zoned crystalline detrital grains versus authigenic grains is not known; it can only be said that both detrital and authigenic grains are present (e.g. Figure 4.1 A), and that the actual detrital proportion of apatite is lower than what is measured.

The Hibernia Formation equivalent is generally well-discriminated, and does not show systematic correlations (within standard error of values) with any other intervals. The values of MZi versus RZi overlap with the Jurassic Sandstone # 1, and RZi versus ATi values overlap with the Albian Sandstones in Blue H-28. It should be noted, however, that one data point, consisting of a sample between 3255m and 3260m, plots away from the two data points from between 3260m and 3270m, due to a differences in RZi and ATi caused by an apparent decrease in rutile grains and increase in tourmaline grains between 3255 m and 3260 m. Another important note is that authigenic growth of rutile and TiO_2 was noted in thin sections of this sandstone (Chapter 3), and should be considered as a possible cause of the high rutile grain counts between 3260 m and 3270 m. It has been postulated that TiO_2 formation occurs due to dissolution and very local (cm-scale) redistribution of Ti ions from Ti-bearing detrital minerals such as biotite,

Figure 4.12: Apatite grains from Jurassic Sandstone #1 (3615m-3620m). Such grains are present, and have many pores, concentric or irregular zoning, and pyrite inclusions (bright mineral). They are similar to the authigenic apatite described by Pe-Piper and Weir-Murphy 2008 from Early Cretaceous clastics in the nearby Scotian Basin.

sphene, ilmenite or rutile (Morad, 1986). Since rutile was the primary Ti-bearing mineral observed in thin section and in heavy mineral mounts between 3260 m and 3270 m, and only titanite and rutile were present between 3255 m and 3260 m, it is most likely that the authigenic TiO_2 observed formed by very local redistribution of Ti ions from detrital rutile, with some possible sourcing from unstable detrital titanite. Thus, the amount of rutile measured may be representative of the original detrital amounts. In any case, MZi and RZi values for the Hibernia Formation and the Jurassic Sandstone #1 are in close agreement. These units are differentiated by ATi values; however, this has already been shown to be influenced by diagenetic growth of apatite in Jurassic Sandstone #1; and thus, taking this into account, the Hibernia Formation and the Jurassic Sandstone #1 are considered to have similar heavy mineral provenance signatures. In addition, Jurassic Sandstone #1 is characterized by low ATi, RZi and MZi values, and has a provenance signature most similar to Jurassic Sandstone #1 and the Hibernia Formation Equivalent, only differing by having distinctively higher modal amounts of zircon and tourmaline (FIG).

The average values of provenance-sensitive heavy mineral ratios from the Baccalieu sandstone in Mizzen L-11 and Berriasian sandstones in Baccalieu I-78 are very close in all cross-plots and average values overlap within error in cross-plots of RZi versus MZi versus RZi (Figure 4.10). The ratio values for most intervals are variably similar to other intervals due to significant variations between some provenance-sensitive mineral pairs and not others between intervals; however, these two intervals have consistently similar provenance-sensitive heavy mineral indexes, and most average mineral indexes have values within a range of 10. This data may support a stratigraphic correlation, which would be expected given the age, modal composition (see Chapter 3) and down hole locations of these formations; however, the data set herein is too limited to correlate these intervals based on the standard errors of only a few data points. One thing that can be noted, however, is that the heavy mineral assemblages, as shown in figures 3.3 and 3.5, are very similar between the Baccalieu Sandstone in Mizzen L-11 and the Berriasian sandstones and shales in Baccalieu I-78, with each major heavy detrital phase having the same range of percentage of heavy minerals. Such a correlation is not evident between any other combinations of two studied intervals, further implying some genetic relationship or correlation between these two units. There is little evidence in either sandstone for dissolution of grains during burial diagenesis; both units are uniquely unaffected by intrastratial solution, and therefore the diagenetic modifications on the heavy mineral assemblages are considered negligible.

The standard errors of the average values of the Albian Sandstone in Blue H-28 only overlap with other intervals in RZi vs. ATi plot, where values overlap with the Hibernia Formation equivalent. In all other ratio cross-plots this interval is well discriminated. This is not surprising because the Albian Sandstone in Blue H-28 is much younger than the other intervals, and is located almost 200 km to the northwest of the other intervals, and therefore should not be expected to correlate to the older sampled locations, in the Northern Flemish Pass Basin; although shared provenance signatures may exist due to similar regional sources.

It should be noted that none of the samples contained significant amounts of detrital chromite; and therefore, ultramafic rocks are interpreted not to have been present in the source areas for any of the sandstones studied herein.

4.4.3 Maturity and sedimentary recycling

The ZTR index (as explained in section 3.2) is used as an indicator of mineralogical maturity and sedimentary recycling, as outlined in Section 4.2.3. This tool is used to assess the potential of sedimentary recycling, along with other lines of evidence in this thesis, including estimated framework sandstone compositions and detrital zircon grain morphologies. It should be noted that there is no standard value above which is indicative of sedimentary recycling, and there are other variables, such as the composition of crystalline basement and/or weathering profiles in the drainage systems, could affect ZTR values, and these factors are also outlined in Section 4.2.3.

Figure 4.12 shows plots of all ZTR values and averaged ZTR values from each interval. Most of the ZTR values from studied intervals fall between 80 and 95, indicating varying degrees of mineralogical maturity/submaturity and sedimentary recycling in most intervals. This is consistent with interpretations made in Chapter 3, based on bulk petrography of thin sections. Also, this is not surprising given the abundance of pre-Mesozoic clastic sequences present in the regional pre-Mesozoic basement (see section 1.3). One sample from Jurassic sandstone # 2 in Mizzen L-11 has a high ZTR value of 95.5, which is interpreted as representing dominantly recycled detritus in this interval, but should not discount the effects of weathering, which are poorly constrained. Other high ZTR values, particularly for the Avalon Formation Equivalent, may be caused by diagenetic $TiO2$ growth, so caution must be used. For this particular interval, if one eliminates rutile from the ZTR equation, values range from 20 to 50; however, the extent of diagenetic rutile growth, if any, has not been quantified. Jurassic Sandstone # 1, which is approximately 150 m above Jurassic Sandstone # 2, has contrastingly low values, ranging between 58.9 and 71.6, with an average value of 63.4. However, low ZTR values in this interval are caused by an abundance of apatite grains, of which a portion has been characterized as authigenic. Therefore, the inherited ZTR value is probably higher, but by how much it is hard to say. Despite this, euhedral calcic amphibole and fluorite grains are present in the heavy mineral separates (Figure 4.1B), suggesting significant first-cycle sourcing from crystalline igneous and/or metamorphic basement rocks.

4.4.4 Summary

Based on the previous descriptions of heavy mineral data and discussion of the significance of heavy mineral data, some general conclusions can be drawn. First of all, Jurassic Sandstone #2, Jurassic Sandstone #1 and the Hibernia Formation equivalent are shown to have a similar provenance signatures characterized by low MZi values and low to moderate RZi values (Figures 4.9, 4.10). Detrital ATi values may be correlative as well, depending on the relative proportion of authigenic apatite in Jurassic Sandstone #1. Additionally, the Albian Sandstone in Blue H-28 is characterized by a provenance signature similar to those of the Jurassic Sandstone #1 and #2 and the Hibernia Formation equivalent.

The Baccalieu Sandstone in Mizzen L-11 and Berriasian Sandstones in Baccalieu I-78 also have similar provenance signatures characterized by moderate MZi, moderate to high RZi and low ATi values (Figures 4.9, 4.10).

The Avalon Formation equivalent is distinguished by a provenance signature characterized by high RZi, moderate to low ATi, and moderate to low MZi values (Figures 4.9, 4.10); though, it should be noted that there may be a diagenetic overprint resulting in increased rutile, but this diagenetic overprint, if it exists, is not constrained.

The ZTR values show an overall enrichment in the ultrastable heavy minerals, which is consistent with significant mineralogical maturity/submaturity and sedimentary recycling. It is also consistent with the findings in the previous chapter, in which the overall mineralogically submaturity of the sandstones and abundance of sedimentary lithic grains was interpreted to have resulted from sedimentary recycling. Weathering may have had an impact increasing this ratio; however, the degree of weathering that modified these sands is not thought to be intense, due to the abundance of relatively unstable sedimentary lithic grains and presence of feldspar grains in the thin sections, as described in Chapter 3. Ultimately, the enrichment of the ultrastable heavy minerals is interpreted to have occurred as an effect of sedimentary recycling.

Chapter 5: Detrital Tourmaline Geochemistry

5.1 Introduction

Detrital tourmaline grains have been analyzed for their major element mineral chemistry to interpret the petrogenesis of the grains. Tourmaline is an ideal mineral for single mineral group varietal provenance analysis since it has multiple chemical end-members that are ultrastable (resistant to solution during chemical weathering and burial diagenesis). Henry and Guidotti (1985) developed a method for using tourmaline grains as an indicator of petrogenesis (mainly granitic versus metasedimentary) based on variations in the molecular proportions of Fe, Mg, Al and Ca. Geochemistry of detrital tourmalines has been used successfully in conjunction with other heavy mineral tools (detrital zircon U-Pb geochronology and heavy mineral ratios) for sedimentary provenance studies in the past (Morton et al. 2005; Piper et al. 2007; Nascimento et al. 2007).

5.2 Methodology

5.2.1 Sampling and Processing

The sampling and processing procedures are the same for the detrital tourmalines as for the detrital heavy minerals, as described in Section 3.2 of this thesis. Detrital tourmalines were located and analyzed directly on the 30 mm heavy mineral mounts.

5.2.2 Mineral Identification and Imaging

Identification of detrital tourmalines from the 30 mm heavy mineral mounts has been performed in automated fashion using a scanning electron microscope (SEM) equipped with and energy dispersive x-ray (EDX) spectrometer mineral liberation analysis (MLA) software in X-Ray modal analysis (XMOD) mode, as described in Section 3.2 of this thesis. The apparatus used includes an FEI Quanta 400 environmental SEM installed with a Bruker AXS XFlash® 3001 SDD x-ray detector at Memorial University in St. John's, Newfoundland. Grains were matched against EDX spectral standards of tourmaline for rapid mineral identification using the X-ray image batch classification function on the Particle-X MLA software program. Locating grains for imaging and chemical analysis was performed during post-processing using a search function on the MLA Viewer software. Back scattered electron imaging of the tourmaline grains was carried out to reveal growth and compositional zoning and grain morphologies using the SEM.

5.2.3 Compositional Analysis

Determination of the major element composition (Na, Mg, Al, Si, K, Ca, Ti, Cr, Mn, Fe) of detrital tourmalines was performed by wavelength-dispersive spectrometry (WDS) using a JEOL-733 electron probe microanalyser at the University of New Brunswick, in Fredericton, New Brunswick. Spot analyses were obtained using a voltage of 15 keV, a beam current of 30 nA, and acquisition times of 30 s on peak, 15 s on high background and 15 s on low background. Analytical standards were natural and synthetic minerals and materials, including jadeite (Na), Olivine (Mg), Corundum (Al), Diopside (Si, Ca), Orthoclase (K), Strontium titanate (Ti), chromium metal (Cr), Bustmanite (Mn) and iron metal (Fe). Minimum detection limits are considered to have been: SiO_2 = 0.02, Al_2O_3 = 0.1, FeO = 0.09, MgO = 0.02, CaO = 0.03, Na_2O = 0.02, TiO_2 = 0.3, in wt% oxide.

Structural formulae were calculated on the basis of 31 anions (O, OH, F), following the methodology of Tindle et al. 2003. Weight percent oxides of B_2O_3, H2O (as OH) and Li_2O3 were calculated assuming the appropriate stoichiometric amounts of B (3 atoms per formula unit), H+F (4 atoms per formula unit) and Li. The amount of Li assigned to the *Y* site is determined by subtracting the amount of cations in the $T + Z + Y$ sites from the ideal sum of the cations occupying the sites (15 atoms per formula unit) [Li = 15 –($T + Z + Y$) or Li = 15 – (Si + Al + Mg + Fe + Mn + Zn+ Ti)]. All Fe and Mn were assumed to be Fe^{2+} and Mn^{2+}.

5.2.4 Theoretical Approach

Henry and Guidotti (1985) described the approach for the use of tourmaline as a petrogenetic indicator. In their study, they plotted the variations in molecular proportions of Mg, Fe and Al (Al-Fe (tot)-Mg ternary diagram) as well as Mg, Fe and Ca (Ca-Fe (tot)-Mg ternary diagram) from tourmalines from various rock types from a variety of previous studies (see Appendix 1 in Henry and Guidotti 1985).

The main advantage of this method is the ability to discriminate between granitic and metamorphic sourced detrital tourmalines, based on variations in the in the Schorl (Fe-rich) and Dravite (Mg-rich) solid solution series. Henry and Guidotti (1985) showed that Fe-rich tourmalines are more commonly derived from granites and Mg-rich tourmalines are more commonly from low-medium grade metasedimentary rocks. This is attributed to the high Mg-Fe partitioning coefficients (generally >1) between tourmalines and common coexisting phases in metasedimentary rocks such as biotite, chlorite, garnet, cordierite and staurolite. One caveat to consider while using this type of discrimination is that it may be limited for some discriminating certain compositions of granites from metasedimentary rocks. For example, peraluminous granites, which contain abundant biotite and often lesser amounts of garnet, could crystallize Mg-enriched tourmalines, that, under this discrimination scheme, would be classified as metasedimentary.

5.3 Tourmaline Data

5.3.1 Introduction

Tourmaline grains from 8 samples were identified and analyzed for chemical composition. Molar proportions of Fe, Mg and Al from all analyzed grains in each sample were plotted on the Al-Fe(tot)-Mg ternary discriminatory diagram of Henry and Guidotti (1985). The fields in this diagram are outlined in Figure 5.1. Results from the chemical analyses can be found in Appendix 3 and Al-Fe(tot)-Mg ternary discriminatory plots of grains from each sample are in Figure 5.2.

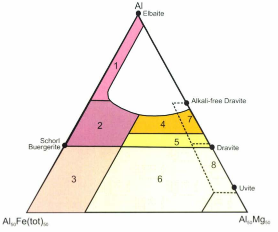

2: Li-poor granitoids and their associated pegmatites and applites

3: Fe-rich tourmaline rocks (hydrothermally altered granites)

4: Metapelites and metapsammites coexisting with an Al-saturating phase

5: Metapelites and metapsammites not coexisting with an Al-saturating phase

6: Fe-rich tourmaline rocks, calc-silicate rocks, and metapelites

7: Low Ca metaultramafics and Cr, V-rich metasediments

8: Metacarbinates and metapyroxenites

Figure 5.1: Al-Fe(tot)-Mg diagram (in molecular proportions) for tourmalines from various rock types. Fe(tot) represents the total Fe in the tourmaline. Several end members are plotted for reference. This diagram is divided into regions that define the compositional range of tourmalines from different rock types. From Henry and Guidotti, 1985.

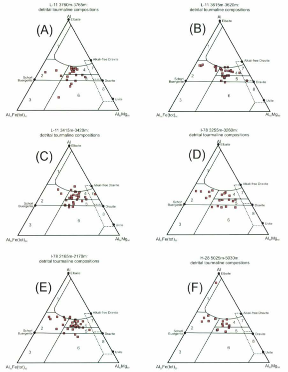

Figure 5.2: Chemical discrimination of detrital tourmalines from this study. See Figure 5.2 for definition of fields. (A) Detrital tourmalines from Jurassic Sandstone #2 in Mizzen L-11 (3760 m-3765 m). (B) Detrital tourmalines from Jurassic Sandstone #1 in Mizzen L-11 (3615 m-3620 m). (C) Detrital tourmalines from Baccalieu Sandstone in Mizzen L-11 (3415m-3420m). (D) Detrital tourmalines from Hibernia Formation Equivalent in Baccalieu I-78 (3255 m-3260 m). (E) Detrital tourmalines from the Avalon Formation Equivalent in Baccalieu I-78(2165 m-2170 m). (F) Detrital tourmalines from the Albian Sandstone in Blue H-28 (5025 m-5030 m).

5.3.2 Mizzen L-11: Jurassic Sandstone # 2

From a sample of heavy minerals taken from between 3760 m and 3765 m in Mizzen L-11, 21 detrital tourmalines were analyzed for chemical composition (Figure 5.2 A). Three grains (14%) plotted in field 2 (Li-poor granites and associated pegmatites and aplites), 9 grains (43%), the largest group of grains, plotted in field 4 (metapelites and metapsammites coexisting with an Al-saturating phase), 5 grains (24%) plotted in field 5 (metapelites and metapsammites) and 4 grains (19%) plotted in field 6 (Fe-rich quartz tourmaline rocks, calc-silicate rocks, and metapelites). Thus, the chemical analyses of detrital tourmalines in this sample indicates a dominance of grains derived from low to moderate grade metasedimentary rocks, with additional input from granitic sources.

5.3.3 Mizzen L-11: Jurassic Sandstone # 1

From a sample of heavy minerals taken between 3415 m and 3420 m in Mizzen L-11, 28 detrital tourmalines were analyzed for chemistry (Figure 5.2 B). Seven grains (25%) plotted in field 2 (Li-poor granites and associated pegmatites and aplites), 14 grains (50%) plotted in field 4 (metapelites and metapsammites coexisting with an Al-saturating phase), 6 grains (21%) plotted in field 5 (metapelites and metapsammites) and 1 grain (4%) plotted in field 6 (Fe-rich quartz tourmaline rocks, calc-silicate rocks, and metapelites). The tourmaline population from this sample is interpreted as having a relatively significant proportion of grains derived from granites, but with most of the grains being derived from low to medium grade metasedimentary rocks coexisting with an Al-silicate mineral phase.

5.3.4 Mizzen L-11: Baccalieu Sandstone

From a sample of heavy minerals taken between 3415 m and 3420 m in Mizzen L-11, 28 detrital tourmalines were analyzed for chemistry (Figure 5.2 C). Only 2 grains (7%) plot in field 2 (Li-poor granites and associated pegmatites and aplites). Additionally, two grains plot within the elbaite-dravite immiscibility gap. The remainder of the grains plot within metasedimentary fields, with 15 grains (54%) that plot in field 4, 7 grains (25%) that plot in field 5, and 2 grains (7%) that plot in field 6. The sampled tourmaline population is therefore interpreted to be dominated by detrital tourmalines from low to medium grade metasedimentary rocks, with very little contribution of tourmalines from granites.

5.3.5 Baccalieu I-78: Hibernia Formation Equivalent

From a sample of heavy minerals taken between 3255 m and 3260 m in Baccalieu I-78, 20 detrital tourmalines were analyzed for chemistry (Figure 5.2 D). Six grains (30%) plotted in field 2 (Li-poor granites and associated pegmatites and aplites), 4 grains (20%) plotted in field 4 (metapelites and metapsammites coexisting with an Al-saturating phase), 5 grains (25%) plotted in field 5 (metapelites and metapsammites) and 5 grains (25%) plotted in field 6 (Fe-rich quartz tourmaline rocks, calc-silicate rocks, and metapelites). The tourmaline population from this sample is interpreted as having a relatively significant granitic derived component, similar in comparison to the data from

Jurassic Sandstone # 1 in Mizzen L-11 (Figure 5.2 B) and the Avalon Formation Equivalent (Figure 5.2 E). However, unlike these populations, metasedimentary tourmalines are interpreted to be mostly derived from metasedimentary rocks that are lower in grade and/or not coexisting with an Al-silicate phase.

5.3.6 Baccalieu I-78: Avalon Fm Equivalent

From a sample of heavy minerals taken between 2165 m and 2170 m in Baccalieu I-78, 31 detrital tourmalines were analyzed for chemistry (Figure 5.2 E). Seven grains (22%) plotted in field 2 (Li-poor granites and associated pegmatites and aplites), 15 grains (48%) plotted in field 4 (metapelites and metapsammites coexisting with an Al-saturating phase), 4 grains (14%) plotted in field 5 (metapelites and metapsammites) and 3 grains (10%) plotted in field 6 (Fe-rich quartz tourmaline rocks, calc-silicate rocks, and metapelites). The remaining 2 grains (6%) plotted in the elbaite-dravite immiscibility gap, but near the boundary between fields 2 and 4. Thus, this tourmaline population is similar to the populations present in Jurassic Sandstone # 1 (Figure 5.2 B), containing a significant amount of grains in field 2 (granitic) with the largest proportions of grains falling in field 4. The tourmaline population is interpreted as being primarily derived from low to moderate grade metasedimentary rocks, with a significant contribution from granites.

5.3.7 Blue H-28: Albian Sandstone

From a sample of heavy minerals taken between 5025m to 5030m in Blue H-28, 17 detrital tourmalines were analyzed for chemistry (Figure 5.2 F). Five grains (30%) plotted in field 2 (Li-poor granites and associated pegmatites and aplites), and an additional grain (5%) plotted in field 1 (Li-rich granitoid pegmatites and aplites). The remaining grains plotted in the metasedimentary fields, with 7 grains (41%) that plotted in field 4 (metapelites and metapsammites coexisting with an Al-saturating phase) and 4 grains (24%) that plotted in field 5 (metapelites and metapsammites). The tourmaline population from this sample is interpreted as primarily derived from low to moderate grade metasedimentary rocks, but with a significant input from granites as well.

Chapter 6: Detrital Zircon Geochronology and Qualitative Analysis

6.1 Introduction

For this study, approximately 40 to 100 detrital zircons per sample have been dated using U-Pb geochronology and described based on Th/U, grain sizes, aspect ratios, zoning and morphology. The methods used in this study are similar to those used by Crowly et al. (2005). Detrital zircon geochronology has been used extensively and with considerable success in many studies of sedimentary provenance (Rainbird et al. 1997; Morton et al. 2005). U-Pb geochronological and qualitative detrital zircon data can be found in Appendix 4 and 5.

6.2 Methodology

6.2.1 Sampling and processing

Cuttings samples weighing 50 to 200 g taken from 5 m well intervals were used to isolate detrital zircon samples. Samples were obtained from the Canada-Newfoundland and Labrador Offshore Petroleum Board (C-NLOPB) and from industry well operators (Petro-Canada and Husky). The cuttings were gently disaggregated and cleaned and sieved to remove all material less than 44 μm, including drilling mud and clays. The dried disaggregated samples were again sieved to isolate the 63-177 μm size fractions. Gravity separation in Methylene Iodide ($\rho = 3.34$ g/cm^3) was used to obtain a fraction of grains with a density greater than 3.34 g/cm^3. These grains were then separated into non-magnetic and paramagnetic fractions using a Franz isodynamic magnetic separator set to 1.7 Amps and 5° rotation. Approximately 70-150 zircons were picked from the non-magnetic and paramagnetic fractions, placed on double-sided tape in a single row lying on their long axes and mounted in 25 mm rings using a 2 part epoxy/resin. The crystals were polished to expose even surfaces at the cores of grains in order to remove the outer surfaces of grains which are typically high in Uranium (Krogh, 1982).

6.2.2 Imaging

The grains were imaged with reflected light and a scanning electron microscope in back-scattered electron mode to reveal growth and compositional zoning. BSE imaging was carried out using the Quanta 400 SEM at Memorial University. Determination of polished cross-sectional areas and length/width aspect ratios of grains were accomplished using MLA software in X-ray modal analysis (XMOD) mode (Gu 2003). The MLA method and SEM conditions during measurement are explained in section 3.2.

6.2.3 Age Dating Analytical Method

Uranium-lead isotope crystallization ages and U and Th concentrations of detrital zircon grains have been determined by laser ablation and inductively coupled plasma mass spectrometry (LA-ICPMS) at the INCO Innovation Centre Laboratory at Memorial University of Newfoundland. The type of in-situ U-Th-Pb dating technique used in the laboratory are described in detailed by Kosler et al. (2002) and Kosler and Sylvester (2003). The instrument consists of a GEOLAS 193 nm excimer laser system connected to a Finnigan ELEMENT XR high-resolution double focusing magnetic sector inductively-coupled plasma mass spectrometer (IC-PMS). The ablation system utilizes an argon-fluorine gas laser emitting at the 193 nm wavelength. The samples were mounted in an airtight sample chamber that was moved beneath a stationary laser (10 μm spot) to produce a square ablation pit measuring 40 x 40 x 15 μm. Zircons which were too small to be ablated using a 40 x 40 x 15 μm ablation pit were ablated using a 30 μm spot at a low frequency (2 Hz) to reduce fractionation. The ablated sample was flushed from the sample cell and carried to the ICPMS using a helium carrier gas.

Instrumental mass bias was corrected using a solution containing ^{203}Tl, ^{205}Tl, ^{209}Bi, ^{237}Np and ^{233}U that was aspirated simultaneously with laser ablation. U/Pb fractionation was limited by rastering and the intercept method was used to correct for any residual fractionation. Accuracy and reproducibility of U-Pb analyses were monitored by measurements of in-house zircon standards of known TIMS U-Pb age (91500 and PL) before and after each 8 unknowns. Data processing was completed using spreadsheet based software (LAMDATE). The ^{207}Pb/^{206}Pb, ^{208}Pb/^{206}Pb, ^{206}Pb/^{238}U and ^{207}Pb/^{235}U ratios were calculated and blank corrected for each analysis.

6.2.4 Qualitative Approaches

In addition to U-Pb geochronology, detrital zircon grains were also analyzed to determine Th/U ratios, grain sizes, grain morphology, zoning typology, and aspect ratios of grains. These qualitative chemical and morphological characteristics of grains are used in conjunction with U-Pb ages (which alone are the most diagnostic for provenance) to further constrain the nature of zircon source rocks (sedimentary, igneous or metamorphic).

For example, morphologies of detrital zircons are used to assess the potential for sedimentary cycling of the zircon grains. Grains are classified as probably first- or multi-cycle based on grain morphology. Any grains that are angular, subhedral or euhedral are interpreted as probable first-cycle grains (derived directly from its igneous or metamorphic crystallization origin), and any grains that are sub-angular, sub-rounded or rounded are interpreted as probable second- or multi-cycle detrital grains (derived directly as a detrital grain from an older sedimentary rock). It may be the case that first-cycle zircons that have travelled long distances may be rounded; however, given the evidence of recycling from previous chapters of this thesis, and the robustness of zircon, rounded zircons are collectively considered to be recycled, for the purpose of identifying recycled age groups that would make provenance interpretations erroneous if considered first cycle. It should be noted that rounded grains may also be of first-cycle metamorphic origin (Hoskin and Schaltegger 2003). The age peaks of fist cycle detrital grains will be useful in determining primary provenance, including constraints on paleodrainage such as direction(s) of transport maximum transport distance.

Other characteristics such as zoning, Th/U, grain size and aspect ratio can give insight into the host rock type of first-cycle detrital zircons (metamorphic versus igneous, and in some cases plutonic versus volcanic). Most igneous zircons have Th/U values greater than 0.5 and dominantly develop oscillatory and/or sector zoning. Metamorphic zircons tend to have lower Th/U, more commonly have rounded or irregular grain morphologies, and more commonly exhibit convolute or irregular zoning patterns. Volcanic zircons can be identified based on their generally small sizes, oscillatory or sector zoning, subhedral morphologies, and high aspect ratios (Hoskin and Schaltegger 2003). By cross-plotting U-Pb age of detrital zircons versus their morphology, Th/U, grain size, zoning and aspect ratios, general interpretations have been made on the nature of zircon source rocks from different age groups, which further helps to constrain sediment provenance.

6.2.5 Data Presentation

The ISOPLOT/Ex program of Ken Ludwig was utilized to generate conventional concordia plots and cumulative probability histograms of U-Pb ages. Single grain U-Pb ages with 2σ error ellipses are plotted on a conventional $^{206}Pb/^{238}U$ and $^{207}Pb/^{235}U$ concordia diagram (Figure 6.1). Age versus frequency histograms were plotted using concordant $^{206}Pb/^{238}U$ and $^{207}Pb/^{235}U$ ages (concordance probability > 0.01) and their errors at 2σ. Cumulative probability curves were also generated and overlain on histograms to identify major age groups and peaks associated with the distribution of detrital zircon U-Pb ages in each sample. In addition, all grains are classified as either being interpreted as first- or multi-cycle based on grain morphology (as explained above). First- and multi-cycle zircons are plotted on age histograms to assess the amount of first-cycle detritus and the dominant direct origin (sedimentary/metasedimentary versus igneous/metamorphic) of zircons in each age group (Figure 6.2). In discussions of

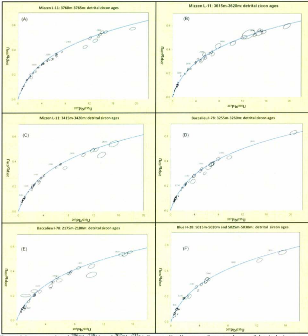

Figure 6.1: conventional $^{206}Pb/^{238}U$ and $^{207}Pb/^{235}U$ Concordia diagrams from analyses of detrital zircons from each sample. Error ellipses are 2σ. Concordant and discordant analyses are included. Diagrams were plotted using the ISOPLOT/Ex program of Ken Ludwig. (A) Mizzen L-11 3760m-3765m, from within the Jurassic Sandstone #2 unit (see figures 2.3 and 2.4). (B) Mizzen L-11 3615m-3620, from within the Jurassic Sandstone #1 unit (see figures 2.3 and 2.6). (C) Mizzen L-11 3415m-3420m, from within the Baccalieu Sandstone unit (see figures 2.3 and 2.8). (D) Baccalieu I-78 3255m-3260m, from within the Hibernia Formation equivalent (see figures 2.10 and 2.11). (E) Baccalieu I-78 2175m-2180m, from within the Avalon Formation equivalent (see figures 2.10 and 2.13). (F) Blue H-28 5015m-5020m and 5025m-5030m, from within the Albian Sandstone unit (see figures 2.22 and 2.23).

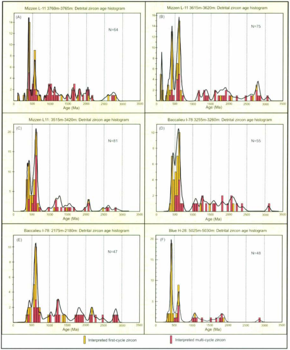

Figure 6.2: Age versus frequency and cumulative probability plots from each sample. Only concordant analyses are included. Diagrams were plotted using the ISOPLOT/Ex program of Ken Ludwig, then redrafted to show probable fist- and muli-cycle grains (A) Mizzen L-11 3760m-3765m, from within the Jurassic Sandstone #2 unit (see figures 2.3 and 2.4). (B) Mizzen L-11 3615m-3620, from within the Jurassic Sandstone #1 unit (see figures 2.3 and 2.6). (C) Mizzen L-11 3415m-3420m, from within the Baccalieu Sandstone unit (see figures 2.3 and 2.8). (D) Baccalieu I-78 3255m-3260m, from within the Hibernia Formation equivalent (see figures 2.10 and 2.11). (E) Baccalieu I-78 2175m-2180m, from within the Avalon Formation equivalent (see figures 2.10 and 2.13). (F) Blue H-28 5015m-5020m and 5025m-5030m, from within the Albian Sandstone unit (see figures 2.22 and 2.23).

numerical ages and corresponding geological Eras, Periods and Stages, the time scale used is the 2009 International Stratigraphic Chart (ICS, 2009).

6.3 Mizzen L-11: Jurassic Sandstone # 2

Detrital zircons were obtained from a cuttings sample taken between 3760 m and 3765 m of Mizzen L-11. From this sample, 121 detrital zircons were mounted and imaged, 96 representative grains were ablated, and 64 yielded usable concordant U-Pb ages with concordance probabilities equal to or greater than 0.01.

6.3.1 Age Groups

The largest proportion of dated detrital zircons grains from this sample are Mid-Paleozoic in age (Early Devonian predominantly), with a significant group of Late Neoproterozoic aged grains, as well as a significant proportion of Mesoproterozoic, Paleoproterozoic and Late Archean aged grains, and several Mesozoic aged grains (Figures 6.1a, 6.2a and 6.3).

One Mesozoic grain is present, and has concordant age of 142 ± 7 Ma (Valanginian-Tithonian).

Middle Paleozoic grains are the most abundant of all dated grains, and comprise 33% of all dated detrital grains. Approximately three quarters of these grains have ages between 395 ± 9 Ma and 421 ± 15 Ma (Late Silurian to Early Devonian), which results in a cumulative probability peak at 410 ± 20 Ma. Also present is one Pennsylvanian aged

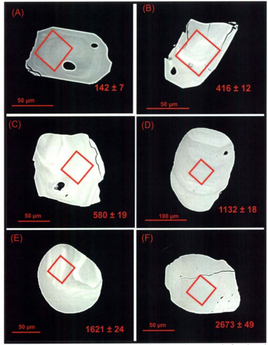

Figure 6.3: BSE images of detrital zircons with locations of 40*40 µm laser raster pits from Jurassic Sandstone #2. (A) Subhedral, concentric oscillatory zoned Mesozoic-aged (Early Cretaceous) detrital zircon; probable first-cycle igneous (volcanic) origin. (B) Euhedral, concentric oscillatory zoned Late Silurian-Early Devonian aged detrital zircon; probable first-cycle igneous origin. (C) Relatively large, angular, concentric oscillatory zoned Late Neoproterozoic aged detrital zircon; probable first- or second-cycle igneous plutonic origin. (D) Relatively large and rounded Mesoproterozoic detrital zircon grain with concentric oscillatory zoning; probable multi-cycle igneous origin. (E) Well rounded Late Paleoproterozoic detrital zircon grain with convoluted zoning; probable multi-cycle metamorphic origin. (F) Sub-round to sub-angular Late Archean detrital zircon with faint oscillatory and/or sector zoning; probably multi-cycle igneous origin.

grains (293 ± 9 Ma), and two Early Ordovician aged grains (472 ± 15 Ma and 467 ± 18 Ma).

Late Neoproterozoic grains comprise 25% of all dated grains in this sample, and most range in age between 546 ± 13 Ma and 733 ± 16 Ma. Over half of the Late Neoproterozoic grains have ages between 560 and 600 Ma, forming a cumulative probability peak at 580 ± 30 Ma. Only one grain in this sample has an age between 750 and 900 Ma, with an age of 855 ± 17 Ma.

Mesoproterozoic, Paleoproterozoic and Late Archean aged grains account for almost half of the dated grains in this sample, and are considerably more abundant in this sample than in all others. Mesoproterozoic grains account for 22% of all dated grains, and have ages ranging from 913 ± 23 Ma and 1512 ± 30 Ma; however, most of the Mesoproterozoic grains have Late Mesoproterozoic ages (900 to 1250 Ma) and this is reflected by cumulative probability peaks at ca. 970 Ma (+100/-50 Ma) and ca. 1130 ± 50 Ma. Paleoproterozoic grains make up 13% of the dated grains in this sample, and range in age between 1622 ± 22 Ma and 2025 ± 39 Ma, with cumulative probability peaks at ca. 1650 ± 50 Ma, 1830 ± 40 Ma and 2030 ± 50 Ma. Late Archean Grains make up about 6% of all dated grains in this sample; have ages ranging between 2537 ± 50 Ma and 2800 ± 31 Ma, with a cumulative probability peak at 2760 ± 60 Ma.

6.3.2 Qualitative analysis of dated grains

Values of Th/U range between 0.2 and 2.3, with most values between 0.2 and 1.2. The two Mesozoic grains have Th/U values between 0.6 and 0.7. Grains from the main

Paleozoic peak are dominated by Th/U values ranging between 0.3 and 1.0. Late Neoproterozoic grains have Th/U values between 0.4 and 1.1, with most of the values between 0.7 and 0.9. Mesoproterozoic grains have on average lower Th/U values, which typically range between 0.2 and 0.7. Most late Paleoproterozoic grains have Th/U Between 0.2 and 0.4 or between 0.6 and 1.0, with no values between 0.4 and 0.6. Most Archean grains have a range of Th/U values between 0.2 and 1.1, but two grains have Th/U > 2.0 (Figure 6.4a).

Dated grains from this sample have cross-sectional areas ranging from 2000 μm^2 to 30000 μm^2, with an average cross-sectional area value of 9250 μm^2 and a median value of 8360 μm^2. The two Mesozoic grains have cross-sectional areas of 7645 μm^2 and 4624 μm^2. The two Carboniferous grains have cross-sectional areas of 4100 μm^2 and 4415 μm^2. Grains from the prominent Late Silurian to Early Devonian peak exhibit a wide and continuous range of cross-sectional area sizes from quite small (2500 μm^2) to relatively large (19000 μm^2). Most of the Neoproterozoic grains have sizes between 3000 μm^2 and 11000 μm^2, with only two other grains with cross-sectional areas of 19180 μm^2 and 16290 μm^2. Grains from the 970 Ma peak mostly have cross-sectional areas between 4000 μm^2 and 10000 μm^2, but two other grains are much larger (>15000 μm^2), and include the largest dated grain in the sample (29260 μm^2) has an age within this peak. Grains from the 1130 Ma peak are larger on average, with most cross-sectional areas between 16000 μm^2 and 24000 μm^2. Paleoproterozoic grains with ages between 1600 and 2200 have cross-sectional areas between 3000 μm^2 and 13000 μm^2. Most Archean grains from the2720 Ma age peak range in cross-sectional area between 7000 μm^2 and 14000 μm^2, but the few other Archean grains have a much wider range in size (Figure 6.5a).

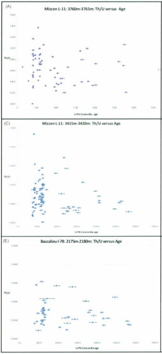

Figure 6.4: Cross-plots of Th/U versus Concordia ages of dated zircons from each interval. Error bars are 2σ. Only concordant U-Pb ages are included. (A) Mizzen L-11 3760m-3765m, from within the Jurassic Sandstone #2 unit (B) Mizzen L-11 3615m-3620, from within the Jurassic Sandstone #1 unit (C) Mizzen L-11 3415m-3420m, from within the Baccalieu Sandstone unit (D) Baccalieu I-78 3255m-3260m, from within the Hibernia Formation equivalent (E) Baccalieu I-78 2175m-2180m, from within the Avalon Formation equivalent (F) Blue H-28 5015m-5020m and 5025m-5030m, from within the Albian Sandstone unit.

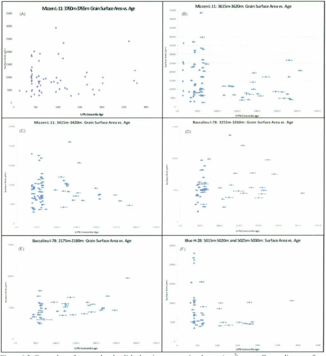

Figure 6.5: Cross-plots of mounted and polished grain cross-sectional areas (μm^2) versus Concordia ages of dated zircons from each interval. Error bars are 2σ. Only concordant U-Pb ages are included. (A) Mizzen L-11 3760m-3765m, from within the Jurassic Sandstone #2 unit (B) Mizzen L-11 3615m-3620, from within the Jurassic Sandstone #1 unit (C) Mizzen L-11 3415m-3420m, from within the Baccalieu Sandstone unit (D) Baccalieu I-78 3255m-3260m, from within the Hibernia Formation equivalent (E) Baccalieu I-78 2175m-2180m, from within the Avalon Formation equivalent (F) Blue H-28 5015m-5020m and 5025m-5030m, from within the Albian Sandstone unit.

Aspect ratios of dated zircon grains in this sample range from 1.03 to 2.2. The two Mesozoic grains have aspect ratios of 1.32 and 1.55. Aspect ratios of the two Carboniferous grains are both 1.32. Grains from the Late Silurian to Early Devonian peak have aspect ratios ranging between 1.05 and 1.83. Late Neoproterzoic grains have a similar range in aspect ratios, except most are lower than 1.4. Most Mesoproterozoic grains have aspect ratios between 1.2 and 1.4, and only a few grains are more elongate than this. The Paleoproterozoic and Archean grains are for the most part more equant, with aspect ratios ranging between 1.04 and 1.35 (Figure 6.6a).

A variety of zoning types are present from dated grains in this sample, but the main types represent are concentric oscillatory (43%) and convolute/irregularly (23%) zoned grains (Figure 6.7a). The Mesozoic grains are centered concentric oscillatory zoned. Paleozoic and Late Neoproterozoic grains have a mixture of zoning types, including concentric and planar oscillatory, cryptic/irregular, sector + oscillatory, and unzoned. Most Mesoproterozoic and Paleoproterozoic grains have either off-centered concentric oscillatory or cryptic/irregular zoning types, although the Paleoproterozoic grains are dominated by off-centered concentric oscillatory zoning. Archean grains are dominated by off-centered concentric oscillatory zoned and unzoned grains (Figure 6.8a).

A range of morphologies are present, but the most abundant grain morphology is sub-rounded, and approximately 30% of the dated grains are so (Figure 6.9a). Grain morphologies show a close relationship with age, with the younger grains being more commonly euhedral, subhedral and angular and older grains being more commonly sub-angular, sub-rounded and rounded, representing increased mechanical abrasion with zircon age. The Mesozoic grains are euhedral-subhedral, and Paleozoic grains are

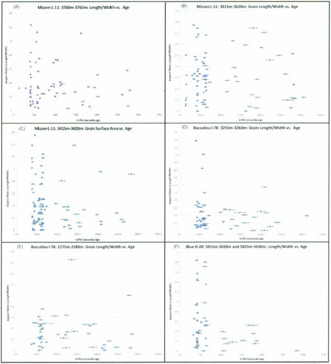

Figure 6.6: Cross-plots of mounted and polished grain aspect ratios (length/width) versus Concordia ages of dated zircons from each interval. Error bars are 2σ. Only concordant U-Pb ages are included. (A) Mizzen L-11 3760m-3765m, from within the Jurassic Sandstone #2 unit (B) Mizzen L-11 3615m-3620, from within the Jurassic Sandstone #1 unit (C) Mizzen L-11 3415m-3420m, from within the Baccalieu Sandstone unit (D) Baccalieu I-78 3255m-3260m, from within the Hibernia Formation equivalent (E) Baccalieu I-78 2175m-2180m, from within the Avalon Formation equivalent (F) Blue H-28 5015m-5020m and 5025m-5030m, from within the Albian Sandstone unit.

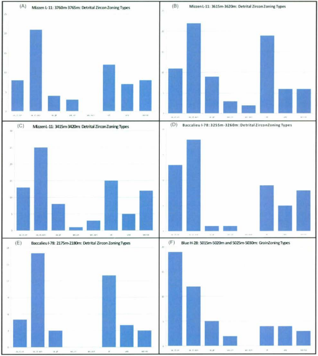

Figure 6.7: Frequency plots of grain zoning types of dated zircons from each interval. Only concordant U-Pb ages are included. oc,ct,cn = oscillatory concentric centered; oc,ct,ocn= oscillatory concentric off-centered; oc,pl = oscillatory planar; sec,cn = sector centered; sec,ocn = sector, off-centered; ot = convolute/irregular/other; unz = unzoned; sec+oc = sector plus oscillatory. (A) Mizzen L-11 3760m-3765m, from within the Jurassic Sandstone #2 unit (B) Mizzen L-11 3615m-3620, from within the Jurassic Sandstone #1 unit (C) Mizzen L-11 3415m-3420m, from within the Baccalieu Sandstone unit (D) Baccalieu I-78 3255m-3260m, from within the Hibernia Formation equivalent (E) Baccalieu I-78 2175m-2180m, from within the Avalon Formation equivalent (F) Blue H-28 5015m-5020m and 5025m-5030m, from within the Albian Sandstone unit.

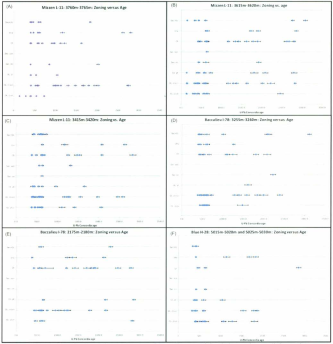

Figure 6.8: Cross plots of grain zoning types verses Concordia ages of dated zircons from each interval. Only concordant U-Pb ages are included. Error bars are 2σ. oc,ct,cn = oscillatory concentric centered; oc,ct,ocn= oscillatory concentric off-centered; oc,pl = oscillatory planar; sec,cn = sector centered; sec,ocn = sector, off-centered; ot = convolute/irregular/other; unz = unzoned; sec+oc = sector plus oscillatory. (A) Mizzen L-11 3760m-3765m, from within the Jurassic Sandstone #2 unit (B) Mizzen L-11 3615m-3620, from within the Jurassic Sandstone #1 unit (C) Mizzen L-11 3415m-3420m, from within the Baccalieu Sandstone unit (D) Baccalieu I-78 3255m-3260m, from within the Hibernia Formation equivalent (E) Baccalieu I-78 2175m-2180m, from within the Avalon Formation equivalent (F) Blue H-28 5015m-5020m and 5025m-5030m, from within the Albian Sandstone unit.

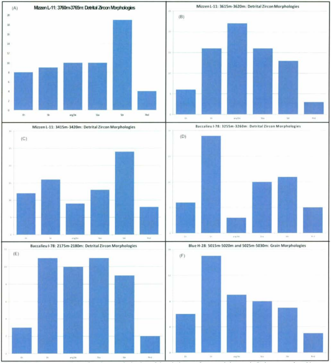

Figure 6.9: Frequency plots of grain morphologies of dated zircons from each interval. Only concordant U-Pb ages are included. Eh = euhedral; Sh = subhedral; ang/bk = angular or broken (possibly during processing); Sba = sub-angular; Sbr = sub-rounded; Rnd = rounded. (A) Mizzen L-11 3760m-3765m, from within the Jurassic Sandstone #2 unit (B) Mizzen L-11 3615m-3620, from within the Jurassic Sandstone #1 unit (C) Mizzen L-11 3415m-3420m, from within the Baccalieu Sandstone unit (D) Baccalieu I-78 3255m-3260m, from within the Hibernia Formation equivalent (E) Baccalieu I-78 2175m-2180m, from within the Avalon Formation equivalent (F) Blue H-28 5015m-5020m and 5025m-5030m, from within the Albian Sandstone unit.

euhedral, angular, sub-angular and sub-rounded. Late Neoproterozoic grains have a mixture of morphologies that include all types from euhedral to round. Grains that make up the Late Mesoproterozoic age peaks are dominantly sub-rounded, with minor sub-angular, angular and subhedral grains also present. Paleoproterozoic grains show a range in morphologies from subhedral to rounded, but most are rounded, sub-rounded or sub-angular. Most Archean grains are angular to sub-round (Figure 6.10a). Approximately 60% of the dated grains in this sample are interpreted as probable multi-cycle grains, and probably derived from sediments or low grade metasedimentary rocks.

6.3.3 Interpretations

The youngest grain in this sample has an age of 142 ± 6 Ma, and therefore defines the maximum depositional age of this unit as Barremian to Valanginian (Early Cretaceous). This is in contrast to the Tithonian (Latest Jurassic) biostratigraphic age of deposition for this interval (Section 3.2.1 of this thesis), but this will be more thoroughly discussed in Chapter 6. The Mesozoic grain is subhedral, below average in size, oscillatory zoned, and has moderate Th/U values. It is interpreted as a first-cycle igneous, possibly volcanic sourced grain. The relatively small size and lack of all crystal faces suggests the grain grew in the interstitial space of cumulative framework minerals, and therefore may have crystallized in the late stage interstitial melt of an intermediate or mafic composition, rather than in a granitic source rock.

The range in size, Th/U values and zoning exhibited by grains from the Late Silurian- Early Devonian age peak indicates a mixture of source types, probably including

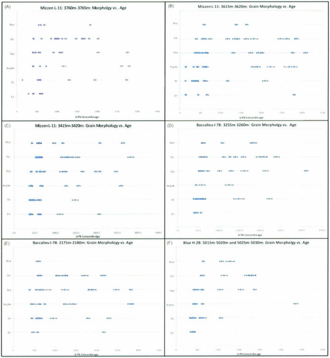

Figure 6.10: Cross plots of grain morphology types verses Concordia ages of dated zircons from each interval. Only concordant U-Pb ages are included. Error bars are 2σ. Eh = euhedral; Sh = subhedral; ang/bk = angular or broken (possibly during processing); Sba = sub-angular; Sbr = sub-rounded; Rnd = rounded. (A) Mizzen L-11 3760m-3765m, from within the Jurassic Sandstone #2 unit (B) Mizzen L-11 3615m-3620, from within the Jurassic Sandstone #1 unit (C) Mizzen L-11 3415m-3420m, from within the Baccalieu Sandstone unit (D) Baccalieu I-78 3255m-3260m, from within the Hibernia Formation equivalent (E) Baccalieu I-78 2175m-2180m, from within the Avalon Formation equivalent (F) Blue H-28 5015m-5020m and 5025m-5030m, from within the Albian Sandstone unit.

igneous plutonic and volcanic grains as well as metamorphic grains. Many of the grains are euhedral, and most of the rest are angular, implying dominantly first- to second-cycle zircons with lesser amounts of sub-angular and sub-round grains that are more likely second- or multiple-cycle detrital grains. The Carboniferous grains are relatively small, oscillatory zoned and subhedral to euhedral. Based on these characteristics, they are interpreted as probable first-cycle volcanic zircons.

Detrital zircons that make up the main Late Neoproterozoic age peak (580 Ma) are dominantly oscillatory zoned, euhedral and subhedral, exhibit a range in sizes and have moderate to high Th/U. The grains from this age group are interpreted to be mainly derived from plutonic ± volcanic igneous sources. A few sub-round and rounded grains are present, and are interpreted as multi-cycle grains.

Most of the Mesoproterozoic grains are sub-angular, sub-round and rounded, have low Th/U (<0.5), are dominantly convolute/irregularly and oscillatory zoned, and are on average bigger than grains of other ages. The Mesoproterozoic grains are interpreted as dominantly multi-cycle, plus possible minor first-cycle, metamorphic grains.

Most of the Paleoproterozoic grains have sub-angular to rounded morphologies, and so are interpreted as dominantly multi-cycle detrital zircon grains. The Th/U values are split between grains with Th/U>0.5 and grains with Th/U<0.5, and most of the grains show concentric oscillatory zoning, indicative of a mixture of igneous and metamorphic original sources.

Most Archean grains are sub-angular to sub-round, and exhibit a variety of zoning types, Th/U values and sizes, implying dominantly multi-cycle grains with a mixture of original sources probably including plutonic and volcanic igneous and metamorphic sources.

6.4 Mizzen L-11: Jurassic Sandstone # 1

Detrital zircons were obtained from a cuttings sample taken between 3615 m and 3620 m. From this sample, 108 detrital zircons were mounted and imaged, 82 representative grains were ablated, and 75 yielded usable concordant U-Pb ages.

6.4.1 Age Groups

The dated detrital zircons in this sample are dominated by grains with Late Neoproterozoic, Early-Mid Paleozoic and Jurassic-Cretaceous ages, with lesser groups of Mesoproterozoic, Paleoproterozoic ages, and a relatively significant group of Late Archean ages (Figures 6.1b, 6.2b and 6.11).

Seven Mesozoic grains are present, with ages between 134 ± 13 Ma and 152.3 ± 9.6 Ma (Early Cretaceous to Late Jurassic) and with a cumulative probability peak at 142 ± 10 Ma (Earliest Cretaceous). Upon closer inspection of these ages, it appears that there are two groupings of Mesozoic ages, one comprising 4 grains with ages between 134 ± 13 Ma and 139.5 ± 3.6 Ma (Valanginian-Berriasian) and one comprising 3 zircons with ages between 149.4 ± 7.6 Ma and 152.3 ± 9.6 Ma (Tithonian-Kimmeridgian).

Paleozoic grains account for 26% of all dated grains. These grains range in age between 293 ± 17 Ma and 482 ± 30 Ma (Pennsylvanian to Early Ordovician), and a cumulative probability peak occurs at 420 ± 30 MA (Late Silurian). Despite the range of

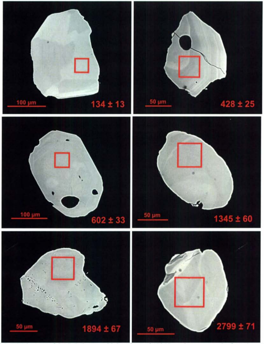

Figure 6.11: BSE images of detrital zircons with locations of 40*40 µm laser raster pits from Jurassic Sandstone #1. (A) Relatively large, subhedral sector + oscillatory zoned Mesozoic aged (Early Cretaceous) detrital zircon; probable first-cycle igneous plutonic origin. (B) Subhedral/ broken or angular and oscillatory zoned Silurian aged detrital zircon; probable first-cycle igneous plutonic or volcanic origin. (C) Large, subhedral and sector + oscillatory zoned Late Neoproterozoic zircon; probably first-cycle igneous plutonic origin. (D) Sub-round and irregularly zoned Mesoproterozoic detrital zircon; probably second- or multi-order metamorphic origin. (E) Sub-angular to sub-round, irregularly zoned Paleoproterozoic detrital zircon; probable first- or muli-order metamorphic origin. (F) Sub-rounded, sector + oscillatory and partially irregulalry zoned Archean detrital zircon; probable multi-order (metamorphosed?) igneous plutonic or volcanic origin.

Paleozoic ages, 14 grains (70% of all Paleozoic and 18% of all dated grains) have ages between 397 ± 31 Ma and 445 ± 18 Ma; therefore, the Paleozoic grain population is dominated by Early Devonian to Late Ordovician grains, with most of the ages being Silurian. No dated grains have ages between 500 and 550 Ma.

Out of all the dated grains, 32% have Late Neoproterozoic ages ranging between 551 ± 20 Ma and 734 ± 45 Ma, with most between 550 and 670 Ma with a cumulative probability peak at 620 ± 60 Ma, making this the largest and most significant age peak from this sample.

The remaining 26% of dated grains have ages older than 1.0 Ga, which have ages ranging between 1.1 and 3.1 Ga (Mesoproterozoic to Late Archean) and several discrete age groupings. There are no grains with ages or associated errors between 750 and 1100 Ma. Mesoproterozoic aged grains account for 8% of all dated grains, and cumulative probability peaks occur at ca. 1170 ± 50 Ma and 1375 ± 100 Ma. Paleoproterozoic grains account for 15% of all dated grains. There are minor age peaks associated with these grains, which occur at ca. 1700 Ma (+75/-50 Ma) and 1900 Ma (+200/-250 Ma) ; however, for the most part, a scattered range of Late Paleoproterozoic ages are present between 1600 and 2100 Ma, rather than discrete groupings of ages. Late Archean aged grains account for 10% of all dated grains in this sample, and range in age between 2600 and 3100 Ma, with a significant cumulative probability peak at ca. 2800 ± 80 Ma.

6.4.2 Qualitative analysis of dated grains

Ratios of Th/U in dated zircon grains in this sample range between 0.1 and 1.3, but variations in the range of Th/U values occur between grains belonging to different age groups. Most of the Mesozoic grains present have Th/U values between 0.8 and 0.9, but one grain has a Th/U value of about 2.3. Most Silurian aged grains have Th/U values between 0.5 and 0.7. Late Neoproterozoic grains that make up the ca. 605 Ma peak appear to bimodal with respect to Th/U, with one group having values between 0.3 and 0.5 and another with values between 0.6 and 1.0. Most of the Mesoproterozoic grains have Th/U >0.5, and the Paleoproterozoic grains have values between 0.2 and 0.45, with several grains that have Th/U >1. Archean grains show the greatest range in Th/U values, ranging from 0.25 to 1.3, with most having values >0.5 (Figure 6.4b).

Dated grains from this sample have cross-sectional areas ranging from 2500 μm^2 to 53000 μm^2, with an average cross-sectional area value of 14700 μm^2 and a median value of 11600 μm^2. The Mesozoic, Paleozoic and Late Neoproterozoic grains show a range in sizes, generally between 5000 μm^2 and 40000 μm^2. Grains from the Silurian age peak comprise a main group of grains with cross-sectional areas between 5000 μm^2 and 15000 μm^2, and a smaller group of larger grains with sizes between 20000 μm^2 and 35000 μm^2. On the other hand, Mesoproterozoic grains are restricted in size, typically between 5000 μm^2 and 15000 μm^2, with most having areas around 13000 μm^2. Paleoproterozoic zircons range in size between 4000 μm^2 and 20000 μm^2, but most are <20000 μm^2. Archean zircons range in size between 4000 μm^2 and 26000 μm^2, but most grains are <10000 μm^2 (Figure 6.5b).

Grains from the Mesozoic age peak are for the most part equant, having aspect ratios less than 0.25. Grains from the Silurian peak have a range in aspect ratios, from equant (1.0) to relatively elongate (1.75), however most are relatively equant, with aspect ratios between 1.0 and 1.4. Younger Paleozoic grains have aspect ratios between 0.25 and 0.5. Aspect ratios of the Neoproterozoic grains range between 1.05 and 1.7 (Figure 6.6b).

Numerous types of compositional zoning were present in the dated zircon grains from this sample, but the most abundant was concentric oscillatory zoning (centered and off-centered), which accounts for 42% of all dated grains (Figure 6.7b). Convoluted/irregular zoning types are also abundant, accounting for 24% of all dated grains. The Mesozoic grains are almost entirely oscillatory-zoned (including planar). Paleozoic and Late Neoproterozoic grains show a range in zoning types that reflects the overall variations in zoning of the entire dated grain population. Mesoproterozoic and Paleoproterozoic grains are split mainly between grains with concentric oscillatory and cryptic/irregular zoning. The Archean grains are dominantly cryptically or sector+oscillatory zoned (Figure 6.8b).

Grain morphologies are variable in the dated grain population. The most abundant type is angular and/or broken grains, but sub-angular, subhedral and sub-rounded grains are also abundant (Figure 6.9b). Morphologies vary as a function of age, with Mesozoic and Paleozoic grains that are dominantly euhedral and subhedral, Late Neoproterozoic grains that are mostly subhedral to sub-angular, and all older grains (>1Ga) that are dominantly angular to rounded (Figure 6.10b). Approximately 28% of the dated grains are interpreted as multi-cycle detrital zircons.

6.4.3 Interpretations

The youngest detrital zircon present in this sample, with an age of 134 ± 13, defines the minimum depositional age of this sandstone unit as probable Valanginian. Even though a range in minimum depositional ages are possible due to the error of this age (any time between Aptian to Tithonian), the presence of three other Valanginian and Berriasian aged grains supports a minimal depositional age of Earliest Cretaceous for this unit. Perhaps the best constraint on the minimum age is one grain with a concordant age of 139.5 ± 3.6 Ma, which, even within error, is Valanginian-Berriasian in age. An error weighted average age was calculated using ages from all the Late Jurassic and Early Cretaceous ages using the ISOPLOT/EX program. The resulting error weighted average age is 141 ± 6.4 Ma (Berriasian, or Earliest Cretaceous) (Figure 6.12). The Mesozoic grains are subhedral to euhedral, most are relatively large and equant, and all have high Th/U are oscillatory zoned. Based on these characteristics, they are interpreted to be of plutonic igneous origin, and probably originated from Zr-rich felsic magmas due to their large grain size and zoning (Figure 6.11a).

Most of the detrital zircons from the Silurian age peak are subhedral, oscillatory zoned, with moderate to large sizes, moderate to high Th/U and relatively small aspect ratios, indicative of a predominance of first-cycle plutonic igneous sources of Silurian detrital zircons. Other grains with convolute zoning, low Th/U, and sub-rounded morphologies may represent metamorphic and/or multi-cycle metasedimentary grains. Several smaller grains with higher aspect ratios are present throughout the range of Paleozoic ages, and these could be volcanic in origin.

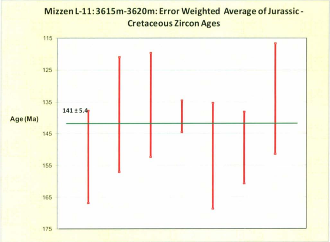

Figure 6.12: Error-weighted average U-Pb Concordia average age from all Late Jurassic and Early Cretaceous grains from the sample in Jurassic Sandstone #1. An age of 141 ± 6.4 Ma places the age of the detrital zircon source or sources in the Berriasian Age of the Early Cretaceous Epoch, and thus defines the maximum depositional age of the unit as no older than Earliest Cretaceous.

The bimodal nature of Th/U and mixture of oscillatory and convolute/irregular zoning in grains comprising the Late Neoproterozoic peak suggests a mixture of igneous and metamorphic sourced grains. Based on grain morphologies, around 40% of the Late Neoproterozoic grains may be multi-cycle; however, most of the interpreted multi-cycle grains are sub-angular, and therefore may just have been transported over longer distances.

Generally, the Mesoproterozoic grains have low Th/U, moderate size, are convolute/irregularly or oscillatory zoned and are mostly sub-rounded, indicating a dominance of multi-cycle metamorphic and igneous grains, with a portion of grains possibly derived directly from metamorphic sources as well. Paleoproterozoic grains display a similar range of characteristics, and so are interpreted similarly. Archean grains are for the most part sub-angular to sub-rounded, relatively small, have a range of Th/U values, and exhibit a variety of zoning types. They are interpreted as dominantly multi-cycle zircon grains initially from a variety of crustal sources, probably including plutonic and volcanic igneous and metamorphic sources.

6.5 Mizzen L-11: Baccalieu Sandstone

Detrital zircons were obtained from a cuttings sample taken between 3415 m and 3420 m. From a cuttings sample from the interval between 3415m and 3420m, 152 detrital zircons were mounted and imaged, 98 representative grains were ablated to yield 81 usable concordant U-Pb ages.

6.5.1 Age Groups

The detrital zircons that were dated show major age groupings in the Late Neoproterozoic and Middle-Late Paleozoic, with some scattered Proterozoic and minor Archean aged zircons. The Neoproterozoic group is by far the most prominent, with 38% of all dated zircons having ages between 558 ± 21 Ma and 732 ± 28 Ma and with a cumulative probability peak of ca. 620 Ma (+50/-60 Ma) (Figures 6.1c, 6.2c and 6.13).

Paleozoic zircons range in age mainly between 370 and 490 Ma (Middle Devonian to Early Ordovician) with only two zircons of Cambrian age. In all, 33% of the dated detrital zircons fall within this range of Middle to Late Paleozoic ages, and cumulative probability peaks are present at 385 Ma (Mid-Devonian) and 435 Ma (Early Silurian). Reflecting these two peaks are 2 major groupings of detrital zircon ages, one in the Late to Middle Devonian with ages ranging between 372 ± 11 Ma and 397 ± 11 Ma (9 grains, or 11% of all dated grains) and one in the Early Devonian to Early Silurian (9 grains, or 12% of all dated grains).

Neoproterozoic grains in this sample have ages ranging between 540 and 735 Ma, but most of the grains (70%) have ages between 600 and 655 Ma with a cumulative probability peak of ages at ca. 620 Ma (+50/-60 Ma).

The remaining 29% of the dated grains have Meso- and Paleoproterozoic and Late Archean ages. Mesoproterozoic grains have a range in ages, with significant age cumulative probability peaks at ca. 1150 Ma (+100/-50 Ma), ca. 1250 Ma (+50/-100 Ma) and ca. 1550 Ma (±50 Ma). Paleoproterozoic grains are primarily represented by a single

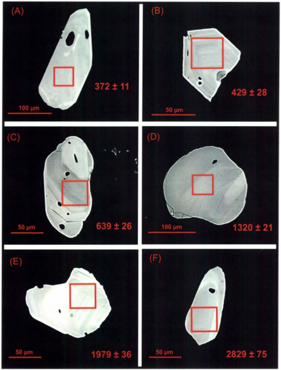

Figure 6.13: BSE images of detrital zircons with locations of 40*40 µm laser raster pits from Baccalieu Sandstone in Mizzen L-11. (A) Relatively large, subhedral oscillatory zoned Late Devonian detrital zircon; probable first-cycle igneous plutonic origin. (B) Euhedral broken and oscillatory zoned Silurian aged detrital zircon; probable first-cycle igneous plutonic origin. (C) Large, sub-round and oscillatory zoned Late Neoproterozoic zircon; probably first- or second-cycle igneous plutonic origin. (D) Sub-round and irregularly zoned Mesoproterozoic detrital zircon; probably second- or multi-order metamorphic origin. (E) Angular oscillatory zoned Paleoproterozoic detrital zircon; probable first- or muli-order igneous origin. (F) Sub-angular, oscillatory and partially irregulalry zoned Archean detrital zircon; probable multi-order (metamorphosed?) igneous plutonic or volcanic origin.

age peak at ca. 2075 Ma (± 30Ma). Only 3 Late Archean grains are present, with a minor age peak at ca. 2630 Ma (±50 Ma).

6.5.2 Qualitative analysis of dated grains

Values of Th/U of dated grains from this sample range from 0.02 to 2.3; however, most grains have values between 0.2 and 0.6. There are some variations in Th/U values with respect to age. Paleozoic and Late Neoproterozoic grains have nearly identical Th/U values between 0.2 and 1.6, with most having values between 0.4 and 1.0. A single Early Devonian grain has a Th/U value of around 2.3. Mesoproterozoic grains are dominated by lower values, ranging between 0.2 and 0.42. Grains from the 2075 Ma Paleoproterozoic peak have Th/U values between 0.5 and 0.85.

Dated grains from this sample have cross-sectional areas ranging from 3000 μm^2 to 26000 μm^2, with an average cross-sectional area value of 8600 μm^2 and a median value of 8000 μm^2. There appears to be some relationship between age and size. Grains from the Paleozoic peak range in area between 3000 μm^2 and 10000 μm^2. Late Neoproterozoic grains show a continuous range in sizes between 4000 μm^2 13000 μm^2 as well as several with sizes >15000 μm^2, and so are on average larger than Paleozoic grains in this sample. Grains from the 1150-1250 Ma peaks are dominantly 8000 μm^2 to 12000 μm^2, and grains from the 1550 Ma peak are dominantly 6000 μm^2 to 8000 μm^2. Grains from the 2075 Ma Paleoproterozoic peak have cross-sectional areas between 6000 μm^2 to 9000 μm^2. Archean grains are smaller, having cross-sectional areas between 4000 μm^2 to 8000 μm^2.

Types of zoning are varied, but are most abundantly centered and off-centered concentric oscillatory (45%), cryptic/irregularly zoned (18%) and sector + oscillatory zoned (14%). There does not appear to be a strong relationship between age and zoning types, except for the fact that all of the sector + oscillatory zoned grains are Paleozoic or Late Neoproterozoic, and most of the planar oscillatory grains have Paleozoic ages.

Morphologies are also quite varied; however, many of the grains (29%) are sub-rounded. Many of the subrounded grains comprise the Late Neoproterozoic age group of detrital zircons. In contrast, most of the Paleozoic grains present are subhedral or euhedral. Older (>1Ga) grains are dominantly sub-angular, sub-rounded or rounded. Approximately 58% of the detrital zircons are interpreted as multi-cycle.

6.5.3 Interpretations

Paleozoic grains can be divided into two groups based on differences in ages and properties. Middle and Late Devonian grains predominantly are elongate, have characteristically low Th/U values of less than 0.5 and a mixture of convoluted/irregularly and oscillatory zoning, indicative of a predominance of metamorphic origin or mixture of grains derived from igneous and metamorphic sources. In contrast, Early Paleozoic grains (Cambrian to Early Devonian) are dominantly more equant, have higher Th/U values (>0.5) and are dominated by oscillatory zoning, indicating a dominance of igneous (probably plutonic) grains in this age range. All of the Paleozoic grains are subhedral to angular, indicating that most or all or first-cycle grains.

Grains from the Neoproterozoic group are equant to elongate, have Th/U values greater than 0.5, show a range in sizes and variety of zoning types and a large proportion of the grains are sub-rounded, with lesser amounts having euhedral to subhedral morphologies. These grains are thus interpreted as dominantly second- or multi- order grains and lesser first-order grains of igneous origin, likely including volcanic and plutonic sources, based on variable zoning, aspect ratios and sizes.

Mesoproterozoic grains in this sample are dominantly subround, relatively large, show a variety of zoning types and have Th/U values of les than 0.5. They are interpreted as possibly first- but probably multiple-cycle grains of dominantly metamorphic origin. Paleoproterozoic grains are dominantly angular to rounded, oscillatory zoned, and have Th/U values greater than 0.5, and are interpreted as multiple-cycle detrital grains of igneous origin. Archean grains are subangular to rounded, oscillatory or convolute zoned, and have Th/U values between 0.4 and 0.6, and are interpreted as multi-cycle grains of mixed origin.

6.6 Baccalieu I-78: Hibernia Formation Equivalent

Detrital zircons were obtained from a cuttings sample taken between 3255 m and 3260 m. From this sample, 86 detrital zircons were mounted and imaged. From this, 82 detrital zircons were processed using MLA to obtain information on cross-sectional area and aspect ratios. Sixty-three of the grains were ablated were ablated using a 40 x 40 x 15 μm raster pit for age dating. Of the 63 ablated samples, 55 produced usable concordant U-Pb ages.

6.6.1 Age Groups

The detrital zircon population comprises a significant Late Neoproterozoic component, with 33% of the grains having ages between 551 ± 50 Ma and 728 ± 35 Ma; although most of the grains have ages between 590 Ma and 630 Ma, forming a cumulative probability peak of 600 Ma (+50/-75 Ma) (Figures 6.1d, 6.2d and 6.14).

A significant Early Paleozoic group of zircons exist as well, with 32% of all dated grains having ages between 392 ± 24 Ma and 537 ± 26 Ma (Devonian-Cambrian) and with a cumulative probability peak of 450 ± 50 Ma (Late Ordovician). However, upon closer inspection, the grains with ages within this range actually comprise 2-3 significant age groupings. The main Paleozoic age group comprises 5 detrital grains (~10% of all dated grains) with ages between 430 ± 36 Ma and 446 ± 23 Ma (Early Silurian to Latest Ordovician). Two grains with ages of 413 ± 26 Ma and 414 ± 31 Ma (Earliest Devonian) were also dated. Four grains were dated with ages ranging throughout the Ordovician (460-485 Ma) and one with an Late-Mid Cambrian age (505 ± 23 Ma). Four grains were dated with Earliest Cambrian Ages ranging between 531 ± 43 Ma and 538 ± 26 Ma; however, it should be noted that these could be latest Neoproterozoic grains, given the error of their ages. In contrast to the Paleozoic aged grains in other samples, the majority of the Paleozoic grains from this sample are Ordovician in age.

The remaining 35% of detrital zircon grains in this sample have Proterozoic ages scattered mostly between 1.0 and 2.5 Ga, with minor probability peaks at ca. 1100 Ma (± 100Ma), ca. 1300 Ma (+75/-50 Ma), ca. 1600 Ma (± 100 Ma), ca. 1820 Ma (+75/-50 Ma),

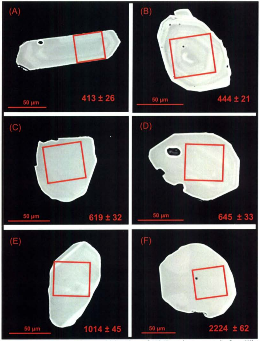

Figure 6.14: BSE images of detrital zircons with locations of 40*40 µm laser raster pits from Hibernia Sandstone in Baccalieu I-78. (A) Relatively elongate, euhedral oscillatory zoned Late Devonian detrital zircon; probable first-cycle igneous volcanic origin. (B) Subhedral and oscillatory zoned Late Ordovician aged detrital zircon; probable first-cycle igneous plutonic origin. (C) Subhedral/broken and faintly oscillatory zoned Late Neoproterozoic zircon; probably first- or second-cycle igneous plutonic origin. (D) Subhedral and oscillatory zoned Late Neoproterozoic detrital zircon; probable first-cycle igneous origin. (E) Angular and sector + oscillatory zoned Mesoproterozoic detrital zircon; probable first- or muli-order igneous origin. (F) Sub-angular, sector zoned Archean detrital zircon; probable multi-cycle igneous plutonic origin.

and ca. 2100 Ma (± 100 Ma). Only one Archean grain was dated, with an age of 3111 ± 43 Ma.

6.6.2 Qualitative analysis of dated grains

Values of Th/U range between 0.1 and 1.9; however, most <1 Ga grains have Th/U values ranging between 0.2 and 1.2, and the >1 Ga grains have Th/U values between 0.2 and 0.8. Other than this, there does not appear to be a strong relationship between Th/U and age grouping.

Dated grains from this sample have cross-sectional areas ranging from 1900 μm^2 to 14000 μm^2, with an average cross-sectional area value of 5600 μm^2 and a median value of 5150 μm^2. There does not appear to be a correlation between age groups and cross-sectional area of grains, and most grains, regardless of age, have cross-sectional areas between 2000 μm^2 and 10000 μm^2, with the greatest concentration with cross-sectional areas between 4000 μm^2 and 6000 μm^2.

Most of the dated grains in this sample (56%) have centered or off-centered concentric oscillatory zoning. Most of the remaining grains have either cryptic/irregular or sector+oscillatory zoning or are unzoned. For the Mesoproterozoic and Paleoproterozoic grains, concentric oscillatory zoned grains are less dominant than they are for Paleozoic and Late Neoproterozoic grains.

With regards to grain morphologies, subhedral grains are the most abundant overall, but sub-angular and sub-rounded grains are also abundant in the dated grain population. There appears to be the regular relationship between grain morphology and age, where older grains (>1 Ga) are dominantly sub-angular to rounded and Paleozoic and Late Neoproterozoic grains are more dominantly subhedral. Approximately 46% of the dated detrital grains are interpreted as multi-cycle.

6.6.3 Interpretations

Paleozoic grains are dominantly subhedral to euhedral, relatively small, oscillatory zoned, and have Th/U values between 0.5 and 1.0, and aspect ratios that range from nearly equant to elongate. These grains are interpreted as dominantly first cycle igneous grains, probably having both volcanic and plutonic origins.

Grains that comprise the Neoproterozoic age peak are dominantly subhedral, oscillatory zoned, equant to slightly elongate, average to large in size, and have Th/U values mostly between 0.5 and 1.0. They are interpreted as first cycle igneous grains, of dominantly plutonic, but also of likely volcanic origin.

Mesoproterozoic grains in this sample vary in size, zoning and Th/U, but most are subangular to rounded, and are therefore interpreted as second- or multiple-cycle detrital grains from a variety of original sources. Paleoproterozoic grains are dominantly rounded to sub-rounded, have Th/U values between 0.4 and 1.0, are average to relatively large, and exhibit a variety of zoning types. They are interpreted as second- or multi-cycle grains of original igneous or metamorphic origin.

6.7 Baccalieu I-78: Avalon Formation Equivalent

Detrital zircons were obtained from a cuttings sample taken between 2175 m and 2180 m. From this sample interval, 69 zircons were mounted and imaged. From this, 47 representative grains were ablated using a 40 x 40 x 15 μm raster pit, and 12 were ablated using a 30 μm laser spot. Of the 59 ablated detrital zircons, 47 produced usable concordant U-Pb ages.

6.7.1 Age Groups

Detrital zircon ages from this sample are characterized by a dominant Late Neoproterozoic grouping, with subordinate (but significant) Mesoproterozoic, Paleoproterozoic and Archean groups, and relatively minor Paleozoic zircons (Figures 6.1e, 6.2e and 6.15).

Approximately 41% of the dated grains are Neoproterozoic in age, and have ages ranging between 566 ± 43 Ma and 749 ± 24 Ma, with a cumulative probability peak at ca. 610 ± 60 Ma.

Five Paleozoic grains are present (approximately 10% of all dated grains), with ages ranging between 383 ± 19 Ma and 484 ± 60 Ma (Mid-Devonian to Early Ordovician) and with a cumulative probability peak at ca. 450 ± 60 Ma (Late Ordovician). The distribution of ages of these grains is essentially similar to those of the Paleozoic grains in the sample from the Hibernia Formation equivalent.

Five detrital zircons (10%) make up a ca. 1250 Ma (+80/-60 Ma) (Mesoproterozoic) peak, and include zircons between the ages of 1175 ± 90 Ma and 1261

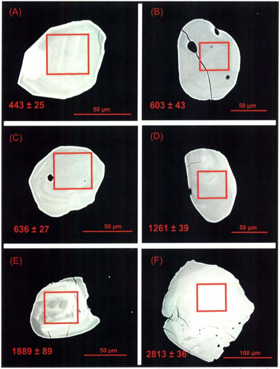

Figure 6.14: BSE images of detrital zircons with locations of 40*40 µm laser raster pits from Avalon Sandstone in Baccalieu I-78. (A) Relatively equant, euhedral oscillatory zoned Late Ordovician detrital zircon; probable first-cycle plutonic igneous origin. (B) Rounded and sector+oscillatory zoned Late Neoproterozoic aged detrital zircon; probable multi-cycle igneous plutonic origin. (C) Subhedral and faintly oscillatory zoned Late Neoproterozoic zircon; probably first-cycle igneous plutonic origin. (D) Sub-rounded and oscillatory zoned Mesoproterozoic detrital zircon; probable multi-cycle igneous origin. (E) Rounded/broken and oscillatory and convolutedly zoned Paleoproterozoic detrital zircon; probable multi-cycle igneous+metamorphic origin. (F) Large sub-angular oscillatory zoned Archean detrital zircon; probable multi-cycle igneous plutonic origin.

± 39 Ma. Paleoproterozoic aged zircons are distributed in two main peaks (ca. 1830 ± 120 Ma and ca. 2175 ± 50 Ma), with ages ranging between 1709 ± 78 Ma and 1920 ± 56 Ma for the ca. 1800 Ma peak and 2125 ± 39 Ma and 2289 ± 48 Ma for the ca. 2200 Ma peak. A minor Archean grouping is also present (3 zircons, or 6%), with a cumulative probability peak at ca. 2800 Ma (+50/-100 Ma) and ages ranging between 2785 ± 48 Ma and 2854 ± 35 Ma.

6.7.2 Qualitative analysis of dated grains

Values of Th/U of the dated grains range between 0.2 and 1.6, except for one grain with an anomalously high Th/U of 3.1. Most of the grains have Th/U values between 0.4 and 0.8. The Late Neoproterozoic grains show a continuous range of Th/U values between 0.35 and 0.85, with several grains having values between 0.9 and 1.1, and then several more with values between 1.4 and 1.6. Most Mesoproterozoic grains have Th/U values between 0.2 and 0.6, with the exception of one grain with a value of 1.4. Paleoproterozoic grains have values between 0.3 and 0.8. The few Archean aged grains have Th/U values between 0.3 and 0.5.

Grain cross-sectional areas range mostly between 2000 μm^2 and 10000 μm^2; however, two large grains, with cross-sectional areas of 21588 μm^2 and 26740 μm^2 are also present. In general, there seems to be an increase in grain size with age, with Late Neoproterozoic grains ranging in size between 2000 μm^2 and 8000 μm^2, Mesoproterozoic and Paleoproterozoic grains ranging in size between 3500 μm^2 and 7000 μm^2, and the largest grains mentioned above have Archean ages.

The dated grains show a variety of zoning types; however, concentric oscillatory zoned grains are by far the most abundant type (50%). Cryptic/irregularly zoned grains are also abundant (28%). There are some apparent variations present between zoning types and age. Late Neoproterozoic and Mesoproterozoic grains are dominated by concentric oscillatory zoned grains, with minor cryptically/irregularly, sector+ oscillatory and unzoned varieties, whereas older grains are relatively more dominated by cryptically/irregularly, sector+ oscillatory and unzoned varieties.

With regards to grain morphologies, the dated grains are mostly subhedral, angular, sub-angular and sub-rounded morphologies, with lesser amounts of euhedral and rounded grains. The regular age verses morphology relationship exists, where the Paleozoic and Late Neoproterozoic grains are dominated by subhedral and euhedral morphologies, whereas older grains are dominated by sub-angular and sub-rounded morphologies. Approximately 66% of the dated detrital zircon grains are interpreted as multi-cycle grains.

6.7.3 Interpretations

Paleozoic grains in this sample are relatively small, euhedral to sub-angular, have Th/U values between 0.3 and 1.5 and exhibit a range of zoning types. They are interpreted as mainly first- or second-cycle grains originally from a mixture of source types. Neoproterozoic grains are dominantly oscillatory zoned and have Th/U values greater than 0.5, but exhibit a variety of sizes, morphologies and aspect ratios. They are interpreted as a mixture of first- and second- or multiple- cycle detrital grains of dominantly original igneous origin. Mesoproterozoic grains are sub-angular to rounded, are oscillatory or cryptically zoned, or unzoned, and exhibit a range of Th/U values. They are interpreted as dominantly recycled detrital grains of original igneous or metamorphic origin. Paleoproterozoic grains are dominantly sub-angular to sub-rounded, have Th/U over 0.5, and are unzoned or oscillatory zoned. They are interpreted as recycled detrital grains of original igneous origin. The three Archean grains present exhibit a variety of zoning types, are angular or sub-angular and have Th/U values less than 0.5, and are interpreted as recycled metamorphic derived detrital zircons.

6.8 Blue H-28: Albian Sandstone

Detrital zircons from samples at from two 5m intervals (5015-5020 m and 5025-5030 m) were used for combined detrital zircon geochronology of this unit. From the sample between 5015 m and 5020 m, 27 grains were mounted and imaged, 19 were ablated and only 12 yielded usable concordant U-Pb ages. From the sample between 5025 m and 5030 m, 46 grains were mounted and imaged, 43 were ablated, and 37 yielded usable concordant U-Pb ages. In all, 48 concordant single detrital zircon ages were used for provenance analysis of this interval.

6.8.1 Age Groups

The predominant age group of detrital zircons in this sample is of Silurian age, with lesser amounts of other grains having other Paleozoic ages. A lesser Late Neoproterozoic group is also present, as well as minor Mesoproterozoic and

Paleoproterozoic groups, and a single Late Archean aged grain (Figures 6.1f, 6.2f and 6.16).

Paleozoic grains range in age between 349 ± 23 Ma and 518 ± 28 Ma (Early Carboniferous to Mid-Cambrian); however, most of grains (approximately 60% of Paleozoic and 18% of all dated zircons) have ages between 418 ± 14 Ma and 436 ± 38 Ma (Silurian) and a cumulative probability peak occurs at ca. 420 ± 20 Ma (Late Silurian).

Late Neoproterozoic grains account for approximately 24% of all grains, and have ages between 576 ± 36 Ma and 647 ± 71 Ma, with a cumulative probability peak at 620 Ma (+30/-50 Ma). Mesoproterozoic grains account for 12% of all dated grains with a cumulative probability peak at ca. 1080 ± 75 Ma. Paleoproterozoic grains account for 10% of all dated grains, with a small cumulative probability peak at ca. 1850 Ma (+50Ma/-120Ma). Only one Late Archean grain was present, with an age of 2852 ± 55 Ma.

6.8.2 Qualitative analysis of dated grains

Values of Th/U of dated grains range between 0.1 and 2.1; with most values occurring between 0.2 and 1.5. Paleozoic grains show a range of values primarily between 0.5 and 1.2, with only a few grains having values greater or less than this range. Late Neoproterozoic grains a have a relatively large range of Th/U values between 0.1 and 1.5, with a group of 4 grains with values between 0.6 and 0.7. Mesoproterozoic grains have Th/U values scattered between 0.4 and 0.9, and grains from the Paleoproterozoic age

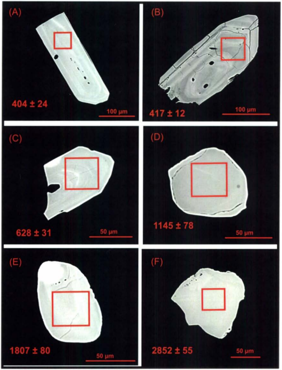

Figure 6.14: BSE images of detrital zircons with locations of 40*40 µm laser raster pits from The Albian aged sandstone in Blue H-28. (A) Elongate, euhedral/broken oscillatory zoned Early Devonian detrital zircon; probable first-cycle igneous volcanic origin. (B) Subhedral/broken and oscillatory (+xenocrystic?) zoned Late Silurian aged detrital zircon; probable first-cycle igneous plutonic origin. (C) Subhedral/broken and oscillatory zoned Late Neoproterozoic zircon; probably first-cycle igneous plutonic origin. (D) Sub-rounded and unzoned Late Mesoproterozoic detrital zircon; probable multi-cycle origin. (E) Rounded and sector + oscillatory zoned Paleoproterozoic detrital zircon; probable muli-order igneous origin. (F) Angular, sector zoned Archean detrital zircon; probable multi-cycle igneous plutonic origin.

group mostly have Th/U values between 0.3 and 0.5, with a couple of grains with values between 0.7 and 0.8. The one Archean grain has a value of approximately 1.55.

Grain cross-sectional areas range from 3864 μm^2 to 22902 μm^2, with an average cross-sectional area of 8410 μm^2 and a median cross-sectional area of 6790 μm^2. In general, the Paleozoic population appears to have the largest grains, as well as exhibiting the most range in sizes.

The most common types of zoning from dated grains in this sample are centered and off-centered concentric oscillatory zoning, which make up 63% of all grains. For the most part, there is not a strong relationship between zoning types and age, except that all of the sector + oscillatory zoned grains are Paleozoic, and the one Archean grain has cryptic/irregular zoning.

A variety of grain morphologies are represented in the dated grains from this sample, but the most abundant morphology type is subhedral (30% of dated grains). Paleozoic grains are dominantly euhedral to subhedral, with some angular and sub-angular grains present. Late Neoproterozoic grains display a range in morphologies from subhedral to rounded. Most of the >1Ga grains are sub-angular to rounded. Approximately 40% of the dated detrital zircons are interpreted as multi-cycle grains.

6.8.3 Interpretations

Paleozoic grains dominantly have Th/U values above 0.5, are mostly euhedral to angular, mostly oscillatory zoned, and exhibit a large range in sizes, but on average are larger than grains from other age groups. They are interpreted as predominantly first-cycle plutonic igneous grains.

Neoproterozoic grains are mostly oscillatory zoned, have Th/U vales above 0.5, have average sizes, but exhibit a mixture of grain morphologies, from euhedral to rounded. They are interpreted as a mixture of first- and multi-cycle detrital grains of predominantly igneous origin.

Mesoproterozoic grains in this sample have Th/U values between 0.3 and 1.0, are mostly subangular to rounded, oscillatory zoned, and exhibit a range in sizes. They are interpreted as second- or multiple-cycle grains of igneous and metamorphic origins. Paleoproterozoic grains are mostly small, sub-rounded, oscillatory or convoluted/irregularly zoned, and have Th/U values between 0.3 and 0.9. They are interpreted as multiple-cycle detrital grains with metamorphic and igneous origins. The single Archean grain is angular, unzoned, relatively large and with a high Th/U value, and is interpreted as a multi-cycle grain of metamorphic origin.

Chapter 7: Discussion and Conclusions

7.1 Introduction

This chapter presents a discussion of U-Pb age data from detrital zircons and other heavy mineral data, with a focus on depositional age constraints, determination of regional sediment source areas, regional paleodrainage orientations and distances, regional uplift, and reinterpretation of Late Jurassic to Early Cretaceous sand depositional models in the Northern Flemish Pass Basin.

7.2 Constraints on Depositional ages

In addition to providing provenance information, dating detrital zircons can provide constraints on the maximum depositional age of clastic sedimentary units, by using the age of youngest dated grain as the date at which depositional age of the unit can not exceed. Most of the intervals from which grains were dated yielded ages no younger than Paleozoic, much older than the generally well established Mesozoic ages for all of the units, and therefore are not useful for bracketing the maximum depositional ages. However, Jurassic Sandstone # 1 and Jurassic Sandstone # 2 in Mizzen L-11 (Figures 1.7 and 2.3) contain Mesozoic detrital zircons with ages that can be compared to existing biostratigraphic age assignments in order to further constrain the depositional ages of these units. Depositional age constraints of these reservoir units are important for synthesizing local and regional depositional models, and the depositional age constraints provided herein are used in conjunction with provenance data from this study and information from previous studies to constrain the orientation and timing of sandstone deposition.

7.2.1 Discussion: age of Jurassic Sandstone # 2

The youngest detrital zircon grain dated from this unit has an age of 141 ± 7 Ma, indicating a maximum depositional age somewhere between the early Tithonian and middle Valanginian, and ranging over the Jurassic-Cretaceous boundary. This unit is included in the biostratigraphic interval between 3735 m and 3823 m, and has been assigned an age of no younger than the earliest Tithonian (Robertson Research, 2003). The U-Pb age of the youngest detrital zircon is consistent with this age assignment, as the error its age overlaps with the previously designated early Tithonian age of this interval. Therefore, the age of Jurassic Sandstone # 2 should continue to be considered early Tithonian (Late Jurassic), as the biostratigraphic age indicates, but should not be considered any older.

7.2.2 Discussion: age of Jurassic Sandstone # 1

Ages of Mesozoic detrital zircons from the Jurassic Sandstone # 1 in Mizzen L-11 indicate an Earliest Cretaceous maximum depositional age. A weighted average age of 141± 5.4 Ma (Berriasian) from all Late Jurassic and Early Cretaceous zircons between the ages of 134-152 Ma, as well as the presence of one grain with an age and error within an Earliest Cretaceous age range (139.5 ± 3.6 Ma, Berriasian) strongly supports an Earliest

Cretaceous, probably Berriasian maximum age of deposition. This is in contrast to the assignment of a Late-Early Tithonian age which was assigned to the interval based on biostratigraphic analysis (Robertson Research 2003). In their report, they state with regards to the interval between 3415 m and 3725 m:

Dating of this interval is based upon overall composition combined with the age assignments to under- and overlying intervals. The dinocyst datum at 3395m in the overlying interval is interpreted to reflect an age no older than intra-late Tithonian and the top of the underlying interval at 3735m is no younger than intra-early Tithonian.

Considering that the age of the interval between 3415 m and 3735 m is constrained by a top no older than middle-late Tithonian and a base no younger than middle-early Tithonian, then much of this interval, including Jurassic Sandstone # 1, could still be interpreted as younger than late Tithonian in age. This biostratigraphic interpretation therefore does not rule out a Berriasian (Earliest Cretaceous) age of deposition for Jurassic Sandstone # 1. It is possible, however, since cutting samples have been used for this interval, that cavings that may have occurred could have contaminated this sample with younger detrital zircons derived from younger intervals above. This is considered unlikely given the abundance of Late Jurassic to Early Cretaceous aged grains in this sample as well as the absence of similarly aged grains in a sample from the Baccalieu Sandstone, located 200 m above this sample interval. If cavings caused such contamination in Jurassic Sandstone # 1, then presumably Berriasian grains would also be present in the Baccalieu Sandstone, either as detrital grains or as contaminants caused by similar caving from above. Therefore, these grains are not considered to be contaminants, and a Berriasian age assignment for this unit should therefore be considered in light of this new evidence. For the purpose of further interpretations in this thesis, the Jurassic Sandstone # 1 is considered to have a Berriasian age in light of this new evidence.

7.2.3 Discussion: age of Baccalieu Sandstone

Although the youngest detrital zircon grain in the Baccalieu Sandstone is Carboniferous, depositional age constraints from older underlying units place age constraints on this sandstone as well. The biostratigraphic age of this unit is cited as early-late Tithonian (Late Jurassic); however, the older down hole Jurassic Sandstone # 1 is herein interpreted as no older than Berriasian; and, therefore the depositional age of the Baccalieu Sandstone is constrained as Berriasian or younger. As discussed above, even if cavings had occurred and contaminated Jurassic Sandstone # 1 with Berriasian aged grains, since no such grains are present in the Baccalieu Sandstone, any caving related contamination must have occurred below the Baccalieu Sandstone. Thus, the age of the Baccalieu Sandstone in Mizzen L-11 is herein definitively constrained as Berriasian or younger.

7.3 Provenance Interpretations

7.3.1 Mizzen L-11: Jurassic Sandstone # 2

A single Mesozoic detrital zircon is present with an age of 141 ± 7. This age matches well with the ages of the Budgell Harbour Stock, located in northern central Newfoundland, as well as a "granite basement" encountered in the bottom section of

Bonavista C-99 on the northeastern Newfoundland Shelf (Helwig et al., 1974; BP Canada, 1975). Another potential source is present in the Avalon Uplift area, where several Mesozoic igneous rocks have been encountered by industry wells, but only one has an age that would match the grains in this sample, a diabase with an age of 135 Ma in the Brant P-87 well in the far southern part of the Avalon Uplift area (Jansa and Pe-Piper, 1998). Potential conjugate margin sources include the Early Cretaceous Porcupine Median high in the Porcupine Basin, or gabbro sills on the Galicia Bank (Tate and Dobson, 1988; Scharer et al., 1995). However, the gabbros on the Galicia Bank are too young to be considered a source, and since the Porcupine Median high has not even been sampled, its exact age is unknown.

Most of the Paleozoic grains in this sample have ages between 395 Ma and 421 Ma (Late Silurian to Early Devonian), with a cumulative probability peak at 410 Ma (Early Devonian). These grains are interpreted as predominantly mixed source first-cycle grains. The east-central Newfoundland interior, comprising rocks of the Gander and Dunnage Zones of the Central Mobile Belt, located to the west and northwest of this unit, is the closest source area for grains of this age. Here, late Silurian to early Devonian plutons are exposed, as well as abundant Silurian volcanic sequences (Dallmeyer et al., 1981; Chorlton and Dallmeyer, 1986; Dickson, 1990; O'Neill, 1991; Valverde-Vaquero et al., 2003). These Silurian to Early Devonian crustal units form a continuation along the Iapetus suture zone, and therefore presumably also exists as pre-Mesozoic basement on now offshore areas of the Irish conjugate margin, which at the time of deposition would have been located several hundred kilometers north and northeast of the sampled sandstone (Figure 7.1). Therefore, parts of the offshore extensions of the Irish conjugate

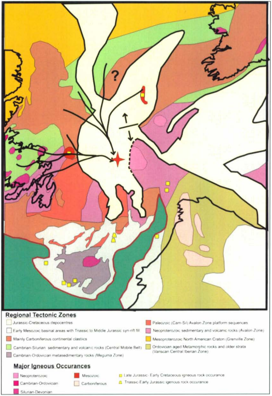

Figure 7.1: Regional provenance interpretation for Jurassic Sandstone #2 in Mizzen L-11. Based on first-cycle zircons with dominantly Silurian-Devonian ages, the most likely source areas include pre-Mesozoic basement comprising syn-orogenic granitoids of the Central Mobile Belt, to the north and/or northwest.

margin (Porcupine Bank and Basin) are potential source areas as well. It should be noted, however, that the pre-Mesozoic geology of these areas is poorly constrained. A significant Iberian source is not likely due to the scarcity of Late Paleozoic (Carboniferous to Permian) aged grains that would be expected to be derived from the extensive Late Paleozoic magmatic rocks on the nearest part of the Iberian massif (Priem and Tex, 1984). Several grains of this age range are present, but they may have been reworked from older foreland sequences on the Grand Banks, as is the case for Albian turbiditic sandstones beneath the continental shelf southeast of the Grand Banks (Hiscott et al. 2008). The Meguma Zone to the south can also be ruled out as a major source of Paleozoic grains due to the absence of Late Devonian (370 Ma- 380 Ma) aged grains that match the age of plutonic emplacement in that area.

A Neoproterozoic age peak consists of grains predominantly 560 and 600 Ma, and these are interpreted as mainly first cycle plutonic and volcanic grains, with minor second cycle grains. The age range and source interpreted source types match well with the young parts of the main arc phase magmatic rocks exposed in the Avalon Zone (Harbour Main volcanics) as well as the ages of the Swift Current granite and Love Cove Group in the Avalon Zone (Krogh et al., 1987).

The >1 Ga grain population is dominantly composed of recycled grains with age peaks at 1.0 Ga, 1.7 Ga, 1.8 Ga and 2.8 Ga. These ages match the all of the ages of detrital zircons present in the Exploits subzone of the Central Mobile Belt (Pollock et al., 2007). However, with the exception of the 1.8 Ga peak, they also match the ages of detrital zircons present in the Paleozoic cover sequences on the Avalon Zone, sedimentary rocks in the Gander Zone, and metasedimentary rocks in the Meguma Zone

(Krogh and Keppie, 1990; O'Neill, 1991; Pollock et al., 2007; White et al., 2008). Thus, the sources of these recycled grains probably include sedimentary rocks in the Central Mobile Belt, but also likely include sources from the Avalon Zone.

Of the possible source areas, a combination of the interior Newfoundland and Bonavista platform areas contain all the potential sources of detrital grains in this sample (Figure 7.1). This area includes Silurian-Devonian granites and Neoproterozoic magmatic rocks that could have provided first-cycle detrital zircons matching the 410 Ma and 580 Ma age peaks from the sample (Dallmeyer et al., 1981; Chorlton and Dallmeyer, 1986; Krogh et al., 1987; Dickson, 1990; O'Neill, 1991). Silurian to Early Devonian granites and the Iapetus terranes and suture zone form a continuation to the Caledonides, and also exist on the exposed Irish conjugate margin as pre-Mesozoic basement (van Staal et al., 1998; Feely et al. 2004). Therefore, parts of the offshore extensions of the Irish conjugate margin (Porcupine Bank and Basin) could be considered potential source areas as well, although with caution, since the nature of the basement has not been determined in this area. Sources of recycled zircon grains are also present on the interior Newfoundland and Bonavista platform areas, and include abundant Paleozoic sedimentary cover sequences containing reworked Paleozoic, Proterozoic and Archean grains with ages matching well with the ages of reworked detrital zircons from this sample (O'Neill, 1991; Pollock et al., 2007; Pollock et al., 2009). Tourmaline discriminations for this sample are also consistent with the Inland Newfoundland source area (Central Mobile Belt) as this area contains a mixture of granitic and low to moderate grade metasedimentary rocks with tourmaline as a common accessory phase (O'Neill, 1991).

Previous sedimentary rocks would have been a major source of detritus in this sandstone, given the abundance of sedimentary lithic grains, mineralogical sub-maturity, high ZTR index value and abundance of recycled detrital zircon grains (~60%). First cycle sources are interpreted to include Silurian-Devonian and Neoproterzoic felsic to intermediate plutonic rocks and volcanic rocks, based on thin section and detrital zircon petrography; and chemistry detrital tourmaline grains show that some first cycle material included metasedimentary rocks. Transport distances are interpreted to have been long, at least for Silurian to Devonian fist-cycle detrital zircon grains, of which the nearest source would have been hundreds of kilometers to the west at the time of deposition. Thus, the catchment area for west to east flowing drainage system connected to this basin-margin sand would have been extensive, sampling much of the Avalon Zone and Central Mobile Belt basement, including abundant cover sequences, granitic, volcanic and metasedimentary rocks, as shown in Figure 7.1.

7.3.2 Mizzen L-11: Jurassic Sandstone # 1

Seven Mesozoic grains are present in the sample with ages ranging between 130 to 155 Ma (Late Jurassic to Early Cretaceous), with an average age of 141 ± 5.4 Ma (Berriasian). Possible source areas for these grains are similar to those outlined previously for the 141 ± 7 Ma grain in Jurassic Sandstone # 2. These grains are interpreted to be of first-cycle plutonic igneous origin, and probably originated from Zr-rich felsic magmas due to their large grain size and oscillatory zoning. Therefore the "granite basement" in Bonavista C-99 is the most likely source of these grains. They are not considered to be ash fall zircons because of their large size, and would have had to have been carried as bed load along with all the sand sized material present.

Early Devonian and Silurian ages dominate the Paleozoic detrital grains in this sample, with most ages falling between 415 Ma and 430 Ma (Silurian). The nearest source of these grains is the Newfoundland interior (Central Mobile Belt) where abundant late Silurian to early Devonian plutons, as well as abundant Silurian volcanic sequences occur (Dallmeyer et al., 1981; Chorlton and Dallmeyer, 1986; Dickson, 1990; O'Neill, 1991; Valverde-Vaquero et al., 2003). Pre-Mesozoic rocks of the Irish conjugate margin, which at the time of deposition would have been located several hundred kilometers northeast and north of the sampled unit, contain similar aged granites and volcanic rocks that could have also contributed first-cycle zircons (Feely et al. 2004).

Other Paleozoic grains in the sample include four Carboniferous grains (1 Pennsylvanian (293 Ma), and 3 Mississippian (325-350 Ma)) as well as one Late Devonian grain (372 Ma). The former Carboniferous grains have ages similar to the ages of Variscan magmatism from the Iberian conjugate margin, which at the time of deposition, would have been located proximally to the east of the sampled unit. The Late Devonian grain has an age that closely matches magmatism in the Meguma Zone, to the south. Because of the scarcity of either of these groups of late Paleozoic grains, the Iberian Margin and Meguma Zone are not considered major sources of sand in this unit. Given the volume of granitic rocks present on the Iberian margin, it would have provided large volumes of detrital zircons if it had been a predominant source area, and therefore the scattered presence of Variscan aged grains does not support Iberian source areas. Instead, these grains are probably reworked from older sedimentary rocks, presumably

Carboniferous sequences offshore, as has been postulated for micas in Albian aged turbiditic sandstones in the Newfoundland Basin.

Late Neoproterozoic grains make up the largest age grouping from this sample, with ages ranging between 550 and 735 Ma, and most having ages between 570 and 670 Ma, covering the entire range of ages of plutonic and volcanic rocks in the Avalon Zone, located west, south and east of the sampled unit (Krogh et al., 1987). Of these detrital zircons, half are interpreted as reworked grains by grain morphology analyses, indicating a significant sourcing from Early Paleozoic cover sequences on the Avalon, and potentially Carboniferous and Permian cover sequences as well (Pollock et al., 2009).

Mesoproterozoic aged detrital zircons, although uncommon in this sample, have ages between 1.2 and 1.5 Ga, and are interpreted as recycled grains. Detrital zircons with these ages are known to exist in Paleozoic cover sequences on the Avalon Zone and Central Mobile Belt, dominantly to the west of the sampled interval, but have not been documented in the sedimentary rocks of the Meguma Zone to the south (Krogh and Keppie, 1990; O'Neill 1991; Pollock et al., 2007; Pollock et al., 2007; White et al., 2008). Recycled Paleoproterozoic grains, with ages ranging between 1.6 and 2.2, and multi-cycle Archean grains, with an age peak at 2.7 Ga, are interpreted to have a similar provenance, as detrital zircons with these ages also occur in sedimentary sequences in the Avalon and Central Mobile Belt Zones (Pollock et al., 2007; Pollock et al., 2009).

Overall, Jurassic Sandstone # 1 in Mizzen L-11 is interpreted to have dominantly distal to proximal first-cycle crystalline granitic and metamorphic sources of zircon from the Avalon Zone and Central Mobile Belt Zones which occur to the west and northwest, including the Bonavista Platform, eastern and central Newfoundland, northeast

Newfoundland shelf area, and potentially parts of the Irish Conjugate Margin (Porcupine Bank and Basin). The Mesozoic grains are interpreted as first-cycle plutonic igneous grains (section 5.4.3), and as such the most likely source is a 145 Ma granitic intrusion currently underlying the West Orphan Basin. Second- and Multiple-cycle detrital zircons display ages that match the ages of detrital zircons present in most Early and Late Paleozoic cover sequences incorporated with or overlying the Avalon Zone and Central Mobile Belt Zones, and therefore are interpreted to be derived from similar pre-Mesozoic sources as the first-cycle grains (Figure 7.2).

Jurassic Sandstone # 1 has a relatively low ZTR indexes (average 63.4), is less mineralogically mature than Jurassic Sandstone #2, containing plagioclase and potassium feldspars in higher modal proportions, and by grain morphology analyses has a higher percentage of first-cycle detrital zircon grains (72%), indicating more significant first cycle sourcing. This interpretation is also supported by other observations, such as the presence of subhedral to angular calcic amphibole grains present in the heavy mineral fraction of this sandstone. However, the lower ZTR index, is at least in part, is overprinted by authigenic growth of apatite, and thus the actual inherited ZTR index is probably higher. Still, more evidence for first-cycle source input can be seen in this unit then is present in Jurassic Sandstone #2 or any other sandstone in this study. Recycling is still considered to have dominated inputs of framework material, evidenced by abundant sedimentary lithic grains and overall mineralogical sub-maturity of the sandstone. The extent of the catchment area for west to east drainage into the basin during the deposition would have been similar to that during deposition of the Jurassic Sandstone #2; again, with a network of rivers sampling much Avalon Zone and Central Mobile Belt basement,

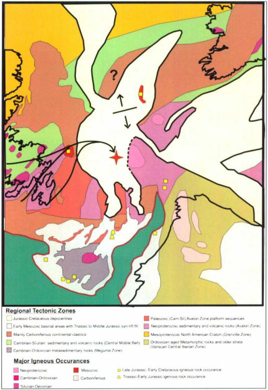

Figure 7.2: Regional provenance interpretation for Jurassic Sandstone #1 in Mizzen L-11. Age peaks of first-cycle zircons match the ages of Avalon arc-phase igneous rocks (Late Neoproterozoic) as well as the ages of orogenic granitoids in the Central Mobile Belt (Silurian-Devonian). Provenance of this unit is similar to the provenance of Jurassic Sandstone #2; however, more first-cycle detritus in the sample indicates denudation of the source area between the times of deposition (Tithonian to Berriasian) of these two units.

as shown in figure 7.2, including cover sequences composed of clastic and carbonate rocks, but also more abundant crystalline rocks such as Silurian-Devonian, Neoproterozoic and enigmatic Mesozoic granitic rocks, volcanic rocks, and metasedimentary rocks. This suggests that between the time of deposition of Jurassic Sandstone #2 and Jurassic Sandstone #1, cover sequences had been denuded from much of the same regional source area to the west. This is also supported by interpretations of heavy mineral signatures in Chapter 4, in which Jurassic Sandstone #1 and Jurassic Sandstone #1 are interpreted to have similar provenance signatures based on overlapping heavy mineral ratios.

7.3.3 Mizzen L-11: Baccalieu Sandstone

The sample from this unit, unlike the two previous units, contained no Mesozoic aged grains, and the youngest detrital zircons are Carboniferous. Essentially there are two age peaks exhibited by the Paleozoic aged grains, one in the Mid-Late Devonian (385 Ma) and one in the Early Devonian to Early Silurian (435 Ma). Such grains may had been derived from Mid-Late Devonian grains is from late Acadian granites in the Meguma Zone, to the south underlying the Avalon Uplift area, or alternatively to the west, in the Gander Zone, where Late Devonian granites are also present (Currie, 1995; Clarke et al., 1997; Kontak et al., 2004). The nearest source of Early Devonian to Late Silurian grains are orogenic granites and volcanics in the Central Mobile Belt, located to the west and northwest of the Baccalieu Sandstone (Dallmeyer et al., 1981; Chorlton and Dallmeyer, 1986; Dickson, 1990; O'Neill, 1991; Valverde-Vaquero et al., 2003).

Neoproterozoic grains in this sample have ages ranging between 540 and 735 Ma, but most of the grains (70%) have ages between 600 and 655 Ma. Based on grain morphological analyses, these Neoproterozoic grains are interpreted as dominantly recycled. The closest source of recycled grains of this age are Paleozoic cover sequences of the Avalon Zone, located to the west, south and east of the Baccalieu Sandstone (Pollock et al., 2009). First-cycle grains from this age group are interpreted to have been derived from the arc-phase volcanic and plutonic rocks of the Avalon Zone, which have similar ages (Krogh et al., 1987). It should be noted, however, that recycled Neoproterozoic detrital zircons with ages between 550 Ma and 700 Ma are also present in the Early Paleozoic metasedimentary rocks of the Meguma Zone, to the south, and could have been sourced from here too (Krogh and Keppie, 1990). The Meguma Zone should be considered a source of these Neoproterozoic grains, given the presence of the Late to Middle Devonian group of detrital zircons in this sample which are herein postulated to be derived from granites in the Meguma Zone, to the south.

Major age peaks from >1Ga detrital zircons occur at 1.2 Ga and 2.1 Ga, and a minor peak occurs at 2.6 Ga. These grains are interpreted as predominantly recycled. Detrital zircons of these ages can be accounted for from cover sequences in the Avalon or Meguma Zones, or in the Central Mobile Belt. Thus these particular age peaks are not diagnostic for the determination of a source area; however, it does argue against sourcing from farther west in the Central Mobile Belt, where 1.6-1.8 Ga detrital grains have been dated in sedimentary rocks, and grains in this range of ages are absent completely in this sample (Krogh and Keppie, 1990; O'Neill 1991; Pollock et al., 2007; White et al., 2008; Pollock et al., 2009).

The ZTR value for this sample is average (88) and just less than half (46%) of the detrital zircon grains are interpreted as recycled, indicating a mixture of crystalline (first-cycle) sources and sedimentary (recycled) sources. Chemistry of detrital tourmalines from this sample shows a dominance of metasedimentary sources, with significantly less granitic grains than in other samples.

Several lines of evidence support a more significant sourcing from the south for the Baccalieu Sandstone, from the Avalon Uplift area which is underlain by the metasedimentary rocks and associated granites of the Meguma Zone. First, and principally, is the Middle to Late Devonian age peak in the detrital zircon population, a possible source of which is granites present in the Meguma Zone (Clarke et al., 1997, Kontak et al., 2004). Secondly, the relative abundance of detrital tourmalines derived from metasedimentary rocks, which corresponds well to source region underlain by the Meguma Zone, in which metapelitic and metapsammitic rocks are extensive and contain tourmaline as a common accessory phase (Raeside et al., 1988). Thirdly, the provenance-sensitive heavy mineral ratios and provenance "fingerprint" of this sandstone are shown to be different from those of the Jurassic Sandstones in Chapter 4, thus indicating some change in provenance.

Overall, first-cycle detrital zircons in the Baccalieu Sandstone are interpreted to have distal sources to the west and potentially to the south, including parts of the basement underlying the Avalon Uplift area. This is contrast to the two older sandstones in this well (Jurassic Sandstone # 1 and #2) which both have similarly interpreted source areas to the west and northwest, on the Bonavista Platform and interior Newfoundland areas, but not source areas far to the south. The drainage area therefore likely encompassed a large area to the south and southwest, as shown in Figure 7.3. This might be expected because many authors have shown that contemporaneous sandstones in the Jeanne d'Arc Basin had significant regional sources to the south, caused by uplift (Tankard and Welsink, 1987; McAlpine, 1990; Sinclair, 1993; Enachescu, 1994). Based on provenance constraints from the zircons, material from this unit is interpreted to have entered the basin from the south. Detrital zircons show evidence for distal transport histories, and such long transport can be applied to quartz grains but probably does not apply to a large proportion of the material in this sandstone, which is made up of relatively unstable mudstone and carbonate grains. The large proportion of lithic grains in the unit suggests that relatively proximal basin margins were uplifted and clastic and carbonate rocks were quickly shed into the basin. This may have occurred in one of two ways: (1) material arriving at the terminus of an extensive drainage system was deposited in an area to the south of the basin, which was subsequently uplifted, resulting in the proximal re-deposition of this material, or (2) unstable lithic material was added very near the end of an extensive drainage system from proximal uplifted areas adjacent to the main river.

7.3.4 Baccalieu I-78: Hibernia Formation Equivalent

Most of the detrital zircons from the sampled section of the Hibernia Formation equivalent have Late Paleozoic and Neoproterzoic ages. The late Paleozoic grains have ages between 392 ± 24 Ma and 537 ± 26 Ma (Devonian-Cambrian), with a cumulative probability peak of ages at 450 ± 50 Ma (Late Ordovician). In fact, the ages of Paleozoic

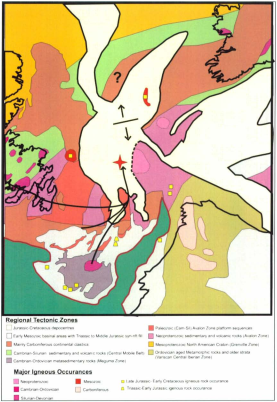

Figure 7.3: Regional provenance interpretation for Baccalieu Sandstone in Mizzen L-11. A Late Devonian (360Ma-380Ma) age group in the first-cycle detrital zircon population is interpreted to be from late orogenic granitoids unique to the Meguma Zone, which at this time was present as pre-Mesozoic basement beneath the Avalon Uplift area, to the south.

grains in this sample are dominantly Ordovician in age, with a small grouping of ages between 460 Ma and 485 Ma that does not exist in other samples. These zircons are interpreted as first-cycle volcanic and plutonic detrital grains. The nearest source of such grains includes granites in the central and westernmost portion of the Central Mobile Belt (Dunnage and Notre Dame subzones), to the west. Potential Conjugate margin sources with similar U-Pb zircon ages occur in orthogneisses in the Central Iberian Zone and granites and volcanic rocks in the Ossa Morena Zone, both on the western Iberian conjugate margin to the east (Capdevila and Mougenot, 1988; Valverde-Vaquero and Dunning, 2000; Romeo et al., 2006; Sola et al., 2008). As well they can be sourced from magmatic rocks from within the Dalradian Supergroup in Northwestern Ireland, to the north (Flowerdew et al., 2005). Orthogneiss from the Central Iberian Zone and igneous rocks from the Ossa Morena Zone can be ruled out as a source of Ordovician grains, since sourcing from these areas would also be expected to be accompanied by voluminous first-cycle detrital material derived from Variscan-aged (Carboniferous to Permian) granitoids, which is not present in this sample (Priem and Tex, 1984; Romeo et al., 2006). The Ordovician magmatics on the Irish margin cannot be ruled out based on ages; however, these rocks are scarcely exposed, especially in comparison to the amounts of exposed Late Silurian and Early Devonian magmatic rocks present on mainland Ireland, and are mafic, and thus would have been an unlikely regional source for detrital zircons (Flowerdew et al., 2005). Multiple, and relatively voluminous sources exist in the western and central portions of the Central Mobile Belt, such as within the Cape Ray Igneous Complex in the Notre Dame Subzone, southwestern Newfoundland, with U-Pb zircon ages between 469 Ma and 488 Ma (Dube et al. 1996); or from the Meelpaeg or Mount

Cormack Subzones, in the Gander Zone, Central Newfoundland, with ages between 458 Ma and 474 Ma (Valverde-Vaquero et al., 2006); these are interpreted as more likely sources due to their closeness, composition and more voluminous exposure.

Additional Paleozoic aged grains, ranging in age from Early Devonian to Late Ordovician, are interpreted to have similar source areas as those similar aged grains from other samples, which include areas to the west and northwest that comprise the Dunnage and Gander Zones in Newfoundland and their extensions on the Irish Conjugate margin and offshore. As previously mentioned, these areas contain abundant Silurian to Devonian aged granitic rocks, matching the ages of the remaining Paleozoic grains in this sample (Dallmeyer et al., 1981; Chorlton and Dallmeyer, 1986; Dickson, 1990; O'Neill, 1991; Valverde-Vaquero et al., 2003).

Neoproterozoic aged grains from this sample have ages predominantly between 590 Ma and 630 Ma, with a cumulative probability peak of ages at 600 Ma (+50/-75 Ma). These grains are interpreted as dominantly second- or multiple-cycle grains and lesser first-order grains of igneous origin, likely including volcanic and plutonic sources. These ages match U-Pb ages from the main arc magmatic rocks in the Avalon Zone, as well as the U-Pb ages of detrital zircons present in Precambrian and Early Paleozoic cover sequences on the Avalon Zone (Krogh et al., 1987; Pollock et al., 2007). Although 550 Ma to 700 Ma aged detrital zircons are also present in the Meguma Zone metasediments, the Meguma Zone is not interpreted to be a major source based on the absence of a Middle-Late Devonian age peak from granitic rocks that would be expected to accompany Meguma Zone sourcing (Clarke et al., 1997; Kontak et al., 2004). Therefore, the Avalon Zone is interpreted as the source of these Neoproterozoic grains.

Major age peaks from >1Ga detrital zircons occur at 1.2 Ga, 1.6 Ga and 2.1 Ga, with a lesser age peak at 2.6 Ga. These grains are interpreted as predominantly recycled. These age peaks overlap with age peaks from detrital zircons present in Paleozoic cover sequences of the Avalon Zone, Central Mobile Belt and Meguma Zone, and thus are not overly diagnostic for provenance interpretations for this unit (Krogh and Keppie, 1990; O'Neill 1991; Pollock et al., 2007; Pollock et al., 2009; White et al., 2008).

The source areas of first-cycle detritus are interpreted predominantly as a combination of interior and eastern Newfoundland and northern and central areas within the Bonavista Platform. These areas include pre-Mesozoic basement comprised of the Central Mobile Belt Zones and the Avalon Zone, which contain Paleozoic and Neoproterozoic igneous rocks best matching the ages of first-cycle grains in this sample. Second- and multiple-cycle grains are interpreted as being derived mainly from Paleozoic cover sequences in the Avalon Zone located to the east and south; however, other Mesozoic rift-related clastics cannot be ruled out as potential direct sources for these recycled grains as well. Overall, the most likely source areas based on the age peaks of detrital zircons in this sample are to the west, and include the areas on the Bonavista Platform and eastern and central Newfoundland (Figure 7.4).

This sandstone has a similar heavy mineral provenance signature as the Jurassic Sandstones in Mizzen L-11 (Chapter 4), and also has similar first-cycle source areas to the west, as evidenced by detrital zircon data. Significant, even dominant, sourcing from pre-existing sedimentary rocks is considered likely based on the high modal proportions of sedimentary lithics and quartz grains, high ZTR index, and a significant majority (60%) of recycled detrital zircons. The catchment area for the west to east directed

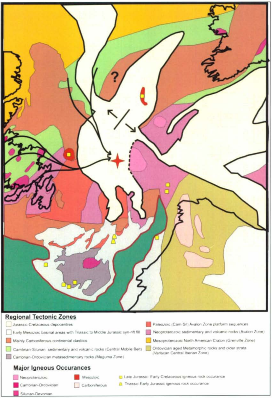

Figure 7.4: Regional provenance interpretation for the Hibernia Formation Equivalent in Baccalieu I-78. Essentially, the provenance of this unit is similar to the provenance of the Jurassic Sandstones #2 and #1 in Mizzen L-11, with source areas dominantly to the west, including rocks of the Avalon Zone and Gander Zone.

drainage system that carried detritus to the basin was as large as for those related to deposition of the Jurassic Sandstones, as evidenced by first-cycle detrital zircons that would have originated several hundred kilometers to the west, and likely sampled material from cover sequences, granitic, volcanic and metasedimentary rocks, as indicated by a mixture of evidence from bulk modal mineralogy, zircon petrography and tourmaline chemistry (Figure 7.4).

.

7.3.5 Baccalieu I78: 5 Avalon Formation equivalent

Detrital zircons ages from this sample are characterized by a dominant Late Neoproterozoic grouping, with subordinate (but significant) Mesoproterozoic, Paleoproterozoic and Archean groups, and, in contrast with previously described samples, relatively minor Paleozoic zircons.

Approximately 40% of the dated grains are Neoproterozoic, having ages ranging between 566 Ma and 750 Ma with an age peak at 610 Ma. These grains are interpreted as a mixture of first- cycle and recycled detrital grains of dominantly igneous origin. The nearest and most likely source of such a large proportion of Late Neoproterozoic grains is the Avalon Zone, which could source both first-cycle grains from arc-phase igneous sources, as well as recycled grains in Precambrian and Paleozoic cover sequences (Krogh et al., 1987; Pollock et al., 2007).

Only five Paleozoic grains are present in this sample, which contrasts greatly with all other samples, in which Paleozoic grains form the largest or second largest age groupings. The ages of the Paleozoic grains cover a wide range, with one Middle

Devonian grain (383 ± 19), two Early Silurian to Late Ordovician grains (425-445 Ma), and two Early Ordovician grains (470-485 Ma). The Middle Devonian age match the age of late orogenic granites in the Meguma Zone, and the Early Silurian to Early Devonian ages match the age of Acadian and Taconic orogenic granitoids present in the Central Mobile Belt (Dallmeyer et al., 1981; Chorlton and Dallmeyer, 1986; Dickson, 1990; O'Neill, 1991; Clarke et al., 1997; Valverde-Vaquero et al., 2003; Kontak et al., 2004). These grains are interpreted as first-cycle based on textural criteria; however, based on their scarcity, it seems difficult to invoke a scenario of direct distal sourcing of these grains from far to the south and west. Significant sourcing from these areas would be expected to provide a larger proportion of detrital zircons with prominent age peaks. Instead, these grains are thus interpreted as second-cycle grains, likely recycled from earlier immature Late Paleozoic continental clastic sediments, which contain detrital grains of these ages, or even potentially from older Mesozoic rift sediments (Murphy and Hamilton, 2000).

The >1Ga detrital zircon populations are characterized by age peaks at 1.3 Ga, 1.8 Ga, 2.2 Ga and 2.8 Ga. These grains are interpreted as dominantly recycled grains of mixed origin (metamorphic and igneous). Detrital zircons from all of these age groups correspond to those present in the Paleozoic cover sequences in the Avalon Zone, and all except for the 1.8 Ga peak correspond to detrital zircon ages in the Meguma Zone, implying a definite recycled Avalon component, but not necessarily a recycled Meguma Zone component (Krogh and Keppie, 1990; Pollock et al., 2007; White et al., 2008). These grains may also have been reworked from older Late Paleozoic or Mesozoic sediments in the area.

ZTR values range between 82.8 and 94.1, with an average value of 88.0, and approximately 66% of the detrital zircon grains are interpreted as recycled, indicating a moderate to high degree of sedimentary recycling. Chemistry of detrital tourmalines from this sample indicates a tourmaline population primarily derived from metasedimentary rocks, but with a significant contribution (roughly one quarter of analyzed tourmalines) from granites as well. A change in provenance from underlying sandstones is indicated by a unique heavy mineral provenance signature from this sandstone (Chapter 4); however, the overprinting effects of diagenesis are not constrained.

The primary source of first-cycle material from this sample appears to be derived from Neoproterozoic arc magmatic rocks in the Avalon Zone, which would have occurred as pre-Mesozoic basement to the south, east and west, as well as beneath this unit. This data argues against any significant distal sources, based on the absence of any significant age groupings of fist-cycle Paleozoic detrital zircons that could be linked to distal sources such as the Meguma Zone to the south, Central Mobile Belt Zones to the west, or the Variscan Iberian Massif to the east. The recycled grains in this sample have a number of potential sources, including Precambrian and Paleozoic cover sequences in the Avalon Zone, Late Paleozoic continental clastic sequences, and earlier Mesozoic rift sediments.

Overall, the provenance data from this unit suggests relatively proximal sources including a mixture of crystalline basement from the Avalon Zone as well as older sedimentary rocks, which could have been sourced from uplifted areas within only 100 km to the west, south or east. Foster and Robinson (1993) presented seismic evidence that this unit prograded from the southeast and the provenance data herein supports this interpretation. Thus, the Avalon Formation Equivalent sandstone is interpreted to have been derived from proximal sources to the southeast, including parts of the Precambrian and Paleozoic Avalon Zone as well as younger sedimentary cover sequences (Figure 7.5).

7.3.6 Blue H-28: Albian Sandstone

The predominant age group of detrital zircons in this sample is Silurian, with lesser amounts of other grains having other Paleozoic ages. A lesser Late Neoproterozoic group is also present, as well as minor Mesoproterozoic and Paleoproterozoic groups, and a single Late Archean aged grain.

These Silurian grains have a cumulative probability peak of ages at ca. 420 ± 20 Ma (Late Silurian), and are interpreted as predominantly first-cycle plutonic igneous grains. These grains are interpreted to have been derived mainly from Silurian plutons and Silurian volcanic sequences present in the Gander and Dunnage Zones of the Central Mobile Belt, which were present in exposed pre-Mesozoic basement highs to the west, and northwest, beyond the basin-bounding Bonavista Fault (Figures 1.8, 1.9, 7.6) (Haworth and Lefort, 1978; Dallmeyer et al., 1981; Chorlton and Dallmeyer, 1986; Dickson, 1990; O'Neill, 1991; Valverde-Vaquero et al., 2003).

A group of Neoproterozoic grains are also present, with ages ranging between 576 Ma and 647 Ma, and a cumulative probability peak at 620 Ma. They are interpreted as second-cycle or recycled grains of dominantly igneous origin. Based on the ages and origin of these grains, they are interpreted to be derived from the nearby Avalon Zone Precambrian basement rocks and Paleozoic cover sequences.

The >1Ga grains constitute a small amount of the grains in this sample, and are dominantly recycled grains of variable crustal origin. The main peaks occur at 1.1 Ga and

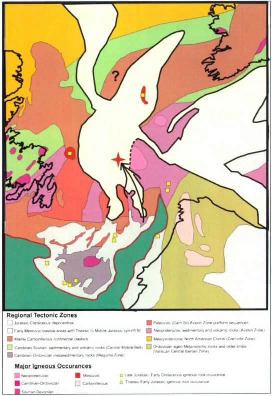

Figure 7.5: Regional provenance interpretation for the Avalon Formation Equivalent in Baccalieu I-78. Detrital zircon age peaks from this unit indicate predominantly Avalon Zone sources. This corroborates well with Foster and Robinson (1993) who interpreted that this unit prograded from the southeast. Thus, proximal sources from the southeast (but, not including the Flemish Cap) are interpreted for this unit.

1.8 Ga. These age groups match ages of detrital zircons present in the Paleozoic cover sequences in the Avalon Zone as well as sedimentary units in the Exploits Subzone of the Central Mobile Belt (O'Neill 1991; Pollock et al., 2007; Pollock et al., 2009). These grains may also have been reworked from continental clastics in the Late Paleozoic Notre Dame and Belle Isle subbasins on the Northeast Newfoundland Shelf; however, ages of detrital zircons within these clastics rocks are unknown.

ZTR values range between 82.1 and 92.7, with an average value of 88.1, and approximately 40% of the detrital zircon grains are interpreted as recycled, indicating a relatively moderate to low degree of sedimentary recycling. Chemistry of detrital tourmalines from this sample indicates a population primarily derived from a mixture of metamorphic and granitic sources.

Overall, this unit is interpreted to have been derived from relatively proximal sources to the west and northwest, on the Bonavista Platform, which includes igneous, metasedimentary and sedimentary rocks that belong to the Avalon Zone, Central Mobile Belt (Gander and Exploits Subzones) and the Notre Dame and Belle Isle subbasins (Figure 7.6). A mixture of Avalon Zone and Central Mobile Belt sources from the west appears to have a consistent heavy mineral provenance signature, as this sandstone has a similar provenance signature to the Hibernia Formation equivalent and Jurassic Sandstones, all of which have similar source regions to the west.

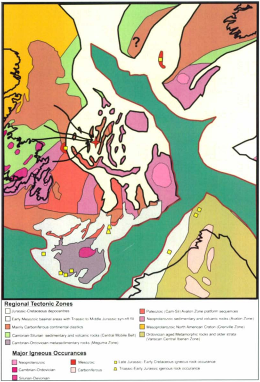

Figure 7.6: Regional provenance interpretation for the Albian sandstone in Blue H-28. A prominent age peak comprising first-cycle Silurian aged detrital zircons indicates proximal sources to the west and northwest, including Silurian orogenic granitoids in the Gander Zone, and minor sourcing from Avalon Zone basement.

7.4 Geological synthesis: Northern Flemish Pass Basin

Jurassic Sandstone # 2 is a Tithonian aged texturally submature sublitharenite and was deposited in or near shallow water adjacent to terrigenous sources (Robertson Research, 2003). Robertson Research (2003) stated that the sand may have been deposited as a gravity flow, but this is conjectural and any number of shallow water or terrestrial depositional settings is possible. Stratigraphically, it fits near the base of the MS1-50 parasequence of Foster and Robinson (1993). According to Foster and Robinson (1993), the MS1-50 parasequence records onlap of sediments from the northwest and progradational deposition in an east-west trending subbasin. Presumably, basin margin uplift occurred either in the north or in the south or both (Foster and Robinson, 1992). The provenance data suggests that detritus was derived from as far as relatively distal (>100km) sources to the west and northwest (Figure 7.1). On the scale of the Baccalieu subbasin, this unit is interpreted to have entered the basin in the Tithonian from the northwest or north as early footwall uplift began at the onset of the MS1-50 parasequence deposition, preceding significant marine transgressions (Figure 7.7). Well control in this area supports the interpretation that this coarse material entered the Baccalieu Subbasin from the northwest, as it is nonexistent or of limited extent towards the southeast; only a thinner and more argillaceous sandstone of the same age is present in Baccalieu I-78, located approximately 25 km to the southeast, at approximately 3750m depth (Jeanne d'Arc Formation Equivalent; Figure 2.10). This may, at best, be directly correlated as a distal equivalent to Jurassic Sandstone # 2 in Mizzen L-11. Jurassic Sandstone # 2 is therefore interpreted to have been deposited into the Baccalieu subbasin from the

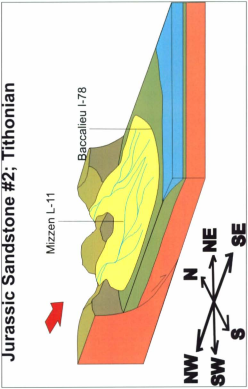

Figure 7.7: Model for the deposition of Jurassic Sandstone #2 in the Tithonian. Jurassic Sandstone #2 was deposited into the Baccalieu subbasin from the west or northwest as a coarse submature deposit during a relative lowstand.

northwest, with the thickest and most arenaceous potions of the unit being limited to northwestern parts of the subbasin.

Jurassic Sandstone # 1 is a texturally mature sublitharenite that was probably deposited during a lowstand in or near shallow water adjacent to terrigenous sources (Robertson Research 2003). A high energy depositional setting where reworking of material occurred is inferred for this unit because of the well sorted nature of material and the presence of ooids. Although it has an assigned age of Tithonian (Roberson Research, 2003), detrital zircon ages herein show evidence that it may be younger (Berriasian). Based on the blocky gamma ray profile, this unit appears to lack any gradation and has sharp lithologic and/or stratigraphic boundaries. It is probably overlain by a flooding surface (Robertson Research, 2003). Based on the above constraints, this thin unit is interpreted to represent a quickly aggrading and prograding sand body, that prograded quickly during a brief lowstand period while accommodation space was low in this part of the subbasin (Figure 7.8). It was subsequently rapidly flooded and buried beneath shales, relating to a sudden highstand. These rapid changes in base level and accommodation space are interpreted to have been tectonically controlled.

The provenance data herein indicates similar paleodrainage orientations as existed for the Jurassic Sandstone # 2, flowing from the west and/or northwest into the subbasin; however, more of the material appears to be first-cycle in nature. This may be the result of previous denudation of sedimentary cover sequences in uplifted source areas. No equivalent unit appears to exist is Baccalieu I-78; therefore, this sandstone is interpreted to be restricted to the western and/or northwestern part of the Baccalieu subbasin, with

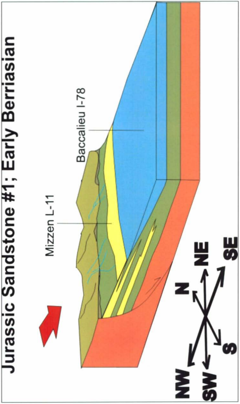

Figure 7.8: Model for the deposition of Jurassic Sandstone #1 in the Tithonian-Berriasian. The sands of Jurassic Sandstone # 2 were rapidly flooded and overlain by shale. Shale deposition continued under shelfal conditions until the early to middle Berriasian, at which time a thin wedge of submature sands comprising Jurassic Sandstone #1 aggraded along the western or northwestern margin of the Baccalieu subbasin, and quickly spread eastward, to a limited extent, during a relative lowstand.

the thickest aggradational accumulations of this unit probably restricted to the northwestern margin (Figure 7.8).

The Baccalieu Sandstone in Mizzen L-11 entered the subbasin from the south and was deposited in a variably restricted shallow water shelf setting with significant terrigenous influences (Figure 7.9). The sands from this unit are thought to have been derived off of an adjacent syn-depositional high, and may have been introduced by gravity flow processes (Robertson Research, 2003). Although a biostratigraphic age of Tithonian has been assigned, detrital zircon constraints from older sands (Jurassic Sandstone #1) suggest it may be younger (Berriasian).

Berriasian aged sandstones and shales are also present in Baccalieu I-78, which have been described and interpreted in Chapters 2, 3 and 4 of this thesis. Based on similarities in ages, modal compositions, stratigraphic positions and heavy mineral provenance signatures, the Baccalieu Sandstone in Mizzen L-11 is interpreted to correlate to the Berriasian sandstones in Baccalieu I-78 (Figure 7.9). The Baccalieu Sandstone in Mizzen L-11 and Berriasian sandstones in Baccalieu I-78 are interpreted as shallow water sandstones deposited as gravity flow or turbidites(?) are a part of an upwards shoaling parasequence that occurs above a sharp flooding surface overlying the shoreface sands of the Jurassic Sandstone # 1 (Foster and Robinson, 1993). The provenance data herein suggests a change in regional paleodrainage into the northern Flemish Pass Basin occurred between deposition of the Jurassic Sandstone # 1, where material came dominantly from the west, and the Baccalieu Sandstone, where material is interpreted to have been derived in part from the south (Figure 7.3). It is possible that the basin flooding

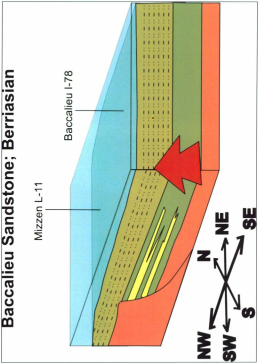

Figure 7.9: Model for the deposition of the Baccalieu Sandstone in the Tithonian-Berriasian. The sands comprising Jurassic Sandstone #1 were quickly flooded, and above this flooding surface began a shoaling upwards parasequence known as MS1-50 (Foster and Robinson, 1993). The sands in MS1-50 were deposited in a shallow water shelf setting and derived in part from the west and in part from the south, at least in the upper part of this parasequence.

noted by Foster and Robinson (1993) and the change in provenance herein are contemporaneous and linked events, both occurring in the Berriasian as the result of uplift and denudation of the Avalon Uplift and subsequent normal movement on the Voyager and Flemish Pass fault zones and down drop of the Flemish Pass Basin. In the Jeanne d'Arc Basin, the Avalon Uplift was a source area for fluvial sandstones of the Jeanne d'Arc Formation in the Tithonian (Late Jurassic) (Tankard and Welsink, 1987; McAlpine, 1990; Sinclair, 1993; Enachescu, 1994). Therefore, the Avalon Uplift had been a positive tectonic element since the Late Jurassic; however, this evidence suggests it reached its maximum uplift and became a dominant regional source of sediments by the Berriasian (Early Cretaceous).

The Hibernia Formation equivalent is a large Berriasian-aged terrestrial sand deposit. Foster and Robinson (1993) place this unit at the top of the upwards shoaling MS1-50 parasequence. Provenance data herein suggests that source areas to the west and northwest, suggesting this deposit must have entered the basin from the west (Figure 7.10). The base of this unit is sharp over the underlying shallow water sands and muds; indicating an abrupt change in lithology and depositional setting. Also, differences in provenance-sensitive heavy mineral ratios and detrital zircon provenance are present between the Hibernia Formation and underlying units. This sudden change in provenance and depositional setting recorded across this contact suggests it is an unconformity and also indicates a rapid change in base level as well as regional paleodrainage orientations (Figure 7.10). These changes are interpreted to record modifications in regional rifting vectors and uplift, relating to the onset of the major NW-SE rifting during the North Atlantic rift stage, causing uplift of new areas during plate re-organization. The Hibernia

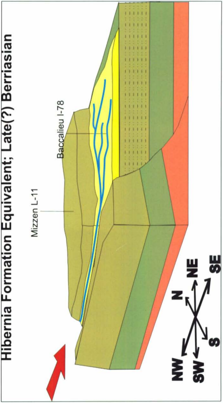

Figure 7.10: Model for the deposition of the Hibernia Formation Equivalent in the Late(?) Berriasian. Rapid uplift and reorientation of the margins of the rift basin occurred in the middle to late Berriasian, which led to erosion of the top of MS1-50 and the eastward progradation of thick submature terrestrial sandstones, known as the Hibernia Formation equivalent.

Formation equivalent is interpreted to have rapidly prograded from the west/northwest as the result of rapid uplift to the west/northwest and increased sediment availability. This basin reorganization and renewed uplift in the Baccalieu Subbasin is interpreted to relate to intensified regional E-W rifting during the culmination of lithospheric attenuation between Iberia and the southern Grand Banks. No correlative unit of the Hibernia Formation Equivalent exists in the Mizzen L-11 well. Therefore, the Mizzen area is interpreted to have been uplifted during this time, and was a site of non-deposition or erosion (Figure 7.10).

The Avalon Formation equivalent entered the Baccalieu subbasin from the southeast during the Valanginian to Hauterivian and was derived primarily from Avalon Zone basement and Late Paleozoic to early Mesozoic sediments from uplifted areas to the southeast including areas around the Beothuk Knoll, Flemish Graben and Flemish Cap (Figures 7.5, 7.11). It is interpreted to have first prograded from the southeast as part of a highstand system tract and then retrograded as part of a transgressive system tract as basin subsidence outpaced sediment input, consistent with the interpretations of Foster and Robinson (1993).

7.4.1 Implications for the Flemish Cap and Local Uplift and Deposition

The granodiorite pluton that comprises the core of the Flemish Cap could not have been a potential source of sediments at the time of deposition of the Avalon Equivalent sandstone, since no ages exist in the detrital zircon population that match the 750 Ma to 830 Ma age of emplacement of the pluton. By this time (Valanginian-Hauterivian, or

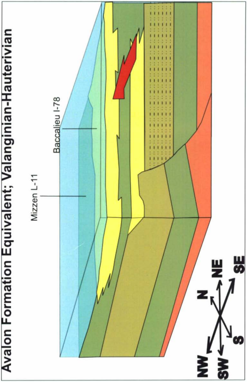

Figure 7.11: Model for the deposition of the Hibernia Formation Equivalent in the Valanginian to Hauterivian. The Hibernia Formation equivalent was overlain by another flooding surface, over which another upwards shoaling sequence was deposited, known as MS2 (Foster and Robinson, 1993). In this part of the basin, the MS2 sequence shoaled upwards from shelfal shales into sandy shelfal sandstones, known as the Avalon Formation equivalent. The Avalon Formation equivalent prograded from the southeast, and then retrograded as basin deepening outpaced sediment input (Foster and Robinson, 1993).

M11 time) seafloor spreading was ongoing between Iberian and the Grand Banks south of the Flemish Cap-Galicia Bank continental segments, however the Flemish Cap and Galicia Bank were still intact, and rifting was focused to the west in the Orphan Basin (Srivastava et al., 2000; Sibuet et al., 2007).

One implication of this is that the Flemish Cap did not exist as a basement high, and was buried, until at least after the Hauterivian-Valanginian (M11 time), and thus not available as an uplifted source area of sediments. This interpretation would imply that the Flemish Cap was buried under Triassic and/or Jurassic syn-rift sediments. However, seismic interpretations across the Flemish Cap show no evidence for extensional basins or syn-rift strata, and for the most part the Flemish Cap is a coherent continental block covered by a veneer of post rift sediments no older than mid- to Late Cretaceous; with the exception of the Flemish Graben, which appears to have a thicker, possibly late syn-rift Cretaceous succession, still probably younger than most of the Late Jurassic to Early Cretaceous rift clastics (Grant, 1973; Enachescu, 1987, 1988; Grant & McAlpine 1990; Hopper et al., 2006). Therefore, the Flemish Cap was unlikely to have been buried by syn-rift strata, and thus should have existed as a basement high and viable source of sediments at this time.

Another possible explanation is that separate drainage systems were taking material from the Flemish Cap-Galicia Bank block and depositing to the south into the incipient Atlantic and Lusitanian Basin, or to the northeast into the Bay of Biscay Basin, instead of the Flemish Pass Basin. This interpretation would imply that some intervening paleogeographic high between the core of the Flemish Cap and the Flemish Pass Basin was diverting drainage systems away. Or, perhaps material was being diverted into and through the Flemish Graben, southwards into the Atlantic Basin.

Finally, a third possibility is that the Flemish Pass granodiorite was not yet exposed, even though the Flemish Cap may have been uplifted and shedding overlying material westward into the Flemish Pass Basin.

There is no evidence to support any distal eastern source areas on the Iberian conjugate margin; and rather, the evidence strongly supports distal to source areas in the northwest, west and south throughout the deposition of the Late Jurassic to Early Cretaceous rift succession in the northern Flemish Pass Basin. Therefore, sediment transport from the Flemish Cap, which was connected to the Iberian margin, into the Flemish Pass Basin, is also not considered likely. Therefore, the most plausible scenario is that material from the Flemish Cap-Galicia Bank was instead somehow diverted south or northeast during the Late Jurassic to Early Cretaceous (Figure 71.12).

7.5 Conclusions:

(1) Depositional histories and areal extents of reservoir sandstones deposited in the northern Flemish Pass Basin during the Late Jurassic to Early Cretaceous (Tithonian to Hauterivian) are further constrained by this study. Jurassic Sandstone # 2 was deposited into the Baccalieu subbasin during the Tithonian from the west or northwest during a relative lowstand or in shallow water (Figure 7.7). The sands were rapidly flooded and overlain by shale. Shale deposition continued under shelfal conditions until the Tithonian or Berriasian. At this time, a thin wedge of sands comprising Jurassic Sandstone # 1

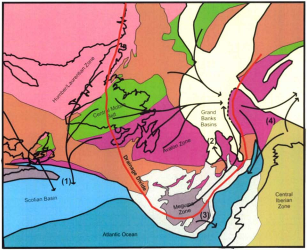

Figure 7.12: Regional paleodrainage patterns and drainage divides as interpreted from this thesis and from previous studies. (1) Pe-Piper and Mackay (2006) interpreted the Newfoundland Humber Zone as a source area for Early Cretaceous sandstones in the Scotian Basin. The Humber Zone is not a major source area for Early Cretaceous sandstones in the Flemish Pass Basin, even though parts of the Gander Zone and Avalon Zone are interpreted as sources; and therefore, a drainage divide is inferred somewhere in between. (2) Paleodrainage into the Jeanne d'Arc Basin in the Late Jurassic as interpreted by Tankard and Welskink (1987) and Enachescu et al. (1994). (3) Provenance of Albian sandstones in the Newfoundland Basin as interpreted by Hiscott et al. (2008). (4) Since neither Iberia nor the Flemish Cap are interpreted as sources of sediment in the Flemish Pass Basin, it is likely that sediment from these areas was instead shed into the Bay of Biscay or Incipient North Atlantic.

aggraded along the western or northwestern margin of the Baccalieu subbasin, and quickly spread eastward, to a limited extent, during a relative lowstand (Figure 7.8). These sands were quickly flooded once again, and above this flooding surface began a shoaling upwards parasequence known as MS1-50 (Foster and Robinson, 1993). The sands in MS1-50 were derived in part from the west and in part from the south, at least in the upper part of this parasequence (Figure 7.9). Rapid uplift and reorientation of the margins of the rift basin occurred in the middle to late Berriasian, which led to erosion of the top of MS1-50 and the eastward progradation of a thick package of submature sandstones, known as the Hibernia Formation equivalent (Figure 7.10). The Hibernia Formation equivalent was overlain by another flooding surface, over which another upwards shoaling sequence was deposited, known as MS2 (Foster and Robinson, 1993). In this part of the basin, the MS2 sequence shoaled upwards from shelfal shales into a sandy upper shelf deposit, known as the Avalon Formation equivalent. The Avalon Formation equivalent prograded from the southeast, and then retrograded as basin deepening outpaced sediment input (Foster and Robinson, 1993) (Figure 7.11).

(2) The regional sedimentary source areas for sandstones in the northern Flemish Pass Basin changed several times throughout the Late Jurassic and Early Cretaceous, between distal western and/or northwestern source areas, to southern and western areas, back to western/northwestern areas, and finally to more proximal areas to the southeast. This has been shown by detrital zircon evidence, and is consistent with variations in heavy mineral provenance signatures. These significant changes in regional paleodrainage patterns over such a short period of time (approximately 10 Ma) are attributed to plate reorganization

accompanying the switch from north-south directed extension to northwest-southeast directed extension at the transition period between the post-Tethys rifting stage and North Atlantic rifting stage. The Avalon Uplift reached its maximum as a regional basement high and source of sediment during the Berriasian, at about the same time as seafloor spreading began between southern Iberia and the Grand Banks (Srivastava et al., 2000). The evidence presented herein indicates some fairly distal source areas to the west of the Northern Flemish Pass Basin, supporting the idea that it could have been in open seaway or syn-depositional communication with the Orphan Basin during this time.

(3) Neither the Iberian Margin nor the Flemish Cap appears to have been sources of sediment for coarse clastics in the northern Flemish Pass Basin during the Late Jurassic to Early Cretaceous North Atlantic rifting, despite their relative proximity to this depocentre. Material from these source areas must have instead been diverted into depocentres to the south or north, including the incipient oceanic Atlantic and Bay of Biscay Basins (Figure 7.12).

(4) The relative scarcity of 1.0 to 1.6 Ga detrital zircons as well as detrital chromites in Late Jurassic and Early Cretaceous sandstones in the Flemish Pass Basin indicates that that Grenville aged basement and Ordovician ophiolites of the Humber Zone in Western Newfoundland were not sources of sediment at this place and time. This is in contrast to the provenance of Early Cretaceous sandstones in the eastern Scotian Basin, where evidence suggests significant sourcing from the Humber Zone, to the north (Pe-Piper and Mackay, 2006.). Therefore, a drainage divide must have existed somewhere east of the

Humber Zone in the Early Cretaceous; west of which sediments were diverted to the south-southeast in the Scotian Basin, and east of which sediments were diverted eastward into the Grand Banks Basins (Figure 7.12).

(5) During the Late Jurassic to Early Cretaceous, large west to east oriented drainage systems were depositing reservoir facies sandstones into the northwestern and western margins of the Flemish Pass Basin. Thus, it is likely that these regional drainage systems also culminated in the East Orphan Basin, to the north, where one might expect to find good quality reservoir facies along the western margin of that basin.

References

Abbink, O., Targarona, J., Brinkhuis, H., and Visscher, H. 2001. Late Jurassic to earliest Cretaceous palaeoclimatic evolution of the southern North Sea. Global and Planetary Change, **30**, 231-256.

Ainsworth, N. R., Riley, L. A., and Sinclair, I.K. 2005. A Mid-Cretaceous (upper Barremian-Turonian) lithostratigraphic and biostratigraphic framework for the Hibernia oilfield reservoir sequence, Jeanne d'Arc Basin, Grand Banks of Newfoundland, *In* Petroleum resources and reservoirs of the Grand Banks, Eastern Canadian Margin *Edited by* R. Hiscott and A. Pulham. Special Paper - Geological Association of Canada, **43**, 45-72.

Alves, Tiago M., Gawthorp, Robert L., Hunt, David W., and Monteiro, Jose H. 2003. Post-Jurassic tectono-sedimentary evolution of the northern Lusitanian Basin (western Iberian margin). Basin Research, **15**, 227-249.

Alves, Tiago M., Manuppella, Giuseppe, Gawthorpe, Robert L., Hunt, David W., and Monteiro, Jose H. 2003. The depositional evolution of diapir- and fault-bounded rift basins; examples from the Lusitanian Basin of west Iberia. Sedimentary Geology, **162**, 273-303.

Amoco Canada Petroleum Company Ltd. 1973. Spoonbill C-30 Well History Report.

Arribas, Jose, and Tortosa, Amparo. 2003. Detrital modes in sedimenticlastic sands from low-order streams in the Iberian Range, Spain; the potential for sand generation by different sedimentary rocks. Sedimentary Geology, **159**, 275-303.

Ascoli, P. 1990. Foraminiferal, ostracode and calpionellid zonation and correlation of 42 selected wells from the north Atlantic margin of North America. Bulletin of Canadian Petroleum Geology, **38**, 485-492.

Balkwill, H. R., and Legall, F. D. 1989. Whale Basin, offshore Newfoundland; extension and salt diapirism. *In* Extensional tectonics and stratigraphy of the North Atlantic margins, *Edited by* A.J. Tankard, and H.R. Balkwill. AAPG Memoir, **46**, 233-245.

Barrs, M.S., Bujak, J.P., and Williams, G.L. 1979. Palynological zonation and correlation of sixty-seven wells, Eastern Canada. Geological Survey of Canada, Paper No. 78-24.

Beard, D. C., and Weyl, P. K. 1973. Influence of Texture on Porosity and Permeability of Unconsolidated Sand. AAPG Bulletin, **57**, 349-369.

Bell, J.S., and Howie, R.D. 1990. Paleozoic Geology. *In* Geology of the Continental Margin of Eastern Canada. *Edited by* M.J. Keen and G.L. Williams, pp. 141-165.

Blasi, A., and Manassero, M. J. 1990. The Colorado River of Argentina; source, climate, and transport as controlling factors on sand composition. Journal of South American Earth Sciences, **3**, 65-70.

Blatt, Harvey, and Christie, John M. 1963. Undulatory extinction in quartz of igneous and metamorphic rocks and its significance in provenance studies of sedimentary rocks. Journal of Sedimentary Petrology, **33**, 559-579.

Blatt, Harvey. 1967. Provenance determinations and recycling of sediments. Journal of Sedimentary Petrology, **37**, 1031-1044.

BP Exploration Canada Ltd. 1975. Bonavista C-99 Well History Report and Logs.

BP Exploration Canada Ltd. 1979. Hare Bay E-21 Well History Report and Logs.

BP Exploration Canada Ltd. 1991. Biostratigrahic Study of Flemish Pass Wells.

Bujak Davies Group. 1987. Palynological Analysis of the Interval 1600-5145 M, Baccalieu I-78, Grand Banks. GSC Open File Report 1870, 16 p.

Burley, S. D. 1986. The development and destruction of porosity within Upper Jurassic reservoir sandstones of the Piper and Tartan fields, outer Moray Firth, North Sea. Clay Minerals, **21**, 649-694.

Cameron, Kenneth L., and Blatt, Harvey. 1971. Durabilities of sand size schist and 'volcanic' rock fragments during fluvial transport, Elk creek, Black Hills, South Dakota. Journal of Sedimentary Petrology, **41**, 565-576.

Canada-Nefoundland and Labrador Offshore Petroleum Board (CNLOPB). 2007. Schedule of wells- Newfoundland offshore area.

Capdevila, R., Mougenot, D. 1988. Pre-Mesozoic basement of the western Iberian continental margin and its place in the Variscan Belt. Proceedings of the Ocean Drilling Program, Scientific Results, **103**, 3-12.

Clarke, D.B., MacDonald, M.A., and Tate, M.C. 1997. Late Devonian mafic-felsic magmatism in the Meguma Zone, Nova Scotia. Memoir - Geological Society of America, **191**, 107-127.

Chevron Canada Resources. 1990. Baccalieu I-78 Palynology Report.

Chian, D, Reid, I.D., and Jackson, H.R. 2001. Crustal structure beneath Orphan Basin and implications for nonvolcanic continental rifting. Journal of Geophysical Research, **106**, 10,923-10,940.

Chorlton, L.B. and Dallmeyer, R.D. 1986. Geochronology of early to middle Paleozoic tectonic development in the Southwest Newfoundland Gander Zone. Journal of Geology, **94**, 67-89.

Colin, Jean-Paul, Ioannides, Nicos S., and Vining, Bernie. 1992. Mesozoic stratigraphy of the *Goban* Spur, offshore South-west Ireland. Marine and Petroleum Geology, **9**, 527-541.

Compton, Robert R. 1962. Manual of Field Geology. New York, John Wiley and Sons.

Cox, Ronadh, and Lowe, Donald R. 1995a. A conceptual review of regional-scale controls on the composition of clastic sediment and the co-evolution of continental blocks and their sedimentary cover. Journal of Sedimentary Research, Section A: Sedimentary Petrology and Processes, **65**, 1-12.

Cox, Ronadh, and Lowe, Donald R.. 1995b. Compositional evolution of coarse clastic sediments in the Southwestern United States from 1.8 to 0.2 Ga and implications for relationships between the development of crustal blocks and their sedimentary cover. Journal of Sedimentary Research, Section A: Sedimentary Petrology and Processes, **65**, 477-494.

Cox, R.A. 2003. Morphological, chemical, and geochronological techniques for characterizing detrital zircon. *In* Geochemistry of Sediments and Sedimentary Rocks: Evolutionary Considerations to Mineral Deposit-Forming Environments *Edited by* D.R. Lentz. Pp. 105-120.

Creaney, S., and Allison, B.H. 1987. An organic geochemical model of oil generation in the Avalon/Flemish subbasin, East Coast Canada. Bulletin of Canadian Petroleum Geology, **35**, 12-23.

Croker, Peter F., and Shannan, P. M. 1987. The evolution and hydrocarbon prospectivity of the Porcupine Basin, offshore Ireland. *In* Petroleum geology of north west Europe *Edited by* J. Brooks and K.W. Glennie, Kenneth W. 633-642.

Croker, Peter F., and Klemperer, Simon L. 1989. Structure and stratigraphy of the Porcupine Basin; relationships to deep crustal structure and the opening of the North Atlantic. *In* Extensional tectonics and stratigraphy of the North Atlantic margins, *Edited by* A.J. Tankard, and H.R. Balkwill. AAPG Memoir, **46**, 445-459.

Crook, Keith A. W. 1968. Weathering and roundness of quartz sand grains. Sedimentology, **11**, 171-182.

Critelli, Salvatore, Arribas, Jose, Le Pera, Emilia, Tortosa, Amparo, Marsaglia, Kathleen M., and Latter, Kelly K. 2003. The recycled orogenic sand provenance from an uplifted thrust belt, Betic Cordillera, southern Spain. Journal of Sedimentary Research, **73**, 72-81.

Currie, K. L. 1995. Plutonic rocks. *In* Geology of the Appalachian-Caledonian Orogen in Canada and Greenland *Edited by* H. Williams. 629-680.

Dallmeyer, R. D., Blackwood, R. F., Odom, A. L. 1981. Age and origin of the Dover Fault; tectonic boundary between the Gander and Avalon zones of the northeastern Newfoundland Appalachians. Canadian Journal of Earth Sciences, **18**, 1431-1442.

Daly, J.S, Flowerdew, M.J. 2005. Grampian and late Grenville events recorded by mineral geochronology near a basement-cover contact in north Mayo, Ireland. Journal of the Geological Society of London, **162**, 163-174.

Davies, P. J., Bubela, B., and Ferguson, J. 1978. The formation of ooids. Sedimentology, **25**, 703-729.

Deon, G., and Timmons, G. 2003.Geological Report on Petro-Canada et al Mizzen L-11.

Demir, Tuncer. 2003. Downstream changes in bed material size and shape characteristics in a small upland stream; Cwm Treweryn, in South Wales. Yerbilimleri, **28**, 33-47.

Desilva, N. 1999. Sedimentary basins and petroleum systems offshore Newfoundland and Labrador. *In* Petroleum Geology of Northwest Europe: Proceedings of the 5th Conference *Edited by* A.J. Fleet and S.R. Boldy. Geological Society, London, pp. 501-515.

Desilva, N. 2000. Flemish pass basin: Hydrocarbon prospectivity and potential deep water development, Journal of Canadian Petroleum Technology, **39**, 22-25.

Dickinson, William R. 1970. Interpreting detrital modes of graywacke and arkose. Journal of Sedimentary Petrology, **40**, 695-707.

Dickinson, W. R.; Suczek, C. A. 1979. Plate tectonics and sandstone compositions. AAPG Bulletin, **63**, 2164-2182.

Dickinson, William R., Beard, L. Sue, Brakenridge, G.R., Erjavec, James L., Ferguson, Robert C., Inman, Kerry F., Knepp, Rex A., Lindberg, F. Alan, and Ryberg, Paul T. 1983. Provenance of North American Phanerozoic sandstones in relation to tectonic setting. GSA Bulletin, **94**, 222-235.

Dickson, W.L. 1990. Geology of the North Bay Granite Suite and metasedimentary rocks in southern Newfoundland (NTS 11P/15E, 11P/16 and 12A/2E). Report - Government of Newfoundland and Labrador. Dept. of Mines and Energy, Geological Survey.

Dill, Harald G. 1995. Heavy mineral response to the progradation of an alluvial fan; implications concerning unroofing of source area, chemical weathering and palaeo-relief (Upper Cretaceous Parkstein fan complex, SE Germany). Sedimentary Geology, **95**, 39-56.

Dingle, R. V., and Scrutton, R. A. 1979. Sedimentary succession and tectonic history of a marginal plateau (Goban Spur, southwest of Ireland). Marine Geology, **33**, 45-69.

Dube, B., Dunning, G.R., Lauziere, K., and Roddick, J.C. 1996. New insights into the Appalachian Orogen from geology and geochronology along the Cape Ray fault zone, southwest Newfoundland. GSA Bulletin, **108**, 101–116.

Enachescu, M.E. 2006. Newfoundland and Labrador Call for Bids NL06-1, Jeanne d'Arc basin.

Enachescu, M.E. 1988. Extended basement beneath the intracratonic rifted basins of the grand banks of Newfoundland. Canadian Journal of Exploration Geophysics, **24**: 48-65.

Enachescu, M.E. 1987. Tectonic and structural framework of the northeast Newfoundland continental margin. *In* Sedimentary Basins and Basin Forming Mechanisms *Edited by* C. Beaumont and A.J. Tankard. Canadian Society of Petroleum Geologists, Calgary. pp. 117-146.

Enachescu, M.E. 1992. Enigmatic basins offshore Newfoundland. Canadian Journal of Exploration Geophysics, **28**, 44-61.

Enachescu, M.E. and Hogg, J. 2004. Compression modified extensional structures (CMES) of the Canadian Atlantic passive margin. CSPG/CSEG/CWLS Annual Convention, Calgary.

Enachescu, M.E., Kearsey, S., Hardy, V., Sinuet, J., Hogg, J., Srivastava, S., Fagan, A., Thompson, T., and Ferguson, R. 2005. Evolution and Petroleum Potential of Orphan Basin, Offshore Newfoundland, and its Relation to the Movement and Rotation of Flemish Cap based on Plate Kinematics of the North Atlantic. *In* 25th annual Gulf Coast section SEPM Foundation, Bob F. Perkins research conference, symposium on Petroleum systems of divergent continental margin basins *Edited by* P.J. R. Post, C. Norman, D.L. Olson, S.L. Palmes, K.T. Lyons, and B. Geoffrey.

Ercilla, G., Garcia-Gil, S., Estrada, F., Gracia, E., Vizcaino, A., Vazquez, Juan T., Diaz, S., Vilas, F., Casas, D., Alonso, B., Danobeitia, J. J., and Farran, M. 2008. High-resolution seismic stratigraphy of the Galicia Bank region and neighbouring abyssal plains (NW Iberian continental margin). Marine Geology, **249**, 108-127.

Esso Resources Canada Ltd. 1986. Esso Parex et al Baccalieu I-78 well history reports and logs.

Feely, M., Coleman, D., Baxter, S., and Miller, B. 2004. U-Pb zircon geochronology of the Galway Granite, Connemara, Ireland: implications for the timing of late Caledonian tectonic and magmatic events and for correlations with Acadian plutonism in New England. Atlantic Geology, **39**, 175-184.

Folk, R.L. 1951. A comparison chart for visual percentage estimation. Journal of Sedimentary Petrology, **21**, 32-33.

Folk, R.L. 1968. Petrology of sedimentary rocks. Austin, Tex., Hemphill's. 170 p.

Foster, D.G. and Robinson, A.G. 1993. Geological history of the Flemish pass basin, offshore Newfoundland. The American Association of Petroleum Geologists Bulletin, **77**, 588-609.

Flowerdew, M.J., Daly, J.S., and Whitehouse, M.J. 2005. 470 Ma granitoid magmatism associated with the Grampian Orogeny in the Slishwood Division, NW Ireland. Journal of the Geological Society of London, **162**, 563-575.

Gradstein, F.M., and Thomas, F.C., 1983. Stratigraphy and depositional environment of Texaco Blue H-28. Report No. EPGS-PAL.1-83FMG/FCT.

Grant, A.C. 1973. Geological and geophysical results bearing upon the structural history of the Flemish cap region. *In* Earth Science Symposium on Offshore Eastern Canada, Geological Survey of Canada paper 71-23, pp. 373-388.

Grant, A.C., and McAlpine, K. D. 1990. The continental margin around Newfoundland. *In* Geology of the continental margin of Eastern Canada, *Edited by* M.J. Keen and G. L. Williams. pp. 239-292.

Grantham, J.H., and Velbel, M.A. 1988. The influence of climate and topography on rock-fragment abundance in modern fluival sands of the southern Blue Ridge Mountains, North Carolina. Journal of Sedimentary Petrology, **58**, 219-227.

Greenough, J.D., Kamo, S.L., and Krogh, T.E. 1993. A Silurian U-Pb age for the Cape St. Mary's sills, Avalon Peninsula, Newfoundland, Canada; implications for Silurian orogenesis in the Avalon Zone. Canadian Journal of Earth Sciences, **30**, 1607-1612.

Gu, Y. 2003. Automated Scanning Electron Microscope Based Mineral Liberation Analysis, An Introduction to JKMRC/FEI Mineral Liberation Analyser. Journal of Minerals & Materials Characterization & Engineering, **2**, 33-41.

Hallsworth, C. R., Morton, A. C., Claoue-Long, J., and Fanning, C. M. 2000. Carboniferous sand provenance in the Pennine Basin, UK; constraints from heavy mineral and detrital zircon age data. Sedimentary Geology, **137**, 147-185.

Haworth, R.T. and Lefort, J.P. 1979. Geophysical evidence for the extent of the Avalon zone in Atlantic Canada. Canadian Journal of Earth Sciences, **16**: 552-567.

Helwig, J., Aronson, J., and Day, D. S. A Late Jurassic Mafic Pluton in Newfoundland. Canadian Journal of Earth Sciences, 1974, **11**, 1314-1319.

Hendriks, M., Jamieson, R. A., Willett, S. D., and Zentilli, M. 1993. Burial and exhumation of the Long Range Inlier and its surroundings, western Newfoundland; results of an apatite fission-track study. Canadian Journal of Earth Sciences , **30**, 1594-1606.

Henry, D.J. and Guidotti, C.V. 1985. Tourmaline as a petrogenetic indicator mineral: an example from the staurolite-grade metapelites of NW Maine. American Mineralogist, **70**, 1-15

Hiscott, R. N., Wilson, R. C. L., Gradstein, F. M., Pujalte, V., Garcia-Mondejar, J., Boudreau, R. R., and Wishart, H. A. 1990. Comparative stratigraphy and subsidence history of Mesozoic rift basins of North Atlantic. AAPG Bulletin, **74**, 60-76.

Hiscott, R.N., Marsaglia, K.M., Wilson, R.L., Robertson, A.H. F., Karner, G.D., Tucholke, B.E., Pletsch, T., and Petschick, R. 2008. Detrital sources and sediment delivery to the early post-rift (Albian-Cenomanian) Newfoundland Basin east of the Grand Banks; results from ODP Leg 210. Bulletin of Canadian Petroleum Geology, **56**, 69-92.

Holford, S.P., Green, P.F., Duddy, I.R., Turner, J.P., Hillis, R.R., and Stoker, M.S. 2009. Regional intraplate exhumation episodes related to plate-boundary deformation. GSA Bulletin, **121**, 1611-1628.

Hopper, J.R., Funck, T., Tucholke, B.E., Louden, K.E., Holbrook, W.S., and Larsen, H.C. 2006. A deep seismic investigation of the Flemish Cap margin; implications for the origin of deep reflectivity and evidence for asymmetric break-up between Newfoundland and Iberia. Geophysical Journal International, **164**, 501-515.

Hoskin, Paul W. O., and Schaltegger, Urs. 2003. The composition of zircon and igneous and metamorphic petrogenesis. *In* Zircon *Edited by* J.M. Hanchar, and P.W.O. Hoskin. Reviews in Mineralogy and Geochemistry, **53**, 27-62.

Hubbard, R.J. 1988. Age and significance of sequence boundaries on Jurassic and Early Cretaceous rifted continental margins. AAPG Bulletin, 72, 49-72.

Hubert, John F. 1962. A zircon-tourmaline-rutile maturity index and the interdependence of the composition of heavy mineral assemblages with the gross composition and texture of sandstones. Journal of Sedimentary Petrology, **32**, 440-450.

International Commission on Stratigraphy (ICS). 2009. International Stratigraphic Chart. http://www.stratigraphy.org/upload/ISChart2009.pdf

Jacobi, R.D. and Kristoffersen, Y. 1981. Transatlantic correlations of geophysical anomalies on newfoundland, british isles, france and adjacent continental shelves, Memoir - Canadian Society of Petroleum Geologists, **7**, 197-229.

Jansa, L.F., and Wade, J.A. 1975. Regional geology. *In* Offshore geology of eastern Canada, Paper - Geological Survey of Canada, **2**, 51-105.

Jansa, L.F., and Pe-Piper, G. 1986. Geology and geochemistry of Middle Jurassic and Early Cretaceous igneous rocks on the eastern North American continental shelf. Open-File Report 1351 - Geological Survey of Canada.

Jansa, L.F., and Pe-Piper, G. 1988. Middle Jurassic to Early Cretaceous igneous rocks along eastern North American continental margin AAPG Bulletin, **72**, 347-366

Johnson, H. Ritchie, J. D., Gatliff, R. W., Williamson, J. P., Cavill, J., and Bulat, J. 2001. Aspects of the structure of the Porcupine and Porcupine Seabight basins as revealed from gravity modeling of regional seismic transects. *In* Mesozoic successions of the Porcupine and North Porcupine basins, offshore Ireland The petroleum exploration of Ireland's offshore basins *Edited by* P.M. Shannon, P.D.W. Haughton, and D.V. Corcoran. Geological Society Special Publications, **188**, 265-274.

Johnsson, M.J., Stallard, R.F.; Meade, R.H. 1988. First-cycle quartz arenites in the Orinoco River basin, Venezuela and Colombia. Journal of Geology, **96**, 263-277.

Johnsson, M.J. 1990. Tectonic versus chemical-*weathering* controls on the composition of fluvial sands in tropical environments. Sedimentology, **37**, 713-726.

Kearsey, S.J. and Enachescu, M.E. 2005. Orphan basin, offshore Newfoundland: Integrated geophysical analysis and evidence for extreme crustal thinning on the conjugate margins. GAC-MAC-CSPG annual meeting, Halifax.

Keen, C.E., Stockmal, G.S., Welsink, H.J., Quinlan, G., and Mudford, B. 1987. Deep crustal structure and evolution of the rifted margin northeast of Newfoundland: Results from LITHOPROBE east, Canadian Journal of Earth Sciences, **24**: 1537-1549.

Keen, C., Peddy, C., de Voogd, B., and Matthews, D. 1989. Conjugate margins of Canada and Europe; results from deep reflection profiling. Geology, **17**, 173-176.

King, L.H., Fader, G.B, Jenkins, W.A.M., and King, E.L. 1986. Occurrence and regional geological setting of Paleozoic rocks on the Grand Banks of Newfoundland. Canadian Journal of Earth Sciences, **23**, 504-526.

King, L.H., Fader, G.B., Poole, W.H., and Wanless, R.K. 1985. Geological setting and age of the Flemish cap granodiorite, east of the grand banks of newfoundland, Canadian Journal of Earth Sciences, **22**: 1286-1298.

Kontak, D.J., Ham, L.J., and Dunning, G. U-Pb dating of the Musquodoboit Batholith, southern Nova Scotia; evidence for a protracted magmatic-hydrothermal event in a Devonian intrusion. Atlantic Geology, **40**, 207-216.

Kosler, J., Fonneland, H., Sylvester, P.J., Tubrett, M., and Pederson, R. 2002. U-Pb dating of detrital zircons for sediment provenance studies - a comparison of laser ablation ICPMS and SIMS techniques, Chemical Geology, **182**: 605-618.

Kosler, J., and Sylvester, P.J. 2003. Present trends and the future of zircon in geochronology; laser ablation ICPMS. *In* Zircon *Edited by* J.M. Hanchar, and P.W.O. Hoskin. Reviews in Mineralogy and Geochemistry, **53**, 243-275.

Kreuger Enterprises, Inc. 1972. Amoco-Imperial Jaeger A-49, K-Ar age determination of granite at 3040 feet.

Krogh, T.E., Strong, D.F., O'Brien, S.J., Papezik, V.S. 1987. Precise U-Pb zircon dates from the Avalon Terrane in Newfoundland. Canadian Journal of Earth Sciences, **25**, 442-453.

Krogh, T. E., and Keppie, J. D. 1990. Age of detrital zircon and titanite in the Meguma Group, southern Nova Scotia, Canada; clues to the origin of the Meguma Terrane. Tectonophysics, **177**, 307-323

Krogh, T. E. 1982. Improved accuracy of U-Pb zircon dating by selection of more concordant fractions using a high gradient magnetic separation technique. Geochimica et Cosmochimica Acta, **46**, 631-635.

Lilly, H.D. 1966. Submarine surveys on the Great Bank of Newfoundland and in the Gulf of Saint Lawrence. Maritime Sediments, **2**, 12-14

Lefort, J.P. and Haworth, R.T. 1978. Geophysical study of basement fractures on the western european and eastern canadian shelves: Transatlantic correlations, and late hercynian movements. Canadian Journal of Earth Sciences, **15**, 397-404.

Lefort, J.P. 1983. A new geophysical criterion to correlate the Acadian and Hercynian orogenies of Western Europe and eastern America. *In* Contributions to the tectonics and geophysics of mountain chains, *Edited by* R.D. Hatcher, H. Williams, and I. Zietz. Memoir - Geological Society of America, **158**, 3-18.

Ludwig, K.R. 1999. User's manual for Isoplot/Ex version 2.06, a geochronological toolkit for Microsoft Excel.

Masson, D. G., and Miles, P. R. 1984. Mesozoic seafloor spreading between Iberia, Europe and North America. Marine Geology, **56**, 279-287.

Masson, D.G. and Miles, P.R. 1986. Development of hydrocarbon potential of mesozoic sedimentary basins around margins of north atlantic, The American Association of Petroleum Geologists Bulletin, **70**: 721-729.

McAlpine, K. D. 1989. Lithostratigraphy of fifty-nine wells, Jeanne d'Arc Basin Open-File Report - Geological Survey of Canada.

McAlpine, K.D. 1990. Mesozoic stratigraphy, sedimentary evolution, and petroleum potential of the Jeanne d'Arc basin, grand banks of Newfoundland. Geological Survey of Canada Paper 89-17.

McBride, E.F., Abel-Wahab, A., McGilvery, T.A. 1996. Loss of sand-size feldspar and rock fragments along the South Texas barrier island, USA. Sedimentary Geology, **107**, 37-44.

McCracken, J.N., Haager, A., Saunders, K.I., and Veilleux, B.W. 2000. Late Jurassic source rocks in the northern Flemish Pass Basin, Grand Banks of Newfoundland. Proceedings of GeoCanada 2000; the millennium geoscience summit. Abstract Volume, Geological Association of Canada, Vol. 25.

McLennan, S. M., Bock, B., Compston, W., Hemming, S. R., and McDaniel, D. K. 2001. Detrital zircon geochronology of Taconian and Acadian foreland sedimentary rocks in New England. Journal of Sedimentary Research, **71**, 305-317.

Millson, J. A. 1987. The Jurassic evolution of the Celtic Sea basins. *In* Petroleum geology of north west Europe *Edited by* J. Brooks and K. Glennie. pp. 599-610.

Milliken, K.L. 1988. Loss of provenance information through subsurface diagenesis in Plio-Pleistocene sandstones, northern Gulf of Mexico. Journal of Sedimentary Petrology, **58**, 992-1002.

Morad, S. 1986. SEM study of authigenic *rutile*, anatase and brookite in Proterozoic sandstones from Sweden. Sedimentary Geology, **46**, 77-89.

Morton, A. C. 1979. Depth control of intrastratal solution of *heavy minerals* from the Palaeocene of the North Sea. Journal of Sedimentary Petrology, **49**, 281-286.

Morton, A. C. 1984. Stability of detrital *heavy minerals* in Tertiary sandstones from the North Sea basin. Clay Minerals, **19**, 287-308.

Morton, A.C., and Hallsworth, C.R. 1994. Identifying provenance-specific features of detrital heavy mineral assemblages in sandstones. Sedimentary Geology, **90**, 241-256.

Morton, A.C., and Hallsworth, C.R. 1999. Processes controlling the composition of heavy mineral assemblages in sandstones Sedimentary Geology, **124**, 3-30.

Morton, A.C., Knox, R.W., and Hallsworth, C. 2002. Correlation of reservoir sandstones using quantitative heavy mineral analysis. Petroleum Geoscience, **8**, 251-262.

Morton, A. C., Whitham, A. G., and Fanning, C.M. 2005. Provenance of Late Cretaceous to Paleocene submarine fan sandstones in the Norwegian Sea; integration of heavy mineral, mineral chemical and zircon age data. Sedimentary Geology, **182**, 3-28.

Moss, A. J. 1972. Initial fluviatile fragmentation of granitic quartz. Journal of Sedimentary Petrology, **42**, 905-916.

Murphy, J. B., and Hamilton, M.A. 2000 Orogenesis and basin development; U-Pb detrital zircon age constraints on evolution of the late Paleozoic St. Marys Basin, central mainland Nova Scotia. Journal of Geology, **108**, 53-71.

Nascimento, M.D., Goes, A.M., Macambira, M.J.B., and Brod, J.A. 2007. Provenance of Albian sandstones in the Sao Luis-Grajau Basin (northern Brazil) from evidence of Pb-Pb zircon ages, mineral chemistry of tourmaline and palaeocurrent data. Sedimentary Geology, **201**, 21-42.

O'Neill, P.P. Geology of Weir's Pond Area, Newfoundland (NTS 2E/1). Report 91-3 Government of Newfoundland and Labrador. Dept. of Mines and Energy, Geological Survey.

Ouma, J.P.B.M. 1967. Fluviatile morphogenesis of roundness; the Hacking river, New South Wales, Australia. Publication - International Association of Scientific Hydrology, **75**, 319-344.

Pemberton, S.G., Spila, M., Pulham, A.J., Saunders, T., MacEachern, J.A., Robbins, D., and Sinclair, I.K. 2001. Ichnology and Sedimentology of Shallow Marine to Marginal Marine Systems: Ben Nevis & Avalon Reservoirs, Jeanne d'Arc Basin. GAC Short Course, 15. 343 pages.

Pe-Piper, G., and Mackay, M. 2006. Provenance of Lower Cretaceous sandstones onshore and offshore Nova Scotia from electron microprobe geochronology and chemical variation of detrital monazite. Bulletin of Canadian Petroleum Geology, **54**, 366-379.

Pe-Piper, G., and Weir-Murphy, S. 2008. Early diagenesis of inner-shelf phosphorite and iron-silicate minerals, Lower Cretaceous of the Orpheus Graben, southeastern Canada; implications for the origin of chlorite rims. AAPG Bulletin, **92**, 1153-1168.

Petrie, S. H., Brown, J. R., Granger, P. J., and Lovell, J. P. B. 1989. Mesozoic history of the Celtic Sea basins. . *In* Extensional tectonics and stratigraphy of the North Atlantic margins, *Edited by* A.J. Tankard, and H.R. Balkwill. AAPG Memoir, **46**, 433-444.

Pettijohn, F. J. 1975. Sedimentary rocks. Harper & Row, Publ., New York, N.Y., United States. 628 p.

Pettijohn, F. J., Potter, P.E., and Siever, R. 1987. Sand and sandstone. Springer-Verlag : New York, NY, United States. 553 p.

Picard, M. Dane; McBride, Earle F. 2007. Comparison of river and beach sand composition with source rocks, Dolomite Alps drainage basins, northeastern Italy. *In* Sedimentary provenance and petrogenesis; perspectives from petrography and geochemistry *Edited by* J. Arribas, S. Critelli, M.J. Johnsson. Special Paper - Geological Society of America, **420**, 1-12.

Piper, D.J.W., Pe-Piper, G., Hundert, T., and Venugopal, D. V. 2007. The Lower Cretaceous Chaswood Formation in southern New Brunswick; provenance and tectonics. Canadian Journal of Earth Sciences, **44**, 665-677.

Pinheiro, L.D., Wilson, R. C. L.; Pena dos Reis, R., Whitmarsh, R.B., and Ribeiro, A. 1996. The western Iberia margin; a geophysical and geological overview. Proceedings of the Ocean Drilling Program, Scientific Results, **149**, 3-23

Pollock, J. C., Wilton, D. H. C., van Staal, C.R., and Morrissey, K. D. 2007. U-Pb detrital zircon geochronological constraints on the Early Silurian collision of Ganderia and

Laurentia along the Dog Bay Line; the terminal Iapetan suture in the Newfoundland Appalachians. American Journal of Science, **307**, 399-433.

Pollock, J.C., Hibbard, J.P., and Sylvester, P.J. 2009. Early Ordovician rifting of Avalonia and birth of the Rheic Ocean; U-Pb detrital zircon constraints from Newfoundland. Journal of the Geological Society of London, **166**, 501-515.

Priem, Harry N. A., and den Tex, E. 1984. Tracing crustal evolution in the NW Iberian Peninsula through the Rb-Sr and U-Pb systematics of Palaeozoic granitoids; a review. Physics of the Earth and Planetary Interiors, **35**, 121-130.

Potter, P. E. 1978. Petrology and chemistry of modern big river sands. Journal of Geology, **86**, 423-449.

Raeside, R.P., Hill, J.D., and Eddy, Brian G. 1988. Metamorphism of Meguma Group metasedimentary rocks, Whitehead Harbour area, Guysborough County, Nova Scotia. Maritime Sediments and Atlantic Geology, **24**, 1-9.

Rainbird, R. H., McNicoll, V. J., Theriault, R. J., Heaman, L. M., Abbott, J. G., Long, D. G. F., and Thorkelson, D. J. 1997. Pan-continental river system draining Grenville Orogen recorded by U-Pb and Sm-Nd geochronology of Neoproterozoic quartzarenites and mudrocks, northwestern Canada. Journal of Geology, **105**, 1-17.

Reid, Jeffrey C. 1985. Comparison chart for estimating volume percentages of constituents in rocks and concentrates in the range of 1.0 to 0.1 volume percent. American Mineralogist, **70**, 1318-1319.

Romeo, I., Capote, R., Tejero, R., Lunar, R., and Quesada, C. 2006. Magma emplacement in transpression; the Santa Olalla igneous complex (Ossa-Morena Zone, SW Iberia). Journal of Structural Geology, **28**, 1821-1834.

Robertson Research Ltd. 1979. Texaco-Shell et al Blue H-28 micropaleontology, palynology and stratigraphy report.

Robertson Research Ltd. 2003. Petro-Canada et al Mizzen L-11 biostratigraphy report.

Robinson, A. J., and Canham, A. C. Reservoir characteristics of the Upper Jurassic sequence in the 35/8-2 discovery, Porcupine Basin. *In* The petroleum exploration of Ireland's offshore basins *Edited by* P.M. Shannon, P.D.W. Haughton, and D.V. Corcoran. Geological Society Special Publications, **188**, 301-321.

Ruffman, A. and van Hinte, J.E. 1970. Orphan knoll - A "chip" off the North American continent. Maritime Sediments, **6**, 142.

Sanderson, I.D. 1984. Recognition and significance of inherited quartz overgrowths in quartz arenites. Journal of Sedimentary Petrology, **54**, 473-486.

Schaerer, U., Kornprobst, J., Beslier, M.O., Boillot, G., and Girardeau, J. 1995. Gabbro *and* related rock emplacement beneath rifting continental crust; U-Pb geochronological and geochemical constraints for the Galicia passive margin (Spain). Earth and Planetary Science Letters, **130**, 187-200.

Schmidt, V., and McDonald, D. A. 1977. Role of secondary porosity in sandstone diagenesis. AAPG Bulletin, **61**, 1390-1391.

Serra, O. 1984. Fundamentals of well-log interpretation I. The acquisition of logging data. Developments in Petroleum Science, **15A**, Elsevier, Holland. 423p.

Sibuet, J. C., Srivastava, S. P., Enachescu, M., and Karner, G. D. 2007. Early Cretaceous motion of Flemish Cap with respect to North America; implications on the formation of Orphan Basin and SE Flemish Cap-Galicia Bank conjugate margins. Geological Society Special Publications, 63-76.

Sinclair, I.K. 1993. Tectonism: the dominant factor in mid-Cretaceous deposition in the Jeanne d'Arc Basin, Grand Banks. Marine and Petroleum Geology, **10**, 530-549.

Sinclair, Iain K. 1995. Sequence stratigraphic response to Aptian-Albian rifting in conjugate margin basins; a comparison of the Jeanne d'Arc Basin, offshore Newfoundland, and the Porcupine Basin, offshore Ireland. *In* The tectonics, sedimentation and palaeoceanography of the North Atlantic region *Edited by R.A.* Scrutton, M.S. Stoker, G.B. Shimmield, and A.W. Tudhope. Geological Society Special Publications, **90**, 29-49.

Schlumberger, 2010. Oilfield Glossary. http://www.glossary.oilfield.slb.com/

Smale, D., and Morton, A. C. 1987. Heavy mineral suites of core samples from the McKee Formation (Eocene-lower Oligocene), Taranaki; implications for provenance and diagenesis. New Zealand Journal of Geology and Geophysics, **30**, 299-306.

Smith, J., and Higgs, K. T. 2001. Provenance implications of reworked palynomorphs in Mesozoic successions of the Porcupine and North Porcupine basins, offshore Ireland. *In* Mesozoic successions of the Porcupine and North Porcupine basins, offshore Ireland The petroleum exploration of Ireland's offshore basins *Edited by* P.M. Shannon, P.D.W. Haughton, and D.V. Corcoran. Geological Society Special Publications, **188**, 291-300.

Sola, A. R., Pereira, M. F., Williams, I. S., Ribeiro, M. L., Neiva, A. M. R., Montero, P.; Bea, F.; and Zinger, T. 2008. New insights from U-Pb zircon dating of Early Ordovician magmatism on the northern Gondwana margin; the Urra Formation (SW Iberian Massif, Portugal). Tectonophysics, **461**, 114-129.

Srivastava, S. P., Sibuet, J. C., Cande, S., Roest, W. R., and Reid, I. D. 2000. Magnetic evidence for slow seafloor spreading during the formation of the Newfoundland and Iberian margins. Earth and Planetary Science Letters, **182**, 61-76.

Srivastava, S.P. and Verhof, J. 1992. Evolution of Mesozoic sedimentary basins around the north central Atlantic: A preliminary plate kinematic solution. *In* Basins on the Atlantic Seaboard: Petroleum Geology, Sedimentology and Basin Evolution *Edited by* J. Parnell. Geological Society Special Publication no.62, pp. 397-420.

Suttner, L.J., Basu, A., and Mack, G.H. 1981. Climate and the origin of quartz arenites. Journal of Sedimentary Petrology, **51**, 1235-1246.

Tankard, A.J. and Welsink, H.J. 1987. Extensional tectonics and stratigraphy of Hibernia oil field, grand banks, Newfoundland. AAPG Bulletin, **71**, 1210-1232.

Tate, M. P., and Dobson, M. R. 1988. Syn- and post-rift igneous activity in the Porcupine Seabight Basin and adjacent continental margin W of Ireland. Geological Society Special Publications, **39**, 309-334.

Taylor, A., Goldring, R., and Gowland, S. 2003. Analysis and application of ichnofabrics. Earth-Science Reviews, 60, 227-259.

Terry, R. D., and Chilingar, C. V. 1955. Summary of "Concerning some additional aids in studying sedimentary formations" by M. S. Shvetsov. Journal of Sedimentary Petrology, **25**, 229-214.

Texaco Shell et al. 1979. Blue H-28 well history report and logs.

Turrin, B. D., and Hemming, S. R. 2000. 40Ar/39Ar ages from the Newark Basin and the Iberia continental margin, thermochronologic constraints on the kinematics of lithospheric extension and continental breakup. Abstracts with Programs - Geological Society of America, **32**, 80.

Valverde-Vaquero, P., van Staal, C.R., van der Velden, A., and Dunning, G.R. 2003. Acadian orogenesis and high grade metamorphism in the Central Mobile Belt of central Newfoundland. Abstracts with Programs - Geological Society of America, **35**, 23.

Valverde-Vaquero, P., van Staal, C.R., McNicoll, V., and Dunning, G.R. 2006. Mid-Late Ordovician magmatism and metamorphism along the Gander margin in central Newfoundland. Journal of the Geological Society of London, **163**, 347-362.

Valverde-Vaquero, P., and Dunning, G. R. 2000. New U-Pb ages for Early Ordovician magmatism in central Spain. Journal of the Geological Society of London, **157**, 15-26.

Verhoef, J., and Srivastava, S. P. 1989. Correlation of sedimentary basins across the North Atlantic as obtained from gravity and magnetic data, and its relation to the early evolution of the North Atlantic. AAPG Memoir, 46, 131-147.

van Hinte, J.E., Ruffman, A., van den Boogaard, M., Jansonius, J., van Kempen, T.M.G., Melchin, M.J., and Miller, T.H. 1995. Paleozoic microfossils from Orphan Knoll, NW atlantic ocean, Scripta Geologica, **109**.

Weltje, G.J, and von Eynatten, H. 2004. Quantitative provenance analysis of sediments; review and outlook. Sedimentary Geology, **171**, 1-11.

Welsink, H. J., Dwyer, J. D., and Knight, R. J. 1989. Tectono-stratigraphy of the passive margin off Nova Scotia. *In* Extensional tectonics and stratigraphy of the North Atlantic margins, *Edited by* A.J. Tankard, and H.R. Balkwill. AAPG Memoir, **46**, 215-231.

Whetten, J.T., and Hawkins, J.W. 1970. Diagenetic origin of graywacke matrix minerals. Sedimentology, **15**, 347-361.

White, C.E., Waldron, J.W.F., Barr, S.M., Simonetti, A., and Heaman, L.M. 2008. Provenance of the Meguma Terrane, Nova Scotia. Abstracts with Programs - Geological Society of America, **40**, 14-15.

Wilkinson, M., Darby, D., Haszeldine, R.S., and Couples, G.D. 1997. Secondary porosity generation during deep burial associated with overpressure leak-off; Fulmar Formation, United Kingdom Central Graben. AAPG Bulletin, **81**, 803-813.

Williams, H., Dehler, S.A., Grant, A.C., and Oakey, G.N. 1999. Tectonics of Atlantic Canada. Geoscience Canada, **26**: 51-70.

Wilson, R. C. L., Hiscott, R. N., Willis, M. G., and Gradstein, F. M. 1989. The *Lusitanian* Basin of west-central Portugal; Mesozoic and Tertiary tectonic, stratigraphic, and subsidence history. *In* Extensional tectonics and stratigraphy of the North Atlantic margins, *Edited by* A.J. Tankard, and H.R. Balkwill. AAPG Memoir, **46**, 341-361.

Worden, R.H. and Burley, S.D. 2003. Sandstone diagenesis: the evolution of sand to stone. *In* Sandstone Diagenesis: Recent and Ancient *Edited by* S.D. Burley and R.H. Worden, 3-44.

Ziegler, P. A. 1989. Evolution of the North Atlantic; an overview Extensional tectonics and stratigraphy of the North Atlantic margins. *In* Extensional tectonics and stratigraphy of the North Atlantic margins, *Edited by* A.J. Tankard, and H.R. Balkwill. AAPG Memoir, **46**, 111-129.

Appendix 1: Thin Section Petrography

Proportions are visually estimated (see Chapter 3)

QFL proportions are normalized to 100%

Zr= Zircon
Qz= Quartz
Dl= Dolomite
Kl= Kaolinite
Cl= Chlorite
CC= Calcite
Cy= Clay
Org= organic material
Tm= Tourmaline
Od= Ooid
Gl= Glauconite
Rt= Rutile
Sid= Siderite
Py= Pyrite
Ig= intergranular
Itg= intragranular
Fr= fracture
Gr= grain dissolution
Cm= cement dissolution
Ang= angular
Sba= sub-angular
Sbr= sub-rounded
Rnd= rounded
Og= overgrowths present
Eh= euhedral
Mf= microfossils present

Sample		L11 3765.5	L11 3765	L11 3756.5	L11 3640	L11 3634.5	L11 3624	L11 3615.5	L11 3606
%Fw grains		68, 68(r)	60, 61(r)	79, 82(r)	65, 65(r)	70, 72(r)	79, 82(r)	73, 78(r)	70, 80(r)
% FW	%Qtz	60	50	70	55	55	60	60	55
	%Fs	2, 4(r)	1, 3(r)	1, 3(r)	1, 2(r)	1, 3(r)	3, 5(r)	2, 5(r)	3, 7(r)
	%Lth	6	8	10	10	14	16	8, 10(r)	12, 15(r)
Lith types		Sd, Ms	Sd, Ms	Sd, Ms	Ls, Ds Sd, Mt	Ls, Ds, Sd	Ls, Ds, Sd	Sd, Ms, Mt(qtz)	Sd, Ms
% Matrix		0	0	1	0	0	0	0	0
% Cement		30	35	4	32	7	1	2	<<1
% Porosity		4	5	15	3	23	20	25	30
Mtx types									
Cem types		D, Kl, Qz	D, Kl, Qz	Dl, Kl, Qz, Cy	Dl, Kl, Cy	Dl,	Dl	Dl, Kl, Cy	Dl
Primary por types		ig, itg(?)	ig, itg (?)	ig	ig	ig, itg(?)	ig	ig	ig
Secondary por types		gr, itg	gr, itg	gr, itg, cm(?)	itg	gr, itg, cm(?)	gr	gr, itg cm(?)	gr,itg
Auth mins									
Acc/Other		Org		Zr,Tm,Gl	Gl, Od	Od	Zr, Cl, Od		
Grn size range (mm)		0.2-2.0	0.2-1.0	0.2-1.2	0.1-3.0	0.3-1.0	0.2-0.8	0.3-1.5	0.2-0.6
wentworth size class		fine-v.coarse	fine-coarse	fine-v.coarse	v.fine-granule	med-coarse	fine-coarse	med-v.coarse	fine-coarse
Average size		0.6 (coarse)	0.5 (m-c)	0.6 (coarse)	0.7 (coarse)	0.4 (medium)	0.35 (medium)	0.6 (coarse)	0.4 (medium)
Sorting		moderate	moderate	moderate	poor	well	well	well	well
Fw roundness		ang-sbr, og	ang-sbr, og	ang-sbr, og	sba-rnd, eh	sba-rnd, eh	sba-rnd, eh	sba-rnd, eh	sbr-rnd
Q		85.7	82.0	84.3	82.1	76.4	75.9	80.0	71.4
F		5.7	4.9	3.6	3.0	4.2	3.8	6.7	9.1
L		8.6	13.1	12.0	14.9	19.4	20.3	13.3	19.5
Total QFL		100.0	100.0	100.0	100.0	100.0	100.0	100.0	100.0
name		sublitharenite	sublitharenite	sublitharenite	sublitharenite	sublitharenite	sublitharenite	sublitharenite	sublitharenite

T maturity	submature	submature	submature	submature	mature	mature	mature	mature
M maturity	submature	submature	submature	submature	submature	submature	submature	immature

Sample		L11 3426	I78 3304.5 m	I78 3199.4 m	I78 3209	I78 3232.7	I78 3273.5	I78 3292.2
%Fw grains		85,	95	86	85	81	81	95
	%Qtz	55, 55(r)	5	65	70	60	65	15
	%Fs	1	0	1, 3?(r)	1, 4?(r)	1, 3?(r)	1, 5?(r)	0
% FW	%Lth	30, 30(r)	90	20	16	20	15	80
Lith types		Sd, Ls, Ls(od), Ds		Sd, Ls, Ds	Ls, Sd, Ms	Ls, Sd, Ms	Ls, Sd, Ms	Sd
% Matrix		0		4	5	4	14	0
% Cement		15	5	<<1	<<1	<<1	5	5
% Porosity		<<1		10	10	15	0	0
Mtx types								
Cem types		Dl	CC	Dl	Dl	Dl	Dl	Dl
Primary por types				ig	ig	ig		
Secondary por types					fr	fr		
Auth mins		Py			Sid			Py
Acc/Other		Gl, Zr, Tm, Cl, Od	Od	Zr, Tm	Zr, Tm, org	Zr, Tm, org		Gl, Org
Grn size range (mm)		0.05-0.8	0.1-1.3	0.07-0.3	0.1-0.3	0.1-0.3	0.1-0.3	0.3-0.8
wentworth size class		v.fine-coarse		v.fine-med	fine-med	fine-med	fine-med	
Average size		0.15 (fine)		0.2 (fine)	0.2 (fine)	0.2 (fine)	0.2 (fine)	
Sorting		moderate-poor	poor	well	well	well	well	moderate
Fw roundness		ang-sbr	v.ang-ang	ang-sbr	ang-sbr	ang-sbr	ang-sbr	ang-sba
Q		64.0	74.2	77.8	72.3	77.4	88.9	5.3
F		1.2	3.4	4.4	3.6	4.8	4.4	0.0
L		34.9	22.5	17.8	24.1	17.9	6.7	94.7
Total QFL		100.0	100.0	100.0	100.0	100.0	100.0	100.0
name		lithic arenite	Lithic arenite	sublitharenite	sublitharenite	sublitharenite	lithic wacke	Lithic arenite

T maturity	submature	submature	mature	mature	mature	immature	mature
M maturity	immature	immature	submature	submature	submature	submature	immature

Sample		I78 2183 m	I78 2180 m	I78 2177.8	I78 2171
%Fw grains		45	52	68	65
	%Qtz	40	47	60	50
	%Fs	2	3	3	3
% FW	**%Lth**	3	2	5	10
Lith types		Sd	Sd	Sd	Sd
% Matrix		50	40	2	15
% Cement		<<1	<<1	<<1	<<1
% Porosity		5	8	30	20
Mtx types					
Cem types		Sid	Sid	Sid	Sid
Primary por types		ig	ig	ig	ig
Secondary por types		itg??	itg??		
Auth mins		Py, Sid	Py, Sid	Py, Sid	Py, Sid
Acc/Other		Gl, Mf, Org, Zr, Tm	Gl, Mf, Org, Zr, Tm	Gl, Mf, Org, Zr, Tm	Gl, Mf, Org, Zr, Tm, Rt
Grn size range (mm)		0.05-0.15	0.05-0.15	0.05-0.2	0.05-0.17
wentworth size class		v.fine-fine	v.fine-fine		
Average size		0.08 (v.fine)	0.08 (v.fine)	0.09	0.08
Sorting		well	well	well	well
Fw roundness		ang-sba	ang-sba	ang-sba	ang-sba
Q		90.4	88.2	79.4	15.8
F		5.8	4.4	4.8	0.0
L		3.8	7.4	15.9	84.2
Total QFL		100.0	100.0	100.0	100.0

name	lithic wacke	lithic wacke	sublitharenite	lithic wacke
T maturity	immature	immature	immature	immature
M maturity	submature	submature	submature	submature

Appendix 2: Detrital heavy mineral counts

Zr = Zircon grain counts

Mz = Monazite grain counts

Tr = Tourmaline grain counts

Ap = Apatite grain counts

Cr = Chromite grain counts

Il = Ilmenite grain counts

Rt = Rutile grain counts

Ti = Titanite grain counts

Tot particles = total number of grains/particles measured in heavy mineral sample

Yield = (Zr+Mz+Tr+Ap+Il+Rt+Tu)/Tot particles x 100%

ZTR = (Zr+Tr+Rt)/(Zr+Tr+Rt+Ap+Mz+Cr+Ti) x 100

ATI = Ap/(Ap+Tr) x 100

MZI = Mz/(Mz+Zr) x 100

RZI = Rt/(Rt+Zr) x 100

IZI = Il/(Il+Zr) x 100

Interval	Sample	Zr	Mz	Tr	Ap	Cr	Il	Rt	Ti	Tot. particles	Yield	ZTR	ATI	MZI	RZI	IZI
L11 1	L-11 3760	44	2	55	2	2	0	6	1	17531	0.64%	96.3	3.5	4.3	12.0	0.0
L11 2	L-11 3615	28	4	42	57	2	4	21	6	12457	1.32%	59.9	57.6	12.5	42.9	12.5
L11 2	L-11 3620	12	2	22	28	5	6	16	2	9579	0.97%	62.5	56.0	14.3	57.1	33.3
L11 2	L11 3625	26	3	33	28	3	2	27	3	20243	0.62%	71.7	45.9	10.3	50.9	7.1
L11 3	L11 3405	38	10	75	14	0	0	79	0	20243	1.07%	88.9	15.7	20.8	67.5	0.0
L11 3	L-11 3410	33	21	57	13	2	0	76	3	15583	1.32%	83.0	18.6	38.9	69.7	0.0
L11 3	L-11 3415	159	64	222	3	6	1	218	28	20165	3.48%	89.9	1.3	28.7	57.8	0.6
L11 3	L11 3420	213	32	221	22	4	4	284	1	20243	3.86%	92.9	9.1	13.1	57.1	1.8
	I78 4135	12	2	22	11	0	0	12	1	20243	0.30%	76.7	33.3	14.3	50.0	0.0
	I-78 3765	16	5	21	3	0	4	15	3	20243	0.33%	86.7	12.5	23.8	48.4	20.0
	I-78 3295	64	29	77	1	0	4	83	3	15246	1.71%	88.2	1.3	31.2	56.5	5.9
	I-78 3300	31	24	71	3	0	1	92	3	10084	2.23%	87.8	4.1	43.6	74.8	3.1
	I-78 3255	73	11	69	8	2	1	6	17	29779	0.63%	79.3	1.4	13.1	7.6	1.4
	I78 3260	53	9	48	9	1	0	63	0	20243	0.90%	90.1	15.8	14.5	54.3	0.0
	I78 3265	105	13	76	12	2	6	95	3	20243	1.54%	90.8	13.6	11.0	47.5	0.0
	I-78 2165	86	32	103	89	9	326	394	19	20405	5.19%	82.8	46.4	27.1	82.1	79.1
	I-78 2170	34	9	150	37	0	177	422	15	12849	6.57%	92.9	19.8	20.9	92.5	81.3
	I-78 2175	48	17	12	9	2	209	348	25	39134	1.71%	94.0	42.9	26.2	87.9	83.9
	I-78 2180	93	32	226	12	3	251	383	21	20069	5.09%	94.1	5.0	25.6	80.5	73.0
H28 1	H-28 5005	44	1	51	7	2	0	8	5	31245	0.38%	92.8	12.1	2.2	15.4	0.0
H28 1	H-28 5010	14	1	36	9	4	2	8	10	27678	0.30%	85.3	20.0	6.7	36.4	12.5
H28 1	H-28 5015	18	1	29	11	4	4	8	10	31687	0.27%	82.1	27.5	5.3	30.8	18.2
H28 1	H-28 5020	17	0	72	10	0	1	7	4	15044	0.74%	90.6	12.2	0.0	29.2	5.6
H28 1	H-28 5025	7	0	53	10	2	3	29	12	16142	0.72%	89.9	15.9	0.0	80.6	30.0

Area % of mineral phases, normalized to total Area% Mz+Ap+Crm+Il+Rt+T+Z								
Sample	**Mz**	**Ap**	**Cr**	**Il**	**Rt**	**Ti**	**Tr**	**Zr**
L-11 3760	0.695558	2.243264	0.972324	0.662783	3.954843	22.86963	20.51712	48.08449
L-11 3615	2.182629	37.62101	2.354735	0.471338	25.65176	18.16511	4.199019	9.354403
L-11 3620	0.264326	27.40253	0.842538	6.376852	26.52695	26.09034	8.378174	4.118286
L11 3625	2.438435	21.9569	2.007036	0.340369	30.77661	2.895778	24.48153	15.10334
L11 3405	1.927676	6.030839	0	0	39.36903	0	37.23674	15.43572
L-11 3410	3.659259	2.157886	1.286121	0	46.80084	0.069956	26.82021	19.20573
L-11 3415	4.734892	0.081637	0.68658	0.175831	30.87937	13.02619	26.63848	23.77703
L11 3420	2.384697	0	0.301237	0.939619	39.46385	0.059557	29.29117	27.55987
I78 4135	1.653644	18.28018	0	0	40.65489	1.028055	28.09679	10.28644
I-78 3765	5.957109	2.382844	0	2.184273	28.19698	2.621128	19.34075	39.31692
I-78 3295	7.03387	1.747647	0	0.808895	44.65426	0.616817	20.80673	24.33178
I-78 3300	7.359149	0.568911	0	0.575029	43.23423	0.82278	33.10087	14.33902
I-78 3255	6.69509	0.28733	0.605555	3.602435	2.144159	23.86999	15.10489	47.69055
I78 3260	1.832878	4.043064	0.03412	0	47.2	0	24.14377	22.74617
I78 3265	2.530701	0.252562	0.637843	1.200488	33.31825	0.757683	25.73334	35.56913
I-78 2165	1.964486	4.113069	1.265606	27.22081	52.51586	1.97272	3.740503	7.206944

I-78 2170	0.710373	2.607638	0.024091	15.00009	62.343	1.352	13.44126	4.521546
I-78 2175	0.944013	2.638171	1.444399	29.12496	38.25039	1.542388	20.82493	5.23074
I-78 2180	1.661085	0.401479	0.403063	26.14789	45.11783	2.966534	18.55052	4.751602
H-28 5005	0.888593	5.729443	2.765253	1.531831	8.786471	7.871352	24.07825	48.34881
H-28 5010	1.074226	11.70459	4.632601	4.349124	8.452069	16.17307	34.05446	19.55987
H-28 5015	4.166666	17.35445	5.486244	6.477926	8.349329	11.37236	27.13532	19.65771
H-28 5020	0	0.40949	1.813455	1.683457	14.13065	3.002925	61.95645	17.00357
H-28 5025	0.250059	1.22685	2.664688	1.187778	29.56943	6.931312	51.66054	6.509339

Weight % of mineral phases, normalized to total Wht% Mz+Ap+Crm+Il+Rt+T+Z								
Sample	**Mz**	**Ap**	**Cr**	**Il**	**Rt**	**Ti**	**Tr**	**Zr**
L-11 3760	0.880496	1.781778	1.086042	0.789652	4.22106	19.86785	15.27781	56.09531
L-11 3615	2.969797	32.11863	2.827036	0.603602	29.4281	16.96221	3.360823	11.7298
L-11 3620	0.361111	23.48941	1.015625	8.199344	30.55535	24.46129	6.7329	5.184965
L11 3625	3.270325	18.47697	2.375075	0.429636	34.80157	2.665282	19.31388	18.66726

L11 3405	2.569062	5.043103	0	0	44.23779	0	29.19195	18.9581
L-11 3410	4.624271	1.711033	1.434084	0	49.86573	0.060671	19.93717	22.36705
L-11 3415	6.061489	0.065574	0.775538	0.211854	33.33004	11.44417	20.05994	28.05139
L11 3420	3.000466	0	0.334431	1.112702	41.8652	0.051427	21.6792	31.95658
I78 4135	2.231219	15.47606	0	0	46.24995	0.95195	22.30016	12.79066
I-78 3765	4.844936	3.721792	0	2.198363	27.52804	2.686737	25.54603	33.4741
I-78 3295	8.617049	1.343376	0	0.932668	46.12382	0.518583	14.99405	27.47045
I-78 3300	9.439663	0.457882	0	0.694208	46.7579	0.724288	24.97581	16.95025
I-78 3255	8.182231	0.22033	0.652997	4.143644	2.209382	20.02006	10.85885	53.7125
I78 3260	2.309566	3.196593	0.037935	0	50.14611	0	17.89588	26.41392
I78 3265	3.127786	0.195858	0.695588	1.396448	34.71974	0.64266	18.70868	40.51323
I-78 2165	2.290801	3.009429	1.302205	29.87518	51.63298	1.578707	2.565781	7.744925
I-78 2170	0.860278	1.981434	0.025742	17.0969	63.65586	1.123639	9.575106	5.681043
I-78 2175	1.163484	1.3895	1.570747	33.78456	39.74804	1.304602	15.09789	5.94117
I-78 2180	2.019646	0.306275	0.432427	29.92223	46.25225	2.475336	13.26762	5.32421
H-28 5005	1.112193	4.499545	3.053892	1.804506	9.27234	6.761199	17.7277	55.76862
H-28 5010	1.473918	10.07659	5.608473	5.616299	9.777749	15.22887	27.48543	24.73267
H-28 5015	5.561822	14.53513	6.461688	8.138336	9.396761	10.41782	21.30661	24.18182

H-28 5020	0	0.369524	2.301276	2.27873	17.13483	2.963889	52.41519	22.53655
H-28 5025	0.35437	1.090905	3.331994	1.584245	35.33108	6.741073	43.06513	8.5012

Appendix 3: Detrital tourmaline chemistry

Sample No.	L113760T1	L113760T2	L113760T3	L113760T4	L113760T5	L113760T6
SiO2	35.19	33.42	35.45	34.81	35.32	35.31
TiO2	1.05	1.03	1.04	1.04	1.04	1.03
Al2O3	30.04	27.89	33.07	32.42	33.25	31.03
Cr2O3	0.02	0.00	0.02	0.02	0.06	0.02
FeO	4.49	10.73	6.08	7.40	7.23	8.65
MgO	8.35	3.70	5.97	5.34	5.16	5.31
CaO	1.17	0.39	0.29	0.35	0.54	0.81
MnO	0.01	0.11	0.01	0.00	0.07	0.04
Na2O	2.01	1.99	1.69	1.77	1.83	1.95
K2O	0.03	0.05	0.04	0.01	0.05	0.04
H2O*	3.55	3.31	3.61	3.55	3.62	3.57
B2O3*	10.30	9.61	10.46	10.30	10.50	10.34
Li2O*	0.31	0.38	0.26	0.24	0.36	0.33
Total	96.52	92.60	97.99	97.24	99.03	98.43
O=F	0.00	0.00	0.00	0.00	0.00	0.00
Total*	96.52	92.60	97.99	97.24	99.03	98.43
Structural formula based on 31 anions (O, OH, F)						
T:						
Si	5.9400	6.0469	5.8907	5.8723	5.8483	5.9377
Al	0.0600	0.0000	0.1093	0.1277	0.1517	0.0623
B	3.0000	3.0000	3.0000	3.0000	3.0000	3.0000
Z:						
Al	5.9162	5.9474	6.0000	6.0000	6.0000	6.0000
Mg	0.0838	0.0526	0.0000	0.0000	0.0000	0.0000
Cr	0.0000	0.0000	0.0000	0.0000	0.0000	0.0000
Y:						
Al	0.0000	0.0000	0.3671	0.3180	0.3370	0.0874
Ti	0.1327	0.1396	0.1300	0.1315	0.1291	0.1307
Cr	0.0032	0.0004	0.0026	0.0022	0.0077	0.0029
Mg	2.0174	0.9455	1.4789	1.3429	1.2737	1.3311
Mn	0.0015	0.0168	0.0013	0.0000	0.0098	0.0059
Fe2+	0.6338	1.6236	0.8449	1.0440	1.0012	1.2164

Li*	0.2114	0.2742	0.1753	0.1614	0.2415	0.2255
sumY	3.0000	3.0000	3.0000	3.0000	3.0000	3.0000
X:						
Ca	0.2121	0.0759	0.0517	0.0634	0.0960	0.1460
Na	0.6564	0.6973	0.5431	0.5779	0.5880	0.6346
K	0.0060	0.0104	0.0085	0.0013	0.0103	0.0095
OH	4.0000	4.0000	4.0000	4.0000	4.0000	4.0000
F	0.0000	0.0000	0.0000	0.0000	0.0000	0.0000
Cl	0.0000	0.0000	0.0000	0.0000	0.0000	0.0000

Sample No.	L113760T9	L113760T8	L113760T9	L113760T10	L113760T11	L113760T12
SiO2	33.52	33.03	35.78	34.91	35.23	35.31
TiO2	1.03	1.04	1.04	1.04	1.04	1.04
Al2O3	28.64	29.43	31.16	33.01	31.33	32.45
Cr2O3	0.04	0.02	0.03	0.07	0.00	0.04
FeO	9.35	7.13	7.06	6.80	6.84	5.69
MgO	4.99	5.24	6.71	5.64	5.84	6.32
CaO	0.57	0.81	0.70	0.83	0.46	0.71
MnO	0.02	0.02	0.00	0.05	0.03	0.01
Na2O	2.01	1.85	2.20	1.67	1.67	1.81
K2O	0.01	0.26	0.06	0.05	0.04	0.05
H2O*	3.37	3.36	3.61	3.60	3.54	3.60
B2O3*	9.76	9.73	10.47	10.44	10.26	10.43
Li2O*	0.21	0.41	0.29	0.33	0.28	0.37
Total	93.52	92.32	99.11	98.44	96.56	97.84
O=F	0.00	0.00	0.00	0.00	0.00	0.00
Total*	93.52	92.32	99.11	98.44	96.56	97.84
Structural formula based on 31 anions (O, OH, F)						
T:						
Si	5.9711	5.9018	5.9370	5.8121	5.9707	5.8816
Al	0.0289	0.0982	0.0630	0.1879	0.0293	0.1184
B	3.0000	3.0000	3.0000	3.0000	3.0000	3.0000
Z:						
Al	5.9839	6.0000	6.0000	6.0000	6.0000	6.0000
Mg	0.0161	0.0000	0.0000	0.0000	0.0000	0.0000
Cr	0.0000	0.0000	0.0000	0.0000	0.0000	0.0000
Y:						
Al	0.0000	0.0993	0.0308	0.2893	0.2285	0.2520
Ti	0.1380	0.1393	0.1295	0.1300	0.1323	0.1304
Cr	0.0063	0.0035	0.0038	0.0092	0.0000	0.0057
Mg	1.3091	1.3958	1.6598	1.3998	1.4755	1.5694
Mn	0.0031	0.0023	0.0000	0.0068	0.0047	0.0010
Fe2+	1.3929	1.0654	0.9797	0.9468	0.9694	0.7926
Li*	0.1506	0.2944	0.1964	0.2182	0.1896	0.2487

sumY	3.0000	3.0000	3.0000	3.0000	3.0000	3.0000
X:						
Ca	0.1090	0.1557	0.1236	0.1486	0.0839	0.1267
Na	0.6935	0.6400	0.7068	0.5406	0.5499	0.5841
K	0.0018	0.0598	0.0116	0.0099	0.0081	0.0110
OH	4.0000	4.0000	4.0000	4.0000	4.0000	4.0000
F	0.0000	0.0000	0.0000	0.0000	0.0000	0.0000
Cl	0.0000	0.0000	0.0000	0.0000	0.0000	0.0000

Sample No.	L113760T13	L113760T15	L113760T17	L113760T18	L113760T20	L113760T21
SiO2	34.99	33.97	34.18	35.55	34.09	35.36
TiO2	1.04	1.02	1.01	1.04	1.04	1.03
Al2O3	29.11	32.08	31.08	32.22	33.33	29.17
Cr2O3	0.02	0.01	0.00	0.06	0.01	0.06
FeO	8.14	12.34	15.72	7.23	6.87	10.51
MgO	7.04	2.75	1.06	6.04	5.95	5.43
CaO	0.81	0.28	0.10	0.69	0.83	0.23
MnO	0.03	0.17	0.29	0.01	0.05	0.05
Na2O	2.32	1.94	2.07	1.81	2.05	2.59
K2O	0.03	0.07	0.04	0.01	0.04	0.02
H2O*	3.52	3.51	3.48	3.62	3.59	3.52
B2O3*	10.20	10.16	10.09	10.48	10.41	10.21
Li2O*	0.15	0.15	0.13	0.27	0.26	0.19
Total	97.40	98.45	99.26	99.03	98.51	98.38
O=F	0.00	0.00	0.00	0.00	0.00	0.00
Total*	97.40	98.45	99.26	99.03	98.51	98.38

Structural formula based on 31 anions (O, OH, F)

T:						
Si	5.9615	5.8083	5.8889	5.8931	5.6915	6.0165
Al	0.0385	0.1917	0.1111	0.1069	0.3085	0.0000
B	3.0000	3.0000	3.0000	3.0000	3.0000	3.0000
Z:						
Al	5.8067	6.0000	6.0000	6.0000	6.0000	5.8496
Mg	0.1933	0.0000	0.0000	0.0000	0.0000	0.1504
Cr	0.0000	0.0000	0.0000	0.0000	0.0000	0.0000
Y:						
Al	0.0000	0.2730	0.1998	0.1879	0.2499	0.0000
Ti	0.1326	0.1315	0.1314	0.1293	0.1303	0.1315
Cr	0.0027	0.0011	0.0000	0.0081	0.0013	0.0082
Mg	1.5948	0.7009	0.2711	1.4926	1.4809	1.2269
Mn	0.0046	0.0252	0.0429	0.0014	0.0068	0.0067
Fe2+	1.1598	1.7645	2.2650	1.0023	0.9592	1.4955
Li*	0.1054	0.1038	0.0898	0.1783	0.1716	0.1311

sumY	3.0000	3.0000	3.0000	3.0000	3.0000	3.0000
X:						
Ca	0.1478	0.0506	0.0190	0.1227	0.1480	0.0417
Na	0.7670	0.6423	0.6909	0.5825	0.6642	0.8556
K	0.0067	0.0148	0.0096	0.0027	0.0080	0.0051
OH	4.0000	4.0000	4.0000	4.0000	4.0000	4.0000
F	0.0000	0.0000	0.0000	0.0000	0.0000	0.0000
Cl	0.0000	0.0000	0.0000	0.0000	0.0000	0.0000

Sample No.	L113760T16	L113760T19	L113760T14	L113615T1	L113615T2	L113760T3
SiO2	34.79	35.77	34.69	35.14	35.82	35.23
TiO2	1.03	1.03	1.03	0.67	0.33	0.95
Al2O3	30.88	28.05	27.73	35.78	33.54	34.27
Cr2O3	0.17	0.00	0.01	0.00	0.00	0.00
FeO	10.99	10.89	9.66	9.51	7.47	7.10
MgO	4.36	6.72	6.48	3.93	7.07	6.17
CaO	1.09	0.87	1.30	0.48	0.97	0.97
MnO	0.07	0.03	0.01	0.01	0.03	0.01
Na2O	1.75	2.28	1.85	1.81	1.78	1.80
K2O	0.08	0.05	0.02	0.08	0.05	0.04
H2O*	3.55	3.55	3.46	3.70	3.70	3.69
B2O3*	10.29	10.30	10.02	10.72	10.72	10.70
Li2O*	0.24	0.09	0.17	0.22	0.02	0.23
Total	99.30	99.62	96.42	102.07	101.51	101.16
O=F	0.00	0.00	0.00	0.00	0.00	0.00
Total*	99.30	99.62	96.42	102.07	101.51	101.16
Structural formula based on 31 anions (O, OH, F)						
T:						
Si	5.8750	6.0369	6.0172	5.6958	5.8082	5.7204
Al	0.1250	0.0000	0.0000	0.3042	0.1918	0.2796
B	3.0000	3.0000	3.0000	3.0000	3.0000	3.0000
Z:						
Al	6.0000	5.5793	5.6689	6.0000	6.0000	6.0000
Mg	0.0000	0.4207	0.3311	0.0000	0.0000	0.0000
Cr	0.0000	0.0000	0.0000	0.0000	0.0000	0.0000
Y:						
Al	0.0209	0.0000	0.0000	0.5322	0.2175	0.2797
Ti	0.1305	0.1306	0.1346	0.0819	0.0407	0.1155
Cr	0.0223	0.0000	0.0020	0.0000	0.0000	0.0005
Mg	1.0976	1.2700	1.3445	0.9502	1.7100	1.4924
Mn	0.0107	0.0045	0.0017	0.0015	0.0041	0.0012
Fe2+	1.5521	1.5370	1.4013	1.2898	1.0135	0.9638
Li*	0.1659	0.0578	0.1160	0.1443	0.0142	0.1470

sumY	3.0000	3.0000	3.0000	3.0000	3.0000	3.0000
X:						
Ca	0.1970	0.1572	0.2410	0.0835	0.1689	0.1692
Na	0.5744	0.7456	0.6209	0.5690	0.5592	0.5682
K	0.0183	0.0100	0.0043	0.0165	0.0102	0.0088
OH	4.0000	4.0000	4.0000	4.0000	4.0000	4.0000
F	0.0000	0.0000	0.0000	0.0000	0.0000	0.0000
Cl	0.0000	0.0000	0.0000	0.0000	0.0000	0.0000

Sample No.	L113760T4	L113615T5	L113615T6	L113615T7	L113615T8	L113615T9
SiO2	34.85	36.99	36.54	36.35	36.42	35.19
TiO2	0.50	0.35	0.69	0.72	0.57	0.33
Al2O3	35.32	31.87	34.07	30.96	34.24	34.89
Cr2O3	0.00	0.05	0.05	0.00	0.00	0.00
FeO	13.27	8.67	8.12	10.11	4.98	13.93
MgO	1.26	6.61	5.35	6.27	7.68	1.09
CaO	0.07	0.76	0.10	0.08	0.83	0.08
MnO	0.13	0.03	0.18	0.00	0.00	0.22
Na2O	1.97	2.36	2.14	2.81	2.08	1.97
K2O	0.05	0.01	0.05	0.01	0.04	0.05
H2O*	3.63	3.95	3.95	3.94	3.89	4.03
B2O3*	10.53	11.45	11.44	11.43	11.28	11.67
Li2O*	0.24	0.00	0.03	0.00	0.14	0.00
Total	101.82	111.72	110.79	112.79	107.12	117.39
O=F	0.00	0.00	0.00	0.00	0.00	0.00
Total*	101.82	111.72	110.79	112.79	107.12	117.39
Structural formula based on 31 anions (O, OH, F)						
T:						
Si	5.7514	5.9803	5.8895	5.9682	5.8216	5.8055
Al	0.2486	0.0197	0.1105	0.0318	0.1784	0.1945
B	3.0000	3.0000	3.0000	3.0000	3.0000	3.0000
Z:						
Al	6.0000	6.0000	6.0000	5.9591	6.0000	6.0000
Mg	0.0000	0.0000	0.0000	0.0409	0.0000	0.0000
Cr	0.0000	0.0000	0.0000	0.0000	0.0000	0.0000
Y:						
Al	0.6194	0.053	0.362	0.000	0.271	0.590
Ti	0.0622	0.043	0.084	0.088	0.069	0.041
Cr	0.0000	0.007	0.006	0.000	0.000	0.000
Mg	0.3105	1.593	1.287	1.494	1.829	0.269
Mn	0.0178	0.004	0.025	0.000	0.000	0.031
Fe2+	1.8309	1.172	1.095	1.388	0.665	1.922
Li*	0.1593	0.129	0.141	0.029	0.165	0.147

SY	3.0000	3.000	3.000	3.000	3.000	3.000
X:						
Ca	0.0122	0.131	0.018	0.014	0.141	0.015
Na	0.6288	0.739	0.668	0.895	0.643	0.629
K	0.0108	0.003	0.011	0.003	0.008	0.011
OH	4.0000	4.000	4.000	4.000	4.000	4.000
F	0.0000	0.000	0.000	0.000	0.000	0.000
Cl	0.0000	0.000	0.000	0.000	0.000	0.000

Sample No.	L113615T12	L113615T13	L113615T14	L113615T15	L113615T16	L113615T17
SiO2	34.72	36.55	36.31	35.93	35.27	35.95
TiO2	0.10	1.29	0.89	0.66	0.77	0.28
Al2O3	35.25	32.93	32.85	35.33	35.59	33.12
Cr2O3	0.00	0.00	0.00	0.00	0.00	0.00
FeO	14.52	8.49	6.71	8.42	9.73	8.22
MgO	0.82	5.77	7.31	5.08	3.83	6.67
CaO	0.27	0.05	1.19	0.45	0.30	0.87
MnO	0.06	0.09	0.00	0.01	0.09	0.02
Na2O	1.86	2.17	1.91	2.03	1.88	2.09
K2O	0.04	0.12	0.06	0.05	0.05	0.07
H2O*	4.03	3.95	3.91	3.98	3.97	3.93
B2O3*	11.68	11.44	11.34	11.52	11.51	11.38
Li2O*	0.00	0.00	0.09	0.03	0.00	0.00
Total	117.86	111.33	109.26	111.90	112.72	110.83
O=F	0.00	0.00	0.00	0.00	0.00	0.00
Total*	117.86	111.33	109.26	111.90	112.72	110.83
Structural formula based on 31 anions (O, OH, F)						
T:						
Si	5.755	5.906	5.845	5.758	5.718	5.837
Al	0.245	0.094	0.155	0.242	0.282	0.163
B	3.000	3.000	3.000	3.000	3.000	3.000
Z:						
Al	6.000	6.000	6.000	6.000	6.000	6.000
Mg	0.000	0.000	0.000	0.000	0.000	0.000
Cr	0.000	0.000	0.000	0.000	0.000	0.000
Y:						
Al	0.640	0.177	0.078	0.432	0.519	0.175
Ti	0.013	0.156	0.108	0.080	0.094	0.035
Cr	0.000	0.000	0.000	0.000	0.000	0.000
Mg	0.202	1.390	1.755	1.214	0.927	1.615
Mn	0.009	0.013	0.000	0.001	0.012	0.003
Fe2+	2.012	1.147	0.903	1.128	1.319	1.116
Li*	0.123	0.117	0.156	0.145	0.130	0.057

SY	3.000	3.000	3.000	3.000	3.000	3.000
X:						
Ca	0.048	0.008	0.205	0.078	0.052	0.152
Na	0.599	0.680	0.596	0.630	0.591	0.658
K	0.008	0.025	0.012	0.010	0.010	0.014
OH	4.000	4.000	4.000	4.000	4.000	4.000
F	0.000	0.000	0.000	0.000	0.000	0.000
Cl	0.000	0.000	0.000	0.000	0.000	0.000

Sample No.	L113615T18	L113615T19	L113615T20	L113615T21	L113615T22	L113615T23
SiO2	35.89	36.91	35.81	36.20	36.11	36.23
TiO2	0.44	0.20	0.75	0.73	1.03	0.79
Al2O3	35.95	32.12	34.12	30.50	34.13	33.73
Cr2O3	0.01	0.00	0.04	0.06	0.02	0.01
FeO	5.83	1.92	9.47	9.17	8.10	5.34
MgO	6.28	11.31	3.93	7.10	5.07	7.11
CaO	0.67	1.79	0.32	0.84	0.39	0.70
MnO	0.01	0.00	0.12	0.01	0.03	0.01
Na2O	1.81	1.95	1.82	2.31	1.88	1.92
K2O	0.04	0.01	0.05	0.04	0.05	0.04
H2O*	3.91	3.81	3.93	3.91	3.93	3.86
B2O3*	11.34	11.04	11.38	11.33	11.39	11.18
Li2O*	0.11	0.10	0.07	0.00	0.11	0.16
Total	108.11	103.09	111.25	111.32	110.31	106.41
O=F	0.00	0.00	0.00	0.00	0.00	0.00
Total*	108.11	103.09	111.25	111.32	110.31	106.41
Structural formula based on 31 anions (O, OH, F)						
T:						
Si	5.738	5.892	5.860	5.950	5.845	5.857
Al	0.262	0.108	0.140	0.050	0.155	0.143
B	3.000	3.000	3.000	3.000	3.000	3.000
Z:						
Al	6.000	5.934	6.000	5.859	6.000	6.000
Mg	0.000	0.066	0.000	0.141	0.000	0.000
Cr	0.000	0.000	0.000	0.000	0.000	0.000
Y:						
Al	0.513	0.000	0.441	0.000	0.357	0.283
Ti	0.052	0.024	0.093	0.090	0.125	0.096
Cr	0.002	0.000	0.005	0.008	0.003	0.001
Mg	1.496	2.625	0.959	1.599	1.224	1.712
Mn	0.001	0.000	0.016	0.001	0.004	0.002
Fe2+	0.780	0.256	1.296	1.261	1.097	0.722
Li*	0.155	0.094	0.190	0.040	0.191	0.184

SY	3.000	3.000	3.000	3.000	3.000	3.000
X:						
Ca	0.114	0.306	0.056	0.149	0.067	0.121
Na	0.561	0.604	0.576	0.736	0.590	0.602
K	0.009	0.002	0.010	0.009	0.011	0.008
OH	4.000	4.000	4.000	4.000	4.000	4.000
F	0.000	0.000	0.000	0.000	0.000	0.000
Cl	0.000	0.000	0.000	0.000	0.000	0.000

Sample No.	L113615T24	L113615T25	L113615T26	L113615T28	L113615T30	L113615T31
SiO2	35.52	36.19	36.44	36.18	35.93	37.00
TiO2	0.63	0.69	1.37	0.37	1.00	0.40
Al2O3	35.30	33.50	31.47	32.44	34.41	33.80
Cr2O3	0.01	0.02	0.00	0.02	0.05	0.00
FeO	9.72	9.95	8.45	9.01	5.19	2.95
MgO	3.75	4.27	6.45	6.03	7.19	8.98
CaO	0.41	0.51	1.01	1.03	1.36	0.42
MnO	0.07	0.08	0.02	0.04	0.00	0.01
Na2O	1.87	1.64	1.89	1.98	1.66	2.24
K2O	0.07	0.06	0.03	0.06	0.09	0.02
H2O*	3.97	3.95	3.92	3.93	3.89	3.83
B2O3*	11.50	11.45	11.37	11.39	11.28	11.11
Li2O*	0.04	0.00	0.06	0.00	0.24	0.14
Total	112.58	112.24	110.94	111.49	107.43	103.87
O=F	0.00	0.00	0.00	0.00	0.00	0.00
Total*	112.58	112.24	110.94	111.49	107.43	103.87
Structural formula based on 31 anions (O, OH, F)						
T:						
Si	5.762	5.908	5.924	5.898	5.748	5.914
Al	0.238	0.092	0.076	0.102	0.252	0.086
B	3.000	3.000	3.000	3.000	3.000	3.000
Z:						
Al	6.000	6.000	5.953	6.000	6.000	6.000
Mg	0.000	0.000	0.047	0.000	0.000	0.000
Cr	0.000	0.000	0.000	0.000	0.000	0.000
Y:						
Al	0.511	0.355	0.000	0.131	0.235	0.281
Ti	0.077	0.085	0.168	0.045	0.120	0.048
Cr	0.002	0.003	0.000	0.003	0.006	0.000
Mg	0.907	1.040	1.515	1.466	1.715	2.140
Mn	0.009	0.011	0.003	0.006	0.000	0.001
Fe2+	1.319	1.358	1.149	1.229	0.694	0.394
Li*	0.174	0.147	0.164	0.121	0.230	0.135

SY	3.000	3.000	3.000	3.000	3.000	3.000
X:						
Ca	0.071	0.089	0.175	0.181	0.234	0.072
Na	0.589	0.520	0.595	0.625	0.514	0.695
K	0.014	0.013	0.007	0.012	0.018	0.005
OH	4.000	4.000	4.000	4.000	4.000	4.000
F	0.000	0.000	0.000	0.000	0.000	0.000
Cl	0.000	0.000	0.000	0.000	0.000	0.000

Sample No.	L113615T32	L113615T34	L113615T6	L113415IT1	L113415IT4	L113415IT6
SiO2	36.14	36.16	36.54	36.17	35.83	35.25
TiO2	1.80	0.72	0.69	0.28	1.34	1.31
Al2O3	33.51	35.59	34.07	30.10	33.70	33.44
Cr2O3	0.04	0.07	0.05	0.00	0.00	0.04
FeO	5.98	6.73	8.12	11.09	6.61	5.93
MgO	6.55	5.70	5.35	6.34	6.58	7.11
CaO	0.62	0.57	0.10	0.84	1.10	1.54
MnO	0.04	0.03	0.18	0.09	0.02	0.02
Na2O	1.87	1.79	2.14	2.20	1.72	1.64
K2O	0.05	0.05	0.05	0.06	0.08	0.08
H2O*	3.89	3.76	3.72	3.62	3.72	3.70
B2O3*	11.28	10.89	10.78	10.49	10.79	10.72
Li2O*	0.22	0.28	0.22	0.00	0.30	0.32
Total	107.94	102.33	102.03	101.29	101.79	101.11
O=F	0.00	0.00	0.00	0.00	0.00	0.00
Total*	107.94	102.33	102.03	101.29	101.79	101.11

Structural formula based on 31 anions (O, OH, F)

T:						
Si	5.814	5.7715	5.8895	5.9938	5.7710	5.7137
Al	0.186	0.2285	0.1105	0.0062	0.2290	0.2863
B	3.000	3.0000	3.0000	3.0000	3.0000	3.0000
Z:						
Al	6.000	6.0000	6.0000	5.8719	6.0000	6.0000
Mg	0.000	0.0000	0.0000	0.1281	0.0000	0.0000
Cr	0.000	0.0000	0.0000	0.0000	0.0000	0.0000
Y:						
Al	0.168	0.4663	0.3623	0.0000	0.1686	0.1012
Ti	0.217	0.0862	0.0842	0.0354	0.1623	0.1602
Cr	0.005	0.0087	0.0063	0.0005	0.0003	0.0050
Mg	1.572	1.3570	1.2867	1.4382	1.5790	1.7188
Mn	0.006	0.0034	0.0246	0.0133	0.0024	0.0023
Fe2+	0.804	0.8982	1.0949	1.5361	0.8901	0.8039
Li*	0.228	0.1801	0.1411	0.0000	0.1971	0.2087

SY	3.000	3.0000	3.0000	3.0236	3.0000	3.0000
X:						
Ca	0.106	0.0983	0.0178	0.1485	0.1898	0.2682
Na	0.584	0.5550	0.6679	0.7064	0.5374	0.5164
K	0.010	0.0096	0.0112	0.0124	0.0155	0.0156
OH	4.000	4.0000	4.0000	4.0000	4.0000	4.0000
F	0.000	0.0000	0.0000	0.0000	0.0000	0.0000
Cl	0.000	0.0000	0.0000	0.0000	0.0000	0.0000

Sample No.	L113415IT8	L113415IT12	L113415IT13	L113415IT15	L113415IT17	L113415IT18
SiO2	36.30	35.34	34.82	36.41	36.40	36.26
TiO2	0.09	0.85	0.47	0.23	0.58	0.84
Al2O3	31.05	35.57	33.26	33.56	32.53	32.79
Cr2O3	0.00	0.03	0.00	0.00	0.02	0.01
FeO	10.68	7.43	7.34	4.13	6.34	8.53
MgO	6.21	5.08	5.85	8.47	6.94	5.98
CaO	0.17	1.17	0.60	0.76	0.34	0.48
MnO	0.01	0.04	0.01	0.00	0.02	0.07
Na2O	2.25	1.41	1.83	1.92	2.05	2.03
K2O	0.05	0.07	0.06	0.04	0.03	0.03
H2O*	3.63	3.72	3.59	3.71	3.66	3.69
B2O3*	10.52	10.78	10.42	10.75	10.61	10.69
Li2O*	0.00	0.33	0.16	0.14	0.18	0.15
Total	100.96	101.83	98.43	100.12	99.72	101.55
O=F	0.00	0.00	0.00	0.00	0.00	0.00
Total*	100.96	101.83	98.43	100.12	99.72	101.55
Structural formula based on 31 anions (O, OH, F)						
T:						
Si	5.9999	5.6945	5.8111	5.8861	5.9609	5.8963
Al	0.0001	0.3055	0.1889	0.1139	0.0391	0.1037
B	3.0000	3.0000	3.0000	3.0000	3.0000	3.0000
Z:						
Al	6.0000	6.0000	6.0000	6.0000	6.0000	6.0000
Mg	0.0000	0.0000	0.0000	0.0000	0.0000	0.0000
Cr	0.0000	0.0000	0.0000	0.0000	0.0000	0.0000
Y:						
Al	0.0485	0.4508	0.3532	0.2790	0.2391	0.1804
Ti	0.0116	0.1029	0.0594	0.0278	0.0709	0.1023
Cr	0.0000	0.0035	0.0000	0.0000	0.0029	0.0007
Mg	1.5300	1.2212	1.4546	2.0422	1.6951	1.4496
Mn	0.0014	0.0055	0.0017	0.0003	0.0023	0.0101
Fe2+	1.4767	1.0010	1.0245	0.5585	0.8680	1.1595
Li*	0.0000	0.2150	0.1065	0.0923	0.1217	0.0974

SY	3.0682	3.0000	3.0000	3.0000	3.0000	3.0000
X:						
Ca	0.0303	0.2024	0.1081	0.1309	0.0589	0.0843
Na	0.7205	0.4410	0.5935	0.6021	0.6521	0.6406
K	0.0109	0.0146	0.0137	0.0078	0.0071	0.0064
OH	4.0000	4.0000	4.0000	4.0000	4.0000	4.0000
F	0.0000	0.0000	0.0000	0.0000	0.0000	0.0000
Cl	0.0000	0.0000	0.0000	0.0000	0.0000	0.0000

Sample No.	L113415IT19	L113415IT21	L113415IT23	L113415IT24	L113415IT26	L113415IT27
SiO2	36.73	35.31	36.34	36.41	36.37	36.31
TiO2	0.49	1.23	0.75	0.74	0.83	0.45
Al2O3	32.38	31.52	35.24	33.51	32.66	31.90
Cr2O3	0.00	0.02	0.07	0.01	0.04	0.02
FeO	5.94	10.52	5.15	8.34	9.22	8.96
MgO	8.22	5.04	6.90	5.68	5.48	6.66
CaO	0.89	0.27	0.37	0.33	0.19	0.55
MnO	0.03	0.05	0.02	0.06	0.03	0.04
Na2O	2.17	2.43	2.06	2.08	2.34	2.28
K2O	0.03	0.04	0.05	0.03	0.03	0.04
H2O*	3.72	3.61	3.76	3.71	3.68	3.67
B2O3*	10.79	10.46	10.91	10.74	10.68	10.65
Li2O*	0.14	0.14	0.25	0.19	0.18	0.04
Total	101.52	100.64	101.87	101.82	101.73	101.58
O=F	0.00	0.00	0.00	0.00	0.00	0.00
Total*	101.52	100.64	101.87	101.82	101.73	101.58
Structural formula based on 31 anions (O, OH, F)						
T:						
Si	5.9188	5.8638	5.7914	5.8910	5.9193	5.9272
Al	0.0812	0.1362	0.2086	0.1090	0.0807	0.0728
B	3.0000	3.0000	3.0000	3.0000	3.0000	3.0000
Z:						
Al	6.0000	6.0000	6.0000	6.0000	6.0000	6.0000
Mg	0.0000	0.0000	0.0000	0.0000	0.0000	0.0000
Cr	0.0000	0.0000	0.0000	0.0000	0.0000	0.0000
Y:						
Al	0.0683	0.0335	0.4100	0.2803	0.1837	0.0643
Ti	0.0592	0.1537	0.0903	0.0897	0.1011	0.0548
Cr	0.0000	0.0020	0.0086	0.0010	0.0050	0.0030
Mg	1.9749	1.2471	1.6382	1.3695	1.3295	1.6214
Mn	0.0047	0.0072	0.0034	0.0078	0.0045	0.0058
Fe2+	0.7999	1.4611	0.6861	1.1287	1.2555	1.2225
Li*	0.0931	0.0955	0.1633	0.1229	0.1207	0.0282

SY	3.0000	3.0000	3.0000	3.0000	3.0000	3.0000
X:						
Ca	0.1528	0.0484	0.0629	0.0570	0.0336	0.0970
Na	0.6764	0.7830	0.6358	0.6513	0.7370	0.7221
K	0.0057	0.0091	0.0110	0.0060	0.0065	0.0080
OH	4.0000	4.0000	4.0000	4.0000	4.0000	4.0000
F	0.0000	0.0000	0.0000	0.0000	0.0000	0.0000
Cl	0.0000	0.0000	0.0000	0.0000	0.0000	0.0000

Sample No.	L113415IT28	L113415IT29	L113415IT30	L113415IT32	L113415IT33	L113415IT34
SiO2	36.57	35.11	36.33	35.26	36.17	44.08
TiO2	0.53	0.82	0.91	0.54	0.74	0.17
Al2O3	34.81	37.48	30.40	30.58	33.80	28.75
Cr2O3	0.02	0.03	0.04	0.01	0.01	0.02
FeO	5.67	5.65	9.82	11.85	11.12	6.35
MgO	6.92	5.50	7.00	5.43	3.56	6.26
CaO	0.78	0.49	1.03	0.80	0.41	0.07
MnO	0.01	0.04	0.05	0.23	0.22	0.00
Na2O	1.76	2.32	2.19	2.28	1.98	1.83
K2O	0.03	0.06	0.05	0.08	0.07	0.04
H2O*	3.76	3.78	3.67	3.59	3.69	3.94
B2O3*	10.90	10.95	10.63	10.41	10.71	11.42
Li2O*	0.24	0.40	0.05	0.00	0.26	2.61
Total	101.99	102.61	102.16	101.06	102.76	105.54
O=F	0.00	0.00	0.00	0.00	0.00	0.00
Total*	101.99	102.61	102.16	101.06	102.76	105.54
Structural formula based on 31 anions (O, OH, F)						
T:						
Si	5.8323	5.5738	5.9392	5.8876	5.8706	6.7072
Al	0.1677	0.4262	0.0608	0.1124	0.1294	0.0000
B	3.0000	3.0000	3.0000	3.0000	3.0000	3.0000
Z:						
Al	6.0000	6.0000	5.7966	5.9062	6.0000	5.1552
Mg	0.0000	0.0000	0.2034	0.0938	0.0000	0.8448
Cr	0.0000	0.0000	0.0000	0.0000	0.0000	0.0000
Y:						
Al	0.3762	0.5877	0.0000	0.0000	0.3361	0.0000
Ti	0.0636	0.0981	0.1114	0.0679	0.0906	0.0190
Cr	0.0023	0.0035	0.0048	0.0008	0.0011	0.0023
Mg	1.6452	1.3022	1.5022	1.2584	0.8609	0.5753
Mn	0.0019	0.0056	0.0076	0.0319	0.0300	0.0000
Fe2+	0.7562	0.7501	1.3429	1.6553	1.5089	0.8081
Li*	0.1546	0.2529	0.0312	0.0000	0.1725	1.5953

SY	3.0000	3.0000	3.0000	3.0144	3.0000	3.0000
X:						
Ca	0.1333	0.0830	0.1810	0.1422	0.0718	0.0110
Na	0.5444	0.7144	0.6950	0.7386	0.6243	0.5401
K	0.0055	0.0114	0.0108	0.0175	0.0155	0.0087
OH	4.0000	4.0000	4.0000	4.0000	4.0000	4.0000
F	0.0000	0.0000	0.0000	0.0000	0.0000	0.0000
Cl	0.0000	0.0000	0.0000	0.0000	0.0000	0.0000

Sample No.	L113415IT36	L113415IT5	L113415IT9	L113415IT16	L113415IT22	L113415IT37
SiO2	36.46	36.26	35.90	35.90	36.25	36.67
TiO2	0.41	0.47	0.74	0.56	0.66	0.57
Al2O3	35.22	35.18	30.22	30.84	35.40	33.01
Cr2O3	0.11	0.06	0.03	0.00	0.04	0.32
FeO	0.27	6.48	11.73	8.98	6.30	4.17
MgO	10.14	5.92	5.27	6.77	6.20	8.84
CaO	1.13	0.75	0.20	0.83	0.59	1.43
MnO	0.01	0.00	0.03	0.02	0.05	0.02
Na2O	1.97	1.81	2.66	2.13	1.83	1.77
K2O	0.08	0.08	0.04	0.03	0.04	0.02
H2O*	3.79	3.74	3.60	3.62	3.76	3.75
B2O3*	11.00	10.85	10.43	10.49	10.90	10.88
Li2O*	0.30	0.32	0.05	0.06	0.24	0.24
Total	100.88	101.93	100.90	100.22	102.27	101.68
O=F	0.00	0.00	0.00	0.00	0.00	0.00
Total*	100.88	101.93	100.90	100.22	102.27	101.68
Structural formula based on 31 anions (O, OH, F)						
T:						
Si	5.7616	5.8064	5.9841	5.9482	5.7821	5.8582
Al	0.2384	0.1936	0.0159	0.0518	0.2179	0.1418
B	3.0000	3.0000	3.0000	3.0000	3.0000	3.0000
Z:						
Al	6.0000	6.0000	5.9203	5.9702	6.0000	6.0000
Mg	0.0000	0.0000	0.0797	0.0298	0.0000	0.0000
Cr	0.0000	0.0000	0.0000	0.0000	0.0000	0.0000
Y:						
Al	0.3207	0.4462	0.0000	0.0000	0.4372	0.0746
Ti	0.0486	0.0561	0.0932	0.0693	0.0793	0.0689
Cr	0.0133	0.0078	0.0042	0.0000	0.0047	0.0408
Mg	2.3882	1.4140	1.2296	1.6418	1.4744	2.1047
Mn	0.0008	0.0006	0.0047	0.0032	0.0071	0.0022
Fe2+	0.0357	0.8684	1.6356	1.2437	0.8407	0.5566
Li*	0.1927	0.2069	0.0326	0.0420	0.1567	0.1522

SY	3.0000	3.0000	3.0000	3.0000	3.0000	3.0000
X:						
Ca	0.1909	0.1282	0.0353	0.1471	0.1007	0.2445
Na	0.6029	0.5619	0.8590	0.6847	0.5651	0.5479
K	0.0153	0.0161	0.0080	0.0060	0.0075	0.0038
OH	4.0000	4.0000	4.0000	4.0000	4.0000	4.0000
F	0.0000	0.0000	0.0000	0.0000	0.0000	0.0000
Cl	0.0000	0.0000	0.0000	0.0000	0.0000	0.0000

Sample No.	L113415IT5	L113415IT9	L113415IT16	L113415IT22	L113415IT37	I783255T1
SiO2	36.26	35.90	35.90	36.25	36.67	36.85
TiO2	0.47	0.74	0.56	0.66	0.57	1.03
Al2O3	35.18	30.22	30.84	35.40	33.01	28.78
Cr2O3	0.06	0.03	0.00	0.04	0.32	0.01
FeO	6.48	11.73	8.98	6.30	4.17	9.68
MgO	5.92	5.27	6.77	6.20	8.84	6.62
CaO	0.75	0.20	0.83	0.59	1.43	0.31
MnO	0.00	0.03	0.02	0.05	0.02	0.02
Na2O	1.81	2.66	2.13	1.83	1.77	2.65
K2O	0.08	0.04	0.03	0.04	0.02	0.03
H2O*	3.74	3.60	3.62	3.76	3.75	3.62
B2O3*	10.85	10.43	10.49	10.90	10.88	10.49
Li2O*	0.32	0.05	0.06	0.24	0.24	0.40
Total	101.93	100.90	100.22	102.27	101.68	100.49
O=F	0.00	0.00	0.00	0.00	0.00	0.00
Total*	101.93	100.90	100.22	102.27	101.68	100.49

Structural formula based on 31 anions (O, OH, F)

T:						
Si	5.8064	5.9841	5.9482	5.7821	5.8582	6.1061
Al	0.1936	0.0159	0.0518	0.2179	0.1418	0.0000
B	3.0000	3.0000	3.0000	3.0000	3.0000	3.0000
Z:						
Al	6.0000	5.9203	5.9702	6.0000	6.0000	5.6205
Mg	0.0000	0.0797	0.0298	0.0000	0.0000	0.3795
Cr	0.0000	0.0000	0.0000	0.0000	0.0000	0.0000
Y:						
Al	0.4462	0.0000	0.0000	0.4372	0.0746	0.0000
Ti	0.0561	0.0932	0.0693	0.0793	0.0689	0.1285
Cr	0.0078	0.0042	0.0000	0.0047	0.0408	0.0017
Mg	1.4140	1.2296	1.6418	1.4744	2.1047	1.2558
Mn	0.0006	0.0047	0.0032	0.0071	0.0022	0.0029
Fe2+	0.8684	1.6356	1.2437	0.8407	0.5566	1.3414
Li*	0.2069	0.0326	0.0420	0.1567	0.1522	0.2697
SY	3.0000	3.0000	3.0000	3.0000	3.0000	3.0000

X:						
Ca	0.1282	0.0353	0.1471	0.1007	0.2445	0.0542
Na	0.5619	0.8590	0.6847	0.5651	0.5479	0.8516
K	0.0161	0.0080	0.0060	0.0075	0.0038	0.0059
OH	4.0000	4.0000	4.0000	4.0000	4.0000	4.0000
F	0.0000	0.0000	0.0000	0.0000	0.0000	0.0000
Cl	0.0000	0.0000	0.0000	0.0000	0.0000	0.0000

Sample No.	I783255T2	I783255T3	I783255T4	I783255T5	I783255T6	I783255T7
SiO2	36.82	37.00	36.81	35.35	36.42	35.29
TiO2	1.04	1.04	1.04	1.02	1.03	1.03
Al2O3	31.42	32.95	29.01	32.99	34.22	27.55
Cr2O3	0.08	0.01	0.05	0.01	0.01	0.07
FeO	5.24	5.33	5.51	13.22	9.84	10.84
MgO	8.30	7.15	9.10	1.56	3.52	7.27
CaO	0.69	0.89	1.70	0.11	0.12	2.41
MnO	0.04	0.02	0.07	0.00	0.12	0.10
Na2O	2.53	1.86	1.86	2.07	1.84	1.49
K2O	0.04	0.01	0.08	0.05	0.03	0.08
H2O*	3.71	3.73	3.65	3.59	3.70	3.55
B2O3*	10.75	10.82	10.59	10.42	10.72	10.29
Li2O*	0.31	0.41	0.39	0.38	0.35	0.07
Total	100.97	101.23	99.86	100.77	101.92	100.04
O=F	0.00	0.00	0.00	0.00	0.00	0.00
Total*	100.97	101.23	99.86	100.77	101.92	100.04

Structural formula based on 31 anions (O, OH, F)

T:						
Si	5.9549	5.9425	6.0434	5.8971	5.9048	5.9581
Al	0.0451	0.0575	0.0000	0.1029	0.0952	0.0419
B	3.0000	3.0000	3.0000	3.0000	3.0000	3.0000
Z:						
Al	5.9439	6.0000	5.6133	6.0000	6.0000	5.4401
Mg	0.0561	0.0000	0.3867	0.0000	0.0000	0.5599
Cr	0.0000	0.0000	0.0000	0.0000	0.0000	0.0000
Y:						
Al	0.0000	0.1795	0.0000	0.3833	0.4436	0.0000
Ti	0.1268	0.1260	0.1288	0.1282	0.1256	0.1308
Cr	0.0097	0.0009	0.0064	0.0010	0.0009	0.0087
Mg	1.9450	1.7119	1.8405	0.3871	0.8508	1.2699
Mn	0.0061	0.0031	0.0099	0.0000	0.0166	0.0142
Fe2+	0.7087	0.7159	0.7565	1.8443	1.3342	1.5305
Li*	0.2036	0.2627	0.2578	0.2561	0.2282	0.0458

SY	3.0000	3.0000	3.0000	3.0000	3.0000	3.0000
X:						
Ca	0.1202	0.1534	0.2984	0.0202	0.0215	0.4362
Na	0.7924	0.5789	0.5931	0.6682	0.5780	0.4882
K	0.0086	0.0023	0.0169	0.0098	0.0065	0.0165
OH	4.0000	4.0000	4.0000	4.0000	4.0000	4.0000
F	0.0000	0.0000	0.0000	0.0000	0.0000	0.0000
Cl	0.0000	0.0000	0.0000	0.0000	0.0000	0.0000

Sample No.	I783255T8	I783255T9	I783255T10	I783255T11	I783255T12	I783255T13
SiO2	35.77	36.89	37.25	36.54	37.31	35.66
TiO2	1.03	1.04	1.03	1.04	1.04	1.03
Al2O3	28.08	29.01	33.69	33.50	32.77	28.98
Cr2O3	0.00	0.09	0.00	0.04	0.02	0.00
FeO	12.19	8.16	11.05	7.66	6.40	10.54
MgO	4.87	7.36	3.08	5.74	7.67	5.86
CaO	1.10	0.54	0.14	0.65	0.69	0.79
MnO	0.11	0.00	0.08	0.08	0.06	0.21
Na2O	2.07	2.59	1.88	1.81	2.41	2.27
K2O	0.06	0.02	0.02	0.06	0.04	0.06
H2O*	3.53	3.63	3.73	3.72	3.78	3.56
B2O3*	10.24	10.53	10.80	10.78	10.97	10.31
Li2O*	0.40	0.42	0.40	0.30	0.28	0.18
Total	99.45	100.28	103.14	101.91	103.44	99.44
O=F	0.00	0.00	0.00	0.00	0.00	0.00
Total*	99.45	100.28	103.14	101.91	103.44	99.44
Structural formula based on 31 anions (O, OH, F)						
T:						
Si	6.0731	6.0873	5.9926	5.8886	5.9114	6.0142
Al	0.0000	0.0000	0.0074	0.1114	0.0886	0.0000
B	3.0000	3.0000	3.0000	3.0000	3.0000	3.0000
Z:						
Al	5.6188	5.6418	6.0000	6.0000	6.0000	5.7604
Mg	0.3812	0.3582	0.0000	0.0000	0.0000	0.2396
Cr	0.0000	0.0000	0.0000	0.0000	0.0000	0.0000
Y:						
Al	0.0000	0.0000	0.3804	0.2513	0.0305	0.0000
Ti	0.1309	0.1285	0.1244	0.1256	0.1239	0.1305
Cr	0.0004	0.0113	0.0000	0.0045	0.0023	0.0000
Mg	0.8514	1.4523	0.7387	1.3790	1.8116	1.2337
Mn	0.0162	0.0000	0.0103	0.0109	0.0078	0.0301
Fe2+	1.7308	1.1261	1.4866	1.0324	0.8480	1.4866
Li*	0.2703	0.2818	0.2597	0.1962	0.1758	0.1192

SY	3.0000	3.0000	3.0000	3.0000	3.0000	3.0000
X:						
Ca	0.2002	0.0950	0.0246	0.1120	0.1169	0.1436
Na	0.6829	0.8291	0.5849	0.5645	0.7408	0.7408
K	0.0137	0.0035	0.0039	0.0120	0.0090	0.0131
OH	4.0000	4.0000	4.0000	4.0000	4.0000	4.0000
F	0.0000	0.0000	0.0000	0.0000	0.0000	0.0000
Cl	0.0000	0.0000	0.0000	0.0000	0.0000	0.0000

Sample No.	I783255T14	I783255T15	I783255T16	I783255T17	I783255T18	I783255T19
SiO2	32.69	36.39	36.42	35.63	36.00	34.82
TiO2	1.02	1.04	1.04	1.02	1.04	1.03
Al2O3	31.44	33.73	31.14	31.20	33.24	31.88
Cr2O3	0.00	0.06	0.02	0.01	0.02	0.01
FeO	13.98	6.04	8.24	12.67	6.51	11.47
MgO	0.64	6.05	6.11	3.09	5.92	3.54
CaO	0.26	0.59	0.79	0.29	0.66	0.53
MnO	0.12	0.05	0.12	0.18	0.06	0.06
Na2O	1.87	1.90	2.16	2.16	2.30	1.95
K2O	0.08	0.05	0.02	0.06	0.11	0.04
H2O*	3.38	3.71	3.65	3.58	3.69	3.56
B2O3*	9.79	10.75	10.58	10.38	10.69	10.32
Li2O*	0.30	0.42	0.33	0.25	0.48	0.24
Total	95.57	100.77	100.63	100.53	100.72	99.44
O=F	0.00	0.00	0.00	0.00	0.00	0.00
Total*	95.57	100.77	100.63	100.53	100.72	99.44
Structural formula based on 31 anions (O, OH, F)						
T:						
Si	5.8038	5.8850	5.9806	5.9675	5.8547	5.8659
Al	0.1962	0.1150	0.0194	0.0325	0.1453	0.1341
B	3.0000	3.0000	3.0000	3.0000	3.0000	3.0000
Z:						
Al	6.0000	6.0000	6.0000	6.0000	6.0000	6.0000
Mg	0.0000	0.0000	0.0000	0.0000	0.0000	0.0000
Cr	0.0000	0.0000	0.0000	0.0000	0.0000	0.0000
Y:						
Al	0.3825	0.3138	0.0074	0.1261	0.2259	0.1955
Ti	0.1358	0.1266	0.1278	0.1288	0.1271	0.1300
Cr	0.0001	0.0071	0.0030	0.0017	0.0022	0.0014
Mg	0.1700	1.4586	1.4957	0.7715	1.4353	0.8890
Mn	0.0184	0.0069	0.0168	0.0259	0.0079	0.0084
Fe2+	2.0757	0.8169	1.1316	1.7746	0.8854	1.6159
Li*	0.2174	0.2702	0.2177	0.1714	0.3162	0.1597

SY	3.0000	3.0000	3.0000	3.0000	3.0000	3.0000
X:						
Ca	0.0492	0.1019	0.1394	0.0523	0.1156	0.0964
Na	0.6439	0.5962	0.6871	0.7013	0.7245	0.6355
K	0.0170	0.0113	0.0051	0.0125	0.0234	0.0086
OH	4.0000	4.0000	4.0000	4.0000	4.0000	4.0000
F	0.0000	0.0000	0.0000	0.0000	0.0000	0.0000
Cl	0.0000	0.0000	0.0000	0.0000	0.0000	0.0000

Sample No.	I783255T21	I783255T21	I782165T1	I782165T2	I782165T3	I782165T4
SiO2	36.10	36.10	35.81	35.48	36.35	36.13
TiO2	1.03	1.03	0.33	0.76	1.43	1.92
Al2O3	30.61	30.61	35.20	34.44	33.99	33.34
Cr2O3	0.04	0.04	0.00	0.00	0.00	0.00
FeO	9.09	9.09	10.96	11.63	6.98	7.50
MgO	5.60	5.60	2.25	2.55	5.81	5.68
CaO	0.51	0.51	0.21	0.35	0.67	0.60
MnO	0.02	0.02	0.03	0.06	0.01	0.04
Na2O	1.93	1.93	1.67	1.88	1.57	1.57
K2O	0.04	0.04	0.04	0.04	0.03	0.02
H2O*	3.60	3.60	3.66	3.66	3.73	3.71
B2O3*	10.42	10.42	10.60	10.60	10.81	10.76
Li2O*	0.27	0.27	0.35	0.31	0.32	0.30
Total	99.27	99.27	101.11	101.77	101.70	101.57
O=F	0.00	0.00	0.00	0.00	0.00	0.00
Total*	99.27	99.27	101.11	101.77	101.70	101.57
Structural formula based on 31 anions (O, OH, F)						
T:						
Si	6.0215	6.0215	5.8707	5.8180	5.8448	5.8379
Al	0.0000	0.0000	0.1293	0.1820	0.1552	0.1621
B	3.0000	3.0000	3.0000	3.0000	3.0000	3.0000
Z:						
Al	6.0000	6.0000	6.0000	6.0000	6.0000	6.0000
Mg	0.0000	0.0000	0.0000	0.0000	0.0000	0.0000
Cr	0.0000	0.0000	0.0000	0.0000	0.0000	0.0000
Y:						
Al	0.0175	0.0175	0.6702	0.4732	0.2876	0.1865
Ti	0.1295	0.1295	0.0401	0.0936	0.1725	0.2330
Cr	0.0057	0.0057	0.0000	0.0000	0.0000	0.0000
Mg	1.3925	1.3925	0.5510	0.6224	1.3936	1.3675
Mn	0.0028	0.0028	0.0036	0.0085	0.0016	0.0060
Fe2+	1.2680	1.2680	1.5028	1.5953	0.9389	1.0140
Li*	0.1840	0.1840	0.2322	0.2069	0.2058	0.1930

SY	3.0000	3.0000	3.0000	3.0000	3.0000	3.0000
X:						
Ca	0.0914	0.0914	0.0369	0.0608	0.1160	0.1037
Na	0.6237	0.6237	0.5295	0.5990	0.4909	0.4916
K	0.0094	0.0094	0.0076	0.0078	0.0057	0.0036
OH	4.0000	4.0000	4.0000	4.0000	4.0000	4.0000
F	0.0000	0.0000	0.0000	0.0000	0.0000	0.0000
Cl	0.0000	0.0000	0.0000	0.0000	0.0000	0.0000

Sample No.	I782165T5	I782165T6	I782165T7	I782165T8	I782165T9	I782165T10
SiO2	43.19	35.63	35.68	35.75	35.61	35.68
TiO2	0.99	0.65	0.65	0.73	0.93	0.32
Al2O3	29.94	34.13	34.03	30.49	29.73	33.98
Cr2O3	0.01	0.06	0.09	0.00	0.00	0.00
FeO	7.12	5.59	5.58	11.77	12.12	13.81
MgO	5.19	6.76	6.57	5.26	5.21	1.44
CaO	0.45	1.17	1.11	0.80	0.75	0.07
MnO	0.02	0.00	0.00	0.04	0.06	0.32
Na2O	1.57	1.78	1.68	2.38	2.38	1.86
K2O	0.01	0.07	0.04	0.08	0.09	0.04
H2O*	3.95	3.70	3.69	3.61	3.59	3.63
B2O3*	11.44	10.72	10.68	10.47	10.39	10.51
Li2O*	2.36	0.34	0.35	0.11	0.10	0.20
Total	106.24	100.60	100.14	101.50	100.95	101.86
O=F	0.00	0.00	0.00	0.00	0.00	0.00
Total*	106.24	100.60	100.14	101.50	100.95	101.86

Structural formula based on 31 anions (O, OH, F)

T:						
Si	6.5613	5.7773	5.8038	5.9321	5.9559	5.8994
Al	0.0000	0.2227	0.1962	0.0679	0.0441	0.1006
B	3.0000	3.0000	3.0000	3.0000	3.0000	3.0000
Z:						
Al	5.3594	6.0000	6.0000	5.8939	5.8164	6.0000
Mg	0.6406	0.0000	0.0000	0.1061	0.1836	0.0000
Cr	0.0000	0.0000	0.0000	0.0000	0.0000	0.0000
Y:						
Al	0.0000	0.2982	0.3280	0.0000	0.0000	0.5212
Ti	0.1128	0.0794	0.0797	0.0907	0.1164	0.0393
Cr	0.0010	0.0078	0.0112	0.0000	0.0000	0.0000
Mg	0.5356	1.6348	1.5926	1.1952	1.1154	0.3543
Mn	0.0020	0.0000	0.0000	0.0060	0.0080	0.0455
Fe2+	0.9045	0.7577	0.7594	1.6331	1.6949	1.9095
Li*	1.4441	0.2220	0.2291	0.0750	0.0654	0.1302

SY	3.0000	3.0000	3.0000	3.0000	3.0000	3.0000
X:						
Ca	0.0740	0.2027	0.1943	0.1426	0.1337	0.0131
Na	0.4626	0.5610	0.5298	0.7660	0.7727	0.5960
K	0.0024	0.0135	0.0082	0.0163	0.0201	0.0088
OH	4.0000	4.0000	4.0000	4.0000	4.0000	4.0000
F	0.0000	0.0000	0.0000	0.0000	0.0000	0.0000
Cl	0.0000	0.0000	0.0000	0.0000	0.0000	0.0000

Sample No.	I782165T11	I782165T12	I782165T13	I782165T14	I782165T15	I782165T16
SiO2	35.52	36.19	35.93	36.47	36.68	36.92
TiO2	0.32	0.09	0.08	1.31	0.68	0.76
Al2O3	34.06	35.10	34.82	30.80	33.66	33.45
Cr2O3	0.00	0.00	0.00	0.00	0.00	0.05
FeO	13.66	10.68	10.96	8.34	6.34	5.04
MgO	1.43	2.49	2.52	6.94	6.62	7.53
CaO	0.09	0.08	0.05	0.36	0.33	0.59
MnO	0.32	0.08	0.11	0.00	0.00	0.00
Na2O	1.90	1.85	1.92	2.43	2.04	2.04
K2O	0.05	0.03	0.02	0.01	0.00	0.02
H2O*	3.62	3.67	3.65	3.67	3.72	3.74
B2O3*	10.50	10.63	10.58	10.62	10.77	10.84
Li2O*	0.21	0.36	0.31	0.15	0.24	0.29
Total	101.68	101.25	100.94	101.12	101.09	101.28
O=F	0.00	0.00	0.00	0.00	0.00	0.00
Total*	101.68	101.25	100.94	101.12	101.09	101.28

Structural formula based on 31 anions (O, OH, F)

T:						
Si	5.8809	5.9154	5.9035	5.9671	5.9175	5.9185
Al	0.1191	0.0846	0.0965	0.0329	0.0825	0.0815
B	3.0000	3.0000	3.0000	3.0000	3.0000	3.0000
Z:						
Al	6.0000	6.0000	6.0000	5.9066	6.0000	6.0000
Mg	0.0000	0.0000	0.0000	0.0934	0.0000	0.0000
Cr	0.0000	0.0000	0.0000	0.0000	0.0000	0.0000
Y:						
Al	0.5287	0.6767	0.6465	0.0000	0.3173	0.2387
Ti	0.0392	0.0107	0.0102	0.1612	0.0824	0.0917
Cr	0.0000	0.0000	0.0000	0.0005	0.0000	0.0069
Mg	0.3539	0.6075	0.6163	1.6001	1.5924	1.8002
Mn	0.0449	0.0110	0.0157	0.0000	0.0000	0.0000
Fe2+	1.8923	1.4606	1.5059	1.1416	0.8550	0.6751
Li*	0.1409	0.2335	0.2055	0.0967	0.1529	0.1874

SY	3.0000	3.0000	3.0000	3.0000	3.0000	3.0000
X:						
Ca	0.0163	0.0143	0.0090	0.0632	0.0569	0.1011
Na	0.6104	0.5852	0.6129	0.7709	0.6390	0.6343
K	0.0096	0.0062	0.0043	0.0028	0.0003	0.0034
OH	4.0000	4.0000	4.0000	4.0000	4.0000	4.0000
F	0.0000	0.0000	0.0000	0.0000	0.0000	0.0000
Cl	0.0000	0.0000	0.0000	0.0000	0.0000	0.0000

Sample No.	I782165T17	I782165T18	I782165T19	I782165T16	I782165T17	I782165T18
SiO2	37.21	37.00	36.38	36.92	37.21	37.00
TiO2	1.00	0.11	0.58	0.76	1.00	0.11
Al2O3	32.98	31.14	28.10	33.45	32.98	31.14
Cr2O3	0.00	0.01	0.00	0.05	0.00	0.01
FeO	5.27	6.74	9.94	5.04	5.27	6.74
MgO	7.35	8.25	8.05	7.53	7.35	8.25
CaO	0.42	0.52	1.59	0.59	0.42	0.52
MnO	0.00	0.00	0.01	0.00	0.00	0.00
Na2O	2.03	2.39	1.96	2.04	2.03	2.39
K2O	0.01	0.02	0.03	0.02	0.01	0.02
H2O*	3.74	3.68	3.61	3.74	3.74	3.68
B2O3*	10.83	10.66	10.46	10.84	10.83	10.66
Li2O*	0.31	0.12	0.07	0.29	0.31	0.12
Total	101.14	100.62	100.77	101.28	101.14	100.62
O=F	0.00	0.00	0.00	0.00	0.00	0.00
Total*	101.14	100.62	100.77	101.28	101.14	100.62

Structural formula based on 31 anions (O, OH, F)

T:						
Si	5.9729	6.0316	6.0475	5.9185	5.9729	6.0316
Al	0.0271	0.0000	0.0000	0.0815	0.0271	0.0000
B	3.0000	3.0000	3.0000	3.0000	3.0000	3.0000
Z:						
Al	6.0000	5.9835	5.5050	6.0000	6.0000	5.9835
Mg	0.0000	0.0165	0.4950	0.0000	0.0000	0.0165
Cr	0.0000	0.0000	0.0000	0.0000	0.0000	0.0000
Y:						
Al	0.2108	0.0000	0.0000	0.2387	0.2108	0.0000
Ti	0.1211	0.0134	0.0728	0.0917	0.1211	0.0134
Cr	0.0000	0.0010	0.0000	0.0069	0.0000	0.0010
Mg	1.7585	1.9888	1.4990	1.8002	1.7585	1.9888
Mn	0.0000	0.0000	0.0017	0.0000	0.0000	0.0000
Fe2+	0.7074	0.9195	1.3814	0.6751	0.7074	0.9195
Li*	0.2023	0.0774	0.0451	0.1874	0.2023	0.0774

SY	3.0000	3.0000	3.0000	3.0000	3.0000	3.0000
X:						
Ca	0.0717	0.0902	0.2824	0.1011	0.0717	0.0902
Na	0.6306	0.7558	0.6331	0.6343	0.6306	0.7558
K	0.0026	0.0032	0.0067	0.0034	0.0026	0.0032
OH	4.0000	4.0000	4.0000	4.0000	4.0000	4.0000
F	0.0000	0.0000	0.0000	0.0000	0.0000	0.0000
Cl	0.0000	0.0000	0.0000	0.0000	0.0000	0.0000

Sample No.	I782165T19	H285025T1	H285025T4	H285025T5	H285025T7	H285025T13
SiO2	36.38	35.69	36.36	36.52	35.66	35.26
TiO2	0.58	1.03	0.93	0.52	0.43	0.43
Al2O3	28.10	31.20	32.78	32.48	31.16	33.24
Cr2O3	0.00	0.00	0.00	0.00	0.00	0.00
FeO	9.94	10.47	6.19	6.59	8.46	11.68
MgO	8.05	5.48	7.23	7.36	7.15	2.93
CaO	1.59	0.88	0.71	0.70	0.93	0.08
MnO	0.01	0.04	0.00	0.00	0.00	0.19
Na2O	1.96	1.92	1.94	2.14	2.09	2.04
K2O	0.03	0.02	0.01	0.02	0.04	0.04
H2O*	3.61	3.63	3.70	3.69	3.62	3.59
B2O3*	10.46	10.51	10.72	10.71	10.49	10.41
Li2O*	0.07	0.12	0.21	0.18	0.03	0.19
Total	100.77	100.99	100.78	100.90	100.04	100.08
O=F	0.00	0.00	0.00	0.00	0.00	0.00
Total*	100.77	100.99	100.78	100.90	100.04	100.08

Structural formula based on 31 anions (O, OH, F)

T:						
Si	6.0475	5.9034	5.8957	5.9291	5.9088	5.8889
Al	0.0000	0.0966	0.1043	0.0709	0.0912	0.1111
B	3.0000	3.0000	3.0000	3.0000	3.0000	3.0000
Z:						
Al	5.5050	5.9862	6.0000	6.0000	5.9932	6.0000
Mg	0.4950	0.0138	0.0000	0.0000	0.0068	0.0000
Cr	0.0000	0.0000	0.0000	0.0000	0.0000	0.0000
Y:						
Al	0.0000	0.0000	0.1600	0.1433	0.0000	0.4310
Ti	0.0728	0.1283	0.1129	0.0632	0.0530	0.0545
Cr	0.0000	0.0005	0.0000	0.0000	0.0000	0.0000
Mg	1.4990	1.3365	1.7474	1.7805	1.7581	0.7294
Mn	0.0017	0.0053	0.0000	0.0000	0.0000	0.0269
Fe2+	1.3814	1.4479	0.8398	0.8945	1.1717	1.6309
Li*	0.0451	0.0815	0.1400	0.1185	0.0172	0.1273

SY	3.0000	3.0000	3.0000	3.0000	3.0000	3.0000
X:						
Ca	0.2824	0.1563	0.1231	0.1212	0.1643	0.0149
Na	0.6331	0.6172	0.6101	0.6740	0.6729	0.6590
K	0.0067	0.0050	0.0023	0.0034	0.0077	0.0095
OH	4.0000	4.0000	4.0000	4.0000	4.0000	4.0000
F	0.0000	0.0000	0.0000	0.0000	0.0000	0.0000
Cl	0.0000	0.0000	0.0000	0.0000	0.0000	0.0000

Sample No.	H285025T14	H285025T15	H285025T16	H285025T19	H285025T21	H285025T23
SiO2	35.88	36.11	35.71	35.72	44.29	35.54
TiO2	1.61	0.55	0.72	0.27	0.00	1.71
Al2O3	32.77	35.31	32.29	32.97	38.98	30.57
Cr2O3	0.00	0.00	0.01	0.00	0.00	0.00
FeO	7.98	5.89	6.38	8.42	2.63	10.57
MgO	5.70	6.25	7.18	6.13	0.56	5.30
CaO	0.47	0.75	1.15	0.71	0.46	0.30
MnO	0.06	0.01	0.01	0.07	0.00	0.07
Na2O	2.01	1.74	1.81	1.89	0.19	2.18
K2O	0.04	0.04	0.02	0.02	0.08	0.04
H2O*	3.68	3.74	3.65	3.65	4.10	3.60
B2O3*	10.67	10.84	10.58	10.58	11.88	10.44
Li2O*	0.28	0.29	0.23	0.07	3.13	0.11
Total	101.15	101.53	99.74	100.51	106.30	100.43
O=F	0.00	0.00	0.00	0.00	0.00	0.00
Total*	101.15	101.53	99.74	100.51	106.30	100.43

Structural formula based on 31 anions (O, OH, F)

T:						
Si	5.8459	5.7893	5.8670	5.8682	6.4766	5.9161
Al	0.1541	0.2107	0.1330	0.1318	0.0000	0.0839
B	3.0000	3.0000	3.0000	3.0000	3.0000	3.0000
Z:						
Al	6.0000	6.0000	6.0000	6.0000	6.0000	5.9144
Mg	0.0000	0.0000	0.0000	0.0000	0.0000	0.0856
Cr	0.0000	0.0000	0.0000	0.0000	0.0000	0.0000
Y:						
Al	0.1378	0.4609	0.1197	0.2525	0.7183	0.0000
Ti	0.1976	0.0664	0.0893	0.0331	0.0000	0.2135
Cr	0.0000	0.0000	0.0012	0.0000	0.0000	0.0000
Mg	1.3853	1.4932	1.7579	1.5021	0.1218	1.2288
Mn	0.0080	0.0014	0.0009	0.0100	0.0000	0.0095
Fe2+	1.0875	0.7901	0.8765	1.1572	0.3219	1.4716

Li*	0.1839	0.1879	0.1545	0.0451	1.8380	0.0767
SY	3.0000	3.0000	3.0000	3.0000	3.0000	3.0000
X:						
Ca	0.0815	0.1284	0.2028	0.1254	0.0718	0.0533
Na	0.6336	0.5405	0.5777	0.6036	0.0544	0.7036
K	0.0083	0.0077	0.0046	0.0039	0.0152	0.0090
OH	4.0000	4.0000	4.0000	4.0000	4.0000	4.0000
F	0.0000	0.0000	0.0000	0.0000	0.0000	0.0000
Cl	0.0000	0.0000	0.0000	0.0000	0.0000	0.0000

Sample No.	H285025T22	H285025T6	H285025T8	H285025T12	H285025T20
SiO2	35.40	36.25	35.01	35.65	36.00
TiO2	0.99	0.43	0.51	0.27	0.68
Al2O3	32.65	34.23	34.56	35.19	34.22
Cr2O3	0.00	0.00	0.00	0.00	0.00
FeO	6.60	9.39	12.73	11.12	7.52
MgO	6.41	4.18	1.84	2.43	5.62
CaO	0.53	0.12	0.29	0.11	0.45
MnO	0.01	0.00	0.01	0.22	0.01
Na2O	2.02	1.63	1.72	1.83	2.01
K2O	0.02	0.03	0.06	0.05	0.04
H2O*	3.63	3.67	3.62	3.66	3.70
B2O3*	10.51	10.63	10.48	10.60	10.72
Li2O*	0.24	0.18	0.24	0.27	0.26
Total	99.00	100.73	101.06	101.40	101.22
O=F	0.00	0.00	0.00	0.00	0.00
Total*	99.00	100.73	101.06	101.40	101.22
Structural formula based on 31 anions (O, OH, F)					
T:					
Si	5.8556	5.9274	5.8044	5.8432	5.8348
Al	0.1444	0.0726	0.1956	0.1568	0.1652
B	3.0000	3.0000	3.0000	3.0000	3.0000
Z:					
Al	6.0000	6.0000	6.0000	6.0000	6.0000
Mg	0.0000	0.0000	0.0000	0.0000	0.0000
Cr	0.0000	0.0000	0.0000	0.0000	0.0000
Y:					
Al	0.2214	0.5241	0.5575	0.6402	0.3710
Ti	0.1227	0.0528	0.0638	0.0327	0.0834
Cr	0.0000	0.0005	0.0000	0.0000	0.0000
Mg	1.5800	1.0191	0.4551	0.5931	1.3573
Mn	0.0014	0.0004	0.0012	0.0301	0.0011
Fe2+	0.9134	1.2835	1.7653	1.5244	1.0195
Li*	0.1610	0.1197	0.1570	0.1795	0.1678

SY	3.0000	3.0000	3.0000	3.0000	3.0000
X:					
Ca	0.0933	0.0203	0.0509	0.0192	0.0775
Na	0.6468	0.5163	0.5537	0.5822	0.6316
K	0.0051	0.0052	0.0121	0.0100	0.0086
OH	4.0000	4.0000	4.0000	4.0000	4.0000
F	0.0000	0.0000	0.0000	0.0000	0.0000
Cl	0.0000	0.0000	0.0000	0.0000	0.0000

Appendix 4: U-Pb isotopic age data from detrital zircons

		Measured Isotopic Ratios							Calculated Ages										
Sample	Grain ID	207Pb/235U	1s error	206Pb/238U	1s error	Rho	207Pb/206Pb	1s error	207Pb/235U	1s error	206Pb/238U	1s error	207Pb/206Pb	1s error	U-Pb/Pb-Pb	Concordia	2s error	MSWD	Probability
									Ma	Ma	Ma	Ma	Ma	Ma	concordancy	age (Ma)	Ma	(of concordance)	
L113760Z	_001	2.315	0.160	0.179	0.010	0.420	0.088	0.001	1217	49	1061	57	1372	17	77	1150	91	7.22	0.007
L113760Z	_003	12.125	0.216	0.496	0.010	0.547	0.178	0.001	2614	17	2595	42	2637	9	98	2616	33	0.30	0.584
L113760Z	_004	19.342	0.417	0.571	0.009	0.363	0.241	0.001	3059	21	2911	37	3130	8	93	DISCORDANT			
L113760Z	_006	0.476	0.038	0.066	0.002	0.167	0.057	0.001	395	26	413	11	505	34	82	411	21	0.44	0.505
L113760Z	_007	0.578	0.023	0.075	0.002	0.262	0.058	0.000	463	15	468	10	536	18	87	467	18	0.07	0.787
L113760Z	_008	1.609	0.041	0.158	0.003	0.375	0.072	0.001	974	16	946	17	975	18	97	961	27	2.33	0.127
L113760Z	_009	2.072	0.032	0.190	0.002	0.352	0.079	0.000	1139	10	1123	11	1172	12	96	1132	18	1.76	0.185
L113760Z	_010	2.074	0.049	0.187	0.003	0.351	0.081	0.001	1140	16	1103	17	1223	20	90	1122	27	3.95	0.047
L113760Z	_011	0.507	0.011	0.064	0.001	0.349	0.055	0.000	417	7	402	6	421	19	96	407	10	3.57	0.059
L113760Z	_012	0.737	0.022	0.095	0.002	0.262	0.057	0.001	560	13	584	9	496	23	118	577	16	2.89	0.089
L113760Z	_013	1.726	0.031	0.170	0.002	0.349	0.074	0.000	1018	11	1014	12	1051	12	96	1016	19	0.12	0.734
L113760Z	_014	0.704	0.025	0.083	0.002	0.282	0.063	0.001	541	15	515	10	697	29	74	521	18	2.91	0.088
L113760Z	_015	35.593	0.640	0.757	0.014	0.515	0.333	0.001	3655	18	3631	51	3629	7	100	3657	35	0.28	0.596
L113760Z	_016	5.693	0.150	0.325	0.008	0.481	0.123	0.001	1930	23	1814	40	1996	8	91	1922	46	11.11	0.001
L113760Z	_017	0.500	0.017	0.067	0.001	0.280	0.056	0.001	412	11	417	8	471	22	88	415	14	0.19	0.661
L113760Z	_018	4.166	0.069	0.291	0.004	0.407	0.102	0.000	1667	14	1649	20	1666	9	99	1663	26	0.99	0.319
L113760Z	_020	0.515	0.014	0.067	0.001	0.298	0.055	0.000	422	10	420	7	426	19	98	420	12	0.05	0.825
L113760Z	_021	0.476	0.014	0.063	0.001	0.309	0.055	0.001	395	9	397	7	431	23	92	396	13	0.02	0.899
L113760Z	_022	14.765	0.243	0.544	0.010	0.541	0.194	0.001	2800	16	2801	40	2776	9	101	2800	31	0.00	0.984
L113760Z	_023	1.644	0.027	0.160	0.002	0.370	0.072	0.001	987	11	959	11	994	15	96	974	18	5.43	0.020
L113760Z	_024	13.004	0.334	0.475	0.011	0.452	0.193	0.001	2680	24	2506	48	2768	9	91	DISCORDANT			
L113760Z	_025	5.262	0.068	0.317	0.004	0.453	0.118	0.001	1863	11	1775	18	1923	8	92	DISCORDANT			
L113760Z	_026	14.135	0.270	0.541	0.010	0.507	0.191	0.001	2759	18	2789	44	2749	11	101	2757	36	0.63	0.429
L113760Z	_030	0.486	0.014	0.065	0.001	0.313	0.055	0.001	402	10	408	7	418	21	97	406	13	0.26	0.610
L113760Z	_031	0.782	0.021	0.093	0.002	0.375	0.060	0.000	587	12	575	11	604	17	95	580	19	0.77	0.380
L113760Z	_032	4.200	0.110	0.289	0.007	0.478	0.103	0.001	1674	22	1635	36	1684	17	97	1670	43	1.45	0.229
L113760Z	_033	0.494	0.017	0.066	0.001	0.267	0.057	0.001	408	12	412	7	493	24	83	411	14	0.12	0.725
L113760Z	_034	0.715	0.026	0.093	0.002	0.227	0.058	0.001	548	15	573	9	524	26	110	568	17	2.60	0.107
L113760Z	_035	6.354	0.142	0.367	0.007	0.437	0.123	0.001	2026	20	2015	34	2003	8	101	2025	39	0.13	0.722

		Measured Isotopic Ratios							Calculated Ages										
Sample	Grain ID	207Pb/235U	1s error	206Pb/238U	1s error	Rho	207Pb/206Pb	1s error	207Pb/235U	1s error	206Pb/238U	1s error	207Pb/206Pb	1s error	U-Pb/Pb-Pb	Concordia	2s error	MSWD	Probability
									Ma	Ma	Ma	Ma	Ma	Ma	concordancy (%)	age (Ma)	Ma	(of concordance)	
L113760Z	_037	13.831	0.236	0.523	0.008	0.450	0.190	0.001	2738	16	2714	34	2739	11	99	2738	32	0.66	0.418
L113760Z	_038	1.844	0.040	0.170	0.003	0.404	0.076	0.001	1061	14	1014	16	1089	15	93	1043	25	7.94	0.005
L113760Z	_039	0.888	0.020	0.103	0.002	0.366	0.061	0.000	645	11	631	10	642	14	98	637	17	1.54	0.215
L113760Z	_042	5.918	0.112	0.327	0.006	0.453	0.129	0.001	1964	16	1826	27	2078	8	88	1946	33	31.70	0.000
L113760Z	_043	2.068	0.102	0.202	0.005	0.266	0.076	0.001	1138	34	1188	29	1108	26	107	1168	49	1.73	0.188
L113760Z	_044	0.984	0.029	0.109	0.003	0.416	0.065	0.001	696	15	667	15	772	16	86	682	26	3.17	0.075
L113760Z	_045	1.352	0.026	0.140	0.002	0.337	0.069	0.001	868	11	846	10	885	18	96	855	17	3.35	0.067
L113760Z	_048	0.524	0.016	0.067	0.001	0.365	0.056	0.001	428	10	417	9	466	22	90	421	16	0.95	0.330
L113760Z	_049	0.801	0.048	0.101	0.003	0.223	0.062	0.001	598	27	621	16	676	32	92	616	30	0.68	0.410
L113760Z	_050	0.460	0.039	0.067	0.001	0.089	0.075	0.002	385	27	417	6	1066	48	39	416	12	1.45	0.229
L113760Z	_051	0.815	0.024	0.096	0.002	0.278	0.061	0.001	605	14	592	9	652	20	91	596	17	0.81	0.368
L113760Z	_055	2.412	0.088	0.203	0.004	0.297	0.083	0.001	1246	26	1193	24	1268	16	94	1215	40	3.21	0.073
L113760Z	_057	2.630	0.059	0.215	0.005	0.536	0.086	0.000	1309	16	1256	27	1343	11	94	1306	33	5.21	0.022
L113760Z	_062	0.521	0.014	0.065	0.001	0.241	0.057	0.001	426	9	409	5	488	26	84	412	10	3.03	0.082
L113760Z	_063	0.383	0.013	0.047	0.001	0.259	0.057	0.001	329	9	298	5	501	31	60	302	10	10.80	0.001
L113760Z	_064	6.552	0.125	0.352	0.008	0.625	0.139	0.001	2053	17	1942	40	2213	16	88	DISCORDANT			
L113760Z	_069	0.566	0.026	0.076	0.001	0.181	0.060	0.001	456	17	474	8	594	25	80	472	15	1.13	0.287
L113760Z	_072	0.519	0.011	0.065	0.001	0.298	0.055	0.000	425	7	407	5	430	20	95	411	9	5.85	0.016
L113760Z	_073	5.080	0.068	0.327	0.004	0.432	0.112	0.001	1833	11	1822	18	1838	9	99	1831	22	0.40	0.528
L113760Z	_079	0.497	0.021	0.064	0.002	0.315	0.057	0.000	410	14	400	10	492	16	81	403	19	0.46	0.499
L113760Z	_080	4.910	0.063	0.308	0.004	0.490	0.111	0.000	1804	11	1732	19	1815	5	95	DISCORDANT			
L113760Z	_082	0.312	0.011	0.047	0.001	0.253	0.051	0.001	275	8	298	5	244	30	122	293	9	7.06	0.008
L113760Z	_083	4.933	0.081	0.314	0.004	0.432	0.111	0.000	1808	14	1760	22	1823	8	97	1800	27	5.72	0.017
L113760Z	_087	3.998	0.060	0.282	0.003	0.353	0.101	0.001	1634	12	1599	15	1646	10	97	1622	22	4.83	0.028
L113760Z	_088	0.503	0.009	0.062	0.001	0.338	0.057	0.000	414	6	389	4	492	17	79	DISCORDANT			
L113760Z	_089	7.425	0.093	0.382	0.005	0.542	0.137	0.000	2164	11	2085	24	2192	5	95	DISCORDANT			
L113760Z	_091	0.673	0.019	0.089	0.001	0.236	0.057	0.001	523	11	553	7	483	26	114	546	13	6.36	0.012
L113760Z	_092	1.481	0.079	0.162	0.002	0.142	0.078	0.001	923	32	969	14	1151	26	84	963	26	2.03	0.154
L113760Z	_095	1.699	0.029	0.165	0.002	0.436	0.073	0.000	1008	11	987	14	1019	9	97	1002	21	2.47	0.116

		Measured Isotopic Ratios							Calculated Ages										
Sample	Grain ID	207Pb/235U	1s error	206Pb/238U	1s error	Rho	207Pb/206Pb	1s error	207Pb/235U	1s error	206Pb/238U	1s error	207Pb/206Pb	1s error	U-Pb/Pb-Pb	Concordia	2s error	MSWD	Probability
									Ma	Ma	Ma	Ma	Ma	Ma	concordancy (%)	age (Ma)	Ma	(of concordance)	
L113760Z	_096	3.303	0.071	0.257	0.004	0.359	0.094	0.000	1482	17	1473	20	1507	8	98	1478	30	0.19	0.664
L113760Z	_097	1.126	0.049	0.110	0.001	0.152	0.079	0.002	766	23	671	8	1182	38	57	DISCORDANT			
L113760Z	_098	0.800	0.022	0.091	0.002	0.356	0.063	0.001	597	12	562	10	706	19	80	575	18	7.07	0.008
L113760Z	_099	0.795	0.027	0.096	0.002	0.333	0.061	0.001	594	15	591	13	624	20	95	592	22	0.02	0.886
L113760Z	_101	0.697	0.020	0.087	0.001	0.260	0.059	0.001	537	12	538	8	572	25	94	538	14	0.01	0.933
L113760Z	_102	6.395	0.120	0.356	0.006	0.425	0.128	0.001	2032	17	1964	27	2068	7	95	2022	33	7.22	0.007
L113760Z	_103	0.527	0.013	0.066	0.001	0.330	0.055	0.001	430	9	410	7	399	25	103	416	12	4.61	0.032
L113760Z	_104	6.579	0.057	0.366	0.003	0.527	0.125	0.000	2056	8	2009	16	2027	5	99	DISCORDANT			
L113760Z	_105	0.153	0.009	0.022	0.001	0.207	0.056	0.001	145	8	142	4	460	40	31	142	7	0.15	0.696
L113760Z	_106	0.775	0.022	0.095	0.002	0.285	0.061	0.001	583	12	586	9	632	18	93	585	16	0.07	0.784
L113760Z	_107	1.394	0.038	0.155	0.002	0.272	0.069	0.001	886	16	929	13	901	27	103	913	23	5.82	0.016
L113760Z	_108	3.002	0.112	0.226	0.005	0.322	0.089	0.001	1408	28	1311	29	1407	14	93	DISCORDANT			
L113760Z	_109	0.783	0.024	0.098	0.002	0.258	0.059	0.001	587	14	600	9	577	25	104	597	17	0.82	0.366
L113760Z	_110	13.555	0.185	0.506	0.007	0.522	0.187	0.001	2719	13	2639	31	2716	9	97	DISCORDANT			
L113760Z	_111	0.780	0.019	0.091	0.002	0.345	0.060	0.001	585	11	562	9	605	20	93	571	16	3.82	0.051
L113760Z	_112	3.976	0.060	0.278	0.004	0.438	0.101	0.000	1629	12	1582	18	1638	8	97	1621	24	7.67	0.006
L113760Z	_113	0.524	0.017	0.066	0.001	0.283	0.061	0.001	428	11	409	7	626	26	65	413	14	2.59	0.108
L113760Z	_114	0.486	0.010	0.063	0.001	0.333	0.055	0.000	402	7	391	5	405	16	97	395	9	2.60	0.107
L113760Z	_115	0.112	0.006	0.021	0.001	0.238	0.042	0.001	108	5	137	3	-242	47	-57	DISCORDANT			
L113760Z	_116	4.366	0.090	0.288	0.005	0.438	0.107	0.000	1706	17	1632	26	1747	7	93	1693	33	9.65	0.002
L113760Z	_117	11.311	0.301	0.425	0.011	0.473	0.189	0.001	2549	25	2283	48	2730	8	84	DISCORDANT			
L113760Z	_118	1.881	0.034	0.177	0.002	0.386	0.075	0.000	1075	12	1052	14	1062	10	99	1065	21	2.46	0.117
L113760Z	_119	3.507	0.071	0.256	0.004	0.397	0.097	0.000	1529	16	1471	21	1561	7	94	1512	30	7.44	0.006
L113760Z	_120	1.078	0.021	0.119	0.002	0.345	0.063	0.000	743	10	726	9	709	14	102	733	16	2.19	0.139
L113760Z	_121	0.528	0.027	0.064	0.002	0.303	0.058	0.001	431	18	403	12	535	29	75	409	23	2.25	0.134
L113615Z	_001	0.877	0.078	0.100	0.005	0.284	0.064	0.006	639	42	614	29	680	29	90	620	54	0.33	0.560
L113615Z	_002	0.825	0.031	0.110	0.003	0.396	0.055	0.003	611	17	670	19	488	26	137	DISCORDANT			
L113615Z	_003	0.919	0.034	0.103	0.003	0.360	0.065	0.003	662	18	634	16	675	25	94	645	28	2.00	0.150
L113615Z	_004	0.201	0.019	0.024	0.001	0.175	0.062	0.006	186	16	151	5	662	58	23	152	10	4.80	0.030
L113615Z	_005	0.477	0.035	0.064	0.003	0.295	0.054	0.005	396	24	397	17	458	35	87	397	31	0.00	0.950

		Measured Isotopic Ratios							Calculated Ages										
Sample	Grain ID	207Pb/235U	1s error	206Pb/238U	1s error	Rho	207Pb/206Pb	1s error	207Pb/235U	1s error	206Pb/238U	1s error	207Pb/206Pb	1s error	U-Pb/Pb-Pb	Concordia	2s error	MSWD	Probability
									Ma	Ma	Ma	Ma	Ma	Ma	concordancy (%)	age (Ma)	Ma	(of concordance)	
L113615Z	_006	0.522	0.022	0.070	0.002	0.308	0.054	0.003	427	15	434	11	413	29	105	432	20	0.22	0.640
L113615Z	_007	0.742	0.033	0.098	0.003	0.309	0.055	0.003	564	19	600	16	424	38	142	587	28	3.10	0.079
L113615Z	_008	0.914	0.042	0.109	0.003	0.303	0.061	0.003	659	22	669	18	667	20	100	666	32	0.18	0.670
L113615Z	_009	7.785	0.411	0.429	0.017	0.366	0.132	0.009	2206	48	2302	75	2063	17	112	2223	90	0.70	0.190
L113615Z	_010	5.382	0.215	0.359	0.012	0.416	0.109	0.006	1882	34	1977	57	1754	18	113	1894	67	3.30	0.071
L113615Z	_011	0.988	0.048	0.104	0.003	0.348	0.069	0.004	698	24	635	20	923	31	69	656	36	5.80	0.016
L113615Z	_012	5.666	0.175	0.327	0.010	0.502	0.126	0.005	1926	27	1824	49	1927	12	95	1922	53	5.90	0.016
L113615Z	_013	0.846	0.047	0.101	0.003	0.249	0.061	0.004	622	26	619	16	753	30	82	619	30	0.02	0.890
L113615Z	_014	0.538	0.028	0.069	0.002	0.304	0.056	0.003	437	19	433	13	477	23	91	434	25	0.06	0.810
L113615Z	_015	0.849	0.042	0.104	0.003	0.257	0.059	0.003	624	23	638	16	696	24	92	634	29	0.33	0.560
L113615Z	_017	2.877	0.074	0.238	0.004	0.362	0.088	0.003	1376	19	1379	23	1366	18	101	1377	34	0.01	0.910
L113615Z	_018	2.598	0.076	0.225	0.005	0.353	0.084	0.003	1300	22	1308	25	1251	15	105	1303	38	0.10	0.760
L113615Z	_019	0.502	0.029	0.072	0.002	0.185	0.050	0.003	413	20	450	9	431	28	104	445	18	3.40	0.066
L113615Z	_020	0.837	0.087	0.099	0.006	0.304	0.062	0.007	618	48	607	36	650	24	93	DISCORDANT			
L113615Z	_021	5.548	0.169	0.343	0.008	0.380	0.117	0.004	1908	26	1903	38	1839	13	103	1907	50	0.02	0.890
L113615Z	_022	0.724	0.064	0.105	0.003	0.159	0.050	0.005	553	38	641	17	639	33	100	629	33	5.40	0.020
L113615Z	_023	0.916	0.042	0.103	0.002	0.242	0.064	0.003	660	22	633	14	777	34	81	638	25	1.40	0.240
L113615Z	_024	0.713	0.021	0.090	0.002	0.382	0.058	0.002	546	12	555	12	554	19	100	551	20	0.37	0.540
L113615Z	_025	0.495	0.035	0.069	0.002	0.229	0.052	0.004	408	24	433	13	384	28	113	428	25	1.07	0.300
L113615Z	_026	2.137	0.059	0.200	0.004	0.332	0.078	0.003	1161	19	1173	20	1110	15	106	1167	32	0.32	0.570
L113615Z	_028	3.150	0.084	0.238	0.005	0.396	0.096	0.003	1445	20	1375	26	1386	14	99	1422	38	7.30	0.007
L113615Z	_029	0.788	0.032	0.108	0.002	0.236	0.053	0.002	590	18	660	12	505	24	131	DISCORDANT			
L113615Z	_030	0.174	0.014	0.021	0.001	0.304	0.059	0.006	163	12	136	7	774	41	18	139	13	0.49	0.027
L113615Z	_031	0.785	0.041	0.096	0.003	0.325	0.059	0.004	588	23	590	19	579	24	102	590	34	0.01	0.930
L113615Z	_034	0.715	0.056	0.090	0.004	0.263	0.057	0.005	548	33	558	22	581	25	96	556	40	0.09	0.760
L113615Z	_035	0.846	0.035	0.102	0.002	0.292	0.060	0.003	623	19	628	14	658	23	95	626	26	0.06	0.800
L113615Z	_036	12.237	0.436	0.502	0.012	0.344	0.177	0.008	2623	33	2622	53	2594	18	101	2623	54	0.00	0.980
L113615Z	_037	6.873	0.250	0.359	0.012	0.465	0.139	0.007	2095	32	1977	58	2077	10	95	2086	65	5.40	0.021
L113615Z	_038	0.489	0.037	0.066	0.002	0.231	0.054	0.004	405	25	411	14	519	26	79	410	26	0.07	0.800
L113615Z	_039	0.358	0.044	0.061	0.003	0.183	0.042	0.006	311	33	385	17	17	36	2312	372	31	4.90	0.026

		Measured Isotopic Ratios							Calculated Ages										
Sample	Grain ID	207Pb/235U	1s error	206Pb/238U	1s error	Rho	207Pb/206Pb	1s error	207Pb/235U	1s error	206Pb/238U	1s error	207Pb/206Pb	1s error	U-Pb/Pb-Pb	Concordia	2s error	MSWD	Probability
									Ma	Ma	Ma	Ma	Ma	Ma	concordancy (%)	age (Ma)	Ma	(of concordance)	
L113615Z	_040	3.985	0.076	0.291	0.005	0.459	0.099	0.003	1631	15	1647	25	1496	12	110	1633	31	0.48	0.490
L113615Z	_042	6.276	0.133	0.366	0.008	0.530	0.124	0.004	2015	19	2009	39	1877	11	107	2015	37	0.04	0.850
L113615Z	_043	2.671	0.142	0.236	0.007	0.283	0.082	0.005	1320	39	1368	37	1344	29	102	1345	60	1.08	0.300
L113615Z	_044	0.837	0.031	0.101	0.002	0.291	0.060	0.003	617	17	618	13	600	26	103	618	23	0.00	0.970
L113615Z	_045	0.491	0.039	0.069	0.003	0.226	0.051	0.005	406	27	432	15	348	34	124	427	28	0.91	0.340
L113615Z	_046	0.133	0.015	0.022	0.001	0.191	0.045	0.006	127	14	138	6	199	45	69	136	12	0.63	0.430
L113615Z	_050	0.719	0.035	0.094	0.002	0.256	0.056	0.003	550	21	577	14	462	21	125	570	26	1.50	0.220
L113615Z	_051	2.206	0.095	0.195	0.005	0.324	0.082	0.004	1183	30	1151	29	1153	16	100	1166	49	0.85	0.360
L113615Z	_052	1.405	0.062	0.180	0.005	0.305	0.057	0.003	891	26	1069	27	503	28	212	DISCORDANT			
L113615Z	_053	4.357	0.154	0.319	0.007	0.317	0.099	0.004	1704	29	1783	35	1626	22	110	1732	50	4.42	0.036
L113615Z	_054	0.331	0.020	0.047	0.001	0.253	0.052	0.004	291	15	293	9	333	24	88	293	17	0.03	0.867
L113615Z	_055	4.976	0.274	0.307	0.017	0.506	0.118	0.009	1815	47	1725	84	1753	10	98	1812	93	1.56	0.212
L113615Z	_056a	0.504	0.034	0.067	0.002	0.224	0.054	0.004	414	23	419	12	523	30	80	418	23	0.04	0.841
L113615Z	_056b	15.598	0.336	0.544	0.012	0.508	0.208	0.006	2853	21	2800	50	2762	10	101	2855	41	1.52	0.218
L113615Z	_057	0.820	0.038	0.101	0.003	0.284	0.059	0.003	608	21	621	16	592	23	105	617	29	0.33	0.565
L113615Z	_061	0.475	0.023	0.064	0.001	0.229	0.054	0.003	394	16	401	9	462	30	87	400	16	0.17	0.679
L113615Z	_062	14.084	0.259	0.519	0.010	0.525	0.197	0.005	2755	17	2696	43	2680	13	101	2759	34	2.65	0.103
L113615Z	_063	0.503	0.025	0.067	0.002	0.262	0.055	0.003	414	17	416	11	378	28	110	416	20	0.02	0.887
L113615Z	_065	0.794	0.067	0.098	0.003	0.178	0.059	0.005	593	38	603	17	769	30	78	602	33	0.06	0.803
L113615Z	_066	0.909	0.095	0.123	0.004	0.163	0.053	0.006	656	51	749	24	601	37	125	734	45	3.36	0.067
L113615Z	_067	19.544	0.508	0.594	0.018	0.579	0.239	0.009	3069	25	3006	72	2955	9	102	3076	48	1.07	0.301
L113615Z	_068	0.550	0.028	0.071	0.002	0.268	0.056	0.003	445	18	440	11	471	21	93	441	21	0.07	0.797
L113615Z	_069	0.845	0.056	0.098	0.003	0.236	0.063	0.005	622	31	601	18	710	30	85	605	34	0.43	0.510
L113615Z	_070	0.793	0.046	0.099	0.003	0.283	0.058	0.004	593	26	611	19	553	29	110	605	34	0.42	0.517
L113615Z	_071	1.008	0.043	0.103	0.003	0.347	0.071	0.004	708	22	630	18	790	24	80	DISCORDANT			
L113615Z	_072	14.773	0.557	0.537	0.016	0.407	0.200	0.010	2801	36	2771	69	2716	12	102	2799	71	0.23	0.635
L113615Z	_073	0.836	0.045	0.087	0.003	0.334	0.070	0.004	617	25	539	19	847	15	64	DISCORDANT			
L113615	_001	0.161	0.009	0.024	0.001	0.358	0.049	0.000	152	8	152	6	161	21	95	152	11	0.01	0.927
L113615	_002	14.826	0.226	0.562	0.010	0.555	0.187	0.001	2804	15	2876	39	2712	10	106	2797	29	4.54	0.033

		Measured Isotopic Ratios							Calculated Ages										
Sample	Grain ID	207Pb/235U	1s error	206Pb/238U	1s error	Rho	207Pb/206Pb	1s error	207Pb/235U	1s error	206Pb/238U	1s error	207Pb/206Pb	1s error	U-Pb/Pb-Pb	Concordia	2s error	MSWD	Probability
									Ma	Ma	Ma	Ma	Ma	Ma	concordancy (%)	age (Ma)	Ma	(of concordance)	
L113615	_003	0.370	0.035	0.056	0.002	0.199	0.053	0.001	319	26	353	13	337	35	105	348	25	1.69	0.194
L113615	_004	0.159	0.007	0.023	0.001	0.329	0.050	0.000	150	6	149	4	187	23	80	149	8	0.02	0.888
L113615	_005	0.527	0.021	0.068	0.002	0.423	0.060	0.001	429	14	423	14	598	24	71	426	23	0.18	0.674
L113615	_006	10.333	0.382	0.451	0.015	0.450	0.162	0.001	2465	34	2402	67	2480	10	97	2462	69	1.14	0.286
L113615	_007	0.595	0.028	0.079	0.003	0.427	0.057	0.001	474	18	491	19	504	26	98	482	30	0.75	0.388
L113615	_008	0.832	0.072	0.099	0.008	0.446	0.060	0.001	615	40	611	45	618	33	99	613	72	0.01	0.929
L113615	_009	0.488	0.024	0.070	0.003	0.374	0.053	0.001	403	16	438	15	332	32	132	421	26	3.75	0.053
L113615	_010	0.772	0.015	0.094	0.001	0.330	0.061	0.000	581	8	582	7	639	16	91	582	12	0.01	0.909
L113615	_011	0.147	0.003	0.022	0.000	0.307	0.048	0.000	139	3	140	2	112	18	125	140	3	0.05	0.825
L113615	_012	0.394	0.019	0.055	0.003	0.489	0.054	0.001	337	14	343	16	366	25	94	339	26	0.16	0.691
L113615	_013	12.951	0.862	0.527	0.031	0.448	0.179	0.002	2676	63	2728	133	2644	20	103	2677	125	0.19	0.665
L113615	_014	0.123	0.012	0.022	0.001	0.274	0.058	0.001	118	11	139	7	514	54	27	134	13	3.89	0.049
L113615	_015	15.190	0.194	0.556	0.008	0.585	0.193	0.001	2827	12	2850	34	2772	6	103	2825	23	0.60	0.439
L113615	_016	4.866	0.129	0.307	0.007	0.420	0.115	0.001	1796	22	1728	34	1872	8	92	1783	44	4.66	0.031
L113615	_018	3.927	0.138	0.289	0.011	0.547	0.099	0.001	1619	28	1634	56	1603	18	102	1619	57	0.10	0.747
L113615	_019	0.540	0.016	0.067	0.001	0.334	0.059	0.000	439	11	418	8	554	17	75	424	15	3.57	0.059
L113615	_020	0.373	0.018	0.053	0.002	0.401	0.054	0.001	322	13	335	13	359	23	93	329	22	0.79	0.375
L113615	_022	0.846	0.061	0.107	0.004	0.276	0.067	0.001	622	34	654	25	852	42	77	644	44	0.77	0.380
L113615	_023	0.729	0.034	0.088	0.004	0.512	0.059	0.001	556	20	545	25	581	29	94	553	38	0.24	0.627
L113415Z	_001	0.854	0.043	0.103	0.002	0.231	0.064	0.001	627	23	634	14	730	25	87	633	26	0.08	0.775
L113415Z	_002	0.419	0.021	0.061	0.002	0.268	0.052	0.001	355	15	383	10	272	27	141	376	18	3.35	0.067
L113415Z	_004	0.793	0.036	0.099	0.002	0.250	0.061	0.001	593	20	611	13	655	19	93	607	24	0.76	0.384
L113415Z	_005	1.612	0.059	0.160	0.005	0.393	0.071	0.000	975	23	956	25	952	13	100	967	40	0.47	0.491
L113415Z	_007	0.860	0.038	0.098	0.002	0.252	0.064	0.001	630	21	602	13	739	25	81	607	24	1.74	0.187
L113415Z	_008	0.451	0.031	0.061	0.002	0.179	0.056	0.001	378	22	382	9	437	27	88	382	18	0.05	0.830
L113415Z	_009	0.442	0.019	0.060	0.001	0.272	0.055	0.001	372	13	373	8	426	20	88	373	16	0.01	0.929
L113415Z	_010	0.941	0.044	0.104	0.003	0.309	0.063	0.001	673	23	638	18	714	28	89	649	32	2.04	0.153
L113415Z	_011	0.875	0.023	0.099	0.002	0.423	0.060	0.000	638	12	610	13	608	15	100	625	21	4.32	0.038
L113415Z	_012	0.620	0.017	0.077	0.002	0.426	0.056	0.000	490	10	476	11	449	14	106	483	18	1.58	0.209

		Measured Isotopic Ratios							Calculated Ages										
Sample	Grain ID	207Pb/ 235U	1s error	206Pb /238U	1s error	Rho	207Pb/ 206Pb	1s error	207Pb /235U	1s error	206Pb/238 U	1s error	207Pb/206 Pb	1s error	U-Pb/Pb-Pb	Concordia	2s error	MSWD	Probability
									Ma	Ma	Ma	Ma	Ma	Ma	concordancy (%)	age (Ma)	Ma	(of concordance)	
L113415Z	_013	0.818	0.030	0.096	0.002	0.331	0.060	0.001	607	17	594	14	585	19	101	598	25	0.55	0.459
L113415Z	_014	2.275	0.108	0.214	0.005	0.252	0.081	0.001	1205	34	1253	27	1213	21	103	1234	47	1.67	0.197
L113415Z	_015	0.738	0.031	0.091	0.002	0.243	0.058	0.001	561	18	561	11	532	26	106	561	21	0.00	0.993
L113415Z	_016	3.303	0.151	0.232	0.012	0.560	0.092	0.000	1482	36	1344	62	1475	10	91	1479	71	7.31	0.007
L113415Z	_017	2.198	0.088	0.196	0.006	0.361	0.078	0.001	1180	28	1154	31	1141	14	101	1169	48	0.62	0.431
L113415Z	_018	0.711	0.024	0.087	0.002	0.352	0.058	0.000	545	14	537	12	535	16	100	540	21	0.29	0.593
L113415Z	_019	0.905	0.043	0.102	0.003	0.300	0.061	0.001	655	23	624	17	640	28	97	632	31	1.60	0.205
L113415Z	_020	0.848	0.038	0.100	0.002	0.271	0.061	0.001	623	21	616	14	632	20	97	618	26	0.13	0.721
L113415Z	_021	1.125	0.042	0.113	0.004	0.515	0.066	0.000	765	20	688	25	806	11	85	742	39	11.53	0.001
L113415Z	_022	2.492	0.067	0.209	0.005	0.450	0.081	0.000	1270	19	1222	27	1214	10	101	1258	37	3.63	0.057
L113415Z	_023	0.653	0.021	0.092	0.002	0.328	0.051	0.001	511	13	566	11	262	29	216	DISCORDANT			
L113415Z	_024	0.537	0.017	0.072	0.001	0.306	0.056	0.000	437	11	450	8	435	19	103	446	15	1.25	0.264
L113415Z	_025	0.688	0.031	0.087	0.002	0.298	0.057	0.001	531	18	540	14	505	21	107	537	25	0.20	0.655
L113415Z	_026	10.379	0.249	0.452	0.011	0.488	0.154	0.001	2469	22	2405	47	2396	8	100	2470	44	2.44	0.118
L113415Z	_027	0.498	0.033	0.068	0.002	0.237	0.056	0.001	410	23	423	13	462	24	91	421	25	0.31	0.580
L113415Z	_029	0.774	0.027	0.100	0.002	0.320	0.058	0.001	582	15	615	13	540	22	114	602	23	3.98	0.046
L113415Z	_030	13.267	0.531	0.452	0.019	0.531	0.193	0.001	2699	38	2405	85	2768	9	87	DISCORDANT			
L113415Z	_031	0.891	0.033	0.100	0.003	0.390	0.061	0.000	647	18	613	17	623	14	98	628	29	3.08	0.079
L113415Z	_032	3.046	0.077	0.243	0.005	0.437	0.086	0.001	1419	19	1403	28	1332	14	105	1416	37	0.41	0.521
L113415Z	_033	0.551	0.018	0.072	0.001	0.315	0.057	0.001	445	12	449	9	475	20	94	448	16	0.06	0.803
L113415Z	_035	0.519	0.028	0.069	0.003	0.354	0.056	0.001	424	19	431	16	453	22	95	429	28	0.11	0.738
L113415Z	_036	0.643	0.050	0.078	0.003	0.220	0.062	0.001	504	31	484	16	691	33	70	487	30	0.41	0.520
L113415Z	_037	0.592	0.025	0.071	0.002	0.326	0.059	0.001	472	16	441	12	585	26	75	450	22	3.30	0.069
L113415Z	_038	0.513	0.016	0.065	0.002	0.389	0.055	0.000	421	11	409	10	427	16	96	414	17	1.15	0.284
L113415Z	_039	0.916	0.018	0.104	0.002	0.383	0.061	0.000	660	10	637	9	634	13	100	648	16	4.72	0.030
L113415Z	_040	7.433	0.272	0.348	0.009	0.360	0.140	0.001	2165	33	1924	44	2233	11	86	DISCORDANT			
L113415Z	_042	0.757	0.066	0.094	0.004	0.247	0.059	0.001	573	38	580	24	578	21	100	579	44	0.04	0.841
L113415Z	_043	0.498	0.042	0.067	0.003	0.261	0.056	0.001	410	29	417	18	443	22	94	416	33	0.06	0.807
L113415Z	_044	0.958	0.051	0.122	0.003	0.199	0.063	0.001	682	26	744	15	714	26	104	732	28	5.31	0.021

		Measured Isotopic Ratios							Calculated Ages										
Sample	Grain ID	207Pb/235U	1s error	206Pb/238U	1s error	Rho	207Pb/206Pb	1s error	207Pb/235U	1s error	206Pb/238U	1s error	207Pb/206Pb	1s error	U-Pb/Pb-Pb	Concordia	2s error	MSWD	Probability
									Ma	Ma	Ma	Ma	Ma	Ma	concordancy (%)	age (Ma)	Ma	(of concordance)	
L113415Z	_048	0.978	0.016	0.113	0.002	0.540	0.061	0.000	692	8	690	12	648	10	106	692	16	0.08	0.774
L113415Z	_049	0.894	0.025	0.100	0.003	0.516	0.061	0.000	649	14	613	17	628	11	98	639	26	5.29	0.021
L113415Z	_050	0.835	0.037	0.093	0.003	0.406	0.061	0.001	616	20	573	20	654	22	88	592	34	3.98	0.046
L113415Z	_053	0.770	0.033	0.092	0.003	0.321	0.059	0.001	580	19	566	15	568	24	100	571	27	0.46	0.497
L113415Z	_055	0.572	0.022	0.068	0.002	0.288	0.060	0.001	460	15	426	9	607	25	70	433	18	4.92	0.027
L113415Z	_056	0.522	0.022	0.069	0.002	0.313	0.055	0.001	426	15	427	11	411	23	104	427	20	0.00	0.948
L113415Z	_057	0.824	0.040	0.106	0.003	0.243	0.060	0.001	610	23	652	15	601	24	109	641	27	3.21	0.073
L113415Z	_058	11.816	0.268	0.490	0.012	0.547	0.173	0.001	2590	21	2572	53	2584	9	100	2591	42	0.16	0.691
L113415Z	_061	0.831	0.018	0.100	0.002	0.439	0.060	0.000	614	10	616	11	613	13	100	615	18	0.02	0.880
L113415Z	_062	0.468	0.028	0.066	0.002	0.240	0.056	0.001	390	19	410	11	459	30	89	406	21	1.10	0.294
L113415Z	_063	0.863	0.097	0.100	0.003	0.134	0.078	0.002	632	53	613	18	1139	53	54	614	35	0.12	0.730
L113415Z	_064	0.907	0.029	0.103	0.002	0.347	0.063	0.001	655	16	630	13	697	17	90	640	24	2.31	0.129
L113415Z	_066	0.998	0.054	0.103	0.003	0.312	0.070	0.001	703	28	631	20	924	28	68	650	38	5.99	0.014
L113415Z	_067	0.494	0.033	0.062	0.003	0.390	0.058	0.001	408	22	386	19	531	26	73	394	35	0.87	0.352
L113415Z	_068	0.703	0.041	0.096	0.002	0.212	0.060	0.001	541	25	590	14	598	26	99	580	26	3.87	0.049
L113415Z	_069	2.484	0.048	0.207	0.004	0.567	0.080	0.000	1267	14	1211	24	1191	8	102	1267	28	8.26	0.004
L113415Z	_070	4.092	0.095	0.287	0.008	0.626	0.099	0.001	1653	19	1624	42	1602	10	101	1656	37	0.72	0.397
L113415Z	_074	0.419	0.044	0.078	0.002	0.119	0.058	0.001	355	31	485	12	521	48	93	DISCORDANT			
L113415Z	_076	12.399	0.276	0.495	0.012	0.545	0.177	0.001	2635	21	2591	52	2621	7	99	2639	41	0.99	0.320
L113415Z	_078	0.621	0.059	0.090	0.002	0.135	0.066	0.001	491	37	553	14	798	37	69	547	26	2.96	0.085
L113415Z	_079	0.737	0.037	0.103	0.003	0.274	0.056	0.001	560	22	632	17	439	26	144	607	29	9.43	0.002
L113415Z	_081	0.868	0.051	0.106	0.003	0.232	0.063	0.001	635	27	648	17	709	31	91	645	31	0.23	0.630
L113415Z	_082	3.349	0.071	0.242	0.005	0.475	0.092	0.000	1493	17	1395	25	1476	10	95	DISCORDANT			
L113415Z	_084	0.542	0.017	0.067	0.002	0.441	0.055	0.000	440	11	420	11	431	11	97	430	19	2.82	0.093
L113415Z	_085	2.576	0.051	0.217	0.004	0.507	0.080	0.000	1294	15	1267	23	1209	11	105	1291	29	1.83	0.176
L113415Z	_086	2.675	0.057	0.223	0.005	0.518	0.081	0.000	1322	16	1299	26	1212	10	107	1320	31	1.01	0.314
L113415Z	_087	0.701	0.034	0.091	0.002	0.210	0.060	0.001	539	20	561	11	610	23	92	558	21	1.12	0.289
L113415Z	_088	0.834	0.032	0.099	0.002	0.300	0.060	0.001	616	18	610	14	621	27	98	612	24	0.09	0.765
L113415Z	_089	3.671	0.097	0.270	0.006	0.455	0.093	0.000	1565	21	1539	33	1486	9	104	1561	41	0.75	0.387

		Measured Isotopic Ratios							Calculated Ages										
Sample	Grain ID	207Pb/235U	1s error	206Pb/238U	1s error	Rho	207Pb/206Pb	1s error	207Pb/235U	1s error	206Pb/238U	1s error	207Pb/206Pb	1s error	U-Pb/Pb-Pb	Concordia	2s error	MSWD	Probability
									Ma	Ma	Ma	Ma	Ma	Ma	concordancy (%)	age (Ma)	Ma	(of concordance)	
L113415Z	_090	0.836	0.028	0.100	0.002	0.367	0.060	0.000	617	15	612	14	604	17	101	614	24	0.08	0.778
L113415Z	_091	0.723	0.060	0.091	0.004	0.256	0.060	0.001	552	36	559	23	616	22	91	558	42	0.04	0.848
L113415Z	_092	2.227	0.135	0.195	0.009	0.393	0.079	0.001	1190	42	1150	50	1184	14	97	1175	77	0.59	0.443
L113415Z	_094	2.137	0.117	0.176	0.008	0.426	0.082	0.001	1161	38	1042	45	1257	19	83	1114	71	6.88	0.009
L113415(2)	_001	0.438	0.014	0.060	0.001	0.255	0.054	0.001	369	10	373	6	389	26	96	372	11	0.20	0.658
L113415(2)	_004	0.493	0.010	0.066	0.001	0.330	0.055	0.000	407	7	412	5	403	16	102	411	9	0.54	0.462
L113415(2)	_007	0.666	0.022	0.085	0.002	0.290	0.059	0.000	518	14	526	10	551	17	95	524	18	0.29	0.592
L113415(2)	_008	0.457	0.016	0.060	0.001	0.258	0.056	0.001	382	11	376	7	447	24	84	377	12	0.24	0.621
L113415(2)	_009	2.162	0.057	0.201	0.003	0.281	0.079	0.001	1169	18	1183	16	1170	16	101	1177	27	0.48	0.489
L113415(2)	_010	0.451	0.008	0.061	0.001	0.289	0.055	0.000	378	5	384	4	400	20	96	382	7	0.97	0.325
L113415(2)	_011	0.439	0.017	0.064	0.001	0.193	0.057	0.001	370	12	401	6	492	35	82	397	11	6.91	0.009
L113415(2)	_012	6.660	0.142	0.374	0.006	0.405	0.129	0.001	2067	19	2048	30	2081	7	98	2064	37	0.47	0.495
L113415(2)	_013	0.482	0.013	0.061	0.001	0.282	0.056	0.001	399	9	384	6	456	25	84	388	11	2.61	0.106
L113415(2)	_014	0.533	0.015	0.069	0.001	0.278	0.057	0.001	434	10	428	6	474	21	90	430	12	0.34	0.558
L113415(2)	_015	6.027	0.123	0.354	0.007	0.501	0.121	0.001	1980	18	1951	35	1968	7	99	1979	36	0.90	0.342
L113415(2)	_016	0.591	0.023	0.075	0.002	0.293	0.058	0.001	471	14	463	10	514	26	90	465	18	0.28	0.597
L113415(2)	_017	6.736	0.101	0.380	0.005	0.416	0.128	0.001	2077	13	2078	22	2065	10	101	2078	26	0.00	0.969
L113415(2)	_020	0.897	0.034	0.105	0.002	0.285	0.063	0.001	650	18	642	13	702	28	91	644	24	0.20	0.657
L113415(2)	_021	15.216	0.603	0.542	0.020	0.471	0.200	0.001	2829	38	2791	85	2829	6	99	2829	75	0.26	0.611
L113415(2)	_023	0.815	0.019	0.100	0.001	0.249	0.060	0.000	605	11	614	7	601	16	102	612	12	0.58	0.448
L113415(2)	_025	3.592	0.133	0.265	0.007	0.343	0.101	0.001	1548	29	1518	34	1640	12	93	1536	52	0.68	0.411
L113415(2)	_026	0.867	0.027	0.104	0.001	0.217	0.062	0.001	634	15	639	8	666	24	96	638	15	0.10	0.753
I783255Z	_002	0.680	0.059	0.086	0.004	0.259	0.058	0.001	527	36	533	23	546	31	98	531	43	0.02	0.881
I783255Z	_004	0.641	0.052	0.088	0.003	0.200	0.063	0.001	503	32	542	17	701	29	77	535	32	1.40	0.237
I783255Z	_006	0.822	0.058	0.104	0.004	0.300	0.059	0.001	609	32	640	26	563	27	114	629	45	0.79	0.374
I783255Z	_007	0.503	0.038	0.070	0.002	0.218	0.057	0.001	414	26	434	14	505	29	86	431	26	0.62	0.432
I783255Z	_008	0.802	0.058	0.101	0.003	0.200	0.065	0.001	598	33	623	17	758	25	82	619	32	0.58	0.448
I783255Z	_009	3.793	0.133	0.278	0.009	0.462	0.094	0.001	1591	28	1579	45	1510	11	105	1590	56	0.09	0.762
I783255Z	_010	0.731	0.037	0.088	0.003	0.380	0.059	0.000	557	22	545	20	551	17	99	550	35	0.27	0.606

		Measured Isotopic Ratios							Calculated Ages										
Sample	Grain ID	207Pb/235U	1s error	206Pb/238U	1s error	Rho	207Pb/206Pb	1s error	207Pb/235U	1s error	206Pb/238U	1s error	207Pb/206Pb	1s error	U-Pb/Pb-Pb	Concordia	2s error	MSWD	Probability
									Ma	Ma	Ma	Ma	Ma	Ma	concordancy (%)	age (Ma)	Ma	(of concordance)	
I783255Z	_011	7.087	0.253	0.381	0.015	0.558	0.127	0.001	2122	32	2080	71	2058	10	101	2125	63	0.52	0.471
I783255Z	_013	0.659	0.047	0.075	0.004	0.399	0.060	0.001	514	29	469	26	611	37	77	486	46	2.18	0.140
I783255Z	_014	0.815	0.025	0.090	0.003	0.509	0.061	0.001	605	14	555	16	633	18	88	DISCORDANT			
I783255Z	_015	5.138	0.209	0.334	0.011	0.421	0.107	0.001	1842	35	1857	55	1757	12	106	1845	67	0.08	0.778
I783255Z	_016	2.608	0.094	0.218	0.007	0.416	0.083	0.001	1303	27	1271	35	1279	19	99	1294	50	0.90	0.343
I783255Z	_019	0.708	0.028	0.086	0.003	0.369	0.059	0.000	544	17	533	15	564	16	94	537	26	0.33	0.564
I783255Z	_020	0.539	0.036	0.084	0.002	0.216	0.051	0.001	438	24	520	15	234	37	223	500	27	11.32	0.001
I783255Z	_022	0.787	0.056	0.085	0.005	0.391	0.064	0.001	589	32	528	28	729	25	73	551	50	3.34	0.068
I783255Z	_025	1.350	0.042	0.116	0.005	0.630	0.073	0.001	868	18	708	26	1013	28	70	DISCORDANT			
I783255Z	_026	9.817	0.349	0.428	0.011	0.367	0.152	0.001	2418	33	2298	50	2371	13	97	2392	64	6.04	0.014
I783255Z	_027	0.612	0.017	0.070	0.002	0.586	0.057	0.001	485	10	435	13	497	22	87	DISCORDANT			
I783255Z	_028	3.744	0.311	0.235	0.015	0.386	0.108	0.001	1581	67	1361	79	1763	19	77	1483	125	7.22	0.007
I783255Z	_029	0.771	0.103	0.096	0.007	0.260	0.058	0.001	580	59	593	39	522	43	114	590	72	0.04	0.839
I783255Z	_030	0.524	0.032	0.061	0.002	0.274	0.062	0.001	428	21	385	12	689	25	56	392	24	4.07	0.044
I783255Z	_031	0.556	0.020	0.071	0.002	0.387	0.056	0.000	449	13	441	12	459	18	96	444	21	0.27	0.603
I783255Z	_034	1.756	0.066	0.164	0.006	0.448	0.074	0.001	1029	24	981	30	1050	15	93	1014	45	2.74	0.098
I783255Z	_035	5.686	0.214	0.300	0.010	0.448	0.132	0.001	1929	32	1691	50	2119	14	80	DISCORDANT			
I783255Z	_041	0.880	0.063	0.100	0.004	0.273	0.064	0.001	641	34	612	23	755	34	81	619	42	0.64	0.425
I783255Z	_042	6.339	0.381	0.350	0.015	0.351	0.131	0.001	2024	53	1936	71	2106	18	92	1997	99	1.48	0.223
I783255Z	_043	0.662	0.023	0.080	0.002	0.394	0.059	0.001	516	14	496	13	585	19	85	505	23	1.70	0.192
I783255Z	_044	0.804	0.050	0.098	0.004	0.336	0.061	0.001	599	28	603	24	653	26	92	602	42	0.02	0.881
I783255Z	_045	1.059	0.048	0.119	0.003	0.320	0.065	0.001	733	23	724	20	771	18	94	728	35	0.13	0.714
I783255Z	_046	0.851	0.036	0.099	0.003	0.326	0.063	0.001	625	20	611	16	694	17	88	616	29	0.43	0.512
I783255Z	_049	1.860	0.058	0.186	0.004	0.355	0.082	0.001	1067	21	1102	22	1244	25	89	1082	35	2.07	0.150
I783255Z	_050	0.559	0.052	0.066	0.003	0.221	0.066	0.001	451	34	409	16	802	28	51	414	31	1.47	0.226
I783255Z	_053	0.751	0.025	0.090	0.002	0.411	0.062	0.001	569	14	554	14	657	18	84	562	24	0.87	0.352
I783255Z	_054	2.078	0.074	0.184	0.004	0.333	0.083	0.001	1142	25	1090	24	1265	22	86	1114	40	3.35	0.067
I783255Z	_055	20.460	0.463	0.628	0.015	0.524	0.226	0.001	3113	22	3141	59	3023	8	104	3111	43	0.29	0.589
I783255Z	_060	7.919	0.278	0.415	0.012	0.396	0.135	0.001	2222	32	2236	53	2158	13	104	2224	62	0.09	0.770

		Measured Isotopic Ratios							Calculated Ages										
Sample	Grain ID	207Pb/235U	1s error	206Pb/238U	1s error	Rho	207Pb/206Pb	1s error	207Pb/235U	1s error	206Pb/238U	1s error	207Pb/206Pb	1s error	U-Pb/Pb-Pb	Concordia	2s error	MSWD	Probability
									Ma	Ma	Ma	Ma	Ma	Ma	concordancy (%)	age (Ma)	Ma	(of concordance)	
I783255Z	_063	0.771	0.044	0.099	0.003	0.256	0.063	0.001	580	25	606	17	709	25	85	599	31	0.95	0.331
I783255Z	_064	0.890	0.072	0.102	0.007	0.419	0.062	0.001	646	39	626	41	675	18	93	637	67	0.23	0.633
I783255Z	_066	6.844	0.255	0.373	0.013	0.474	0.131	0.001	2091	33	2045	62	2118	11	97	2089	66	0.73	0.393
I783255Z	_067	0.616	0.028	0.077	0.002	0.321	0.061	0.001	488	17	476	13	651	23	73	480	24	0.39	0.530
I783255Z	_068	6.799	0.342	0.375	0.015	0.408	0.130	0.001	2086	45	2051	72	2092	11	98	2080	87	0.26	0.609
I783255Z	_069	2.432	0.176	0.210	0.012	0.395	0.083	0.001	1252	52	1230	64	1270	26	97	1245	95	0.11	0.737
I783255Z	_072	1.075	0.058	0.093	0.002	0.210	0.079	0.002	741	28	576	13	1160	38	50	DISCORDANT			
I783255Z	_073	0.883	0.047	0.105	0.003	0.283	0.063	0.001	643	25	645	18	693	23	93	645	33	0.01	0.916
I783255Z	_074	3.933	0.212	0.280	0.013	0.419	0.101	0.001	1621	44	1593	64	1645	13	97	1615	84	0.21	0.644
I783255Z	_075	0.754	0.063	0.101	0.004	0.235	0.059	0.001	571	37	620	23	569	27	109	608	43	1.68	0.195
I783255Z	_076	0.671	0.020	0.071	0.002	0.496	0.059	0.001	521	12	445	13	556	26	80	DISCORDANT			
I783255Z	_077	0.572	0.024	0.070	0.002	0.340	0.062	0.001	459	15	438	12	670	26	65	445	22	1.76	0.185
I783255Z	_078	4.942	0.182	0.319	0.012	0.507	0.108	0.001	1810	31	1783	58	1760	11	101	1809	62	0.27	0.600
I783255Z	_079	0.698	0.032	0.087	0.002	0.305	0.061	0.001	538	19	539	15	622	30	87	538	26	0.00	0.968
I783255Z	_084	0.896	0.036	0.099	0.003	0.323	0.068	0.001	650	19	608	15	858	18	71	621	27	4.27	0.039
I783255Z	_087	0.490	0.070	0.072	0.002	0.092	0.069	0.001	405	48	448	11	898	43	50	446	23	0.84	0.360
I783255Z	_088	0.798	0.031	0.095	0.002	0.327	0.061	0.001	596	17	587	14	649	19	90	590	25	0.24	0.624
I783255Z	_090	3.012	0.099	0.235	0.006	0.420	0.089	0.001	1411	25	1359	34	1404	12	97	1397	48	2.49	0.115
I783255Z	_092	0.643	0.026	0.075	0.001	0.243	0.063	0.001	504	16	466	9	711	31	66	471	17	5.49	0.019
I783255Z	_094	0.568	0.028	0.076	0.002	0.309	0.057	0.001	457	18	470	14	490	21	96	465	25	0.44	0.509
I783255Z	_095	0.895	0.064	0.109	0.005	0.292	0.062	0.001	649	34	669	27	673	27	100	663	47	0.30	0.585
I783255Z	_096	0.535	0.023	0.068	0.003	0.430	0.055	0.001	435	15	425	15	423	24	101	430	26	0.36	0.550
I783255Z	_097	0.820	0.071	0.097	0.003	0.187	0.077	0.001	608	40	597	19	1131	32	53	598	36	0.07	0.789
I783255Z	_098	0.801	0.066	0.100	0.005	0.300	0.063	0.001	598	37	615	29	693	22	89	609	52	0.19	0.661
I783255Z	_099	0.524	0.030	0.065	0.002	0.307	0.072	0.001	428	20	409	14	976	35	42	413	26	0.86	0.354
I783255Z	_100	2.436	0.038	0.205	0.004	0.561	0.085	0.000	1253	11	1200	19	1322	8	91	DISCORDANT			
I783255Z	_101	2.490	0.048	0.210	0.004	0.481	0.080	0.000	1269	14	1231	21	1204	10	102	1263	27	4.35	0.037
I78_3255	_098	0.914	0.067	0.102	0.005	0.353	0.070	0.001	659	36	628	31	923	34	68	640	55	0.64	0.423
I78_3255	_002	0.901	0.077	0.104	0.012	0.695	0.071	0.001	652	41	637	72	951	29	67	654	81	0.08	0.775

		Measured Isotopic Ratios							Calculated Ages										
Sample	Grain ID	207Pb/235U	1s error	206Pb/238U	1s error	Rho	207Pb/206Pb	1s error	207Pb/235U	1s error	206Pb/238U	1s error	207Pb/206Pb	1s error	U-Pb/Pb-Pb	Concordia	2s error	MSWD	Probability
									Ma	Ma	Ma	Ma	Ma	Ma	concordancy (%)	age (Ma)	Ma	(of concordance)	
I782175Z	_001	0.949	0.033	0.105	0.003	0.387	0.064	0.001	677	17	641	17	750	23	85	657	28	3.66	0.056
I782175Z	_002	3.201	0.166	0.235	0.010	0.413	0.097	0.001	1457	40	1361	53	1565	17	87	1428	76	3.57	0.059
I782175Z	_003	10.343	0.359	0.441	0.015	0.489	0.162	0.002	2466	32	2354	67	2479	19	95	2466	64	3.76	0.053
I782175Z	_005	1.650	0.186	0.102	0.004	0.170	0.098	0.004	989	71	626	23	1590	69	39	DISCORDANT			
I782175Z	_008	7.349	0.155	0.382	0.011	0.691	0.130	0.001	2155	19	2086	52	2095	15	100	2168	34	2.80	0.094
I782175Z	_009	0.918	0.026	0.103	0.003	0.485	0.062	0.000	661	14	632	16	659	17	96	652	25	3.59	0.058
I782175Z	_010	1.632	0.113	0.152	0.009	0.422	0.074	0.001	983	44	911	50	1052	27	87	953	79	2.03	0.154
I782175Z	_012	0.756	0.044	0.094	0.004	0.324	0.061	0.001	572	26	580	21	644	25	90	577	37	0.09	0.759
I782175Z	_013	0.851	0.058	0.098	0.005	0.350	0.066	0.001	625	32	602	28	818	21	74	611	49	0.44	0.509
I782175Z	_014	4.691	0.229	0.281	0.011	0.390	0.122	0.001	1766	41	1594	54	1986	14	80	DISCORDANT			
I782175Z	_015	1.079	0.062	0.099	0.004	0.333	0.080	0.001	743	30	611	22	1186	29	52	DISCORDANT			
I782175Z	_018	0.587	0.034	0.077	0.004	0.454	0.058	0.001	469	22	477	24	533	31	90	472	39	0.12	0.730
I782175Z	_020	0.906	0.066	0.106	0.004	0.251	0.067	0.001	655	35	648	23	843	38	77	649	42	0.04	0.847
I782175Z	_022	1.245	0.565	0.203	0.009	0.047	0.105	0.004	821	255	1192	46	1722	75	69	1175	90	2.94	0.086
I782175Z	_023	2.423	0.373	0.239	0.009	0.124	0.115	0.003	1249	111	1384	48	1886	40	73	1364	90	1.51	0.220
I782175Z	_025	0.839	0.044	0.095	0.004	0.443	0.062	0.001	618	24	584	26	682	28	86	603	43	1.68	0.194
I782175Z	_026	0.821	0.041	0.098	0.004	0.420	0.061	0.001	609	23	603	24	640	28	94	606	40	0.05	0.832
I782175Z	_029	0.563	0.023	0.070	0.002	0.405	0.055	0.000	454	15	435	14	431	13	101	443	25	1.35	0.246
I782175Z	_031	5.604	0.187	0.351	0.010	0.418	0.115	0.001	1917	29	1937	47	1874	16	103	1920	56	0.22	0.638
I782175Z	_032	2.511	0.104	0.204	0.006	0.360	0.087	0.001	1275	30	1196	33	1361	16	88	1238	53	4.83	0.028
I782175Z	_033	0.863	0.023	0.101	0.002	0.329	0.060	0.000	632	12	619	10	616	17	101	624	18	0.88	0.347
I782175Z	_034	1.135	0.029	0.119	0.003	0.425	0.065	0.000	770	14	724	15	775	12	93	749	24	8.85	0.003
I782175Z	_037	5.864	0.343	0.325	0.012	0.303	0.129	0.001	1956	51	1815	56	2083	11	87	1889	89	4.87	0.027
I782175Z	_039	0.848	0.024	0.095	0.002	0.356	0.060	0.000	624	13	588	11	609	17	97	601	20	6.65	0.010
I782175Z	_040	0.748	0.138	0.094	0.004	0.103	0.063	0.001	567	80	582	21	699	36	83	581	42	0.03	0.859
I782175Z	_041	1.824	0.052	0.171	0.004	0.369	0.075	0.001	1054	19	1018	20	1058	14	96	1037	32	2.74	0.098
I782175Z	_042	1.079	0.203	0.105	0.020	0.506	0.068	0.001	743	99	646	117	875	29	74	707	188	0.80	0.372
I782175Z	_043	0.453	0.029	0.061	0.002	0.211	0.058	0.001	379	20	384	10	522	31	73	383	19	0.05	0.825
I782175Z	_044	2.372	0.046	0.201	0.003	0.443	0.082	0.000	1234	14	1178	18	1238	10	95	DISCORDANT			

		Measured Isotopic Ratios							Calculated Ages										
Sample	Grain ID	207Pb/235U	1s error	206Pb/238U	1s error	Rho	207Pb/206Pb	1s error	207Pb/235U	1s error	206Pb/238U	1s error	207Pb/206Pb	1s error	U-Pb/Pb-Pb	Concordia	2s error	MSWD	Probability
									Ma	Ma	Ma	Ma	Ma	Ma	concordancy (%)	age (Ma)	Ma	(of concordance)	
I782175Z	_046	0.618	0.048	0.069	0.007	0.651	0.061	0.001	489	30	432	42	631	23	69	484	60	3.13	0.077
I782175Z	_047	0.835	0.029	0.099	0.002	0.283	0.062	0.001	616	16	608	11	684	18	89	610	21	0.24	0.625
I782175Z	_049	10.322	0.577	0.371	0.018	0.445	0.196	0.005	2464	52	2034	87	2795	45	73	DISCORDANT			
I782175Z	_050	20.434	1.542	0.496	0.012	0.162	0.271	0.007	3112	73	2597	52	3313	38	78	DISCORDANT			
I782175Z	_051	0.750	0.030	0.090	0.003	0.400	0.061	0.001	569	18	553	17	631	28	88	560	29	0.68	0.408
I782175Z	_052	2.492	0.070	0.210	0.005	0.448	0.082	0.001	1270	20	1231	28	1236	14	100	1261	39	2.16	0.142
I782175Z	_054	0.860	0.045	0.104	0.002	0.229	0.062	0.001	630	24	637	15	677	24	94	636	27	0.08	0.772
I782175Z	_056	1.168	0.112	0.098	0.002	0.124	0.093	0.003	786	53	601	14	1485	56	40	DISCORDANT			
I782175Z	_057	0.539	0.021	0.067	0.002	0.415	0.056	0.001	438	14	420	13	461	27	91	428	23	1.51	0.219
I782175Z	_058	0.747	0.087	0.092	0.004	0.174	0.063	0.001	566	51	566	22	701	29	81	566	43	0.00	1.000
I782175Z	_059	0.695	0.021	0.069	0.001	0.267	0.068	0.001	536	13	428	7	857	29	50	DISCORDANT			
I782175Z	_061	5.049	0.121	0.312	0.008	0.510	0.109	0.001	1828	20	1750	37	1786	10	98	1825	41	5.87	0.015
I782175Z	_062	7.508	0.154	0.398	0.009	0.533	0.127	0.001	2174	18	2158	40	2060	9	105	2175	37	0.23	0.632
I782175Z	_065	14.530	0.365	0.537	0.012	0.443	0.183	0.001	2785	24	2772	50	2678	8	104	2785	48	0.08	0.773
I782175Z	_066	0.634	0.020	0.067	0.002	0.421	0.061	0.001	499	13	421	11	623	25	68	DISCORDANT			
I782175Z	_067	0.792	0.025	0.093	0.002	0.380	0.060	0.001	592	14	574	13	611	20	94	582	23	1.49	0.222
I782175Z	_068	0.868	0.054	0.101	0.004	0.299	0.062	0.001	634	29	621	22	671	18	92	625	40	0.19	0.661
I782175Z	_069	4.860	0.113	0.310	0.007	0.463	0.109	0.001	1795	20	1739	33	1779	10	98	1789	39	3.75	0.053
I782175Z	_070	2.406	0.158	0.207	0.011	0.388	0.081	0.000	1245	47	1213	56	1228	12	99	1233	85	0.30	0.586
I782175Z	_071	14.940	0.289	0.534	0.011	0.541	0.189	0.001	2811	18	2758	47	2735	8	101	2816	36	1.78	0.182
I782175Z	_072	4.672	0.115	0.263	0.006	0.453	0.122	0.001	1762	21	1507	30	1979	9	76	DISCORDANT			
I782175Z	_074	7.111	0.156	0.384	0.008	0.498	0.128	0.001	2125	20	2094	39	2070	10	101	2125	39	0.83	0.361
I782175Z	_075	1.140	0.046	0.112	0.003	0.280	0.071	0.001	773	22	686	15	957	26	72	DISCORDANT			
I782175Z	_076	8.529	0.224	0.428	0.010	0.457	0.136	0.001	2289	24	2295	46	2177	8	105	2289	48	0.02	0.879
I782175Z	_077	15.621	0.282	0.554	0.009	0.444	0.195	0.001	2854	17	2842	37	2785	7	102	2854	34	0.12	0.724
H285025Z	_001	0.845	0.053	0.097	0.005	0.414	0.060	0.001	622	29	596	30	617	31	97	609	50	0.67	0.415
H285025Z	_002	15.593	0.451	0.543	0.014	0.453	0.203	0.002	2852	28	2796	59	2847	13	98	2852	55	1.16	0.282
H285025Z	_004	0.538	0.030	0.068	0.003	0.371	0.057	0.001	437	20	424	17	487	28	87	429	30	0.40	0.529
H285025Z	_005	0.382	0.027	0.057	0.002	0.261	0.055	0.001	328	20	356	13	410	31	87	349	23	1.92	0.165

		Measured Isotopic Ratios							Calculated Ages										
Sample	Grain ID	207Pb/235U	1s error	206Pb/238U	1s error	Rho	207Pb/206Pb	1s error	207Pb/235U	1s error	206Pb/238U	1s error	207Pb/206Pb	1s error	U-Pb/Pb-Pb	Concordia	2s error	MSWD	Probability
									Ma	Ma	Ma	Ma	Ma	Ma	concordancy (%)	age (Ma)	Ma	(of concordance)	
H285025Z	_008	0.444	0.031	0.066	0.002	0.236	0.056	0.001	373	22	413	13	466	32	89	404	24	3.31	0.069
H285025Z	_010	0.521	0.022	0.069	0.002	0.367	0.056	0.001	426	14	428	13	456	25	94	427	22	0.03	0.874
H285025Z	_011	0.942	0.057	0.058	0.004	0.621	0.124	0.005	674	30	365	26	2009	70	18	DISCORDANT			
H285025Z	_012	0.366	0.020	0.033	0.002	0.593	0.076	0.001	316	15	212	14	1100	25	19	DISCORDANT			
H285025Z	_013	0.493	0.037	0.070	0.003	0.291	0.054	0.001	407	25	434	18	373	30	116	426	33	1.08	0.298
H285025Z	_015	4.886	0.157	0.311	0.009	0.464	0.110	0.001	1800	27	1748	46	1805	15	97	1795	54	1.63	0.202
H285025Z	_016	0.548	0.020	0.064	0.002	0.519	0.059	0.001	443	13	397	15	553	23	72	425	24	11.45	0.001
H285025Z	_018	0.530	0.033	0.071	0.004	0.420	0.055	0.001	432	22	440	23	398	40	110	436	38	0.11	0.740
H285025Z	_019	1.809	0.090	0.188	0.006	0.300	0.074	0.001	1049	32	1111	30	1046	26	106	1082	50	2.87	0.090
H285025Z	_020	0.478	0.026	0.068	0.002	0.273	0.056	0.001	396	18	426	12	451	30	95	418	22	2.57	0.109
H285025Z	_021	1.705	0.104	0.183	0.007	0.299	0.073	0.001	1010	39	1084	37	1006	26	108	1049	60	2.75	0.097
H285025Z	_022	0.848	0.041	0.107	0.003	0.302	0.062	0.001	624	22	653	18	676	24	97	642	32	1.47	0.225
H285025Z	_023	1.136	0.078	0.097	0.003	0.203	0.087	0.002	771	37	595	16	1354	48	44	606	31	19.42	0.000
H285025Z	_024	0.612	0.036	0.053	0.002	0.356	0.084	0.002	485	23	335	14	1299	57	26	351	27	40.92	0.000
H285025Z	_025	5.339	0.120	0.329	0.007	0.484	0.114	0.001	1875	19	1831	35	1861	14	98	1873	38	2.09	0.149
H285025Z	_026	2.643	0.176	0.199	0.013	0.502	0.094	0.001	1313	49	1170	72	1502	14	78	1286	98	5.14	0.023
H285025Z	_027	0.832	0.034	0.099	0.004	0.447	0.061	0.001	615	19	609	21	635	21	96	613	34	0.07	0.793
H285025Z	_028	0.841	0.034	0.104	0.003	0.384	0.062	0.001	620	19	636	19	663	22	96	628	31	0.59	0.444
H285025Z	_029	4.929	0.235	0.324	0.017	0.560	0.106	0.001	1807	40	1807	84	1724	15	105	1807	80	0.00	0.998
H285025Z	_030	5.089	0.187	0.336	0.010	0.399	0.111	0.001	1834	31	1869	48	1813	16	103	1840	60	0.59	0.442
H285025Z	_031	0.477	0.030	0.069	0.002	0.275	0.054	0.001	396	21	430	14	376	29	114	420	26	2.41	0.120
H285025Z	_033	0.751	0.037	0.095	0.004	0.392	0.062	0.001	569	21	583	21	680	30	86	576	36	0.39	0.530
H285025Z	_034	0.546	0.126	0.067	0.003	0.086	0.097	0.003	442	83	419	16	1564	58	27	420	32	0.08	0.780
H285025Z	_035	1.857	0.069	0.181	0.005	0.382	0.076	0.001	1066	24	1074	28	1092	18	98	1069	43	0.08	0.776
H285025Z	_036	0.735	0.035	0.101	0.003	0.288	0.059	0.001	559	21	618	16	579	31	107	597	28	7.05	0.008
H285025Z	_037	0.087	0.007	0.015	0.001	0.252	0.050	0.001	85	6	93	4	172	40	54	92	7	1.69	0.193
H285025Z	_038	0.537	0.026	0.066	0.003	0.430	0.058	0.001	436	17	414	17	522	24	79	425	29	1.45	0.228
H285025Z	_040	0.508	0.013	0.067	0.001	0.392	0.056	0.000	417	9	419	8	434	16	97	418	14	0.08	0.783
H285025Z	_043	2.165	0.141	0.189	0.009	0.364	0.096	0.001	1170	45	1117	49	1540	29	73	1145	78	1.00	0.318

		Measured Isotopic Ratios							Calculated Ages										
Sample	Grain ID	207Pb/235U	1s error	206Pb/238U	1s error	Rho	207Pb/206Pb	1s error	207Pb/235U	1s error	206Pb/238U	1s error	207Pb/206Pb	1s error	U-Pb/Pb-Pb	Concordia	2s error	MSWD	Probability
									Ma	Ma	Ma	Ma	Ma	Ma	concordancy (%)	age (Ma)	Ma	(of concordance)	
H285025Z	_044	3.553	0.151	0.273	0.010	0.422	0.093	0.001	1539	34	1556	50	1480	20	105	1542	65	0.13	0.722
H285025Z	_045	0.672	0.028	0.083	0.003	0.398	0.058	0.001	522	17	511	16	515	21	99	516	28	0.36	0.549
H285025Z	_046	0.936	0.051	0.103	0.004	0.349	0.064	0.001	671	27	633	23	745	20	85	647	41	1.69	0.193
H285025Z	_047	0.856	0.026	0.103	0.002	0.343	0.060	0.000	628	14	630	13	615	16	102	629	22	0.01	0.915
H285025Z	_048	4.275	0.147	0.293	0.010	0.491	0.100	0.001	1689	28	1656	49	1627	13	102	1686	57	0.57	0.449
H285025Z	_049	0.593	0.022	0.060	0.002	0.505	0.068	0.001	473	14	376	14	868	28	43	DISCORDANT			
H285025Z	_050	0.526	0.033	0.059	0.003	0.409	0.062	0.001	429	22	367	18	675	34	54	387	34	7.68	0.006
H285025Z	_051	0.637	0.063	0.042	0.003	0.353	0.135	0.003	500	39	267	18	2168	39	12	DISCORDANT			
H285025Z	_052	0.892	0.218	0.098	0.004	0.088	0.109	0.004	647	117	602	25	1776	61	34	603	49	0.14	0.704

Appendix 5: Qualitative Detrital Zircon Data

Legend:

S. Area: Cross-sectional area, measured in μm^2.

AR: Aspect ratio, measured as the ratio of length/width (in μm).

Morph: Grain morphology:

- **Eh:** Euhedral
- **Sh:** Subhedral
- **Ang:** Angular
- **Sba:** Sub-angular
- **Sbr:** Sub-rounded
- **Rnd:** Rounded
- **Bk:** Broken, inferred as broken during drilling or sample preparation.

Zoning: Growth zoning of zircon crystals, as determined by scanning electron microscope in back-scattered electron mode.

- **Oc, ct:** Oscillatory, concentric.
- **Oc, pl:** Oscillatory, planar.
- **Sec:** Sector zoning.
- **Ot:** Other zoning, mainly convoluted or irregular zoning types.
- **Unz:** Unzoned.
- **Sec+Oc:** Sector and oscillatory zoning.

Conc age: Concordia age, in Ma.

2σ: 2-sigma error of Concordia age, in Ma.

Th: Thorium concentration, in ppm.

U: Uranium concentration, in ppm.

Th/U: Ratio of Th (ppm)/ U (ppm).

Sample	Grain ID	S. area	AR	Morph	Zoning	Conc age	2σ	Th	U	Th/U
L113760Z	_003	23929	1.227	ang/bk	unz	2616	33	152	201	0.757
L113760Z	_006	18164	1.194	ang/bk	oc, pl	411	21	111	115	0.964
L113760Z	_007	20053	1.130	sba-sbr	sec+oc, ocn	467	18	270	308	0.877
L113760Z	_008	29260	1.688	sbr-rnd	oc, ct, ocn	961	27	55	86	0.640
L113760Z	_009	23305	1.359	sbr	oc, ct, ocn	1132	18	58	157	0.371
L113760Z	_010	17317	1.409	sba	ot	1122	27	25	55	0.456
L113760Z	_011	18593	1.068	ang/bk	unz	407	10	239	266	0.899
L113760Z	_012	16287	1.228	sba	unz	577	16	83	94	0.878
L113760Z	_013	19084	1.730	sba-sbr	oc, ct, ocn	1016	19	59	162	0.366
L113760Z	_014	9960	1.052	sh/sbr	oc, ct, ocn	521	18	41	67	0.609
L113760Z	_015	9918	1.284	sh	oc, ct, cn	3657	35	67	108	0.617
L113760Z	_017	13866	1.346	sba	oc, ct, cn	415	14	265	309	0.858
L113760Z	_018	11780	1.081	sbr	oc, ct, ocn	1663	26	64	164	0.394
L113760Z	_020	11077	1.477	sbr-sba	ot	420	12	185	325	0.569
L113760Z	_021	12825	1.706	sba	ot	396	13	2	541	0.004
L113760Z	_022	7539	1.287	ang/bk	unz	2800	31	15	70	0.209
L113760Z	_023	9720	1.346	sbr	ot	974	18	59	122	0.479
L113760Z	_026	12620	1.062	sba	oc, ct, ocn	2757	36	57	53	1.065
L113760Z	_030	8364	1.090	sbr	sec	406	13	206	299	0.691
L113760Z	_031	2846	1.103	ang	oc, ct, ocn	580	19	177	290	0.610
L113760Z	_032	7057	1.130	sbr	oc, ct, ocn	1670	43	39	49	0.793
L113760Z	_033	9489	1.522	sbr	sec+oc, ocn	411	14	124	247	0.504
L113760Z	_034	8254	2.125	sh	ot	568	17	74	91	0.812
L113760Z	_035	9880	1.200	sba	oc, ct, ocn	2025	39	74	216	0.340
L113760Z	_037	8577	1.574	ang/ sh	oc, ct, ocn	2738	32	23	34	0.686
L113760Z	_038	5320	1.250	sbr	oc, pl	1043	25	86	157	0.550
L113760Z	_039	3937	1.176	eh/bk	sec+oc	637	17	253	328	0.772
L113760Z	_042	4864	1.330	sh	oc, ct, ocn	1946	33	84	252	0.333
L113760Z	_043	5772	1.382	sba	unz	1168	49	16	35	0.459
L113760Z	_044	9207	1.240	rnd	ot	682	26	313	296	1.057
L113760Z	_045	8045	1.291	sbr	sec	855	17	73	120	0.603
L113760Z	_048	4967	1.073	eh	sec+oc, ocn	421	16	302	349	0.866
L113760Z	_049	6779	1.747	sbr	unz	616	30	44	61	0.714
L113760Z	_050	4582	1.300	eh	oc, ct, ocn	416	12	143	453	0.316
L113760Z	_051	8280	1.323	eh	sec+oc, ocn	596	17	101	135	0.750
L113760Z	_055	5305	1.244	sbr	ot	1215	40	27	134	0.203
L113760Z	_057	2645	1.030	sh	oc, ct, ocn	1306	33	122	185	0.659
L113760Z	_062	10359	1.202	sbr	oc, ct, ocn	412	10	65	136	0.479
L113760Z	_069	3156	1.098	sba	unz	472	15	202	247	0.816
L113760Z	_072	8462	1.630	ang	oc, pl	411	9	131	190	0.687
L113760Z	_073	3126	1.056	rnd	sec+oc, ocn	1831	22	45	111	0.404
L113760Z	_079	2364	1.130	ang	ot	403	19	300	577	0.519
L113760Z	_082	4416	1.320	eh	oc, ct, cn	293	9	64	155	0.413
L113760Z	_083	5132	1.340	sbr	oc, ct, ocn	1800	27	139	141	0.991

Sample	Grain ID	S. area	AR	Morph	Zoning	Conc age	2σ	Th	U	Th/U
L113760Z	_087	10116	2.110	sbr	ot	1622	22	124	131	0.949
L113760Z	_091	6304	1.986	rnd	oc, ct, cn	546	13	46	108	0.423
L113760Z	_092	4150	1.382	sbr	ot	963	26	45	147	0.305
L113760Z	_095	7611	1.202	sbr	oc, ct, ocn	1002	21	84	357	0.235
L113760Z	_096	3382	1.267	sbr	oc, ct, ocn	1478	30	101	303	0.332
L113760Z	_098	7585	1.126	eh	oc, ct, ocn	575	18	139	141	0.991
L113760Z	_099	4473	1.563	sh	oc, ct, ocn	592	22	191	270	0.706
L113760Z	_101	6167	1.691	sbr-sba	oc, pl	538	14	202	147	1.368
L113760Z	_102	7524	1.512	sbr	sec	2022	33	124	172	0.722
L113760Z	_103	8683	1.833	ang	sec+oc, cn	416	12	125	158	0.792
L113760Z	_105	4625	1.324	sh	oc, ct, cn	142	7	91	137	0.665
L113760Z	_106	4716	1.343	ang/sh	oc, ct, ocn	585	16	117	235	0.497
L113760Z	_107	8185	1.350	sba	ot	913	23	32	38	0.847
L113760Z	_109	19182	1.037	rnd	ot	597	17	115	129	0.893
L113760Z	_111	10435	1.108	sh	oc, ct, cn	571	16	149	208	0.717
L113760Z	_113	7349	2.230	eh	oc, ct, ocn	413	14	48	164	0.292
L113760Z	_114	10161	1.275	ang-sba	sec+oc, ocn	395	9	558	624	0.894
L113760Z	_118	8615	1.724	sba	oc, ct, ocn	1065	21	126	360	0.349
L113760Z	_120	9432	1.243	ang	oc, ct, cn	733	16	118	362	0.326
L113760Z	_121	12335	1.250	eh	oc, ct, cn	409	23	184	157	1.170
L113615Z	_001	39648	1.408	sh, sba/bk	oc, ct, ocn	620	54	88	105	0.840
L113615Z	_003	32788	1.184	sba-sbr	ot	645	28	89	103	0.867
L113615Z	_004	24514	1.118	eh, bk	oc, ct, ocn	152	10	376	442	0.851
L113615Z	_005	37072	1.461	sbr	oc, pl	397	31	58	128	0.454
L113615Z	_006	31066	1.356	eh-sh, bk	sec+oc	432	20	100	126	0.789
L113615Z	_007	53578	1.427	sbr	oc, pl	587	28	71	100	0.716
L113615Z	_008	20370	1.374	eh-sh	oc, ct, cn	666	32	172	179	0.962
L113615Z	_009	17080	1.458	ang-sba	oc, ct, ocn	2223	90	34	108	0.318
L113615Z	_010	14056	1.03	ang-sba	ot	1894	67	28	82	0.344
L113615Z	_011	25060	1.035	ang	unz	656	36	26	41	0.644
L113615Z	_012	19334	1.123	sba-sbr	sec, cn	1922	53	168	151	1.115
L113615Z	_013	17066	1.281	sbr	oc, ct, ocn	619	30	52	71	0.737
L113615Z	_014	32130	1.27	eh-sh,/bk	sec, cn	434	25	376	308	1.219
L113615Z	_015	22358	1.313	eh-sh,/bk	oc, ct, cn	634	29	91	113	0.801
L113615Z	_017	11648	1.309	rnd	oc, ct, ocn	1377	34	41	83	0.494
L113615Z	_018	11928	1.632	sba	oc, ct, ocn	1303	38	41	230	0.180
L113615Z	_019	13034	1.688	eh, bk	oc, ct, ocn	445	18	163	252	0.650
L113615Z	_021	9954	1.286	sbr,bk	unz	1907	50	41	97	0.425
L113615Z	_022	10066	1.521	sba,bk	ot	629	33	77	105	0.728
L113615Z	_023	17136	1.252	ang-sba	sec, ocn	638	25	47	72	0.654
L113615Z	_024	20944	1.441	sba-ang/bk	oc, ct, cn	551	20	92	274	0.335
L113615Z	_025	12376	1.158	sbr/bk	oc, ct, ocn	428	25	110	190	0.579
L113615Z	_026	6580	1.174	sh/bk	ot	1167	32	27	181	0.148
L113615Z	_030	25592	1.503	ang/bk	oc, ct, ocn	139	13	49	81	0.606
L113615Z	_031	10486	1.312	rnd, bk	oc, ct, ocn	590	34	66	140	0.476

Sample	Grain ID	S. area	AR	Morph	Zoning	Conc age	2σ	Th	U	Th/U
L113615Z	_034	8190	1.079	sbr-rnd	oc, ct, ocn	556	40	67	136	0.491
L113615Z	_035	6342	1.217	ang	ot	626	26	68	173	0.393
L113615Z	_036	8414	1.333	sbr, bk	ot	2623	54	17	32	0.527
L113615Z	_037	6118	1.707	sh/bk	oc, pl	2086	65	70	165	0.427
L113615Z	_038	23114	1.667	sba-sbr	oc, ct, ocn, xc	410	26	54	95	0.569
L113615Z	_039	22680	1.487	sba	oc, ct, ocn	372	31	52	83	0.619
L113615Z	_040	5320	1	sbr-rnd	oc, ct, ocn	1633	31	63	152	0.411
L113615Z	_042	7308	1.57	sba-sbr,bk	oc, ct, ocn	2015	37	49	168	0.289
L113615Z	_043	11578	1.39	sbr	ot	1345	60	25	25	1.013
L113615Z	_044	13454	1.061	ang	unz	618	23	77	70	1.096
L113615Z	_045	24304	1	sba-ang/bk	ot	427	28	70	93	0.755
L113615Z	_046	14588	1.049	eh, bk	oc, ct, cn	136	12	51	108	0.476
L113615Z	_050	9618	1.062	ang	oc, pl	570	26	61	174	0.353
L113615Z	_051	11802	1.275	sbr	oc, ct, ocn	1166	49	77	194	0.395
L113615Z	_053	7854	1.04	sba-sbr,bk	unz	1732	51	9	22	0.426
L113615Z	_054	8526	1.319	sh	oc, ct, cn	293	17	224	436	0.513
L113615Z	_055	7084	1.746	sba-sbr	oc, pl	1812	93	71	305	0.233
L113615Z	_056a	8540	1.224	eh-sh	oc, ct, cn	418	23	71	305	0.233
L113615Z	_056b	4004	1.113	sbr-rnd,bk		2855	41	90	103	0.867
L113615Z	_057	6188	1.314	sh/bk	unz	617	29	84	85	0.982
L113615Z	_061	5852	1.047	eq-elp, sh	oc, ct, ocn	400	16	108	182	0.592
L113615Z	_062	7210	1.031	sba-sbr	sec+oc	2759	35	19	70	0.265
L113615Z	_063	7728	1.314	sba-ang	oc, ct, ocn	416	20	127	221	0.572
L113615Z	_065	33460	1.479	sh/bk	sec+oc	602	33	105	155	0.675
L113615Z	_066	24402	1.259	sbr-rnd	oc, pl, ocn	734	45	29	82	0.356
L113615Z	_067	20734	1.123	sba-sbr	sec+oc	3076	48	62	92	0.680
L113615Z	_068	12306	1.376	sba-sbr	oc, pl	441	21	189	337	0.560
L113615Z	_069	8526	1.319	ang-sba	oc, ct, ocn	605	34	143	201	0.713
L113615Z	_070	17150	1.1	sh	ot	605	34	21	58	0.356
L113615Z	_072	26642	1.12	eq, ang	oc, pl	2799	71	73	69	1.061
L113615	_011	6346	1.064	ang/bk	oc, pl	140	2	2567	1123	2.285
L113615	_001	36246	1.323	ang/bk	oc, cn, ocn	152	11	867	991	0.874
L113615	_002	17081	1.514	eh/bk	ot	2798	29	103	83	1.247
L113615	_003	15023	1.335	eh-sh	oc, ct, cn	348	25	50	99	0.504
L113615	_004	9021	1.239	eh	sec+oc, cn	149	8	576	724	0.796
L113615	_005	8849	1.143	sh/sbr	oc, ct, cn	426	23	102	167	0.613
L113615	_006	8644	1.5	sbr	oc, ct, cn	2462	69	108	515	0.211
L113615	_007	8026	1.333	sba	ot	482	30	46	130	0.354
L113615	_008	6620	1.287	ang-sba	sec, cn	613	72	85	116	0.736
L113615	_009	6757	1.745	sh, bk	ot	421	26	59	81	0.727
L113615	_010	6517	1.17	sh	oc, ct, cn	582	12	62	307	0.201
L113615	_012	5214	1.287	sh,bk	sec+oc, cn	339	26	358	1146	0.312
L113615	_013	4768	1.1	ang	ot	2677	130	83	64	1.293
L113615	_014	21029	1.1	sh, bk	oc, ct, cn	134	13	90	112	0.807
L113615	_015	4322	1.237	sba-sbr	oc, ct, ocn	2825	24	246	361	0.680

Sample	Grain ID	S. area	AR	Morph	Zoning	Conc age	2σ	Th	U	Th/U
L113615	_016	4013	1.146	ang	ot	1783	44	121	317	0.382
L113615	_018	3773	1.593	sbr	ot	1619	57	107	116	0.929
L113615	_019	2950	1.094	sh	ot	424	15	310	479	0.648
L113615	_020	2950	1.774	ang/bk	oc, ct, ocn	329	22	814	1108	0.734
L113615	_022	2401	1.321	sba-sbr	ot	644	44	35	85	0.412
L113415Z	_001	9842	1.378	sba	oc, pl	633	26	90	88	1.018
L113415Z	_002	9856	2.38	eh	oc, ct, cn	376	18	41	78	0.527
L113415Z	_004	16856	1.287	eh	oc, ct, ocn	607	24	199	326	0.609
L113415Z	_005	8653	1.43	sbr-rnd	oc, pl	967	40	407	313	1.300
L113415Z	_007	7140	2.047	sh/sbr	oc, ct, ocn	607	24	64	138	0.463
L113415Z	_008	7700	1.224	sh, bk	ot	382	18	154	375	0.412
L113415Z	_009	8792	2.169	sh, bk	oc, ct, cn	373	16	77	371	0.209
L113415Z	_010	10724	1.506	sh/sbr	sec+oc, ct, ocn	649	32	134	132	1.014
L113415Z	_011	6664	1.853	sba-sbr	ot	625	21	289	228	1.265
L113415Z	_012	6132	1.123	sh, bk	oc, ct, ocn	483	18	424	554	0.766
L113415Z	_013	5516	1	sh, bk	oc, ct, ocn, xc	598	25	87	162	0.536
L113415Z	_014	10360	1.159	sba-sbr	oc, ct, ocn	1234	47	41	29	1.427
L113415Z	_015	8218	1.286	rnd	sec, ct, ocn, xc	561	21	84	74	1.140
L113415Z	_017	8358	1.378	sbr, bk	oc, ct, ocn	1169	48	37	156	0.234
L113415Z	_018	9114	1.267	sbr, bk	oc, ct, ocn	540	21	332	241	1.376
L113415Z	_019	12852	1	sbr, bk	unz	632	31	44	48	0.913
L113415Z	_020	6972	1.089	sbr	oc, ct, cn	618	26	202	140	1.438
L113415Z	_022	10122	1.324	ang	ot	1258	37	82	264	0.310
L113415Z	_024	6944	1.413	sbr	sec+oc, ct, cn	446	15	115	298	0.384
L113415Z	_025	10234	1.479	sbr-rnd	sec+oc, ct, cn	537	25	77	159	0.486
L113415Z	_026	7336	1.276	sba	oc, ct, ocn	2469	45	49	137	0.361
L113415Z	_027	2954	1.133	eh	sec+oc, nct, cn	421	25	159	179	0.887
L113415Z	_029	8162	1.333	sba-sbr	sec+oc, ct, cn	602	23	103	117	0.883
L113415Z	_031	8148	1.119	rnd	sec, cn	628	29	9	566	0.015
L113415Z	_032	6006	2.382	sbr	oc, ct, cn	1416	37	38	92	0.414
L113415Z	_033	6482	2.547	eh, bk	oc, pl	448	16	195	188	1.033
L113415Z	_035	3570	1.103	eh, bk	oc, ct, ocn	429	28	402	439	0.917
L113415Z	_036	6062	1.133	sh/sba	ot	487	30	70	86	0.817
L113415Z	_037	6496	1.38	sh, bk	oc, ct, cn	450	22	189	406	0.466
L113415Z	_038	9142	1.446	sh, bk	oc, ct, ocn	414	17	149	483	0.308
L113415Z	_039	5796	1.4	sh	sec+oc, ct, cn	648	16	200	383	0.521
L113415Z	_042	3598	1.383	sh	sec+oc, ct, ocn	579	44	177	196	0.901
L113415Z	_043	3836	1.103	sh, bk	sec+oc, ct, cn	416	33	147	230	0.641
L113415Z	_044	3682	1.383	sba	sec+oc, ct, ocn	732	28	108	125	0.868
L113415Z	_048		1.33	ang/bk	ot	692	16	253	886	0.285
L113415Z	_049	9324	1.933	sh	oc, ct, ocn	639	26	1143	1146	0.998
L113415Z	_050	6342	1.747	eh	sec+oc, ct, cn	592	34	94	287	0.329
L113415Z	_053	6706	1.494	sbr	oc, ct, ocn	571	27	62	88	0.703
L113415Z	_055	9170	1.306	ang	oc, pl	433	18	76	49	1.539
L113415Z	_056	9492	1	ang-sba	sec+oc, ct, ocn	427	20	103	120	0.858

Sample	Grain ID	S. area	AR	Morph	Zoning	Conc age	2σ	Th	U	Th/U
L113415Z	_057	9856	1.103	sbr, bk	oc, ct, ocn	641	27	67	69	0.975
L113415Z	_058	5838	1.17	ang-sba	oc, ct, ocn	2591	42	120	227	0.528
L113415Z	_061	4102	1.756	eh	oc, ct, ocn	615	18	289	387	0.746
L113415Z	_062	8806	1	sba	oc, pl	406	21	174	74	2.335
L113415Z	_063	10388	1.263	rnd	oc, ct, oc, xc	614	35	37	64	0.580
L113415Z	_064	7224	1	ang	sec, nct	640	24	95	140	0.678
L113415Z	_066	4914	1.5	sba	ot	650	38	14	25	0.551
L113415Z	_067	4116	1.75	eh, bk	oc, pl	394	45	84	97	0.866
L113415Z	_068	8792	1.09	sbr	oc, ct, ocn	580	26	37	88	0.428
L113415Z	_070	5936	1.329	sba	oc, pl	1656	37	383	360	1.062
L113415Z	_076	6437	1.13	rnd, bk	unz	2638	41	252	447	0.563
L113415Z	_078	17514	1.185	sba	oc, pl	547	26	45	74	0.619
L113415Z	_081	11578	2.176	sbr	ot	643	31	9	40	0.226
L113415Z	_084	7672	1.386	rnd	oc, ct, ocn	430	19	626	949	0.659
L113415Z	_085	8232	1.076	sbr	oc, ct, ocn	1291	29	64	153	0.418
L113415Z	_086	21028	1.024	sbr	sec, nct	1320	31	122	326	0.374
L113415Z	_087	16282	1.517	sbr, bk	oc, ct, cn	558	21	99	115	0.857
L113415Z	_088	11984	1	rnd	sec+oc, ct, ocn	612	24	46	70	0.648
L113415Z	_089	15652	1.053	ang	oc, ct, ocn	1561	41	135	345	0.390
L113415Z	_090	26138	1.059	sba-sbr	ot	614	24	136	247	0.551
L113415Z	_091	11368	1.164	sbr-rnd	oc, ct, ocn	558	42	75	112	0.671
L113415Z	_092	4200	1.169	sba	unz	1175	77	47	123	0.385
L113415Z	_094	12000	1.8	eh	N/A	1111	71	201	264	0.763
L113415(2)	_001	17941	2.012	sh	ot	372	11	30	170	0.179
L113415(2)	_004	6432	1.612	eh/bk	oc, ct, ocn	411	9	159	290	0.547
L113415(2)	_007	7103	1.14	sbr	oc, ct, cn	524	18	293	267	1.097
L113415(2)	_008	9457	1.67	sh/bk	oc, ct, ocn	377	12	94	228	0.412
L113415(2)	_009	11089	1.052	rnd/ bk	unz	1177	27	128	75	1.714
L113415(2)	_010	6589	2.11	eh	oc, ct, cn	382	7	108	403	0.267
L113415(2)	_011	9898	1.023	ang	oc, ct, ocn	397	11	41	103	0.400
L113415(2)	_012	7356	1.95	eh	oc, ct, cn	2064	37	95	136	0.697
L113415(2)	_013	5311	1.21	sh	ot	388	11	71	403	0.176
L113415(2)	_014	8934	1.16	sba	oc, ct, ocn	430	12	237	298	0.794
L113415(2)	_015	9117	1.25	sba	oc, ct, ocn	1979	36	125	151	0.830
L113415(2)	_016	10326	1.91	sh	oc, ct, cn	465	18	70	146	0.481
L113415(2)	_017	7528	1.14	sbr	unz	2078	26	39	67	0.581
L113415(2)	_020	6584	2.24	sbr	ot	644	24	66	91	0.730
L113415(2)	_021	4692	1.91	sbr	ot	2829	75	43	151	0.287
L113415(2)	_023	6319	1.09	rnd	ot	2078	26	193	365	0.527
L113415(2)	_025	7899	1.12	sbr/ bk	ot	1536	52	49	185	0.262
L113415(2)	_026	4763	1.18	sbr	oc, ct, cn	638	15	283	241	1.175
I783255Z	_002	8162	1.616	sh-sbr	oc, ct, cn	531	43	104	62	1.681
I783255Z	_004	5054	1.147	sh	oc, ct, cn	535	32	111	175	0.635
I783255Z	_006	6188	1.128	sh	unz	629	45	28	38	0.732
I783255Z	_007	5782	1.078	eh	sec+oc, cn	431	26	135	144	0.938

Sample	Grain ID	S. area	AR	Morph	Zoning	Conc age	2σ	Th	U	Th/U
I783255Z	_008	5166	1.146	sba-sbr	oc, ct, ocn	619	32	43	115	0.378
I783255Z	_009	12040	1.413	sba-sbr	oc, ct, ocn	1590	56	53	180	0.297
I783255Z	_010	4648	1.5	sba-sbr	oc, ct, ocn	550	35	173	222	0.780
I783255Z	_011	4970	1.462	sba	sec+oc, ocn	2125	63	141	356	0.397
I783255Z	_013	6258	1.111	sh	sec+oc, cn	486	46	289	302	0.959
I783255Z	_015	7714	1.349	rnd	oc, ct, ocn	1845	67	118	144	0.819
I783255Z	_016	5796	1.293	sba	oc, ct, ocn	1294	50	29	93	0.309
I783255Z	_019	4970	1.098	sba	ot	537	26	290	311	0.932
I783255Z	_022	5992	1.493	sba	oc, ct, cn	551	50	108	135	0.805
I783255Z	_026	7532	1.211	sbr	oc, ct, ocn	2392	64	40	82	0.479
I783255Z	_028	4858	1.469	sh	oc, ct, cn	1483	130	46	89	0.516
I783255Z	_029	2758	1.143	ang	unz	590	72	42	40	1.047
I783255Z	_030	2730	1.143	sh	oc, ct, ocn	392	24	98	431	0.227
I783255Z	_031	4130	1.344	sh	oc, ct, cn	444	21	296	383	0.772
I783255Z	_034	5362	1.479	sba-sbr	sec+oc, cn	1014	45	163	246	0.662
I783255Z	_041	5572	1.333	rnd	oc, ct, cn	619	42	48	46	1.046
I783255Z	_042	3794	1.5	sbr	oc, ct, ocn	1997	99	20	34	0.609
I783255Z	_043	3962	1.281	sh	oc, ct, cn	505	23	144	265	0.542
I783255Z	_044	4690	1.133	sh	oc, ct, ocn	602	42	230	239	0.964
I783255Z	_045	9898	1.392	sba	oc, ct, ocn	728	35	14	169	0.086
I783255Z	_046	8820	2	sh	oc, ct, cn	616	29	137	238	0.577
I783255Z	_049	3570	1.231	rnd	ot	1082	35	292	155	1.891
I783255Z	_050	4116	1.667	eh	unz	414	31	43	83	0.511
I783255Z	_053	8218	2.643	eh	oc, ct, cn	562	24	148	260	0.570
I783255Z	_054	2310	1.561	sbr	ot	1114	40	134	178	0.753
I783255Z	_055	4508	1.385	sba	sec+oc, cn	3111	43	111	161	0.692
I783255Z	_060	9772	1.101	sh	sec, cn	2224	62	31	45	0.694
I783255Z	_063	5068	1.286	sh	oc, ct, cn	599	31	92	170	0.539
I783255Z	_064	5978	1.183	sbr	oc, ct, ocn	637	67	365	316	1.155
I783255Z	_066	5404	2.143	sbr	sec+oc, ocn	2089	66	76	160	0.475
I783255Z	_067	5404	1.714	eh, bk	oc, ct, ocn	480	24	71	149	0.480
I783255Z	_068	4410	1	sbr	ot	2080	87	39	115	0.337
I783255Z	_069	3850	1.545	ang	ot	1245	95	49	224	0.217
I783255Z	_073	5236	1.147	sh	oc, ct, cn	645	33	117	114	1.030
I783255Z	_074	4508	1.2	sba	oc, pl	1615	84	70	101	0.689
I783255Z	_075	5152	1.667	rnd	oc, ct, ocn	608	43	76	95	0.792
I783255Z	_077	3052	1.25	sh, bk	oc, ct, ocn	445	22	122	179	0.684
I783255Z	_078	5404	1	rnd	ot	1809	62	73	100	0.730
I783255Z	_079	9716	1.24	sba	oc, ct, ocn	538	26	59	149	0.396
I783255Z	_084	2380	1.667	sh	oc, ct, cn	621	27	96	195	0.494
I783255Z	_087	1610	1.765	ang	unz	446	23	348	598	0.582
I783255Z	_088	7014	3.019	sh	oc, ct, cn	590	25	54	278	0.193
I783255Z	_090	7658	1.124	sbr	oc, ct, ocn, xc	1397	48	66	209	0.317
I783255Z	_092	5474	1.092	sh, ang/bk	oc, ct, ocn	471	17	278	776	0.358
I783255Z	_094	5950	1.627	sh	ot	465	25	249	311	0.800

Sample	Grain ID	S. area	AR	Morph	Zoning	Conc age	2σ	Th	U	Th/U
I783255Z	_095	5096	1.049	sbr	ot	663	47	53	71	0.744
I783255Z	_096	4298	1.147	eh, ang/bk	ot	430	26	134	140	0.957
I783255Z	_097	2380	1.306	sh, ang/bk	oc, ct, ocn	598	36	83	137	0.608
I783255Z	_098	4970	1.324	sh	sec+oc, cn	609	52	229	248	0.922
I783255Z	_099	4984	3.375	eh-sh	sec+oc, cn	413	26	182	199	0.916
I783255Z	_101	13664	1.043	sbr	unz	1263	27	653	534	1.223
I782175Z	_001	5642	1.047	sba-sbr	oc, pl	657	28	154	160	0.967
I782175Z	_002	3850	1.344	sh, ang/bk	ot	1428	76	87	168	0.522
I782175Z	_003	4578	1.053	sba-sbr	ot	2466	64	58	52	1.110
I782175Z	_008	4816	1.098	eh, bk	oc, pl	2168	34	267	491	0.542
I782175Z	_009	4298	1.403	sbr-rnd,bk	oc, pl, xc	652	25	681	1181	0.577
I782175Z	_010	5880	1.627	sh, bk	oc, ct, ocn	953	79	302	212	1.421
I782175Z	_011	4228	1	sh	sec+oc, ct, ocn	577	37	180	243	0.741
I782175Z	_012	4550	1.469	sh	sec+oc, ct, ocn	611	49	165	329	0.503
I782175Z	_013	4018	1.469	sbr-rnd	ot	1709	78	345	341	1.010
I782175Z	_017	3542	1.5	sh-eh,bk	oc, ct, cn	472	39	93	137	0.684
I782175Z	_019	3276	1.755	sh, bk	oc, ct, cn, xc	649	42	28	43	0.639
I782175Z	_021	3780	1.224	sbr-sba	oc, ct, ocn	1175	90	243	435	0.559
I782175Z	_022	6650	2.65	ang, bk	unz	1364	90	282	203	1.390
I782175Z	_024	7700	1.211	sbr	sec, ct, cn	603	43	213	273	0.781
I782175Z	_025	2436	1.556	sbr-rnd	N/A	606	40	74	110	0.677
I782175Z	_026	3892	1.127	sh	oc, ct, ocn	443	25	397	857	0.463
I782175Z	_028	5558	1.479	sba-sbr	ot	1920	56	64	103	0.622
I782175Z	_029	5152	1.643	sba-sbr	unz	1238	53	127	41	3.108
I782175Z	_030	5320	1.146	sh-eh,bk	oc, ct, ocn, xc	624	18	63	169	0.371
I782175Z	_031	4858	1.147	sh, bk	oc, ct, ocn	749	24	341	439	0.777
I782175Z	_035	5740	1.235	sh	oc, ct, ocn	601	20	141	202	0.699
I782175Z	_036	2632	1.071	sbr-rnd	ot	581	42	53	107	0.491
I782175Z	_037	4424	1.286	sba-sbr	oc, ct, ocn	1037	32	52	170	0.307
I782175Z	_038	3080	1.489	sba	ot	707	190	257	239	1.076
I782175Z	_039	3276	1.109	sba	unz	383	19	28	67	0.413
I782175Z	_040	4466	1.284	ang	ot	1219	26	53	223	0.239
I782175Z	_042	N/A	N/A	ang	oc, ct, ocn	484	60	74	335	0.222
I782175Z	_043	3444	1.442	sh	oc, ct, cn	610	21	187	225	0.831
I782175Z	_046	3878	1.617	sh	oc, ct, ocn	560	29	36	91	0.398
I782175Z	_047	5418	1.333	sbr	oc, ct, ocn	1261	39	103	177	0.582
I782175Z	_051	3864	1.333	sbr	oc, ct, ocn, xc	605	27	327	400	0.816
I782175Z	_052	3542	1.5	ang-sba	ot	428	23	149	103	1.443
I782175Z	_053	6846	1.232	sba-sbr	ot	566	43	108	70	1.532
I782175Z	_055	5376	1.448	sba-sbr	ot	1825	41	167	219	0.761
I782175Z	_058	9688	2	sbr, bk	ot, xc	2785	48	96	203	0.471
I782175Z	_060	5782	1.435	eh, bk	oc, ct, ocn	582	23	73	158	0.461
I782175Z	_061	5432	1.38	sba	oc, ct, ocn	625	40	207	201	1.032
I782175Z	_062	5852	1.302	sba-sbr	oc, ct, ocn	1789	39	105	149	0.705
I782175Z	_063	5656	1.047	ang-sba	oc, ct, ocn	1233	85	102	247	0.415

Sample	Grain ID	S. area	AR	Morph	Zoning	Conc age	2σ	Th	U	Th/U
I782175Z	_064	26740	1.043	sba	oc, ct, cn, xc	2815	36	114	301	0.380
I782175Z	_068	6846	1.167	sba	sec+oc, ct, ocn	2289	48	135	247	0.548
I782175Z	_069	21588	1.292	sbr, bk	oc, pl, xc	2854	35	71	192	0.371
I782175Z	_070	5656	1.047	ang-sba	oc, ct, ocn	1233	85	102	247	0.415
I782175Z	_071	26740	1.043	sba	oc, ct, cn, xc	2815	36	114	301	0.38
I782175Z	_074	4592	1.038	sba-sbr	unz	2125	39	81	116	0.702
I782175Z	_076	6846	1.167	sh, sba/bk	sec+oc, ct, ocn	2289	48	135	247	0.548
I782175Z	_077	21588	1.292	sbr, bk	oc, pl, xc	2854	35	71	192	0.371
H285025Z	_001	15498	2.714	sh	oc, ct, cn	609	50	241	371	0.650
H285025Z	_002	10612	1	ang-sba	ot	2852	55	170	110	1.551
H285025Z	_004	9520	2.429	eh	oc, ct, cn	429	30	330	297	1.110
H285025Z	_005	15344	1.654	eh, bk	sec+oc, ct, cn	349	23	94	181	0.520
H285025Z	_008	21728	2.84	eh, bk	oc, ct, cn	404	24	270	215	1.253
H285025Z	_010	6944	1.771	eh	oc, pl	427	22	188	237	0.792
H285025Z	_013	10766	1.364	sh	oc, ct, ocn	426	33	100	191	0.526
H285025Z	_015	10164	1.351	sbr-rnd	oc, ct, ocn	1795	54	80	239	0.334
H285025Z	_018	6790	1.117	sh, bk	sec+oc, ct, cn	436	38	139	188	0.743
H285025Z	_019	10024	1.248	rnd	oc, ct, cn	1082	50	47	54	0.875
H285025Z	_020	5026	1.211	eh, bk	oc, ct, cn	418	22	102	163	0.625
H285025Z	_021	8512	1.388	sba-sbr	oc, pl	1049	60	37	46	0.810
H285025Z	_022	6874	1.6	sbr	ot	642	32	105	134	0.783
H285025Z	_025	5026	1.2	sba, bk	oc, ct, ocn	1873	39	138	176	0.786
H285025Z	_026	4158	1.179	rnd	oc, ct, cn	1286	98	101	227	0.445
H285025Z	_027	7378	2.8	sba	oc, ct, ocn	613	34	269	185	1.454
H285025Z	_028	4648	1.507	eh, bk	oc, ct, cn	628	31	128	212	0.604
H285025Z	_029	4466	1.516	sbr	oc, ct, cn	1807	80	166	358	0.463
H285025Z	_030	4508	1.147	sba-sbr	unz	1840	60	63	85	0.734
H285025Z	_031	4690	1.253	sba, bk	sec+oc, ct, cn	420	26	206	234	0.882
H285025Z	_032	4242	1.406	sba, bk	ot	476	33	101	201	0.501
H285025Z	_033	3864	1	sh	oc, ct, cn	576	36	42	203	0.209
H285025Z	_034	7448	1.378	sh, bk	oc, ct, cn	420	32	206	184	1.121
H285025Z	_035	4004	1	sh	oc, ct, cn	1069	43	180	401	0.448
H285025Z	_036	5516	1.667	sbr	oc, ct, ocn	597	28	98	73	1.340
H285025Z	_038	5250	1.089	sh, bk	oc, ct, cn	425	29	243	305	0.798
H285025Z	_040	10220	1.056	ang	unz	418	14	138	684	0.202
H285025Z	_043	4914	1.147	sbr-rnd	unz	1145	78	12	20	0.592
H285025Z	_044	4900	1.211	sba-sbr	oc, ct, ocn	1542	65	98	271	0.362
H285025Z	_045	5306	1.578	sba-sbr	oc, ct, cn	518	28	96	183	0.522
H285025Z	_046	9030	1.523	sh, bk	oc, ct, cn	647	71	311	674	0.462
H285025Z	_047	4284	1.25	sba-sbr	oc, ct, cn	629	22	56	467	0.121
H285025Z	_048	4634	1.516	sba-sbr	unz	1686	57	35	100	0.356
H285025Z	_050	8246	1.929	sh, bk	oc, pl	387	34	652	310	2.102
H285025Z	_052	15498	1.98	sh	oc, cn, ocn	603	49	50	75	0.668
H28_5015	_001	20360	2.46	sh-ang	oc, pl	418	9	356	269	1.323
H28_5015	_003	10074	1.174	ang/bk	oc, ct, ocn	423	19	188	194	0.967

Sample	Grain ID	S. area	AR	Morph	Zoning	Conc age	2σ	Th	U	Th/U
H28_5015	_005	22903	1.618	sh/bk	oc, ct, ocn	420	15	123	206	0.600
H28_5015	_008	10454	2.571	eh/bk	oc, pl	421	22	157	199	0.789
H28_5015	_009	11377	1.955	sh/bk	oc, pl	420	15	142	203	0.699
H28_5015	_012	10062	1.324	sh/bk	oc, ct, ocn	327	15	317	536	0.592
H28_5015	_017	6688	1.179	eh	oc, ct, ocn	415	15	147	141	1.042
H28_5015	_019	3420	1.16	sba	oc, ct, ocn	424	18	189	300	0.630
H28_5015	_020	5993	1.608	eh	oc, ct, ocn	423	15	437	442	0.987
H28_5015	_022	4731	1.1	sba	ot	646	28	67	64	1.043
H28_5015	_023	5532	2.35	eh	oc, pl	632	12	192	281	0.682
H28_5025	_025	5026	1.07	sh	oc, ct, ocn	380	40	183	390	0.469
H28_5025	_032	4242	1.35	ang/bk	ot	476	33	101	201	0.501